Association of Arterial Stiffness and Changes in Brain Structure and Function in the UK Biobank

Association of Arterial Stiffness and Changes in Brain Structure and Function in the UK Biobank

By Elric Y. Allison, H.B.Kin

A Thesis Submitted to the School of Graduate Studies in Partial Fulfilment of the Requirements for the Degree Master of Science

McMaster University © Copyright by Elric Y. Allison, June 2022

M.Sc. Thesis – E.Y. Allison; McMaster University – Department of Kinesiology McMaster University MASTER OF SCIENCE (2022) Hamilton, Ontario (Kinesiology)

TITLE: Association of Arterial Stiffness and Changes in Brain Structure and Function in the UK Biobank

AUTHOR: Elric Y. Allison, H.B.Kin (Lakehead University)

SUPERVISOR: Dr. Baraa K. Al-Khazraji, PhD

NUMBER OF PAGES: 258

ACKNOWLEDGEMENTS

I would like to begin by thanking my supervisor, Dr. Baraa Al-Khazraji. I am so grateful for your mentorship. Your leadership by example has shown me what is means to be a great scientist, mentor, and person. Your person-first approach to mentorship was and continues to be instrumental in pushing me through feelings of doubt and burnout. You have showed me that good, rigorous science does not need to be at the expense of mental and physical wellbeing. I also want to thank you for always embracing and fostering my creativity and having an open mind on the numerous occasions that I have come to you with impractical project ideas ("maybe for your PhD"). Despite all the hinderances of the pandemic, you have always put me in a position to be productive and pursue ideas that I found interesting. Without your guidance this project would not have been possible.

Thank you to Dr. Kurt Smith, for being the person who sparked my passion for science and physiology. You started me on this path and were fundamental in setting the stage for my future development as a scientist. Beers owed.

Thank you to my supervisory committee members Dr. Aimee Nelson and Dr. Michael Noseworthy. While our meetings have been infrequent, your guidance and expertise have been crucial in the design of my M.Sc. project. With each comment and piece of advice, you have both strengthened this project significantly. Thank you both for all your help in taking this project from an idea to its current form.

I also want to thank the entire lab, from my fellow graduate student Michelle Mei to our undergraduate students and volunteers. Despite being a young lab, the culture that we have built together has made it an absolute pleasure to work with all of you. I cannot wait to see how we grow as a team and what we are able to accomplish together in the coming years.

I want to thank my mom and Sasan, for your unconditional love and support throughout the entirety of my studies. Thank you for always supporting me and allowing me to follow my interests. Thank you for listening to me talk about my research and being patient with me during times of high stress. Thank you for the countless home cooked meals and food deliveries provided over the last two years. Your support is never taken for granted.

Chloe, I cannot thank you enough for your unwavering support. It is difficult to imagine how I would have gotten through this period without you. Thank you for creating a space to unplug and an environment to laugh and have fun, even in the most stressful of times. No matter how my day goes, it is an absolute joy and privilege to end each one with you.

LAY ABSTRACT

Arterial stiffening both accompanies the normal aging process and can progress due to acquired health conditions. As arteries begin to stiffen the ability to buffer high pressure blood flow is impaired and can put microvasculature at risk of damage. Microvascular damage in the brain can disrupt blood and subsequent oxygen delivery to the brain. When delivery to the brain does not meet the metabolic demand, changes in brain structure brain can occur. Changes in brain structure are associated with impaired brain function, as well as potentially accelerating the progression of neurological diseases. What remains unclear is whether arterial stiffness impacts brain structure differently across regions or all regions homogenously. The purpose of this thesis was to examine the relationship between arterial stiffness and structural and functional changes in the brain over time (objective 1: 2-5 years; objective 2: 8-11 years). Our observations suggest that the progression of arterial stiffness had an effect that was equivalent to approximately 30% of the rate of grey matter tissue loss associated with normal healthy aging (~0.25% reduction in grey matter per year). We found no effect of changes in arterial stiffness on the progression of total grey matter volume, white matter lesions or brain function. We did observe a significant negative relationship between arterial stiffness at baseline and total grey matter volume 8-11 years later. We found no relationship between baseline arterial stiffness and brain structure or function 8–11-years post-baseline. Taken with the effects of normal aging, the loss of tissue in select brain regions associated with changes in arterial stiffness may result in grey matter reductions beyond the range associated with what is considered healthy or normal aging. The association of arterial stiffness and total grey matter volume 8-11 years later suggests that changes in whole brain structure are the product of long-term exposure to arterial stiffness.

ABSTRACT

While evidence suggests there is indeed a relationship between arterial stiffness and changes in brain structure and function cross-sectionally, the longitudinal relationship between arterial stiffness and changes in brain structure and function is unclear. Also unclear is whether a regional effect of arterial stiffness on brain structure exists, or if the effect is homogenous across brain regions. Using a healthy cohort of the UK Biobank study (N = 1858, mean±SD: 61 ± 7 years), we investigated the longitudinal association between changes in arterial stiffness index (ASI) and brain structure (grey matter cortical thickness, whole brain grey matter volume, white matter hyperintensity volume) and function (cognitive performance in 6 tests) over 2.5 ± 1 years. We also examined the association between baseline ASI and all structural and functional brain outcomes 8-11 years post-baseline (N = 630). Prior to post-hoc correction, we observed a significant effect of changes in ASI over 2.5 ± 1 years on grey matter cortical thickness in 11 brain regions contributing to reductions between 0.0004-0.0024mm annually, but none of the 11 regions remained significant post-correction. Following correction there was also no effect of changes in ASI on whole brain grey matter volume (p = 0.76), white matter hyperintensity volume (p = 0.84), or cognitive performance in the domains of interest. Baseline ASI was not associated with regional grey matter cortical thickness, white matter hyperintensity volume, or cognitive function, but did have a significant negative association with whole brain grey matter volume 8.5 ± 1.05 **(p = 0.015) years later** and 11 ± 1.02 **(p = 0.03)** years later. Our findings suggest that taken with the effect of age, elevations in ASI may have an additive effect to accelerate changes in brain structure beyond the range that is to be expected as a part of normal aging. Our findings also suggest the relationship between ASI and reductions in whole brain grey matter volume may require long-term exposure to elevations in arterial stiffness in otherwise healthy older adults.

TABLE OF CONTENTS

CHAPTER I

Literature Review

Arterial Stiffness

Arterial Structure

Arteries have three primary layers of tissue: intima, media, and adventitia (*Figure 1*). All cells within the vasculature including endothelial cells of the intima, smooth muscle cells of the media, and fibroblasts of the adventitia, are sensitive to mechanical stimuli. The intrinsic cells within each layer typically seek to establish and maintain a preferred mechanical homeostatic state (or vascular tone) (Humphrey & Tellides, 2019). Many vascular conditions appear to arise with compromised or a loss of homeostasis. One pathophysiological consequence of disrupted vascular homeostasis, either via the process of normal aging or through disease pathways such as atherosclerosis, diabetes mellitus (Fjell et al., 2014; Ramanoël et al., 2018; Thambisetty et al., 2010), or obesity, is stiffening of the arterial wall. Arterial stiffening is an early-stage modification to the composition and function of the vascular system, and is the precursor to several pathological conditions including atherosclerosis (Fernandes et al., 2008), hypertension (Laurent et al., 2006), and various other cardiovascular diseases (Vlachopoulos et al., 2010). As a result, assessment of subclinical changes in the elastic properties of arteries are often used for risk stratification purposes (Pereira et al., 2015). It is important to note that arterial stiffness is more common in central and conduit arteries such as the aorta, and less frequent in peripheral arteries (Zieman et al., 2005). Vessel stiffening typically develops from complex interactions involving structural and cellular factors (Lacolley et al., 2020).

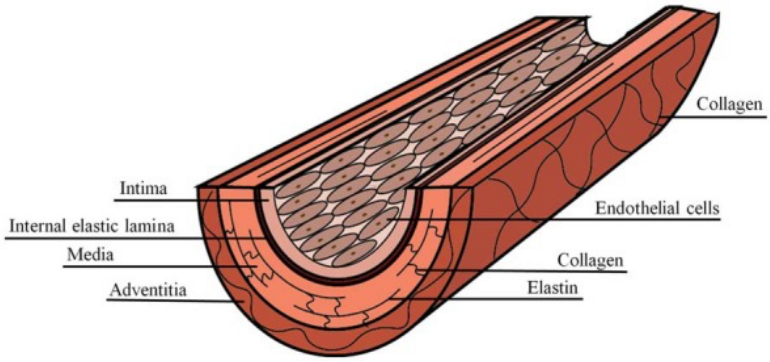

Figure 1. Composite structure of elastic artery (Kohn et al., 2015).

Structural factors contributing to arterial stiffness

Structural properties of the vascular wall are largely dependent on the joint contributions of two primary scaffolding proteins within the extracellular matrix: elastin and collagen (Zieman et al., 2005). The presence of elastin affords arteries the ability to distend during systole and recoil during diastole, which causes a dampening of high systolic pressures ejected from the heart prior to reaching distal arteries, microvasculature, and end-organs, while the presence of collagen provides strength and structure to prevent vessel failure or rupture when exposed to high systolic pressures (Cecelja & Chowienczyk, 2009; Messerli et al., 1985; Stakos et al., 2010; Wagenseil & Mecham, 2012; Xu et al., 2000). Under normal conditions, the relative composition of these two proteins within the vasculature is held stable by a cyclical process of production and degradation via catabolic matrix metalloproteases (MMPs). These MMP's allow for synthesis of new proteins within the extracellular matrix of the vessel by degrading collagen and elastin. As a product of both normal aging and disease such as diabetes or obesity, there may be a disruption of the balance between production and degradation via MMPs which may potentially result in an overabundance of collagen, and a degradation in elastin within the vessel wall (Wagenseil & Mecham, 2012). Elevations in arterial stiffness can also occur via advanced glycolytic end products (AGEs), which

act to form cross-links between long-lived proteins such as collagen. AGEs-linked collagen is stiffer, disorganized, and more resistant to MMP degradation, leading to accumulation of structurally and functionally inadequate collagen formations (Zieman et al., 2005). Shifting the balance of extracellular matrix composition in favour of collagen greatly contributes to arterial stiffness, as collagen fibres are ~100-1000 times stiffer than elastin fibres (Wagenseil & Mecham, 2012). Disruption in the collagen and elastin production and degradation cycle may stem from vascular trauma leading to an increase of pro-inflammatory cytokines, growth factors, and vascular adhesion molecules (Zieman et al., 2005). Taken together, these structural changes contribute to the stiffening of the arterial wall (Zieman et al., 2005). Another factor contributing to increased collagen production is increased luminal pressure by way of chronic elevations in blood pressure (Xu et al., 2000). Increased collagen synthesis is related to elevated arterial stiffness in individuals with treated hypertension (Stakos et al., 2010).

Cellular and neural factors contributing to arterial stiffness

The two most prominent cellular factors influencing arterial stiffness are endothelial cell signalling and smooth muscle cell tone (Zieman et al., 2005). Endothelial function is largely defined by the vasodilatory response to stimuli, both mechanical (shear stress) and cellular (e.g., acetylcholine) (Ballermann et al., 1998; Wilson et al., 2016). In healthy vessels, the response to either mechanical or cellular stimuli triggers a cascade leading to increased nitric oxide production by endothelial cells, which subsequently leads to smooth muscle cell relaxation (vasodilation) (Ballermann et al., 1998). Impairments in production of nitric oxide by endothelial cells are a hallmark of endothelial dysfunction and has been frequently associated with the progression of arterial stiffening and elevated risk of cardiovascular diseases (Hadi et al., 2005; Jadhav & Kadam, 2005; van Bussel et

al., 2011). Vascular smooth muscle cells are similarly responsive to both mechanostimulation (smooth muscle cell stretch), and hormonal factors such as angiotensin-II, endothelin-1, oxidative stress, and nitric oxide (Zieman et al., 2005).

Additionally, there is a significant role of sympathetic nerve activity on vascular tone (Nardone et al., 2020). Evidence suggests that chronic elevations in sympathetic outflow may contribute to increased vascular remodelling by acting on the α-adrenergic receptors of vascular smooth muscle (Nardone et al., 2020). The relationship between elevations in sympathetic nerve activity and arterial stiffening across multiple indices including carotid intima media thickness, aortic wave reflection characteristics, pulse wave velocity, augmentation index, and arterial compliance has been reported frequently in the literature (Holwerda, Luehrs, DuBose, Collins, et al., 2019; Holwerda, Luehrs, DuBose, Majee, et al., 2019; Millar et al., 2019; Nardone et al., 2020; Swierblewska et al., 2010; Tanaka et al., 2017). The dynamic interplay between mechanical, cellular, and neural factors contribute to regulate vascular smooth muscle tone, and in healthy vessels allow for vasoconstriction and vasodilation to regulate blood flow to match metabolic demand at rest and during physiological challenges.

Atherosclerotic stiffening

In addition to the factors intrinsic to the vessel and age-related vascular stiffening, disease states and vascular injury are also strongly associated with the progression of arterial stiffness. Atherosclerosis is a chronic vascular condition that leads to vessel stiffening via build-up of plaques on the arterial wall (Bergheanu et al., 2017). While many risk factors may contribute to

the build-up of arterial plaques including hypertension, smoking, and hyperglycemia, hypercholesterolemia is believed to be one of the most potent triggers for the development of atherosclerosis (Bergheanu et al., 2017). Description of the full process behind the development of atherosclerotic vascular stiffening is beyond the scope of this literature review but has been described elegantly by several (Bentzon et al., 2014; Bergheanu et al., 2017; Moore & Tabas, 2011; Rafieian-Kopaei et al., 2014).

Measurement of Arterial Stiffness

Regional pulse wave velocity (PWV)

The current gold standard measurement approach for the assessment of arterial stiffness is pulse wave velocity (PWV). This measurement technique provides essential information about the state of the systemic arterial system. PWV is defined as the velocity at which systolic pressure waves propagate along the arterial tree (Pereira et al., 2015). As previously mentioned, when functioning optimally, arteries are capable of distending during systole and recoil during diastole, allowing elastic arteries to act as a buffer, preventing high pressure waves from reaching distal microvasculature or end-organs (Belz, 1995). Higher values of PWV correspond to lower distensibility and compliance of the vessel, and therefore, is an indication of stiffer vessels. Regional PWV is a widely accepted approach for the quantification of arterial stiffness and is assessed by measuring the propagation time of systolic pulse waves to travel between two measurement sites. The most frequently used arterial segment when measuring regional PWV is the segment between the carotid and the femoral arteries (Millasseau et al., 2005; Pereira et al., 2015). It is important to note that the measure of carotid-femoral PWV (cfPWV) presents with limitations, as it is an averaged value of PWV over the length of the segment between each vessel,

that may or may not account for potential differences in the mechanical and elastic properties of the two arteries (Pereira et al., 2015). In addition, because cfPWV is an averaged value, potential variations in arterial properties between the two measurement sites can go undetected (Darwich et al., 2015). At early stages of age-related vascular stiffening or atherosclerosis, fibrous spots contributing to the stiffening of the arterial wall are not uniformly distributed, and as such using a measure such as cfPWV is unable to provide any information about specific areas of stiffness or abnormalities (Darwich et al., 2015). Additionally, although the length of the arterial segment between each site is measured, the curvatures or irregularities within the arterial segment are not considered and could serve as a contributing factor leading to inaccurate estimation of PWV. Measurement of cfPWV can also be greatly influenced and confounded by the presence of abdominal obesity, which can influence and skew the measurement of the distance between each measurement site (*Equation 1)* (Calabia et al., 2011; Pereira et al., 2015).

$$PWV = D \text{ (meters)}/Dt \text{ (seconds)} \qquad \textit{Equation 1.}$$

D is the distance between measurement point 1 and measurement point 2, and Dt is the transit or propagation time (i.e., the time required for the foot of the pressure wave to travel the full distance of the segment).

The devices most frequently used to measure regional PWV include the PulsePen® (DiaTecne, Milan, Italy), Complior® (Colson, France), and SphygmoCor® (AtCor Medical, Sydney, Australia) (Rajzer et al., 2008; Salvi et al., 2004). All three of the devices are approaches that rely on the use of tonometry-based techniques (Pereira et al., 2015). The PulsePen® is a device composed of one

tonometer and an integrated ECG unit. Typically, to quantify cfPWV, two PulsePen® units are required, one at each measurement site. The delay between systolic pulse waves is determined by applanation tonometry obtained at each measurement site, and is then synchronized with the ECG signal (Salvi et al., 2004). The Complior® uses two pressure mechanotransducers directly applied to the surface of the skin at two measurement sites. In comparison to the PulsePen®, the Complior® does not include an integrated ECG unit (Rajzer et al., 2008). SphygmoCor® analyzes the pulse wave at two measurement sites, simultaneously estimating the delay in pulse wave propagation between the proximal and distal measurement sites with respect to the ECG wave, via integrated ECG unit, to calculate PWV (Rajzer et al., 2008). While measuring the same construct, the values derived from each device differ to varying degrees. For example, in a comparative study of these devices, PWV derived from the Complior® was a mean 1.4m/s higher than SphygmoCor® derived PWV (Rajzer et al., 2008). Despite being the gold standard approach for measurement of PWV, tonometry is highly dependent on operator skill, meaning that inter-user reliability may confound measurements (Laurent et al., 2006). As a result, sufficient training is required for operators of tonometry-based techniques used in both research and clinical settings for PWV assessment.

Table 1. Distribution of pulse wave velocity (PWV) values (m/s) in the reference value population (N=11,092) according to age and blood pressure category (The Reference Values for Arterial Stiffness' Collaboration, 2010). Age category is reported in years, PWV reference ranges are reported as means and 95% CI.

	Blood Pressure Category				
Age	Optimal	Normal	Pre-HT	Grade I HT	Grade II HT
<30	6.1 (4.6–7.5)	6.6 (4.9–8.2)	6.8 (5.1–8.5)	7.4 (4.6–10.1)	7.7 (4.4–11.0)
30-39	6.6 (4.4–8.9)	6.8 (4.2–9.4)	7.1 (4.5–9.7)	7.3 (4.0–10.7)	8.2 (3.3–13.0)
40-49	7.0 (4.5–9.6)	7.5 (5.1–10.0)	7.9 (5.2–10.7)	8.6 (5.1–12.0)	9.8 (3.8–15.7)
50-59	7.6 (4.8–10.5)	8.4 (5.1–11.7)	8.8 (4.8–12.8)	9.6 (4.9–14.3)	10.5 (4.1-16.8)
60-69	9.1 (5.2–12.9)	9.7 (5.7–13.6)	10.3 (5.5–15.1)	11.1 (6.1–16.2)	12.2 (5.7–18.6)
>70	10.4 (5.2-15.6)	10.4 (5.2–15.6)	11.8 (5.7–17.9)	12.9 (6.9–18.9)	14.0 (7.4–20.6)

Local pulse wave velocity

Local PWV differs from regional PWV as it measures the systolic pulse wave at a single measurement site. By measuring PWV at a single arterial segment, typically the aorta or the carotid arteries, the local approach to measurement of PWV avoids the previously mentioned limitations of regional PWV such as different mechanical properties of arterial segments, curvatures in the arterial segment between the measurement sites, and measurement errors associated with abdominal obesity (Pereira et al., 2015). Understanding and considering the heterogeneity between stiffness states and mechanical properties of segments along the entire arterial system can provide more nuanced insight into what is happening at the point of measurement. Local PWV is typically measured via two primary non-invasive approaches; Phase-contrast (PC) MRI and Doppler ultrasound (Pereira et al., 2015). PC-MRI assessment of local PWV is an accurate assessment approach as it provides both high temporal and spatial resolution (Pereira et al., 2015). PC-MRI allows the direct imaging of the thoracic and abdominal aorta without operating under any

anatomical assumptions (i.e., lack of curvature along the arterial segment). This direct measurement of the path length of the systolic pressure wave makes the use of PC-MRI measurement approaches a useful technique for the assessment of arterial stiffness compared to tonometry and ultrasound based-techniques (Joly et al., 2009; Pereira et al., 2015). There are multiple approaches to assessing arterial stiffness via ultrasound. One Doppler ultrasound technique for the assessment of local PWV estimates the time delay (pulse wave transit time) between vessel distension at two close positions along the length of the same arterial segment of interest (Calabia et al., 2011; Pereira et al., 2015). Another Doppler ultrasound-based approach estimates local PWV by calculating the ratio between change in blood velocity and change in vessel cross-sectional area over the duration of one cardiac cycle (Pereira et al., 2015; Rabben et al., 2004). Using ultrasound-based approaches for the assessment of PWV is highly user-dependent, and as such require significant training for reliable measurements (Calabia et al., 2011; Pereira et al., 2015). While regional PWV is accepted as the 'gold standard' methodological approach for the measurement of arterial stiffness, local PWV may be the more clinically insightful and relevant method. This is especially true in clinically relevant cases such as early-stage arterial stiffening, where homogeneity of vascular stiffening or mechanical properties of the vessel cannot be assumed confidently (Laurent et al., 2006).

Arterial stiffness index (ASI)

The previously highlighted techniques for the assessment of arterial stiffness all come with the caveat of requiring skilled technicians to complete these assessments, as well as the cost and accessibility of equipment (pressure transducers, ultrasound, MRI), which may pose a barrier to data collection (S. R. Alty et al., 2007). One suggested alternative and potentially more widely

applicable technique for the estimation of arterial stiffness is the contour of the digital volume pulse (DVP) (S. R. Alty et al., 2007). The DVP is created by two components: the pressure transmitted from the left ventricle directly to the finger, and the transmission of the pressure from the left ventricle to the lower body, and reflected back via the aorta (Fung et al., 2019).

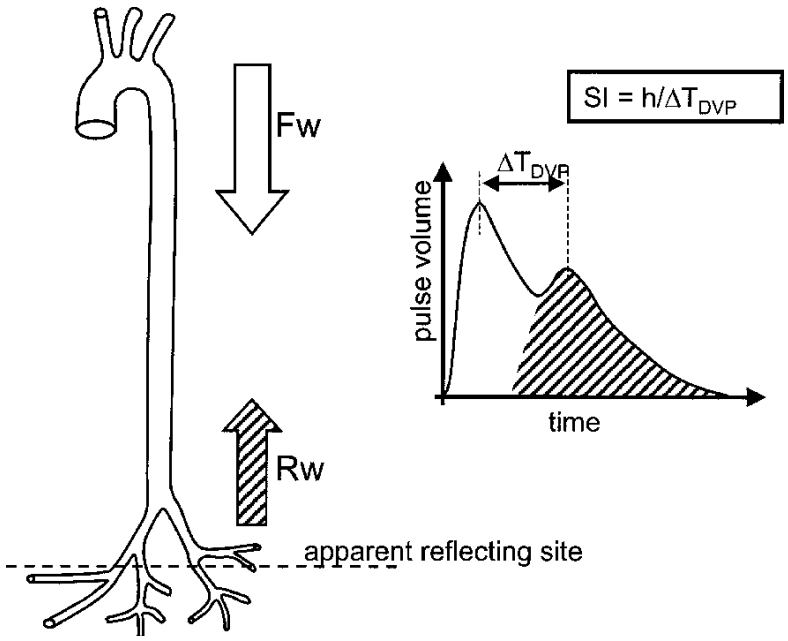

Figure 2. Estimation of arterial stiffness via digital volume pulse (DVP) (Millasseau et al., 2002)

The DVP waveform can be quickly and efficiently acquired by using photoplethysmography at the tip of the finger, an approach that measures the absorption of infrared light at the point of measurement to quantify volumetric variations of blood flow (Castaneda et al., 2018). Though this approach can be confounded by factors such as temperature and perfusion of the hand, the DVP contour is mainly determined by characteristics of the heart and large arteries (S. R. Alty et al., 2007). Arterial stiffness index (ASI) is a non-invasive, photoplethysmography derived index measure of vascular stiffness shown to be correlated with cfPWV ($r = 0.65$, Millasseau et al., 2002) ($r = 0.58$, Woodman et al., 2005). Much like the values derived from all PWV measures, higher

ASI values reflect stiffer arterial walls, characterized by faster arrival of the reflected waveform (Fung et al., 2019). ASI is a simple, fast, and inexpensive approach requiring minimal user training, making it favourable for large scale studies (Millasseau et al., 2002). Measurement of ASI via finger photoplethysmography obtains the systolic pulse waveform during a 10- to 15-second measurement. The shape of the waveform is directly related to the time it takes for the pulse wave to travel through the arterial tree in the lower body, and to be reflected to the finger (Millasseau et al., 2002). In other words, ASI is characterized as the time interval between the peaks of the direct and reflected components of the DVP contour, divided by the individual's height (Fung et al., 2019). Estimation of arterial stiffness via ASI is illustrated in *Figure 2,* where *h* represents the height of the subject, and ΔT represents the temporal difference between the arrival of the direct and reflected components of the DVP contour (Millasseau et al., 2002). While ASI is not the gold standard measurement technique for the assessment of arterial stiffness, it has been demonstrated to be a simple, quick, cost effective, and easily reproducible alternative requiring little-to-no training allowing for the estimation of arterial stiffness. Additionally, ASI has been shown to be an independent predictor of cardiovascular disease, myocardial infarction, and all-cause mortality in a 169,613 subject subsample of the United Kingdom (UK) Biobank cohort (Said et al., 2018). ASI also allows for data collection in a seated position, rather than a supine position as required by many of the other approaches for the measurement of PWV, further contributing to the convenience of this approach (Fung et al., 2019). For all these reasons, ASI is favourable for large scale population-based studies spanning multiple assessment centers, as it is easily accessible, requires little training, and reduces inter-user variability during the measurement process (Millasseau et al., 2002).

FreeSurfer Image Processing Pipeline

FreeSurfer is a freely available set of software tools used for the automated processing and study of cortical and subcortical anatomy (https://surfer.nmr.mgh.harvard.edu/fswiki/FreeSurferAnalysisPipelineOverview). FreeSurfer conducts analysis on brain MR images by reconstructing a 3D input image into a 2D surface based representation of the brain (Fischl & Dale, 2000). The use of surface-based representations for analysis of brain MRI is advantageous over volume based approaches as it provides several different morphological phenotypes including volumes, cortical thicknesses, surface area, and curvature compared to volume alone (Fischl & Dale, 2000). FreeSurfer requires several steps to reconstruct the 3D MR image into a 2D surface representation (Dale et al., 1999). The first step is a non-linear registration to a standard space atlas. Following registration, the bias field of the input image is estimated by measuring the variation of voxel intensities in the cerebral white matter. Each voxel intensity is divided by the bias field value to remove the effects of the field. Following bias field correction, the skull is then stripped to remove all non-brain tissues in the image. Once non-brain tissues have been removed from the image, the FreeSurfer tool automatically classifies tissues in the image as either white matter or non-white matter based on intensity values and neighbouring voxel intensity values. An initial surface is then generated by following the outline of the defined white matter boundary, which is defined as the *orig.mgz* surface (https://surfer.nmr.mgh.harvard.edu/fswiki/recon-all). This initial surface is further refined by determining and following the intensity gradients between the white and grey matter labelled the *white surface* or *white.mgz* (https://surfer.nmr.mgh.harvard.edu/fswiki/recon-all). When the white matter boundary is established, the boundary is expanded outwards towards the outer boundary of the grey matter, which is labelled as the *pial surface*, or *pial.mgz* by Freesurfer (https://surfer.nmr.mgh.harvard.edu/fswiki/recon-all). The difference between the white surface

and the pial surface is used to estimate the measure of grey matter cortical thickness (Fischl & Dale, 2000). Once each tissue type has been classified, the surface of each hemisphere is individually inflated into a smooth 'boxing glove' shaped representation while still maintaining all the morphological characteristics including cortical folding, gyri, and sulci of the cortical surface. The initial inflated surface is then further inflated into a spherical representation, further facilitating inter-subject registration with the FreeSurfer standard space template sphere *FSaverage* (https://surfer.nmr.mgh.harvard.edu/fswiki/FsAverage) along two dimensions (latitude and longitude). Once registered to *FSaverage*, the spherical surface representation is parcellated according to a standardized atlas, and in the case of the present study was parcellated according to the Desikan-Killiany atlas, which are then mapped back onto the individual surface reconstruction, providing image derived phenotypes (IDPs) for 34 bilateral (68 total) cortical regions (https://surfer.nmr.mgh.harvard.edu/fswiki/CorticalParcellation).

UK Biobank Magnetic Resonance Image Data Collection and Processing

T1 MRI

The full UK biobank T1 brain MRI processing pipeline is described in detail in the work from Alfaro-Almagro et al (Alfaro-Almagro et al., 2018) and supplementary materials provided by the UK Biobank data showcase (https://biobank.ndph.ox.ac.uk/showcase/ukb/docs/brain_mri.pdf). In summary, the raw MR images enter the pipeline and are preprocessed by conducting bias field correction and defacing to protect the anonymity of the UK biobank participants. From this point, the field of view (FoV) is cut down to reduce the amount of non-brain tissue present in the image. Primarily, the portion of the image that is removed includes the space above the head, and any tissues below the brain such as the neck. Additionally, all images fed through the UK Biobank

brain MRI processing pipeline are anonymized or 'defaced' automatically by masking out voxels in the face and ear regions without loss of brain voxel resolution. After the FoV is cut down, the gradient distortion correction is applied. These preliminary steps result in a reduced FoV T1 brain MR image. The image is then non-linearly warped to a standard space T1 template (http://www.bic.mni.mcgill.ca/ServicesAtlases/ICBM152NLin6). A standard-space brain mask is then back-transformed into the T1 space and applied to the reduced-FoV T1 image to generate a brain-extracted T1 image. Following the creation of the brain-extracted T1-image, tissue-specific segmentation is applied using an automated segmentation tool developed by Zhang and colleagues (Zhang et al., 2001). Using the automated segmentation tool, tissues can then be classified as one of the following: cerebrospinal fluid, brain grey matter, and white matter, as well as partial volume images for each tissue type. This image processing step is also used to generate a fully bias-field-corrected version of the brain-extracted T1 image. The external surface of the skull on the newly generated fully bias-field-corrected brain-extracted T1image is then estimated from the original T1 image and used to normalize brain tissue volumes to total head size. Both normalized and non-normalized volumes of different tissue types and total brain volume are generated as IDPs and are accessible from the UK Biobank database (https://biobank.ndph.ox.ac.uk/showcase/label.cgi?id=100). The automated segmentation tool developed by Zhang and colleagues is also used to generate 139 grey matter IDPs. This is done by summing the partial grey matter volume estimates within 139 regions of interest, both cortical and subcortical. These regions of interest are defined in the standard space T1 template and combine parcellations from several atlases (the Harvard- Oxford cortical and subcortical atlases https://fsl.fmrib.ox.ac.uk/fsl/fslwiki/Atlases and the Diedrichsen cerebellar atlas (https://www.diedrichsenlab.org/imaging/atlasPackage.htm). The previously estimated warp field

is then applied to the regions of interest to generate a version of the regions in native space, for masking onto the segmented T1 image. Both shapes and volumes of subcortical structures are modelled using an integrated registration and segmentation tool (Patenaude et al., 2011). Shapes and volumes are for 15 different subcortical structures are stored in a subfolder, and a single summary image with a unique integer value for each structure is saved within the folder. The respective volumes of each individual subcortical structure are saved as IDPs in the UK Biobank database.

As part of the UK Biobank image processing pipeline T1 images are also processed using the freely available segmentation software FreeSurfer (https://surfer.nmr.mgh.harvard.edu). FreeSurfer is a tool developed at Harvard university, and is used to model the cortical surface anatomy, relying on surface atlases to map different neuroanatomical IDPs according to the atlas regional surface areas, volumes, and mean cortical thickness (Desikan et al., 2006; Fischl et al., 2002). FreeSurfer also provides the ability to extract subcortical regions according to the selected standard atlas, resulting in additional IDPs. “Grey-white” contrast cortical region IDPs are also created and represent the contrast between white (W) and grey (G) matter pixel intensities and expressed by the following equation (W-G)/((W+G)/2) (Alfaro-Almagro et al., 2018). Following FreeSurfer modelling, outputs are then manually quality control checked using a supervised random forest based machine learning approach to automatically identify problematic images based on a comprehensive range of imaging derived metrics including measures of asymmetry, normalized intensity per subcortical structure, and matrices to detect alignment that can classify images as usable or unusable for analysis. The full scope of the machine learning algorithm developed by Klapwijk and colleagues is described elsewhere (Klapwijk et al., 2019). Any

FreeSurfer outputs that fail the quality check are not included in the final FreeSurfer IDPs folder of the UK Biobank dataset. Where available, T2-FLAIR images can be used alongside T1 images to achieve a more accurate model of the cortical surface compared to T1 images alone. For some derived measures such as regional cortical thicknesses, there is a clear bias in the estimation of regional thicknesses when using both T2-FLAIR and T1 vs. T1 alone. It is recommended by the developers of the UK Biobank image processing pipeline to use both T1 and T2-FLAIR inputs (Alfaro-Almagro et al., 2018).

T2-FLAIR MRI

The full T2-FLAIR image processing pipeline is similar to the T1 pipeline, with some key differences. As done in the T1 image, the original T2-FLAIR image is first corrected for gradient distortion, after which a linear registration using an automated image registration tool is applied to transform the gradient corrected T2-FLAIR image into the corrected standard space T1 template. Following the transformation of the T2-FLAIR image into the T1 space, T1 brain and defacing masks are applied to preserve anonymity. The final difference in the T2-FLAIR image processing pipeline is the correction of residual bias field inhomogeneities using the values derived from the automated segmentation of the T1 image. The total volume of white matter hyperintensities is estimated to generate a final IDP. The lesion segmentation is automatically conducted using a tool developed by Griffanti and colleagues (Alfaro-Almagro et al., 2018; Griffanti et al., 2016).

Arterial Stiffness, Pulsatility, and the Brain

In healthy vessels, central elastic arteries expand and recoil within each cardiac cycle to effectively dampen high pressure pulsatile flow ejected from the heart, which acts to protect less elastic distal arteries, microvasculature, and end-organs (Tarumi et al., 2014). Windkessel function is characterized by the innate ability of elastic arteries to expand and recoil in response to high pressure systolic flow. Aging or pathology associated with stiffening of the vascular wall may lead to impairments in Windkessel function, resulting in augmented pulsatility of blood flow, and in turn leading to an increased risk of microvascular and end-organ damage (Tarumi et al., 2014). This is especially true in the context of cerebral hemodynamics. High pulsatile flow reaching and potentially damaging micro vessels within the cerebral circulation has been identified as an independent risk factor for the development of cerebrovascular disease (Scuteri et al., 2011). A hallmark of cerebrovascular disease is the chronic disruptions or attenuation in perfusion to cerebral tissues (Alosco et al., 2014).

Hypoperfusion of neural tissue has been linked to structural changes in neural tissue integrity such as grey matter (GM) atrophy (Alosco et al., 2014) and white matter hyperintensities (WMH) (Gupta et al., 2012). Recent cross-sectional work conducted as a part of the Framingham Heart Study demonstrated that aortic stiffness as measured by cfPWV was associated with reduced total brain volume, elevations in WMH volume, and significant impairments in cognitive performance related to cerebrovascular dysfunction in older adults (Tsao et al., 2013). They also observed that for each SD increase in cfPWV, there was a reduction in total brain volume equivalent to 1.2 years of aging (Tsao et al., 2013). The AGES study from Mitchell *et al.*, showed a similar relationship, highlighting an association between elevated arterial stiffness and cerebrovascular dysfunction,

leading to greater WMH volume and significant reductions in cognitive performance, while elevations in pulsatility index (PI) was related to reductions in both white matter volume and GM volume (Mitchell et al., 2011). Findings across the literature are consistent, and systematic reviews and meta-analyses have corroborated the relationship between arterial stiffness (measured via cfPWV) and cerebrovascular disease (van Sloten et al., 2015). Both reductions in GM volume and elevated WMH volume are of great clinical relevance, as structural changes in brain tissue beyond the rate expected in normal aging is linked to impaired neurological function including deficits across multiple cognitive domains, as well as increasing the risk for the progression of neurodegenerative disorders such as vascular dementia, Parkinson's disease, and Alzheimer's disease (Arvanitakis et al., 2016; Pasha et al., 2015; Soriano-Raya et al., 2012). Beyond changes in neurological function and health, cerebrovascular disease also dramatically increases the risk of adverse cerebrovascular outcomes such as stroke or cerebrovascular accident (Gupta et al., 2012).

Cortical grey matter (GM) in healthy aging

When considering the structure of the grey matter tissue in the brain, there are three main indices that are used to describe grey matter structure: 1) cortical surface area, 2) cortical thickness, and 3) grey matter volume (GMV) (Winkler et al., 2010). Evidence suggests that measures of cortical surface area and cortical thickness are genetically and phenotypically independent, and GMV is a function of the two independent indices, while more heavily influenced by cortical surface area (Panizzon et al., 2009; Winkler et al., 2010). Acquired from T1-weighted MRI, GM cortical thickness is measured by the distance between the outer surface of the cerebral white matter and the inner surface of the pia mater. GM cortical thickness seems to be a more robust measure than volumetric measures for detection of differences between functionally healthy and pathological

brains, including cognitive impairment and neurodegenerative conditions including Parkinson's disease (Winkler et al., 2010). Work from Hutton and colleagues involved a comparative analysis between thickness and volumetric based measures of grey matter atrophy and determined that thickness was indeed believed to be a more sensitive measure of age-related decline in grey matter (Hutton et al., 2009). The greater sensitivity of cortical thickness measures in comparison to GMV is likely due to the reliance of GMV on cortical surface area, and therefore is prone to being confounded by cortical folding (Hutton et al., 2009).

Changes in brain structure, and specifically atrophy of grey matter is expected with normal aging. A gradual reduction of ~0.02-0.06mm per decade in GM cortical thickness is believed to be a normal part of the aging process; whereas GM cortical thinning exceeding 0.06mm per decade may be considered indicative of pathology (Thambisetty et al., 2010). Whole-brain atrophy rate as measured by GMV is believed to be within a range of 0.2-0.7% reduction per year (Enzinger et al., 2005; Scahill et al., 2003; Sluimer et al., 2008). In a study investigating both GMV and cortical thickness, Hutton et al., determined that there was an age-related global decline in whole brain GMV of approximately 2.6mL per year, and an age-related global decline in mean cortical thickness of 0.0086mm per year in 48 otherwise healthy subjects (age range: 20-60 years) (Hutton et al., 2009). These values of age-related reductions in grey matter are variable across the literature, with work from Lemaitre et al., reporting an age-related reduction of 3.68mL and 0.004mm in GMV and mean cortical thickness per year, respectively in 216 healthy subjects aged 18-87 (Lemaitre et al., 2012). Findings from Thambisetty et al., support the findings from Lemaitre, and also reported an approximate 0.004mm reduction in mean cortical thickness per year (reported as ~0.4mm reduction per decade) in 66 older adults with no evidence of neuropathology (Thambisetty

et al., 2010). Quantitative analyses based solely on volumetric representations of the brain are still common across the literature, despite belief that analysis of surface area and thickness independently are the more comprehensive approach. Volumetric approaches such as voxel-based morphometry (VBM) classify voxels according to different tissue types (grey and white matter, cerebrospinal fluid). Due to GMV being a function of two independent indices, there is likely information to be derived from cortical surface area and cortical thickness measures that is not captured with GMV (Winkler et al., 2010). Furthermore, because GMV is the function of two independent indices, it can complicate interpretation of volumetric based findings (Fjell et al., 2014). Volumetric approaches still quantify the volume of grey matter per voxel, and provide a fast, straightforward approach for the analysis of brain structure that still allows for comparisons across subjects despite variability in head and brain size, as volumetric indices are typically normalized to head size (Winkler et al., 2010).

Atrophy of grey matter tissues in the brain is not homogenous across different regions of the brain or between measurement approaches of grey matter, and as such a measure such as whole brain GMV or global mean cortical thickness is an oversimplification of the atrophic patterns likely occurring as either a part of normal aging or as a consequence of pathology (Ramanoël et al., 2018). A review from Fjell et al., suggests that the most drastic age-related reductions in grey matter occurred in the frontal and temporal lobes, independent of any evidence of pathology (Fjell et al., 2014). Other more recent cross-sectional work corroborated these findings, identifying that when comparing healthy middle aged adults (aged 40 ± 8) to older adults (aged 70 ± 6.5), older age was associated with significantly smaller bilateral GMV in the frontal and temporal regions, while also detecting significant age related reductions in the parietal and occipital regions

(Ramanoël et al., 2018). The work from Thambisetty and colleagues also reported an "anterior-posterior gradient" for the structural change in grey matter over the decade long study, with frontal and parietal regions exhibiting the greatest rates of reduction in cortical thickness (Thambisetty et al., 2010). This finding supports the "last in, first out" hypothesis, suggesting that more advanced and late maturing brain regions responsible for higher level cognitive tasks are the most vulnerable to age related changes in structure (Fjell et al., 2014). The anterior-posterior gradient in vulnerability to aging is supported by evidence of age-related declines in cognitive performance across several domains including processing speed and working memory, both of which depend on the integrity of the prefrontal cortex (Lemaitre et al., 2012). Hutton and colleagues also reported the most sensitive cortical regions to age-related declines in grey matter that included the prefrontal, orbitofrontal, and temporal regions, as well as the insula, cingulate and precentral sulci, which is agreement with much of the literature (Hutton et al., 2009; Lemaitre et al., 2012). As previously mentioned, certain cortical regions present with more pronounced reductions in grey matter than others, and as such a metric of whole brain GMV atrophy or global mean cortical thickness, while valuable, is an incomplete representation of age-related reductions in brain volume. Taken together, the evidence points to a clear anterior bias concerning age related declines in cortical grey matter. Another key takeaway is that likely the best and most comprehensive approach to quantifying changes in grey matter is to use both thickness and surface area indices independently, as opposed to volumetric measures; however thickness-based approaches provide greater sensitivity for differentiating between functionally healthy and pathological brains when compared to surface-based or volume-based approaches alone (Winkler et al., 2010).

White matter hyperintensities (WMH) in healthy aging

As previously mentioned, a consequence of cerebrovascular dysfunction or cerebral small vessel disease is hypoperfusion of neural tissues. With hypoperfusion, structural changes in the brain can be detected via MRI. One of the most frequently detected changes in brain structure with MRI is the presence of white matter hyperintensities (WMH). WMH are lesions found deep in cerebral white matter, and correspond to areas of diminished white matter density. WMH are identified as 'bright spots' on T2-FLAIR images indicating damage, or lesions to cerebral white matter (Ramanoël et al., 2018). These lesions within the white matter are typically believed to be of vascular origin, as lesions are typically detected near cerebral microvasculature exhibiting signs of cerebrovascular disease (Chutinet & Rost, 2014; Debette & Markus, 2010). Certain subjective visual rating scales exist for the assessment of WMH severity, such as the Fazekas scale, and the Scheltens scale (Chutinet & Rost, 2014). Both scales take into consideration location, size, and number of hyperintense regions within the white matter. While these visual rating measures may be applicable for clinical diagnosis and regularly used by neuroradiologists, the issue remains that these assessments are subjective in nature when it comes to assessing lesion burden severity. In comparison to the visual rating scales, volumetric methods provide more accurate and reliable measures of WMH severity. Volumetric assessments of WMH are more sensitive than subjective visual scores in detecting memory symptoms, risk of stroke, onset of dementia, stroke severity, and other functional disabilities (Chutinet & Rost, 2014). Evidence suggests that in older adults, WMH volumes is variable across the literature, with any value between 1-14mL considered as normal, as these ranges have been observed over time in the literature in healthy older-adult models (60-85 years at baseline) (Garde et al., 2005; Kramer et al., 2007; Raz et al., 2012; Silbert et al., 2008; Wolfson et al., 2013). An increase of ~0-0.8mL per year in WMH even in healthy individuals is to be expected, with one study by Garde and colleagues observing an average 1.3mL increase

per year in WMH in otherwise healthy Danish older adults (80-85 years of age) (Ramirez et al., 2016; Garde et al., 2005; Kramer et al., 2007; Raz et al., 2012; Silbert et al., 2008; Wolfson et al., 2013). Despite the presence of WMH being a part of normal aging, evidence suggests that increases in WMH volume beyond 0.8mL per year (Ramirez et al., 2016) may be associated with greater cognitive impairment across domains of verbal IQ, memory, and executive function, as well as placing those with elevated WMH burden at greater risk for neurodegenerative diseases such as vascular dementia (Chutinet & Rost, 2014; Garde et al., 2005; Kramer et al., 2007; Schmidt et al., 2005; Silbert et al., 2009).

Cognitive Function

Digit symbol substitution test (DSST)

The digit symbol substitution test (DSST) is a neuropsychological testing tool primarily used by researchers seeking to understand and assess human associative learning, but is also considered to be a measure of complex attention (Jaeger, 2018). The DSST has become a staple in neuropsychological testing due to its sensitivity in the determination of the presence or brain damage, as well as its sensitivity to changes in cognitive function (Jaeger, 2018). The test requires subjects to match symbols to numbers according to a key or legend typically located at the top of the page. The number of correct matches made by the subject within the allotted time (typically 90-120 seconds) determines their DSST score. To avoid training effects, the symbol-digit pairings differ with each test attempt. The DSST is frequently used by researchers largely due to its efficacy in the assessment of a wide range of cognitive operations (Jaeger, 2018). High scoring on the DSST requires motor speed, attention, and visuoperceptual functions. Performance is believed to also be influenced by associative learning (Jaeger, 2018). In addition, the ability or decision to engage in

learning strategies during the test to improve performance calls for executive functions of planning and strategizing (Jaeger, 2018). The notion that DSST called on sub-domains of executive function was supported by Beres and Baron, by measuring the effect of active training on DSST performance (Beres & Baron, 1981). The study observed that improvement in DSST performance occurred with repeated exposure and speculated that this was largely in part due to the executive function of strategizing or the exertion of effort to learn the pairings with each attempt (as pairings cannot be memorized) contributes to improved performance. Additionally, working memory, another sub-domain of executive function, is also believed to be required to hold in mind the rules of the DSST and for the continual updating of the symbol-digit pairings (Jaeger, 2018). For these reasons, the consensus is that the DSST is polyfactorial cognitive test, and impairments in any one of the mentioned cognitive domains is believed to result in a decline in performance (Jaeger, 2018). DSST responses have been described in textbooks to be the "end product of the integration of visual perceptual, oculomotor, fine manual motor, and mental functions" (Walsh, 1978). While the DSST is a polyfactorial test, and multiple domains influence DSST performance, one drawback is the lack of specificity in the determination of which domain is impaired. This inability to precisely determine which domain is being affected makes interpretation of DSST performance difficult and limits its use as a diagnostic tool for specific cognitive domain performance. That said, sensitivity of the DSST to brain damage, cognitive dysfunction, as well as changes in cognitive function across a wide range of clinical populations makes it a practical and effective approach for the assessment of global cognitive performance and the overall condition of the brain when cognitive battery is not feasible or available.

Trail making test A (TmA) and B (TmB)

Both the Trail Making Test part A (TmA) and part B (TmB) are neuropsychological tools used either in isolation or as part of cognitive battery for the detection of cognitive impairment in the domains of processing speed, sequencing, mental flexibility, and visuomotor skills (Bowie & Harvey, 2006). Performance on the trail making tests is considered to be a robust measure that correlates strongly with intelligence, and is a sensitive indicator of neurological impairment (Reitan & Wolfson, 2004; Steinberg et al., 2005; Waldmann et al., 1992). Certain evidence suggests that the trail making tests are also a sensitive measure for the detection of normal-age related declines in concentration, vigilance, and visuospatial ability that occur later in life (Bowie & Harvey, 2006).

In the TmA, the subject being assessed uses a pencil to connect 25 encircled numbers in numerical order. The TmA is presumed to be a test of visual search and motor speed skills. In the TmB, the subject connects 25 encircled numbers and letters in numerical and alphabetical order, respectively, alternating between numbers and letters. The TmB is considered to be a test of higher level cognitive skills such as mental flexibility (Bowie & Harvey, 2006). The numbers and letters are placed in a semi-random fixed order as to avoid overlapping of the lines connecting each encircled number or letter. A subject's performance is determined by the total time required for completion of both the part A and B. A higher time to completion of the two tests suggests greater cognitive impairment (Bowie & Harvey, 2006). A cut-off time of ~300s is typically used as a marker to discontinue the test administration as such is treated as the maximum score for the trail making tests. A full detailed description of the protocols for both the TmA and TmB can be found in publication (Bowie & Harvey, 2006).

Fluid intelligence test

The cognitive domain of fluid intelligence is characterized by one's ability to reason, flexibly engage with the environment, recognize patterns, and solve problems with no prior experience or knowledge (Cochrane et al., 2019). Fluid intelligence is centered around the ability to solve problems that have not been encountered before, distinguishing it from the domain of crystallized intelligence, which is a measure of a subject's respective body of knowledge and specialized problem-solving skills already acquired. Fluid intelligence is a particularly popular measure as it has been suggested to be a measure of high ecological interest, correlating strongly with both academic and occupational success (Gottfredson, 1997; Hunter, 1986; Neisser et al., 1996). Evidence suggests that fluid intelligence is also reduced with advancing age (Kaufman & Horn, 1996). In the context of the UK Biobank, the Fluid Intelligence Test a 2-minute assessment in which subjects are required to answer as many questions as possible, and performance on the Fluid Intelligence Test is determined by the total number of correct answers within the allotted two minutes https://biobank.ndph.ox.ac.uk/ukb/field.cgi?id=20016.

Numeric memory

The numeric memory test, sometimes referred to as the digit span test, is a salient assessment of working verbal memory. Working memory refers to the short term storage and manipulation of information required for complex tasks such as language comprehension, learning, and reasoning (Baddeley Alan, 1992). The numeric memory test assesses numeric memory capacity by presenting a subject with a two-digit number to remember. The number is taken away (i.e., disappears from the screen) and after a short period the subject is asked to recall the two-digit

number presented. Following each correct recall, one digit is added to the number up to a maximum of 12 digits. Numeric memory test performance is determined by the maximum number of digits correctly recalled (https://biobank.ndph.ox.ac.uk/ukb/label.cgi?id=100029).

Pairs matching

The Pairs Matching test, or sometimes referred to as the Episodic memory test, is an assessment of a subject's ability to encode (transforming perceived stimuli into a mental representation), consolidate, and retrieve past events within a given context (Buck et al., 2021). During the pairs matching test, subjects are asked to memorize the position of as many matching pairs of cards as possible. The cards are then turned face down, and the participant is asked to flip as many pairs as possible in the fewest number of attempts. There are a total of two rounds in the pairs matching test. The first round contains three pairs of matching cards (total of six cards), while the second round contains six pairs of matching cards (total of twelve cards). Pairs matching test performance is determined by the number of errors, or incorrect matches per round. In other words, a score of zero is considered a perfect score on the Pairs matching test (https://biobank.ndph.ox.ac.uk/ukb/label.cgi?id=100030).

Linear mixed effects models

Fixed and random effects

Linear mixed effects models (LMM) are an extension of the standard linear regression model that allow for the incorporation of both fixed and random effect terms (Bates et al., 2015). It is crucial to correctly classify variables as either fixed or random factors when fitting LMMs. Fixed factors

can be defined as variables in which all levels of interest are included within the experiment. One example is the use of sex as a fixed effect. If a study design includes both male and female participants, all possible levels of sex exist within the data and as such a fixed-effects specification is appropriate for sex. A grouping variable such as occupation can serve as another example to help in understanding the concept of fixed and random effects. Consider a dataset containing a categorical variable of 'occupation' with 4 levels: Teacher, Police officer, Firefighter, Chef. If researchers have reason to only be interested in generalizing findings to these four occupations, the variable 'occupation' can be fit as a fixed effect. However, if the researchers aim to generalize their findings to all occupations, the variable occupation would instead be fit as a random effect, as the values for this variable are not representative of all levels of interest (Magezi, 2015). Random effect terms of LMMs include random factors, or interactions between fixed and random factors (Magezi, 2015). In simple terms, a factor is considered random if the levels included in the study represent a random subset of a larger set of potential levels (Oberg & Mahoney, 2007). It is not possible to anticipate the contributions of random effects *a priori*, as it is not reasonable to assume that similar shifts in the variation of the data will occur with addition of another level (Oberg & Mahoney, 2007). Consider the frequently used example of a treating physician. If a reseacher hopes to examine the health status of subjects on a criteria of *y*, but want to account for how different physicians may influence health status on criteria *y*, they may use physician as a random effect to examine between group (subjects with the same physician) differences in health status (Magezi, 2015). To extend this example one step further, if researchers wanted to investigate both within-group variance of participant within physician, and variability between physician group, they may use a hierarchial random effect term of individual subject nested within physician (Magezi, 2015). One can examine variance at the individual subject level without nesting within a

group or leveled variable, by fitting individual subject alone as a random effect. By fitting individaul subjects as a random effect, it allows researchers to examine how each subject differs at baseline (random intercept) and how they may change over the course of time or between repeated measures (random slopes). In this example, individual subjects are conisdered to be their own grouping variables, as data will be correlated within subject between repeated measures (Lohse et al., 2020). A more detailed and nuanced explanation of fixed and random effects terms, as well as detailed explanation of the mathematics behind LMMs can be found in online publication (Oberg & Mahoney, 2007).

Linear mixed effects models for longitudinal analysis

Compared to other models used to assess longitudinal changes such as repeated measures ANOVA and latent change score models, LMM offer greater flexibility in the type of data they are able to handle, making them preferable for assessing relationships over two or more time points. LMM are able to handle and effectively model unstructured time series data (when time intervals between visits are not the same across subjects or groups), making these models preferable for trajectory-based investigations such as the proposed study (Lohse et al., 2020). While repeated measures ANOVA models can model mean differences between two (or more) correlated data points, it cannot model directionality of time (Lohse et al., 2020). Compared to repeated measures ANOVA, latent change score models can effectively model directionality of timepoints, however, they are only able to model time as a discrete or structured variable (i.e., timepoint 1, timepoint 2, timepoint 3) and operate under the assumption that all subjects have the same time intervals between each measurement (McNeish & Matta, 2018). Linear mixed effects models provide a versatile and powerful framework to address more complex research questions when compared to traditional

linear regression models, or other repeated measures approaches such as repeated measures ANOVA and latent change score models.

Monte-Carlo simulations, estimating statistical power and sample size

The power of a study is defined as the probability that the test will be able to reject the null hypothesis, assuming the null hypothesis is truly false (Green & MacLeod, 2016). If a study is underpowered, the real effects may go undetected and therefore there is a greater risk of incurring type II error. The widely agreed upon benchmark for a study to be considered 'adequately powered' is 80 percent. In other words, at a given sample size with 80% power, if one was to run a study 100 times, each time with a new sample, one would be able to confidently reject the null hypothesis in 80 of those 100 studies. For these reasons, performing power analyses *a priori* is considered good practice to ensure that the study can test the hypothesis and address the research question at hand (Green & MacLeod, 2016). Monte-Carlo simulations are a flexible and accurate mathematical method that are used to determine necessary sample size when designing a study (Green & MacLeod, 2016). Simulation based approaches for estimating sample size are applicable across a wide range of statistical methods and study designs (Green & MacLeod, 2016). Using statistical software such as R (https://www.r-project.org/) an otherwise complex and computationally expensive approach of conducting simulation-based power analyses are made relatively simple. Using the package *SimR* (https://cran.r-project.org/web/packages/simr/index.html), one begins the process of simulation-based power analyses by first fitting mock, simulated, or pilot data to the statistical model that is to be used in the study to test the hypothesis. Following the model fit, using *SimR*, power is calculated using a Monte-Carlo based approach which iteratively repeats the following three steps: 1) simulate new

values for the response variable using the model provided; 2) refit the model to the new simulated response; 3) apply a statistical test to the simulated fit. In this approach, the tested effect is known to exist, and as such each positive test is a true positive (or a rejection of the null hypothesis when the null hypothesis is indeed false), and each negative test is classified as type II error. The power of the test at a given sample size is calculated from the number of successful rejections of the null hypothesis and the number of type II errors that occur and expressed as a percentage value (Green & MacLeod, 2016). Modifiable parameters in the SimR package include: the number of iterations or simulations to be conducted (default 1000 simulations), the variable to conduct the simulations along (i.e., number of participants vs. total number of observations), the alpha significance level (default $p = 0.05$), and desired main effect of model (default first fixed effect in the model).

Thesis objectives and hypotheses

Evidence suggests there is a cross-sectional association between arterial stiffness and brain structure and function. What remains less understood is the longitudinal relationship between the progression of arterial stiffness and changes in brain structure and function. To our knowledge, no study to date has investigated the longitudinal role of changes in arterial stiffness on changes in regional grey matter cortical thickness. It is currently unclear whether a regional effect of arterial stiffness on changes in brain structure exists, or if the effect is homogenous across all brain regions. The present study is the first to investigate the potential longitudinal relationship between arterial stiffness and changes in regional grey matter cortical thicknesses in a large population-based cohort ($N = 1858$). Our work also aims to extend on previous work (Jochemsen et al., 2015; Suri et al., 2020) by investigating the longitudinal relationship between arterial stiffness and brain volumes (total GMV; WMH volume) and cognitive function. Therefore, in the present study we

analyze a large sub-cohort of middle- to older-aged healthy adults from the UK Biobank population study to 1) examine the relationship between changes in arterial stiffness and changes in brain structure over 2.5 ±1 years; and 2) examine whether indices of arterial stiffness at baseline are associated with brain structure and function approximately a decade later.

CHAPTER II

Manuscript

Introduction

Changes in brain structure (grey matter atrophy, white matter lesions) and function (reductions in cognitive performance) have been established to be present in even healthy subjects as a part of the normal aging process (Thambisetty et al., 2010; Lemaitre et al., 2012; Scahill et al., 2003; Hutton et al., 2009; Raz et al., 2012; Kramer et al., 2007; Resnick et al., 2003; Cornelis et al., 2019; Silbert et al., 2008; Harada et al., 2013). Due to the high metabolic demand of the brain, and its inability to store energy, cerebral tissues require constant and stable blood supply, and therefore are highly vulnerable to changes in vascular function and health (Hoiland et al., 2016; Raichle & Gusnard, 2002). The accumulation of vascular risk factors including smoking, obesity, diabetes mellitus, and hypertension, are suggested to have a role in the acceleration of structural and functional changes in the brain beyond what is expected with normal aging (Alosco et al., 2014; Jochemsen et al., 2015). The potential neurological consequences of accumulated vascular risk factors include impaired cognitive function (Iadecola et al., 2016; Lamar et al., 2015; Llewellyn et al., 2008), vascular dementia (Wiesmann et al., 2013), and Alzheimer's disease (Dickstein et al., 2010). While there are likely several pathological pipelines of this link between cardiovascular and brain health, one proposed mechanism for vascular related changes in brain structure and function is stiffening of central arteries (Hussain et al., 2018; Iadecola et al., 2016; Llewellyn et al., 2008). Arterial stiffening, both a consequence of the normal aging process and a potential acquired condition as a result of lifestyle habits, is a subclinical marker suggested to be a precursor to a myriad of vascular disease states such as hypertension, atrial fibrillation, coronary artery disease, heart failure, and stroke (Chae et al., 1999; Franklin et al., 1997; Mitchell, 2014; Mitchell et al., 2007; Sutton-Tyrrell et al., 2005).

A widely accepted approach for the assessment of central arterial stiffness is pulse wave velocity (PWV), a non-invasive tonometry-derived measurement of the transit time of a systolic pulse wave to travel between two sites, typically the carotid artery and the femoral artery (cfPWV). Pulse wave arterial stiffness index (ASI) provides an index of vascular stiffness similar to cfPWV ($r = 0.65$) (Millasseau et al., 2002). Measurement of ASI is a simple, fast, and inexpensive approach requiring minimal user training, making it favourable for large scale studies (Millasseau et al., 2002). Due to their elastic properties, arteries distend during systole and recoil during diastole, which allows for dampening of high systolic pressures ejected from the heart prior to reaching distal arteries, microvasculature, and end-organs (Chae et al., 1999; Godia et al., 2007; Mitchell, 2008, 2014; Mitchell et al., 2007). As arterial stiffness increases, the vessel's ability to dampen high systolic pressures may be impaired, potentially leading to high pulse pressure waves reaching vessels in the microcirculation (Mitchell, 2008). Within the context of the cerebral vasculature and brain health, the increased pulsatility and high-pressure blood flow secondary to vessel wall stiffening may lead to damage of the fragile cerebral microvasculature. This cascade of events is believed to be a key mechanism behind the onset and progression of cerebrovascular disease (Chae et al., 1999). Cerebrovascular disease predisposes the brain to interruptions or chronic reductions in regional cerebral blood flow, which in turn can lead to hypoperfusive injury within the neural tissue (Chutinet & Rost, 2014; Gupta et al., 2012).

Two structural changes of interest resulting from cerebral hypoperfusion include the atrophy of cortical grey matter (GM) and the accumulation of white matter hyperintensities (WMH) (Alosco et al., 2014; Makedonov et al., 2013). Acquired from T1-weighted anatomical magnetic resonance (MR) images, GM cortical thickness is measured by the distance between the outer surface of the cerebral white matter and the inner surface of the pia mater. Additionally, GM cortical thickness

seems to be more reliable than volumetric measures for detection of differences between functionally healthy and pathological brains, including cognitive impairment and Parkinson's disease (Singh et al., 2006; Sørensen et al., 2014). A gradual reduction of ~0.02-0.06mm per decade in GM cortical thickness is believed to be a normal part of the aging process; whereas GM cortical thinning exceeding 0.06mm per decade may be considered indicative of pathology (Thambisetty et al., 2010). WMH lesions appear as 'bright spots' on T2 fluid-attenuated inversion recovery (FLAIR) images indicating damage to cerebral white matter (Silbert et al., 2008). Evidence suggests that WMH burden beyond the expected +0.8mL increase in WMH per two-year interval accompanying normal aging (Ramirez et al., 2016) is associated with greater cognitive impairment across domains of verbal IQ, memory, and executive function (Garde et al., 2005; Kramer et al., 2007; Schmidt et al., 2005; Silbert et al., 2008). Both GM cortical atrophy and elevated WMH volume are of great clinical relevance, as structural changes in the brain are linked to impaired neurological function including deficits across multiple cognitive domains, as well as increasing the risk for the progression of neurodegenerative disorders such as vascular dementia, Parkinson's disease, and Alzheimer's disease (Arvanitakis et al., 2016; Pasha et al., 2015; Soriano-Raya et al., 2012). Cross-sectionally, measures of arterial stiffness have been shown to be associated with structural changes in neural tissue, observing reductions in cortical GM volume and an elevation in WMH volume, as well as reductions in cognitive performance across domains of memory, processing speed, and executive function (Mitchell et al., 2011). Longitudinally, the relationship between changes in arterial stiffness and brain structure is less clear, with no association of arterial stiffness with the progression of whole brain atrophy or increases in WMH volumes (Jochemsen et al., 2015; Suri et al., 2020). Furthermore, evidence from a large sample (N = 591) suggests that elevations in arterial stiffness is a strong predictor of cognitive decline

longitudinally across multiple domains over 4-years of follow up (Hajjar et al., 2016). While evidence supports the structural and functional relationships between arterial stiffness and brain structure cross-sectionally (Badji et al., 2019; Hajjar et al., 2016; Jochemsen et al., 2015; Mitchell et al., 2011), no study to date has investigated how changes in arterial stiffness may affect the rate of change in GM regional cortical thicknesses, total grey matter volume (GMV), WMH volume, and cognitive performance compared to the effects of normal aging in the same cohort of individuals.

Via data made available from the UK Biobank, we aimed to address two primary objectives. Objective 1 was to investigate how changes in arterial stiffness (assessed via ASI) influences longitudinal structural (i.e., regional GM cortical thickness in 26 regions, whole brain GMV, and whole brain WMH volume) and functional (cognitive performance in six tests) changes in the brain. Objective 2 was to assess the association between baseline ASI and brain structure and function 8-11 years following baseline. For Objective 1, we hypothesized that longitudinal increases in ASI will be associated with longitudinal reductions in regional GM cortical thickness and whole brain GMV, increases in WMH, and reductions in cognitive performance over 2.5 ± 1 years. For Objective 2, we hypothesized that greater ASI at baseline will be associated with brain structure and function in an 8-11 year follow-up.

Methods

Study Population

We analyzed data from the first full release of the UK Biobank database (released in 2012). The UK Biobank is a prospective study of over 500,000 participants recruited in 2006–2010 (Sudlow et al., 2015). Data collected from the participants included questionnaires, physical measures, MRI

imaging data, and ongoing hospital records. UK Biobank received ethical approval from the Northwest Multi-Centre Research Ethics Committee (REC reference: 11/NW/0382). All participants in the UK Biobank gave informed consent for the study via a touch-screen interface that required agreement for all individual statements on the consent form as well as the participant's signature on an electronic pad. In this process, all participants gave informed consent for data linkage as one statement requested consent for access to medical and other health-related records, the long-term storage and use of this and other information about the participants, also after incapacity or death, for health-related research. The UK Biobank consent form is available at: https://www.ukbiobank.ac.uk/media/05ldg1ez/consent-form-uk-biobank.pdf. UK Biobank has approval from the institutional review boards, namely, the North West Multi-centre Research Ethics Committee for the UK, from the National Information Governance Board for Health & Social Care for England and Wales, and from the Community Health Index Advisory Group for Scotland (https://www.ukbiobank.ac.uk/media/0xsbmfmw/egf.pdf). We acquired approval from the UK Biobank to access data based on the proposed research questions (application # 71652) as well as ethics approval from McMaster Research Ethics board (MREB#: 5833) (please see "ethics clearance" component on the project OSF link; Hamilton, ON, Canada).

Study Design

To investigate the role of changes in arterial stiffness on the progression of changes in brain structure and function, we included both male and female middle aged and older adults (61 ± 7 years; age range: 46-81) at a maximum of three time points (baseline, imaging visit 1, imaging visit 2). Participants were excluded from the present analysis if they reported having been diagnosed with diabetes mellitus, hypertension, cardiovascular disease, stroke, angina,

neurodegenerative diseases (dementia, Parkinson's disease, Alzheimer's disease), brain cancer, brain haemorrhage, brain abscess, aneurysm, cerebral palsy, encephalitis, head injury, nervous system infection, multiple sclerosis, head, or neurological injury. Participants were also excluded from analyses if they were missing >5% of data for primary measures, or if they were missing follow up data (first and second imaging visits corresponding with instance 2.0 and instance 3.0) for any of our primary outcome measures of regional GM cortical thickness, grey matter volume, and WMH. Only participants that met all the eligibility criteria, as well as having data for ASI at the first and second imaging visits (corresponding with instance 2.0 and instance 3.0), were included in study analyses. To investigate the role of arterial stiffness on changes in brain structure and function, we used the ASI*instance (instance 2.0 - instance 3.0) interaction as the independent variables in Objective 1 and used ASI at baseline (instance 0.0), adjusted for age, as the independent variable in Objective 2.

Measures

Pulse wave arterial stiffness index (ASI)

ASI was measured during the first visit to the assessment center using the PulseTrace PCA2 (CareFusion, San Diego, CA) (Field-ID 21021) in 169,829 participants from 2006 until 2010 as part of the UK Biobank cohort study. The PulseTrace PCA2 uses finger photoplethysmography to obtain the pulse waveform during a 10- to 15-s measurement using an infrared sensor clipped to the end of the index finger. The measurement was repeated on a larger finger or on the thumb if less than two thirds of the waveform was visible on the display of the PulseTrace PCA2 device, or if the waveform did not stabilize within 1 minute after clipping the infrared sensor to the end of the index finger (protocol:

https://biobank.ndph.ox.ac.uk/showcase/showcase/docs/Pulsewave.pdf). The shape of the waveform is directly related to the time it takes for the pulse wave to travel through the arterial tree in the lower body, and to be reflected to the finger. ASI, while not the gold standard measurement technique for the assessment of arterial stiffness, has been demonstrated to be a simple, quick, and easily reproducible alternative approach for the measurement of arterial stiffness that is favourable for large scale population-based studies such as the UK Biobank. The strength of relationship between cfPWV (applanation tonometry) and ASI is higher than other measures of arterial stiffness such as PWV and arterial compliance (r=0.65 vs. r=0.47, respectively) (Millasseau et al., 2002).

Magnetic resonance imaging (MRI) data and image processing

In 2014, UK Biobank began inviting back 100,000 of the original volunteers for brain, heart, and body imaging. Imaging data for 10,000 volunteers has already been processed and made available for further research (Alfaro-Almagro et al., 2018). The included MRI sequences are T1 (Section T1 pipeline), T2-FLAIR (Section T2 FLAIR pipeline) anatomical scans. All brain MRI data were acquired on the same 3T Siemens Skyra scanner, following a freely available protocol (http://www.fmrib.ox.ac.uk/ukbiobank/protocol/V4_23092014.pdf), documentation (http://biobank.ctsu.ox.ac.uk/crystal/docs/brain_mri.pdf), and publication (Alfaro-Almagro et al., 2018). In brief, data were acquired with a standard Siemens 32-channel head coil. T1-weighted MPRAGE and T2-weighted FLAIR volumes were acquired in sagittal orientation at 1 × 1 × 1 mm and 1.05 × 1 × 1 mm resolution, respectively. Regional GM cortical thicknesses values were extracted from T1-Weighted anatomical scans according to the Desikan-Killiany atlas intrinsic to FreeSurfer (https://surfer.nmr.mgh.harvard.edu/fswiki), an open-source surface-based

segmentation software. Using the Desikan-Killiany atlas, FreeSurfer parcellation generated 34 bilateral cortical parcels, attributed to eight lobar structures.

We investigated changes in GM cortical thickness in 26 (13 per hemisphere) regions based on their associations with the selected cognitive domains for the present study. For executive function the cortical regions included consisted of the caudal middle frontal gyri, rostral anterior cingulate, rostral middle frontal gyri, and superior frontal gyri (Wen et al., 2011). For the domain of working memory, cortical regions included consisted of superior and inferior parietal cortices, superior and inferior temporal cortices, as well as the parahippocampus (Wen et al., 2011). We additionally investigated the lateral occipital lobe and medial-temporal lobe which corresponded with visual and verbal declarative memory, respectively (Wen et al., 2011). For cognitive domains of verbal reasoning and numeric reasoning we included cortical regions of the caudal anterior cingulate and posterior cingulate (Arsalidou et al., 2018; Feng et al., 2021). For the domain of fluid intelligence, all relevant brain regions had already been included among other domains, including the caudal middle frontal gyri, the superior and inferior parietal lobes, rostral anterior cingulate, rostral middle frontal gyri, and the superior frontal lobe (Chen et al., 2020). Finally, for processing speed, literature suggests that this domain is a function of global cortical network connectivity, and as such no additional regions were included to represent this domain (Wen et al., 2011). The full MR image processing and segmentation pipeline is described in detail in publication (Alfaro-Almagro et al., 2018). WMH volumes were extracted from T2-FLAIR MRI using the BIANCA automated segmentation tool, as described in publication (Alfaro-Almagro et al., 2018).

Cognitive outcomes

Cognitive function was assessed using self-administered computerized battery unique to UK Biobank to enable population wide cognitive assessment able to be administered without researcher supervision (https://www.ukbiobank.ac.uk/media/gnkeyh2q/study-rationale.pdf). A detailed description of all tests is provided online (https://biobank.ctsu.ox.ac.uk/crystal/label.cgi?id=116). Brief descriptions of the tests chosen for the purposes of this study are provided below (Cornelis et al., 2019).

Digit symbol substitution test (DSST)

This test for complex processing speed was completed at follow-up on home computers and involves matching numbers to a set of symbols. We used the number of correct substitutions for our analyses. Detailed information on the digit symbol substitution test is provided through the UK Biobank data showcase (https://biobank.ctsu.ox.ac.uk/crystal/field.cgi?id=23324) (Cornelis et al., 2019).

Trail making test A (TmA) and B (TmB)

Trail making test A and B are visual attention tests provide information on visual search, scanning, speed of processing, mental flexibility, and executive functions and were completed at follow-up on home computers. Participants were asked to connect scattered circles containing a sequence of numbers (Trail A) and then to connect circles containing numbers or letters by alternating between them in ascending sequence (Trail B). We used the total time to completion for each test for our analyses. Detailed information on the Trail Making test A

(https://biobank.ctsu.ox.ac.uk/crystal/field.cgi?id=6348) and B (https://biobank.ctsu.ox.ac.uk/crystal/field.cgi?id=6350) is provided through the UK Biobank data showcase (Cornelis et al., 2019).

Fluid intelligence test

Participants were presented with 13 verbal logic/reasoning-type multiple choice questions and had to answer as many as they could within 2 minutes. Incorrect or unanswered questions were scored as zero. The total number of correct answers (maximum of 13) was used for our analysis. Detailed information on the fluid intelligence test is provided through the UK Biobank data showcase (https://biobank.ctsu.ox.ac.uk/crystal/field.cgi?id=20016) (Cornelis et al., 2019).

Numeric memory test

The numeric memory test is designed assess numeric short-term memory, as part of the touchscreen questionnaire. The participant was shown a 2-digit number to remember. The number then disappeared and after a short while they were asked to enter the number onto the screen. The number became one digit longer each time participants remembered a number correctly (up to a maximum of 12 digits). Data to be used in analyses is the maximum number of digits remembered. Detailed information on the numeric memory test is provided through the UK Biobank data showcase (https://biobank.ctsu.ox.ac.uk/crystal/field.cgi?id=4282) (Cornelis et al., 2019).

Pairs matching test

This episodic visual memory test was completed at the assessment centers. Participants were shown 6 pairs of cards for 5 seconds and asked to memorise the position of as many matching pairs of cards as possible. Following the 5 seconds, the cards were turned over. Participants were instructed to select the pairs of cards that had matching symbols in the fewest number of attempts. Two rounds were conducted: the first round used 3 pairs of cards and the second round used 6 pairs of cards. The data from the pairs matching test used for analyses was the total number of incorrect matches made in the respective round. Detailed information on the pairs matching test is provided through the UK Biobank data showcase (https://biobank.ctsu.ox.ac.uk/crystal/field.cgi?id=399) (Cornelis et al., 2019).

Statistical Analysis

For Objective 1, the longitudinal relationship between ASI and the outcome measures of GM cortical thickness (26 regions), WMH volume, and cognitive outcomes for all six tests of interest were examined using a robust linear mixed effects model (LMM). All statistical analyses were conducted in the freely available statistical software R (https://cran.r-project.org). We primarily relied on the package *robustlmm* (https://cran.r-project.org/web/packages/robustlmm/vignettes/rlmer.pdf) to implement the LMMs. The use of robust linear mixed effects models allowed us to identify and consider outliers without necessitating their exclusion by reweighing of residuals according to their distance from the model fit (Koller, 2016). In each model the interaction between ASI and instance (visit number) was treated as the independent variable. The ASI*Instance interaction and all covariates (age, sex, years between visits, waist to hip ratio, self-reported physical activity) were added to the model as fixed effects. Individual observations (subject ID) were fit as a random effect, with random

intercepts, to account for the variability between subjects at baseline as well as allowing each subject to have a different trajectory of changes in brain structure and function (*Equation 1)*. Based on previous research, we analyzed a smaller subset (N = 1801) of our total UK Biobank cohort using LMM, excluding all subjects with WMH volume greater than 15mL to determine whether those with non-healthy levels (>15mL) of WMH influence the relationship between ASI and WMH volume (Garde et al., 2005; Kramer et al., 2007; Raz et al., 2012; Silbert et al., 2008; Wolfson et al., 2013). For our *a priori* sample size calculations, we chose age, sex, and years between visits as our base number of covariates. Where applicable, we conducted paired t-tests (or non-parametric equivalent) to detect whether mean (or median) differences between imaging visits were statistically significant. For Objective 2, we used analyzed a subsample (N = 630 subjects with baseline ASI data) of our healthy UK Biobank sample using linear regressions to test the association between ASI at baseline (collected between 2006-2010) and 26 regional GM cortical thicknesses, whole brain GMV, WMH volume, and cognitive performance in all six tests at the first imaging visit (~8.5 ± 1.05 years post baseline) and second imaging visit (~11 ± 1.02 years post baseline), adjusted for age, to examine the temporal relationship between arterial stiffness at a single point and structural and functional brain health at a 8-11 year follow-up (https://biobank.ndph.ox.ac.uk/showcase/field.cgi?id=53).

Due to the use of several different models for each of our outcome measures using the same predictor variables and covariates, where appropriate, significant p-values were adjusted using the Holm-Bonferroni post-hoc test for multiple comparisons. Significant findings were reported when the adjusted p-value was below the set alpha threshold of p = 0.05 for all outcomes. All analysis code was uploaded to our laboratory's Open Science Framework account and/or our Gitlab

repository for this project. Given the nature of the data, and in compliance with UK Biobank's materials transfer agreement, raw participant level data are not shared, and only aggregated data are presented herein. All values are reported as mean ± SD unless otherwise stated.

The independent variable was ASI * Instance, and the outcome measures of interest were regional GM Cortical Thickness (26 regions), GMV, WMH volumes, DSST, TmA, TmB, Fluid Intelligence Test, Numeric Memory Test, Pairs Matching Test. Covariates included in the model were age, sex, years between visits, waist-to-hip ratio, physical activity levels. The model fit was based off a linear mixed model with fixed effects of ASI*Instance, all covariates, and random effects of Subject ID (*Equation 1*).

$$\text{Outcome} \sim \text{ASI} * \text{Instance} + \text{Covariates} + (1|\text{Subject ID}) + \text{error} \qquad \textit{Equation 1.}$$

A Priori Sample Size Calculation

To calculate required sample size, we used a simulation-based approach using the R package *SimR* (https://cran.r-project.org/web/packages/simr/index.html) (Green & MacLeod, 2016) and tested for the ASI*Instance interaction along the variable "participant" to assess power for a given number of participants. We created a single mock data set based on estimated normative values either from the UK Biobank data showcase or from the literature for all outcomes of interest. For all outcome measures, we included minimum mean differences of interest associated with what is expected during normal aging to conservatively approach our sample size simulations. All reported values in the mock dataset are reported as mean ± SD unless otherwise noted. The mock data set includes ASI values of 9 ± 4m/s based on the values available via the UK Biobank data showcase

(https://biobank.ctsu.ox.ac.uk/crystal/field.cgi?id=21021) and an increase in ASI of 0.5m/s per decade (~0.25m/s per follow up), based on work from the Baltimore Longitudinal study on Aging in which cfPWV was assessed in adults over approximately a decade (AlGhatrif et al., 2013). Due unstructured and non-uniform follow-up times in UK Biobank participants (between 2-5 years between follow up sessions), we also included a continuous variable named "time between visits", in which the value for visit 1 was 0 and visit 2 was a random number between 2-5 years. For our primary outcome variable of GM cortical thickness, we chose to use an approximated mean and SD representative of the mean thickness of most brain regions (2.5 ± 0.25mm) (https://biobank.ctsu.ox.ac.uk/crystal/label.cgi?id=196; field ID range 27174-27296). The minimum mean difference of interest used for the mock cortical GM thickness values was based on the degradation expected in normal aging, ~0.02-0.06mm reduction per decade (Lemaitre et al., 2012). We used a mean GM cortical thickness reduction of ~0.005mm per year as our observed mean difference in the mock data set to conservatively estimate necessary sample size. For whole brain GMV (800 ± 50mL), a mean difference of -3mL per year was included, as this is a conservative reduction in whole brain GMV based on the literature for what is expected in normal aging (Enzinger et al., 2005; Scahill et al., 2003; Sluimer et al., 2008). For WMH values (5 ± 6mL) (https://biobank.ctsu.ox.ac.uk/crystal/field.cgi?id=25781), a mean difference of +1mL of WMH volume per follow up point was used, a slightly greater mean difference than the +0.8mL in WMH volume seen in Ramirez et al., over a 2-year time interval due to a larger time interval between visits in the UK Biobank data (Ramirez et al., 2016). To estimate our necessary sample size to detect normal aging-related changes in cognitive performance, mean differences were taken from Cornelius *et al*., a recent study which used the UK Biobank database to assess cognitive decline across multiple domains cross-sectionally in healthy subjects across several decades of adulthood

(Cornelis et al., 2019). For the Digit Symbol Substitution Test (18 ± 5 correct substitutions) (https://biobank.ctsu.ox.ac.uk/crystal/field.cgi?id=23324), a difference of -1 correct substitutions per follow up was used (Cornelis et al., 2019). For Trail Making Test A (22.9 ± 0.88 seconds) (https://biobank.ctsu.ox.ac.uk/crystal/field.cgi?id=6349) and B (58.0 ± 27 seconds) (https://biobank.ctsu.ox.ac.uk/crystal/field.cgi?id=6351), mean differences of +1.6 seconds for Trail Making A and a mean difference +4 seconds for Trail Making B were used for the mock dataset (~7% increase per ~5 years of age cross-sectionally) (Cornelis et al., 2019). A mean difference of -0.1 correct answers per follow up was used for the minimum change of interest for Fluid Intelligence Test performance (6.15 ± 2 correct answers) (https://biobank.ctsu.ox.ac.uk/crystal/field.cgi?id=20016) (Cornelis et al., 2019). For the Numeric Memory Test (6.7 ± 1.25 correct digit recall) (https://biobank.ctsu.ox.ac.uk/crystal/field.cgi?id=4282) we included a mean difference of -1 correct digit recall per follow up point (Cornelis et al., 2019). For the Pairs Matching Test (2.3 ± 3 errors) (https://biobank.ctsu.ox.ac.uk/crystal/field.cgi?id=399) mean difference of interest, we used a change of +0.07 errors per follow up point (Cornelis et al., 2019). The mock data set also included age (57 ± 8 years) (https://biobank.ctsu.ox.ac.uk/crystal/field.cgi?id=21022), sex (M = 1, F = 2), waist to hip ratio (0.75 ± 0.35) (Molarius et al., 1999), self-reported physical activity (days per week exercising 10+ minutes, ranging from 0-7), and a discrete variable relating to visit number, using values of 1 or 2, corresponding to image visit 1 and 2, respectively. Means and standard deviations for variables of interest and covariates included in the mock dataset are directly based on the values seen in the literature and UK Biobank data showcase (https://biobank.ndph.ox.ac.uk/showcase/). The mock dataset was fit to the LMM in accordance with *Equation 1* using the R package *lme4* (https://cran.r-

project.org/web/packages/lme4/index.html) prior to conducting our *a priori* sample size calculations. Following 1000 simulations of the mock dataset fit to the LMM, using the *SimR* package, it was determined that at any sample beyond 665 subjects, we are >80% powered to test the effect of the ASI and instance interaction effect on all outcomes of interest. All power calculations for outcomes of interest are presented in *Table 1*.

Table 1. Power curve for all outcome measures of interest

Sample Size (n)	5	225	445	665	885	1105	1325	1545	1765	1985
Statistical Power	%	%	%	%	%	%	%	%	%	%
GM Cortical Thickness	0% [0-0]	99% [98-100]	99% [98-100]	99% [98-100]	99% [99-100]	100% [100-100]	100% [100-100]	100% [100-100]	100% [100-100]	100% [100-100]
Whole Brain GMV	0% [0-0]	98% [97-99]	100% [99-100]	100% [99-100]	100% [99-100]	100% [99-100]	100% [99-100]	100% [99-100]	100% [99-100]	100% [99-100]
WMH Volume	0% [0-0]	90% [87-92]	99% [98-99]	99% [98-99]	100% [99-100]	100% [99-100]	100% [99-100]	100% [99-100]	100% [99-100]	100% [99-100]
Digit Symbol Substitution Test	0% [0-0]	99% [98-100]	99% [98-100]	99% [98-100]	100% [99-100]	100% [99-100]	100% [99-100]	100% [99-100]	100% [99-100]	100% [99-100]
Trail Making Test A	0% [0-0]	41% [37-46]	72% [68-76]	90% [87-92]	97% [96-98]	98% [97-99]	100% [99-100]	100% [99-100]	100% [99-100]	100% [99-100]
Trail Making Test B	0% [0-0]	50% [45-54]	82% [78-85]	95% [92-96]	99% [98-99]	99% [98-100]	100% [99-100]	100% [99-100]	100% [99-100]	100% [99-100]

Fluid Intelligence Test	0% [0-0]	30% [26-34]	56% [51-60]	72% [68-76]	83% [79-86]	92% [90-94]	95% [92-97]	98% [96-99]	99% [97-99]	100% [99-100]
Numeric Memory Test	0% [0-0]	52% [48-57]	79% [76-83]	92% [89-94]	97% [95-98]	99% [98-99]	99% [98-99]	99% [98-99]	100% [99-100]	100% [99-100]
Pairs Matching Test	0% [0-0]	39% [34-43]	62% [58-66]	81% [77-84]	91% [88-93]	97% [95-99]	99% [97-99]	99% [98-99]	99% [98-99]	100% [99-100]

*Note: Simulated observed power calculations (rounded to the nearest percentage [95% CI]) based on minimum mean differences of interest from the literature using a mock dataset. Mock data (n=1999) were fit to linear mixed model using lmer() function on R and fit to Outcome ~ ASI*Instance + Age + Sex + Time between visits + (1|Subject ID) + error.*

Results

Table 2. Descriptives of sample population from UKB who met inclusion criteria with no history of stroke, myocardial infarction, cardiovascular disease, hypertension, blood clots, or other comorbid conditions. Reported as mean ± SD unless otherwise stated. Body Mass Index (BMI); Blood pressure (BP); Self-reported physical activity (PA); Hormone replacement therapy (HRT); Digit symbol substitution test performance (DSST)

	First Imaging Visit		**Second Imaging Visit**		
n = 1858	*M*	*SD*	*M*	*SD*	*p*
Female (n)	1007	-	-	-	-
Male (n)	851	-	-	-	-
Age (years)	61	7	64	7	-
Time between assessments (years)	2.57	0.96	-	-	-
Height (cm)	170.43	9.30	-	-	-
Weight (kg)	73.93	14.49	74.17	14.51	**<0.001**
BMI	26.04	4.16	26.04	4.23	0.375
Body Fat (%)	30.40	8.16	30.99	8.33	**<0.001**
Waist Circumference (cm)	86.68	12..27	87.47	12.24	**<0.001**
Hip Circumference (cm)	100.10	8.59	99.41	8.43	**<0.001**
Waist to Hip Ratio	0.86	0.086	0.88	0.087	**<0.001**
Arterial Stiffness Index (m/s)	9.79	2.66	9.13	3.12	**<0.001**
Systolic BP (mmHg)	137.68	18.52	132.12	19.99	0.207
Diastolic BP (mmHg)	77.28	10.46	76.80	9.53	0.341
PA >10 minutes (days/week)	4.02	2.22	4.07	2.25	0.319
Medications (n / %)					
Cholesterol Lowering Medication	83	4.4%	111	5.9%	-
BP Lowering Medication	43	2.3%	51	2.7%	-
Insulin	4	0.2%	3	0.1%	-
HRT	55	2.9%	60	3.2%	-
Oral Contraceptives	8	0.4%	4	0.2%	-
Whole Brain Grey Matter Volume (mL)	805.902	46.330	796.033	45.563	**<0.001**
White Matter Hyperintensities (mL)	4.009	4.914	4.609	5.662	**<0.001**

DSST Performance (correct matches)	20.20	4.79	20.06	5.21	0.961
Trail Making Test A (total time required; s)	20.689	6.633	21.236	10.371	0.008
Trail Making Test B (total time required; s)	50.069	21.133	51.311	25.750	0.007
Fluid Intelligence Test (correct answers)	6.79	2.01	6.75	1.99	0.93
Numeric Memory Test (digits remembered)	6.79	1.39	6.63	1.79	0.33
Pairs Matching Test (incorrect matches)	0.30	0.80	0.29	0.75	0.54

Table 3. Mean grey matter cortical thicknesses for regions of interest reported in mm. All unadjusted p values are result of Wilcoxon rank test to determine whether median values were significantly different between imaging visits. Bonferroni adjusted alpha level of significance is 0.0019 after accounting for 26 regions.

	First Imaging Visit (Left Hemisphere)		**Second Imaging Visit (Left Hemisphere)**			**First Imaging Visit (Right Hemisphere)**		**Second Imaging Visit (Right Hemisphere)**		
Cortical region	*M*	*SD*	*M*	*SD*	*p*	*M*	*SD*	*M*	*SD*	*p*
Caudal Anterior Cingulate	2.7455	0.2796	2.722	0.2865	**$p < 0.001$**	2.8332	0.1421	2.8188	0.1539	**$p < 0.001$**
Caudal Middle Frontal Gyri	2.8717	0.1490	2.8600	0.1560	**$p < 0.001$**	1.9544	0.1366	1.9493	0.1411	$p = 0.0086$
Rostral Anterior Cingulate	2.9061	0.1876	2.8859	0.1917	**$p < 0.001$**	2.9475	0.1972	2.9319	0.1989	**$p < 0.001$**
Rostral Middle Frontal Gyri	2.6852	0.1290	2.6685	0.1387	**$p < 0.001$**	2.6353	0.1181	2.6181	0.1259	**$p < 0.001$**
Superior Frontal Gyri	2.9604	0.1421	2.9387	0.1534	**$p < 0.001$**	2.9186	0.1303	2.8994	0.1408	**$p < 0.001$**
Superior Parietal Cortex	2.4792	0.1270	2.4684	0.1406	**$p < 0.001$**	2.4482	0.1313	2.4356	0.1413	**$p < 0.001$**
Inferior Parietal Cortex	2.6978	0.1183	2.6839	0.1284	**$p < 0.001$**	2.7246	0.1300	2.7081	0.1386	**$p < 0.001$**
Superior Temporal Cortex	2.9868	0.1641	2.9637	0.1692	**$p < 0.001$**	3.0639	0.1592	3.0376	0.1645	**$p < 0.001$**
Middle Temporal Cortex	2.9107	0.1482	2.8891	0.1532	**$p < 0.001$**	2.9957	0.1454	2.9892	0.1505	**$p < 0.001$**
Inferior Temporal Cortex	3.0577	0.1370	3.0411	0.1389	**$p < 0.001$**	3.0323	0.1319	3.0195	0.1387	**$p < 0.001$**
Parahippocampus	2.7828	0.2962	2.7657	0.2953	**$p < 0.001$**	2.7127	0.2522	2.7040	0.2515	**$p < 0.001$**
Posterior Cingulate	2.6985	0.1717	2.6767	0.1742	**$p < 0.001$**	2.7058	0.1759	2.6825	0.1834	**$p < 0.001$**
Lateral Occipital Lobe	2.3203	0.1272	2.3047	0.1340	**$p < 0.001$**	2.3517	0.1348	2.3414	0.1386	**$p < 0.001$**

2

Table 4. Statistical output from linear mixed effects models for each outcome of interest (objective 1). Unadjusted p-value and Holm's corrected p-value are both provided, where the Holm's corrected p value is the final value used to assess significance of findings.

N = 1858	ASI * Instance		Age		Sex		Years between Visits		Waist to hip ratio		Self-reported physical activity	
Outcome	*p*	Holm's corrected *p*	*p*	Holm's corrected *p*	*p*	Holm's corrected *p*	*p*	Holm's corrected *p*	*p*	Holm's corrected *p*	*p*	Holm's corrected *p*
LH Caudal Anterior Cingulate	**0.01**	0.11	**<0.001**	**<0.001**	0.65	-	**<0.001**	**0.0015**	0.029	0.095	0.48	-
LH Caudal Middle Frontal Gyri	**0.034**	0.21	**<0.001**	**<0.001**	0.42	-	**0.006**	**0.036**	0.53	-	0.13	-
LH Rostral Anterior Cingulate	0.35	-	**<0.001**	**<0.001**	0.96	-	**0.007**	**0.036**	0.16	-	0.55	-
LH Rostral Middle Frontal Gyri	0.22	-	**<0.001**	**<0.001**	**0.039**	0.12	0.51	-	0.71	-	0.46	-
LH Superior Frontal Gyri	0.053	-	**<0.001**	**<0.001**	0.37	-	**<0.001**	**0.0014**	0.79	-	0.14	-
LH Superior Parietal Cortex	0.16	-	**<0.001**	**<0.001**	0.39	-	**<0.001**	**<0.001**	0.52	-	**0.038**	**0.038**
LH Inferior Parietal Cortex	**0.023**	0.20	**<0.001**	**<0.001**	**0.026**	0.10	**0.004**	**0.032**	0.91	-	0.061	-

LH Superior Temporal Cortex	0.104	-	**<0.001**	**<0.001**	**0.001**	**0.011**	0.76	-	**0.044**	0.095	0.35	-
LH Middle Temporal Lobe	**0.031**	0.21	**<0.001**	**<0.001**	**<0.001**	**<0.001**	0.28	-	**0.008**	0.056	0.63	-
LH Inferior Temporal Cortex	**0.041**	0.21	**<0.001**	**<0.001**	**<0.001**	**<0.001**	0.19	-	0.53	-	0.83	-
LH Parahippocampus	**0.03**	0.21	**<0.001**	**0.005**	**<0.001**	**<0.001**	0.28	-	0.49	-	0.84	-
LH Posterior Cingulate	0.072	-	**<0.001**	**<0.001**	0.17	-	**0.002**	**0.018**	0.70	-	0.83	-
LH Lateral Occipital Lobe	0.076	-	**<0.001**	**<0.001**	**0.002**	**0.02**	0.10	-	**0.022**	0.095	**0.007**	**0.014**
RH Caudal Anterior Cingulate	0.091	-	**<0.001**	**<0.001**	0.054	-	**0.002**	**0.018**	**0.01**	**0.06**	0.43	
RH Caudal Middle Frontal Gyri	**0.036**	0.21	**<0.001**	**0.016**	**0.005**	**0.04**	0.90	-	**0.001**	**0.009**	0.44	-
RH Rostral Anterior Cingulate	0.63	-	0.24	-	**0.013**	0.078	**0.005**	**0.035**	0.097	-	0.14	-
RH Rostral Middle Frontal Gyri	0.30	-	**<0.001**	**<0.001**	0.69	-	0.53	-	**<0.001**	**0.0012**	0.75	-

RH Superior Frontal Gyri	0.058	-	**<0.001**	**<0.001**	**0.024**	0.12	**0.002**	**0.018**	0.056	-	0.66	-
RH Superior Parietal Cortex	**0.025**	0.20	**<0.001**	**<0.001**	**<0.001**	**0.003**	**0.006**	**0.032**	**0.019**	0.095	0.63	-
RH Inferior Parietal Cortex	0.090	-	**<0.001**	**<0.001**	0.074	-	0.083	-	**0.021**	0.095	0.41	-
RH Superior Temporal Cortex	**0.019**	0.19	**<0.001**	**<0.001**	0.29	-	0.66	-	0.26	-	0.67	-
RH Middle Temporal Lobe	**0.035**	0.21	**<0.001**	**<0.001**	**0.01**	0.07	0.88	-	0.12	-	0.90	-
RH Inferior Temporal Cortex	0.057	-	**<0.001**	**<0.001**	0.47	-	0.44	-	0.40	-	0.76	-
RH Parahippocampus	0.36	-	**<0.001**	**0.012**	**<0.001**	**<0.001**	0.58	-	0.36	-	0.054	-
RH Posterior Cingulate	0.29	-	**<0.001**	**<0.001**	**0.004**	**0.036**	**0.002**	**0.018**	0.55	-	0.83	-
RH Lateral Occipital Lobe	**0.037**	0.21	**<0.001**	**<0.001**	**0.004**	**0.036**	0.92	-	**0.002**	**0.016**	0.36	-
GMV	0.76	-	**<0.001**	-	**<0.001**	-	**<0.001**	**-**	**0.005**	-	0.92	-
WMH	0.84	-	**<0.001**	-	0.23	-	**<0.001**	**-**	**0.005**	**-**	0.36	-
DSST Performance	0.81	-	**<0.001**	**<0.001**	0.56	-	0.99	-	**0.017**	**0.042**	0.72	-

TmA Performance	0.25	-	**<0.001**	**<0.001**	**0.005**	**0.01**	0.23	-	0.83	-	0.63	-
TmB Performance	0.23	-	**<0.001**	**<0.001**	0.35	**-**	0.57	-	0.46	-	0.44	-
Fluid Intelligence Test Performance	**0.029**	0.17	**0.019**	0.11	**0.009**	**0.009**	0.23	-	**0.021**	**0.042**	0.068	-
Numeric Memory Test Performance	0.65	-	**<0.001**	**<0.001**	**<0.001**	**<0.001**	**0.019**	0.114	**<0.001**	**<0.001**	0.42	
Pairs Matching Test Performance	0.74	-	**<0.001**	**<0.001**	**0.001**	**0.003**	0.52	-	**0.014**	**0.042**	0.30	-

Table 5. Statistical output for linear regression analysis for each outcome of interest (objective 2).

N = 630	First Imaging Visit				Second Imaging visit			
	Baseline ASI		Age		Baseline ASI		Age	
Outcome	*p*	Holm's corrected *p*	*p*	Holm's corrected *p*	*p*	Holm's corrected *p*	*p*	Holm's corrected *p*
LH Caudal Anterior Cingulate	0.39	-	**0.001**	**0.027**	0.268	-	**<0.001**	**0.005**
LH Caudal Middle Frontal Gyri	0.053	-	**<0.001**	**<0.001**	**0.023**	0.069	**<0.001**	**<0.001**
LH Rostral Anterior Cingulate	0.62	-	**<0.001**	**0.027**	0.85	-	**<0.001**	**0.004**
LH Rostral Middle Frontal Gyri	0.52	-	**<0.001**	**<0.001**	0.34	-	**<0.001**	**<0.001**
LH Superior Frontal Gyri	0.058	-	**<0.001**	**<0.001**	0.15	-	**<0.001**	**<0.001**
LH Superior Parietal Cortex	0.33	-	**<0.001**	**<0.001**	0.24	-	**<0.001**	**<0.001**
LH Inferior Parietal Cortex	**0.034**	0.068	**<0.001**	**<0.001**	**0.028**	0.069	**<0.001**	**<0.001**
LH Superior Temporal Cortex	0.082	-	**<0.001**	**<0.001**	0.23	-	**<0.001**	**<0.001**
LH Middle Temporal Cortex	**0.014**	0.056	**<0.001**	**<0.001**	0.058	-	**<0.001**	**<0.001**
LH Inferior Temporal Cortex	0.54	-	**0.003**	0.078	0.40	-	**<0.001**	**<0.001**

LH Parahippocampus	0.061	-	0.72	-	0.39	-	**0.024**	0.48
LH Posterior Cingulate	0.76	-	**<0.001**	**<0.001**	0.26	-	**<0.001**	**<0.001**
LH Lateral Occipital Lobe	0.27	-	**<0.001**	**<0.001**	0.46	-	**<0.001**	**<0.001**
RH Caudal Anterior Cingulate	0.49	-	**<0.001**	**<0.001**	0.27	-	**<0.001**	**<0.001**
RH Caudal Middle Frontal Gyri	0.16	-	0.059	-	0.53	-	**0.002**	0.052
RH Rostral Anterior Cingulate	0.26	-	0.30	-	0.85	-	0.78	-
RH Rostral Middle Frontal Gyri	0.84	-	**<0.001**	**<0.001**	0.46	-	**<0.001**	**<0.001**
RH Superior Frontal Gyri	0.45	-	**<0.001**	**<0.001**	0.088	-	**<0.001**	**<0.001**
RH Superior Parietal Cortex	0.21	-	**<0.001**	**<0.001**	0.098	-	**<0.001**	**<0.001**
RH Inferior Parietal Cortex	**0.049**	0.068	**<0.001**	**<0.001**	**0.028**	0.069	**<0.001**	**<0.001**
RH Superior Temporal Cortex	0.31	-	**<0.001**	**<0.001**	0.17	-	**<0.001**	**<0.001**
RH Middle Temporal Cortex	0.87	-	**<0.001**	**<0.001**	0.33	-	**<0.001**	**<0.001**
RH Inferior Temporal Cortex	**0.018**	0.056	**0.003**	0.056	**0.012**	**0.048**	**<0.001**	**<0.001**
RH Parahippocampus	0.66	-	0.055	-	0.063	-	**0.004**	0.10

RH Posterior Cingulate	0.96	-	**<0.001**	**0.005**	0.24	-	**0.004**	0.10
RH Lateral Occipital Lobe	0.91	-	**<0.001**	**<0.001**	0.79	-	**<0.001**	**<0.001**
GMV	**0.015**	-	**<0.001**	**<0.001**	**0.030**	-	**<0.001**	**<0.001**
WMH	0.47	-	**<0.001**	**<0.001**	0.083	-	**<0.001**	**<0.001**
DSST Performance	0.78	-	**<0.001**	**<0.001**	0.71	-	**<0.001**	**<0.001**
TmA Performance	0.71	-	**<0.001**	**<0.001**	0.29	-	**<0.001**	**<0.001**
TmB Performance	0.25	-	**<0.001**	**<0.001**	0.64	-	**<0.001**	**<0.001**
Fluid Intelligence Test Performance	0.37	-	0.296	-	0.71	-	0.25	-
Numeric Memory Test Performance	0.36	-	0.12	-	0.31	-	**0.013**	**0.026**
Pairs Matching Test Performance	**0.034**	0.20	**<0.001**	**<0.001**	0.44	-	0.087	-

A descriptive summary of demographic characteristics and brain measures for the study population can be found in *Table 2*. All values are reported as mean ± SD unless otherwise stated. The mean age of eligible study participants (n = 1858) at the first imaging visit was 61 ± 7 years of age, and the number of males and females was 851 and 1007, respectively. For the present sample, time interval between baseline and the first imaging visit was 8.5 ± 1.02 years, and 2.5 ± 1 years between the first and second imaging visit. All subjects that were missing multiple data points for ASI, regional GM cortical thickness, GMV, or WMH, as well as having any disease conditions as described in the exclusion criteria were excluded from the present analyses. Following Wilcoxon rank tests for non-parametric data, significant differences were detected in weight, BMI, body fat percentage, waist to hip ratio, ASI, GMV, WMH (*Table* 2), and all 26 GM cortical thickness regions (*Table 3*) between the first and second imaging visit. All statistical model outputs for Objective 1 can be found in *Appendix A,* and model outputs for Objective 2 can be found in *Appendix B*.

Objective 1 - Linear Mixed Effect Model Results

Regional Cortical Grey Matter (GM) Thickness

Following linear mixed effect model analysis on 26 cortical regions, prior to post-hoc correction it was determined that there was a significant effect of the ASI*Instance interaction on 11 of the 26 cortical regions analyzed. The 11 brain regions included: the left hemisphere caudal anterior cingulate (***p* = 0.01**), left hemisphere caudal middle frontal gyri (***p* = 0.034**), the right hemisphere caudal middle frontal gyri (***p* = 0.036**), right hemisphere superior parietal cortex (***p* = 0.025),** left hemisphere inferior parietal cortex (***p* = 0.023**), right hemisphere superior temporal cortex (***p* = 0.019**), left hemisphere inferior temporal cortex (***p* = 0.041**), left hemisphere parahippocampus (***p***

= 0.03), left hemisphere middle temporal lobe (***p* = 0.035**), right hemisphere middle temporal lobe (***p* = 0.035**), right hemisphere lateral occipital lobe (***p* = 0.037**). Following post-hoc correction for multiple comparisons using the Holm-Bonferroni method, there was no significant effect of the ASI*Instance interaction on any of the 26 cortical regions analyzed (raw *p* and adjusted *p* reported in *Table 4).* Graphical representation of the effect of the changes in ASI on changes in each regional GM cortical thickness over 2.5 ± 1 years can be seen in *Figures 1-13*. Our linear mixed effects model also detected a significant effect of age in all but one (right hemisphere rostral anterior cingulate) of the 26 cortical regions analyzed (***p* ≤0.001** for all regions in which age effect was detected) and all regions in which an effect was detected prior to correction remained significant following post-hoc correction. There was a significant effect of sex on regional GM cortical thickness in 15 of 26 brain regions prior to post-hoc correction (right hemisphere caudal middle frontal gyri; right hemisphere rostral anterior cingulate; left and right hemisphere rostral middle frontal gyri; right hemisphere superior frontal gyri; right hemisphere superior parietal cortex; left hemisphere inferior parietal cortex; left hemisphere superior temporal cortex; left hemisphere inferior temporal cortex; left and right hemisphere parahippocampus; left and right hemisphere lateral occipital lobes; left and right hemisphere middle temporal lobes). Nine of the 15 regions in which sex differences were detected suggested that the reductions in cortical thickness over the time between imaging visits was greater in males than females (right hemisphere caudal middle frontal gyri; right hemisphere rostral anterior cingulate; left hemisphere superior temporal cortex; left hemisphere inferior temporal cortex; left and right hemisphere lateral occipital lobe; left hemisphere middle temporal lobe; right hemisphere temporal lobe) and six of which (right hemisphere superior frontal gyri; right hemisphere superior parietal cortex; left hemisphere inferior parietal cortex; left and right hemisphere parahippocampus; right hemisphere

posterior cingulate) suggested that the reduction in cortical thickness was greater in female than males over the time between imaging visits. Following post-hoc correction there was a significant effect of sex in 10 total cortical regions including the right hemisphere caudal middle frontal gyri, right hemisphere superior parietal cortex, left hemisphere superior temporal cortex, left hemisphere inferior temporal cortex, left and right hemisphere parahippocampus, left and right hemisphere lateral occipital lobes, left hemisphere middle temporal lobe, and right hemisphere posterior cingulate. Years between visits had a significant effect on GM cortical thickness in 12 of 26 regions analyzed prior to post-hoc correction; however, this should be interpreted with caution as this variable is assessing whether the variability in the time interval between visits in the UK Biobank has a significant influence on outcomes and should not be interpreted as a measure of longitudinal changes or directionality of changes in the outcomes of interest. Following post-hoc correction, all 12 regions in which years between visits had a significant effect remained significant. The regions significantly associated with years between visits included the bilateral caudal anterior cingulate, left hemisphere caudal middle frontal gyri, bilateral rostral anterior cingulate, bilateral superior frontal gyri, bilateral superior parietal cortices, left hemisphere inferior parietal cortex, and bilateral posterior cingulate. There was also a significant effect of waist to hip ratio in 10 of 26 regions analyzed which included the bilateral hemisphere caudal anterior cingulate, right hemisphere caudal middle frontal gyri, right hemisphere rostral middle frontal gyri, right hemisphere superior parietal cortex, right hemisphere inferior parietal cortex, left hemisphere superior temporal cortex, bilateral lateral occipital lobes, and left hemisphere middle temporal lobe; however, following post-hoc correction, only four regions remained significant (**right hemisphere caudal anterior cingulate, right hemisphere caudal middle frontal gyri, right hemisphere rostral middle frontal; right hemisphere lateral occipital lobe**). The covariate of

self-reported physical activity had no effect on 24 of the 26 brain regions. The two brain regions in which self-reported physical activity was significant were the left hemisphere superior parietal cortex and left hemisphere lateral occipital lobe (adjusted $\boldsymbol{p}$ **= 0.038** and **0.014**, respectively). Overall, the linear mixed effects models were able to explain an average of 78 ± 5.5% of total variance across all 26 regions. The raw linear mixed effects model outputs for each region can be found in *Appendix A (A1-A26).*

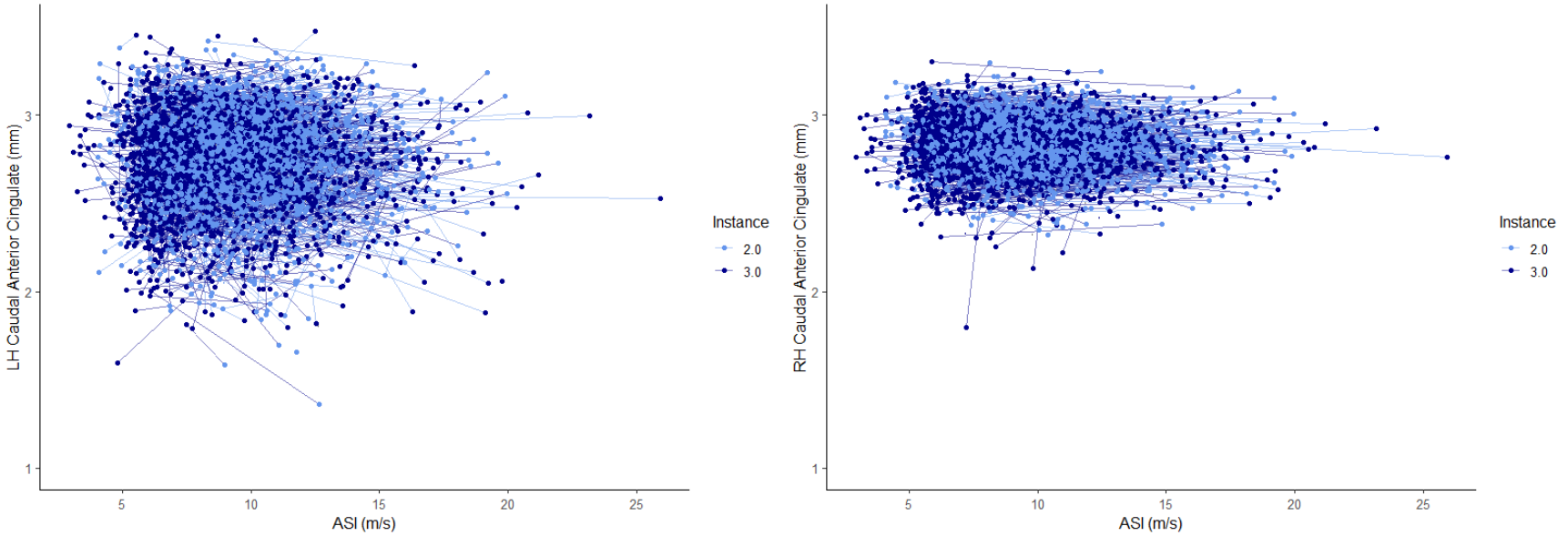

Figure 1. Association of changes in ASI (m/s) and changes in left and right hemisphere caudal anterior cingulate cortical thicknesses (mm) over 2.5 ± 1 years (range 1.1-6.9 years). Each individual line indicates a single participant's trajectory over the two instances (instance 2.0 and 3.0) (N = 1855).

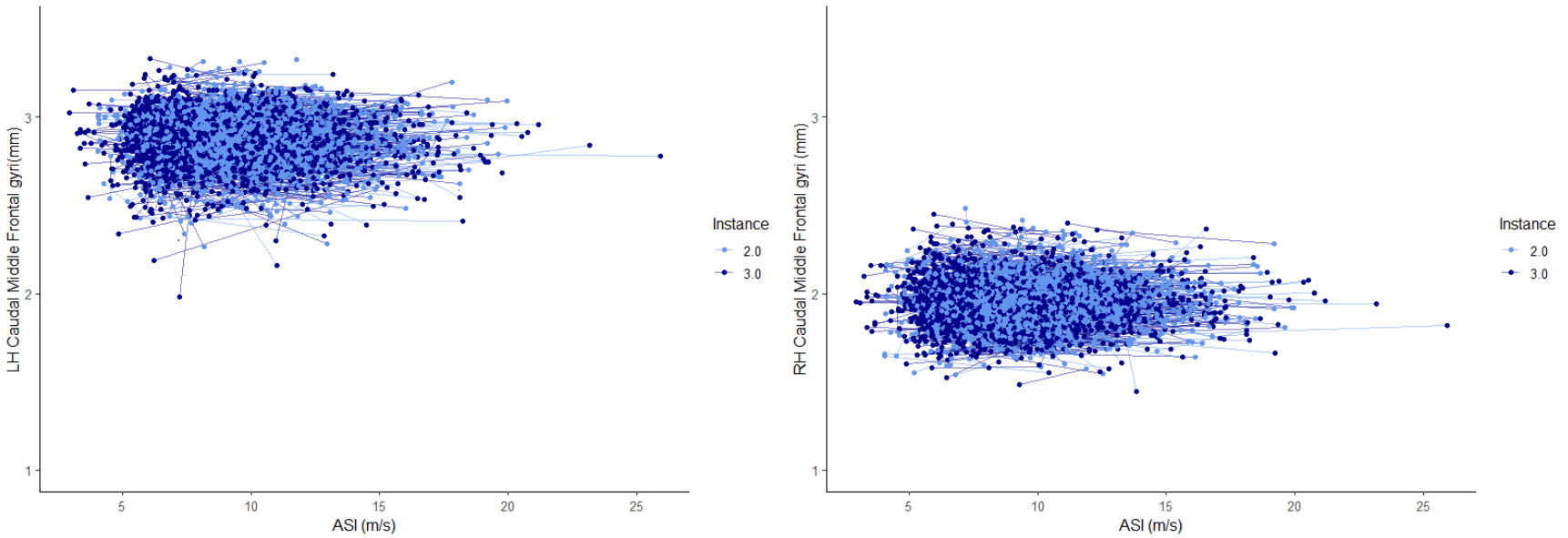

Figure 2. Association of changes in ASI (m/s) and changes in left and right hemisphere caudal middle frontal gyri cortical thicknesses (mm) over 2.5 ± 1 years (range 1.1-6.9 years). Each individual line indicates a single participant's trajectory over the two instances (instance 2.0 and 3.0) (N = 1855).

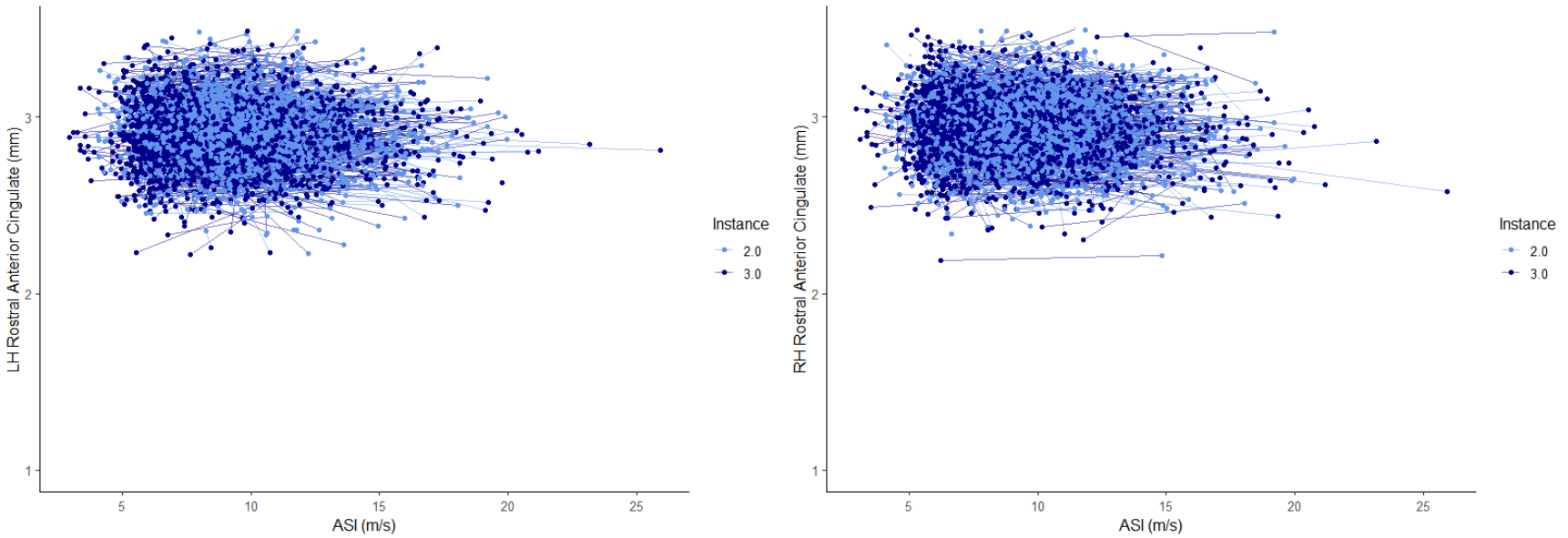

Figure 3. Association of changes in ASI (m/s) and changes in left and right hemisphere rostral anterior cingulate cortical thicknesses (mm) over 2.5 ± 1 years (range 1.1-6.9 years). Each individual line indicates a single participant's trajectory over the two instances (instance 2.0 and 3.0) (N = 1855).

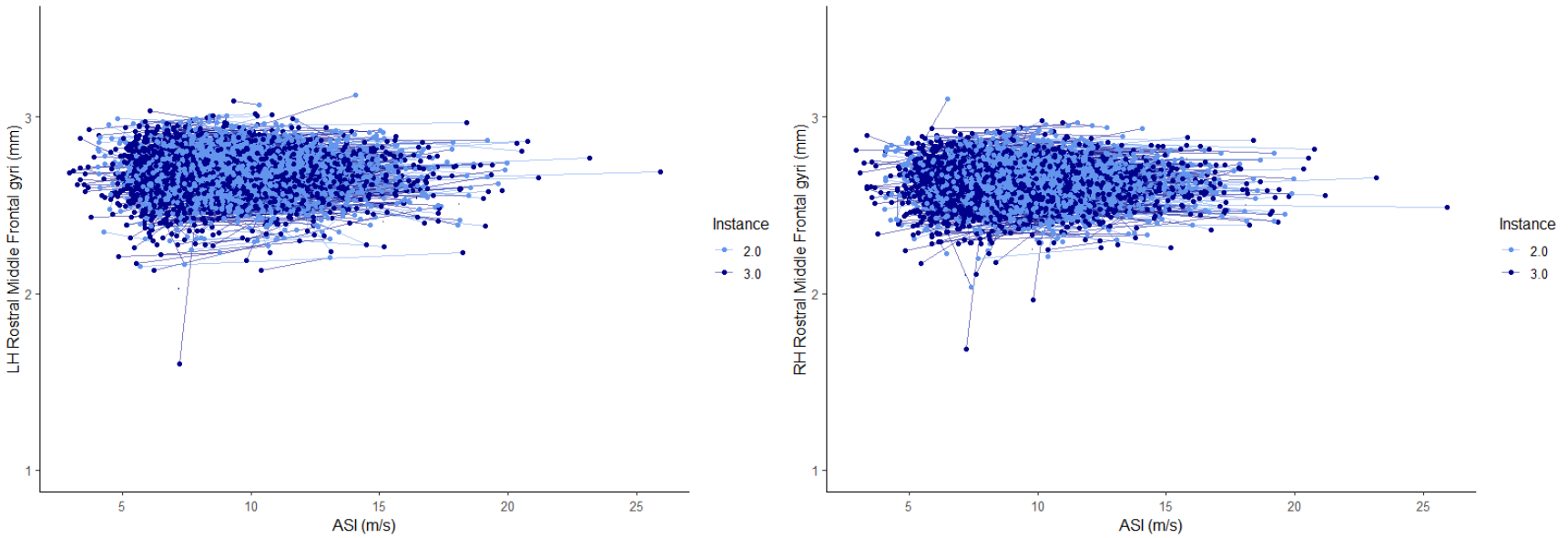

Figure 4. Association of changes in ASI (m/s) and changes in left and right hemisphere rostral middle frontal gyri cortical thicknesses (mm) over 2.5 ± 1 years (range 1.1-6.9 years). Each individual line indicates a single participant's trajectory over the two instances (instance 2.0 and 3.0) (N = 1855).

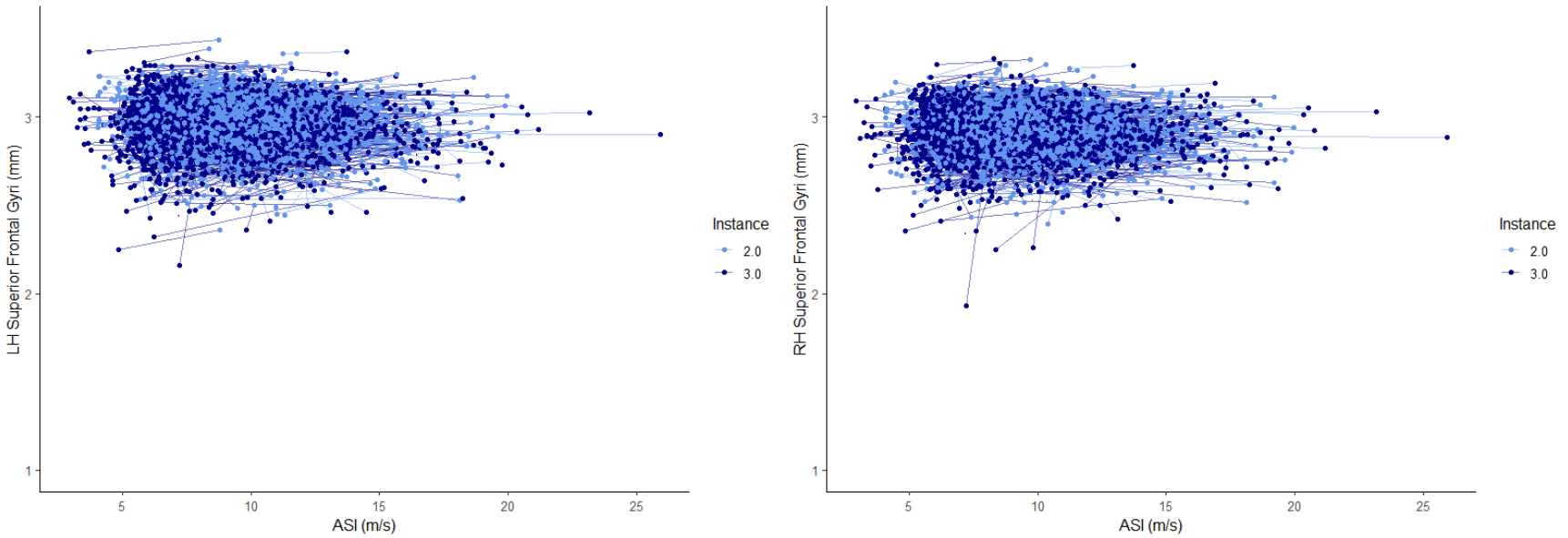

Figure 5. Association of changes in ASI (m/s) and changes in left and right hemisphere superior frontal gyri cortical thicknesses (mm) over 2.5 ± 1 years (range 1.1-6.9 years). Each individual line indicates a single participant's trajectory over the two instances (instance 2.0 and 3.0) (N = 1855).

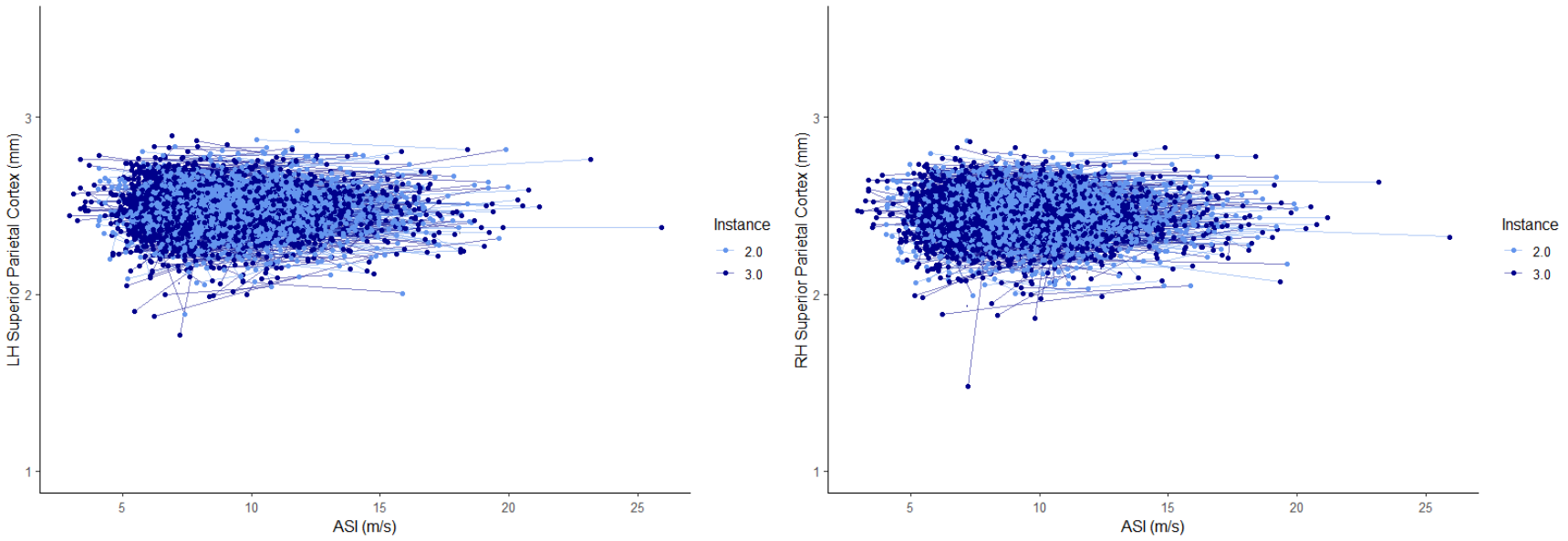

Figure 6. Association of changes in ASI (m/s) and changes in left and right hemisphere superior parietal cortex cortical thicknesses (mm) over 2.5 ± 1 years (range 1.1-6.9 years). Each individual line indicates a single participant's trajectory over the two instances (instance 2.0 and 3.0) (N = 1855).

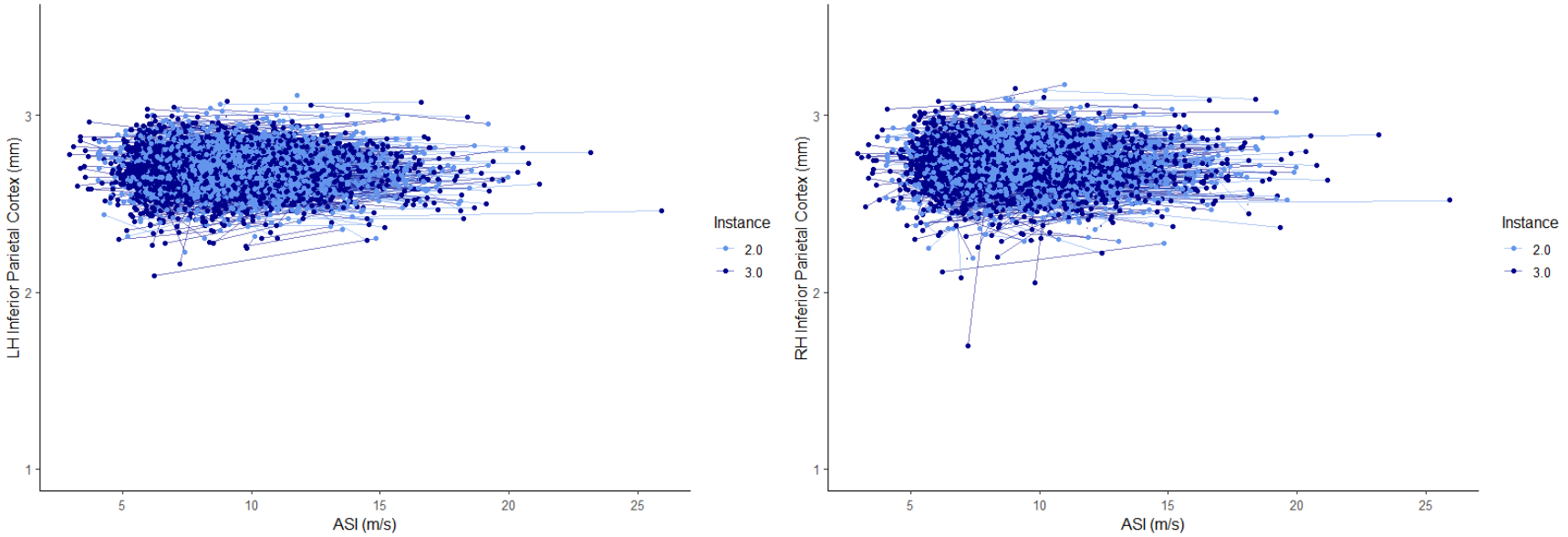

Figure 7. Association of changes in ASI (m/s) and changes in left and right hemisphere inferior parietal cortex cortical thicknesses (mm) over 2.5 ± 1 years (range 1.1-6.9 years). Each individual line indicates a single participant's trajectory over the two instances (instance 2.0 and 3.0) (N = 1855).

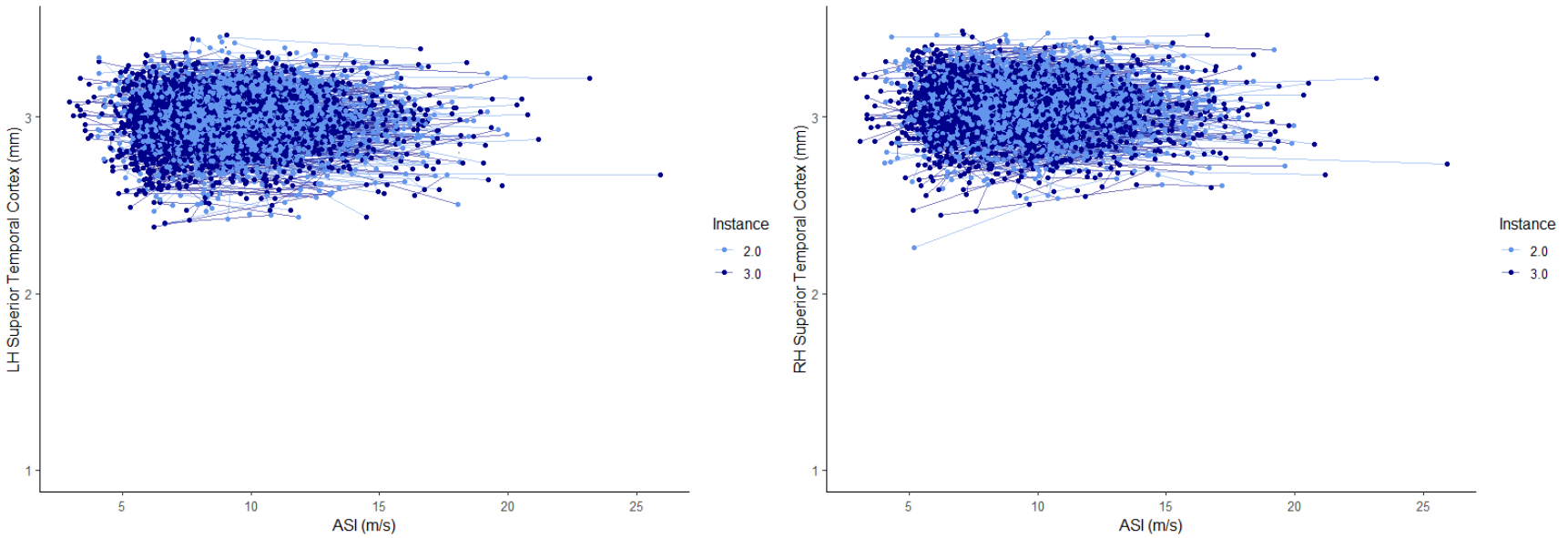

Figure 8. Association of changes in ASI (m/s) and changes in left and right hemisphere superior temporal cortex cortical thicknesses (mm) over 2.5 ± 1 years (range 1.1-6.9 years). Each individual line indicates a single participant's trajectory over the two instances (instance 2.0 and 3.0) (N = 1855).

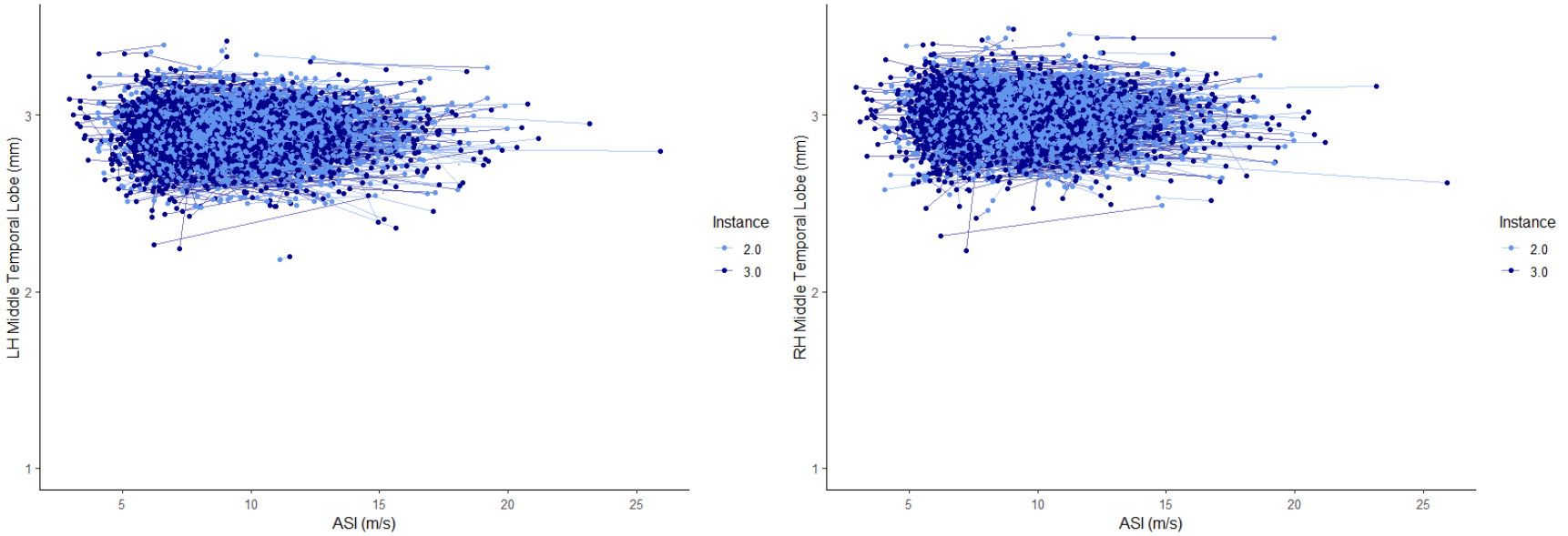

Figure 9. Association of changes in ASI (m/s) and changes in left and right hemisphere middle temporal lobe cortical thicknesses (mm) over 2.5 ± 1 years (range 1.1-6.9 years). Each individual line indicates a single participant's trajectory over the two instances (instance 2.0 and 3.0) (N = 1855).

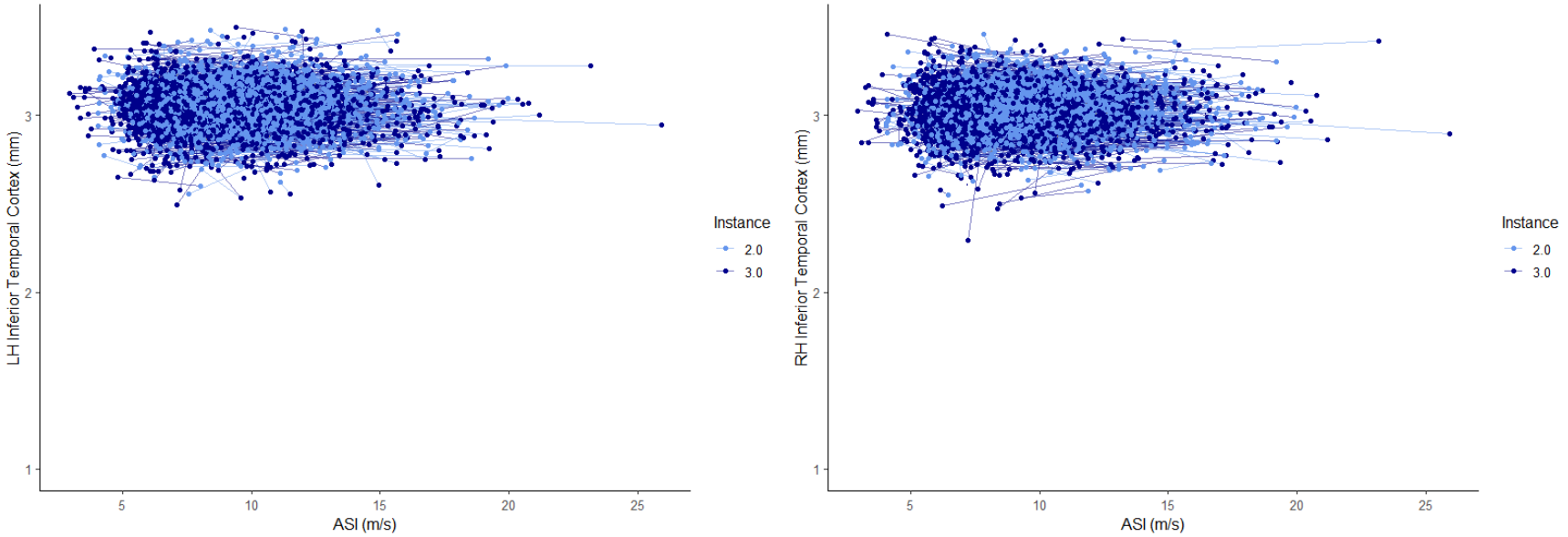

Figure 10. Association of changes in ASI (m/s) and changes in left and right hemisphere inferior temporal cortex cortical thicknesses (mm) over 2.5 ± 1 years (range 1.1-6.9 years). Each individual line indicates a single participant's trajectory over the two instances (instance 2.0 and 3.0) (N = 1855).

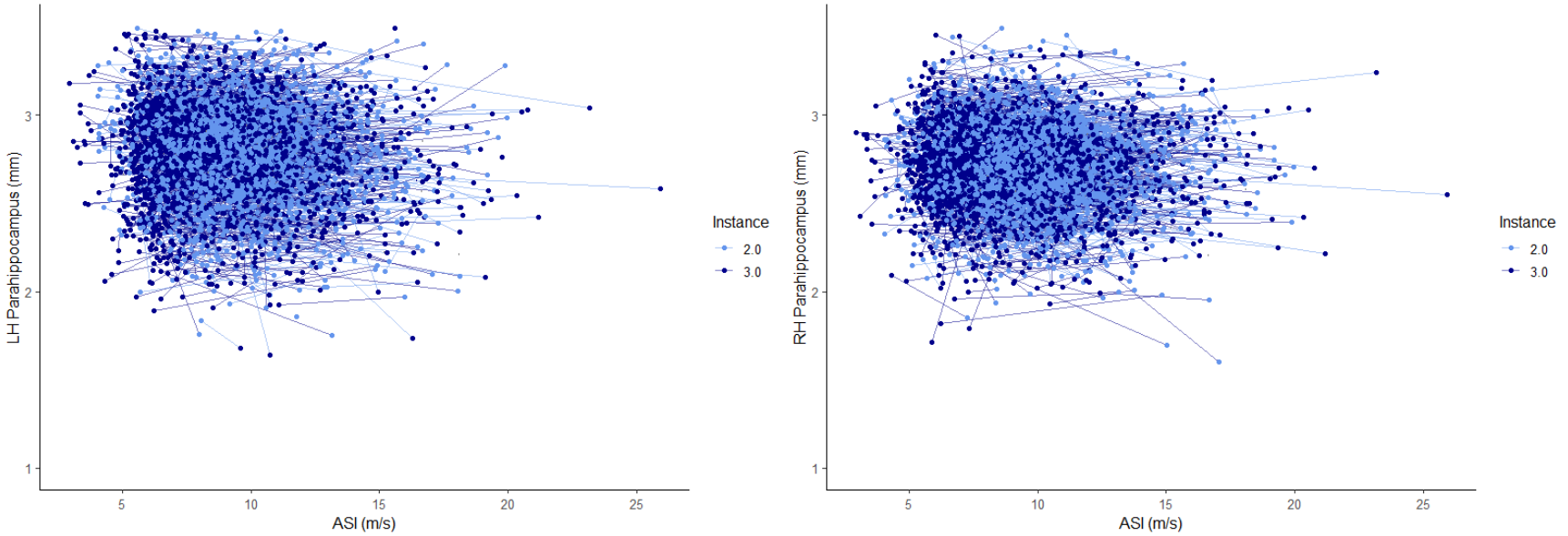

Figure 11. Association of changes in ASI (m/s) and changes in left and right hemisphere parahippocampus cortical thicknesses (mm) over 2.5 ± 1 years (range 1.1-6.9 years). Each individual line indicates a single participant's trajectory over the two instances (instance 2.0 and 3.0) (N = 1855).

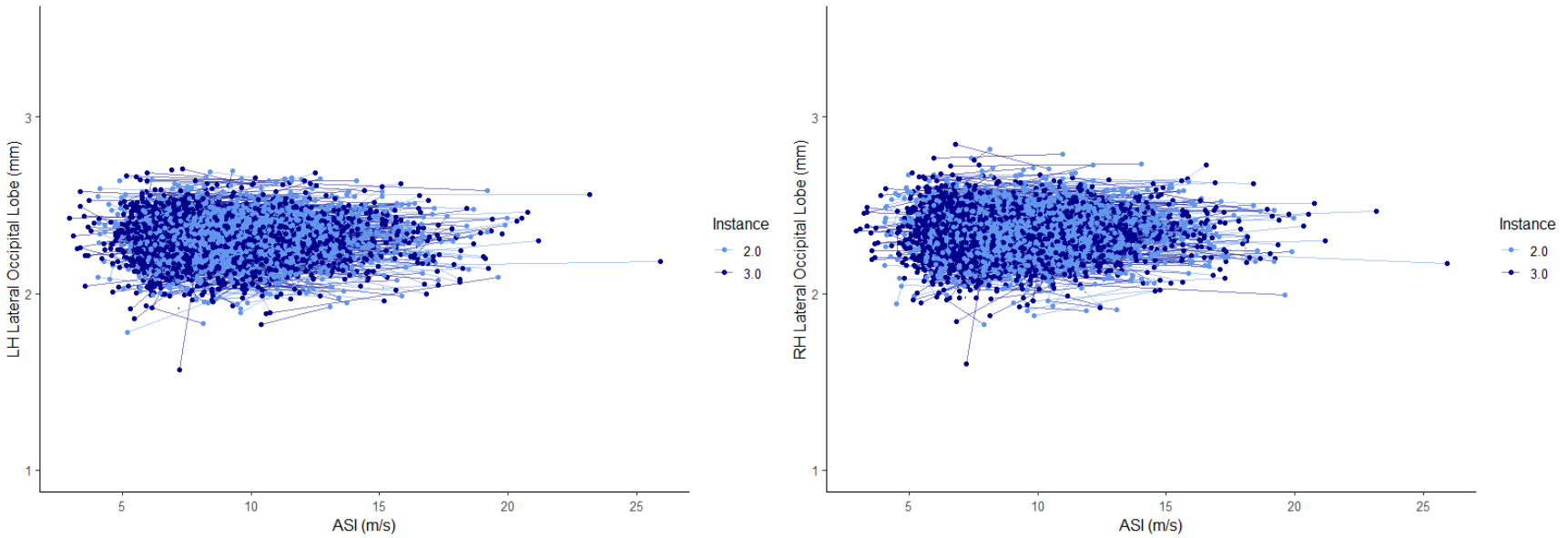

Figure 12. Association of changes in ASI (m/s) and changes in left and right hemisphere lateral occipital lobe cortical thicknesses (mm) over 2.5 ± 1 years (range 1.1-6.9 years). Each individual line indicates a single participant's trajectory over the two instances (instance 2.0 and 3.0) (N = 1855).

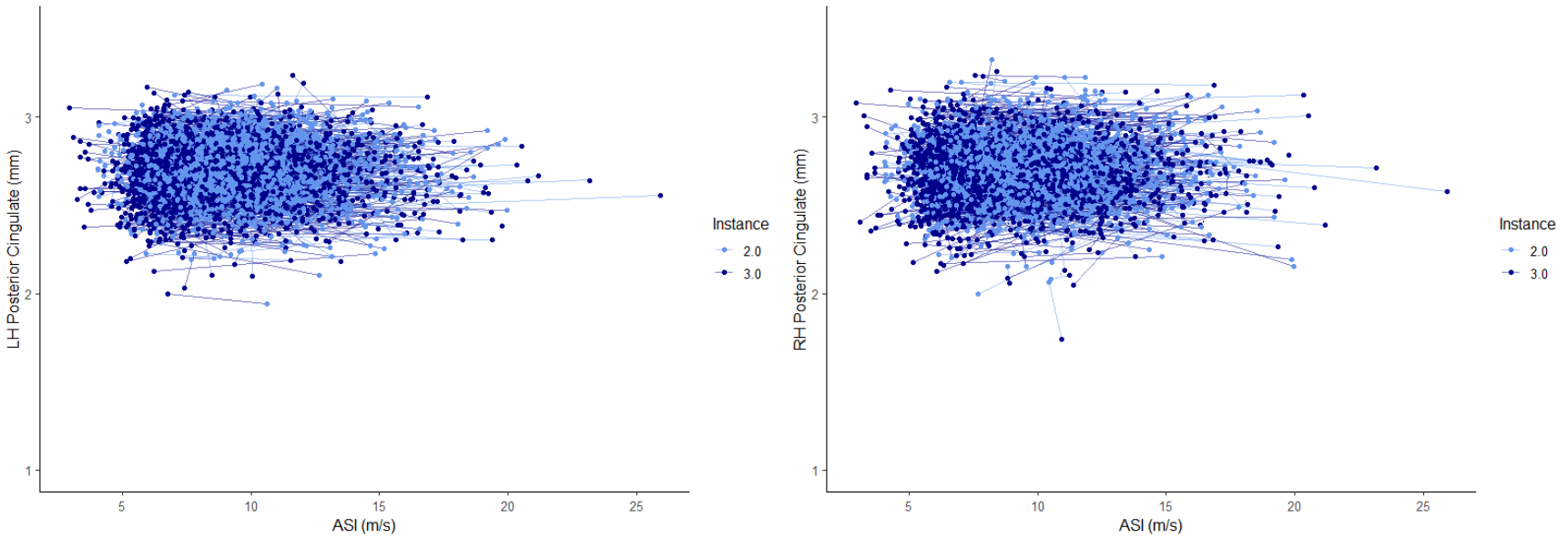

Figure 13. Association of changes in ASI (m/s) and changes in left and right hemisphere posterior cingulate cortical thicknesses (mm) over 2.5 ± 1 years (range 1.1-6.9 years). Each individual line indicates a single participant's trajectory over the two instances (instance 2.0 and 3.0) (N = 1855).

Whole Brain Grey Matter Volume

There was no significant relationship detected between the main effect of the ASI*Instance interaction and whole brain GMV ($p = 0.76$). Graphical representation of the effect of the changes in ASI on changes in whole brain GMV over 2.5 ± 1 years can be seen in *Figure 14*. There was a significant association between age and GMV (***p* < 0.001**), with a 3.699mL reduction in GMV with each year of age. The model also detected significant differences between sexes **(*p* < 0.001)**, suggesting males had a reduction in GMV that was ~20.484mL greater compared to females over 2.5 ± 1 years. The effect of 'Years between visits' was significantly associated with whole brain GMV (***p* < 0.001**). The model also detected a significant effect of waist to hip ratio (***p* = 0.005*)***, suggesting that for every 0.05 unit increase in waist to hip ratio, GMV decreased by ~0.633mL. The linear mixed effects model was able to explain ~96% of the variance in GMV in the present sample. Summary of the linear mixed effects model for GMV (raw and adjusted *p)* can be found in *Table 4.* The raw linear mixed effects model output for GMV can be found in *Appendix A27*.

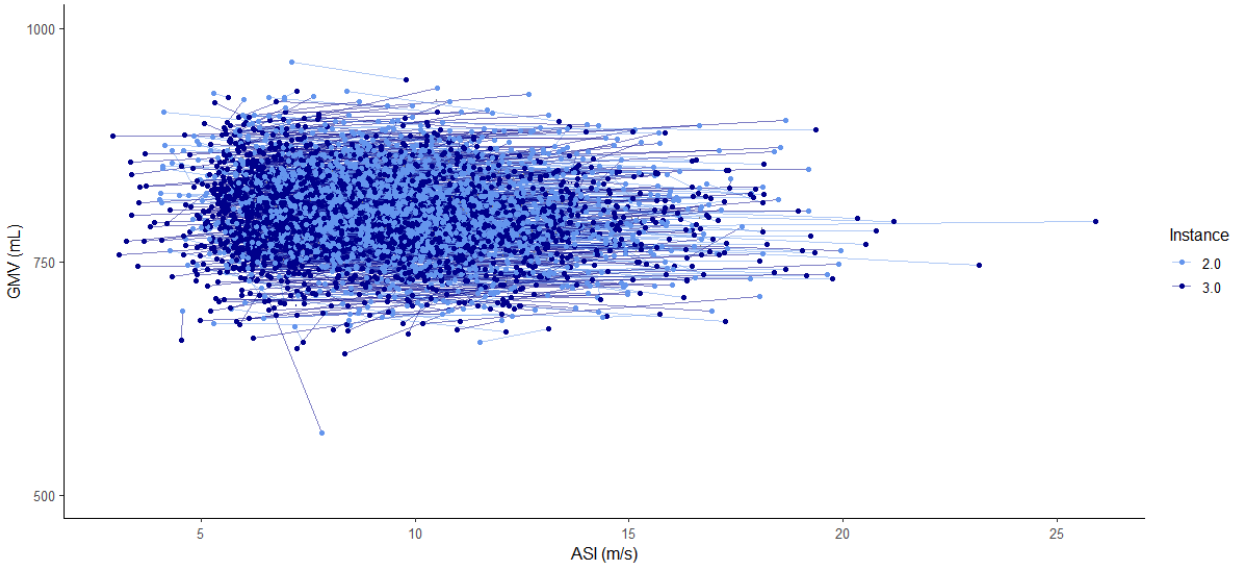

Figure 14. Association of changes in ASI (m/s) and changes in whole brain GMV (mL) over 2.5 ± 1 years (range 1.1-6.9 years). Each individual line indicates a single participant's trajectory over the two instances (instance 2.0 and 3.0) (N = 1858).

White matter hyperintensities (WMH) volume

Similar to GMV, there was no significant effect of ASI*Instance interaction on WMH volume (p = 0.84). Graphical representation of the effect of the changes in ASI on changes in WMH volume over 2.5 ± 1 years can be seen in *Figure 15 and 16 (WMH volume with a maximum value of 15mL).* There was however a significant effect of age **($p < 0.001$)**, with the model estimating a 0.167mL increase in WMH volume with each additional year of age. There was no significant effect of sex (p = 0.23) on WMH volume. A significant effect of years between visits on WMH volume was detected (**$p = 0.005$**). A significant effect of waist to hip ratio was also observed **($p < 0.001$)**, with the model estimating an ~0.105mL increase in WMH volume per 0.05 unit increase in waist to hip ratio. There was no effect of self-reported physical activity on WMH volume over 2.5 ± 1 years

(p = 0.36). Collectively, the linear mixed effects model was able to explain 85% of variance in WMH volume in the UK Biobank subcohort. Summary of the linear mixed effects model for WMH (raw and adjusted *p)* can be found in *Table 4.* The raw linear mixed effects model output for WMH can be found in *Appendix A28.*

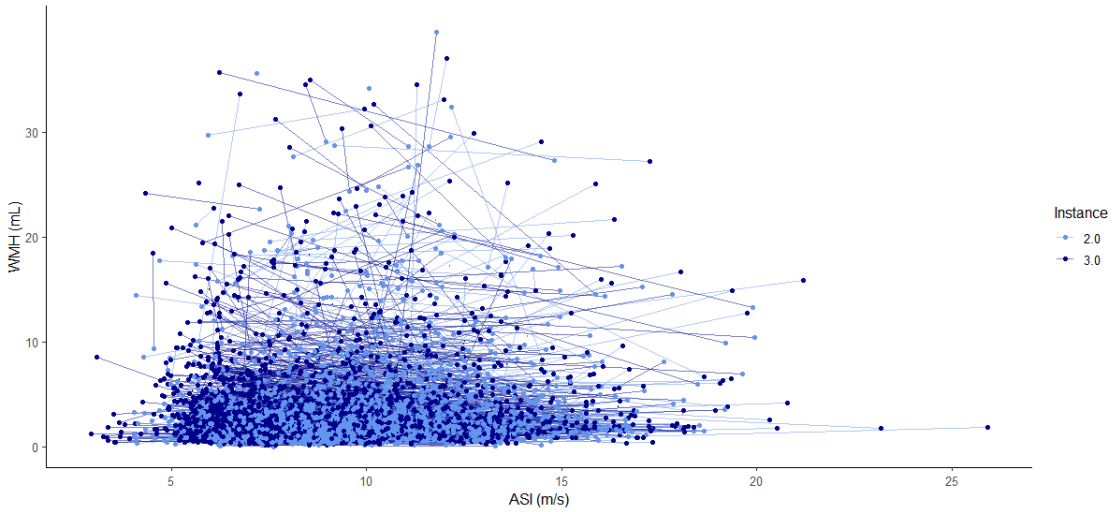

Figure 15. Association of changes in ASI (m/s) and changes in whole brain WMH (mL) over 2.5 ± 1 years (range 1.1-6.9 years). Each individual line indicates a single participant's trajectory over the two instances (instance 2.0 and 3.0) (N = 1858).

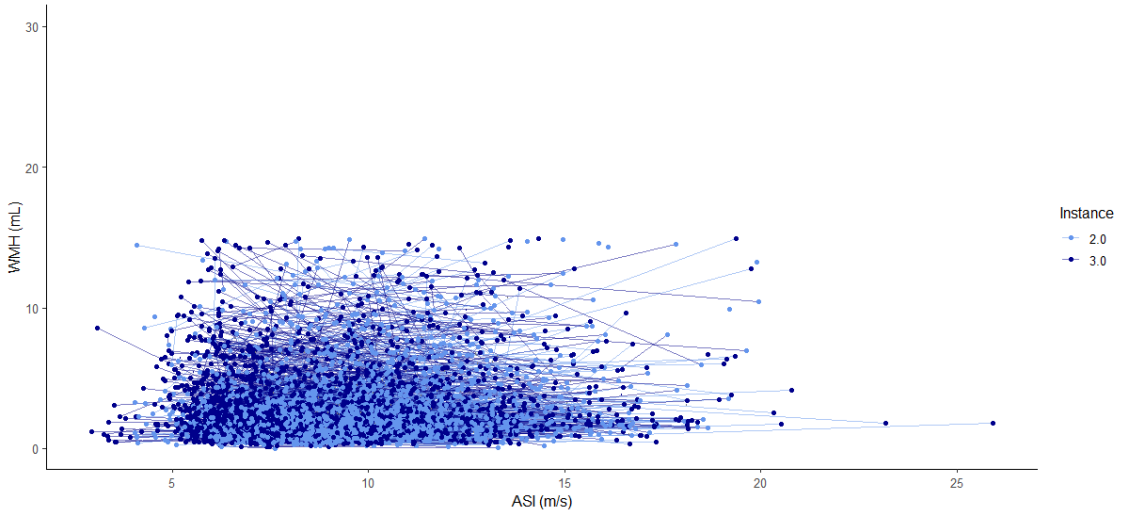

Figure 16. Association of changes in ASI (m/s) and changes in whole brain WMH (mL) over 2.5 ± 1 years (range 1.1-6.9 years) when adjusted to only include max WMH volume of 15mL. Each individual line indicates a single participant's trajectory over the two instances (instance 2.0 and 3.0) (N = 1801).

Cognitive performance

Linear mixed effects model analysis for the six cognitive tests of interest determined that the ASI and instance interaction effect was significant only on Fluid Intelligence Test performance (***p* = 0.029**) prior to post hoc correction and following correction for multiple comparisons using the Holm-Bonferroni method, there was no effect of the ASI*Instance interaction on any of the cognitive tests included in the present study. Graphical representation of the effect of the changes in ASI on changes in each cognitive test performance over 2.5 ± 1 years can be seen in *Figures 17-22*. There was a significant effect of age on all cognitive test performances prior to correction, and five of six remained significant following post-hoc correction using the Holm-Bonferroni method. Significant sex differences were detected in performance of six tests prior to correction,

and following correction remained significant in four of six tests including TmA (***p* = 0.005, adjusted *p* = 0.01**), Fluid Intelligence Test (***p* = 0.009, adjusted *p* = 0.01**), Numeric Memory Test (***p* < 0.001, adjusted *p* < 0.001**), and Pairs Matching Test performance (***p* = 0.001, adjusted *p* = 0.003**). The models also detected a significant effect of waist to hip ratio for cognitive performance in the Digit Symbol Substitution Test (***p* = 0.017, adjusted *p* = 0.042**), Fluid Intelligence Test (***p* = 0.021, adjusted *p* = 0.042**), the Numeric Memory Test (***p* < 0.001, adjusted *p* = <0.001**), and the Pairs Matching Test (***p* = 0.014, adjusted *p* = 0.042**). There was no effect of self-reported physical activity on any of the cognitive tests analyzed. Overall, the linear mixed models were able to explain ~24.4 ± 30.5% of the variance in the cognitive models included. Summary of the linear mixed effects model for all cognitive tests included in analyses (raw and adjusted *p)* can be found in *Table 4.* The raw linear mixed effects model output for cognitive performance for each test can be found in *Appendix A (A29-A34).*

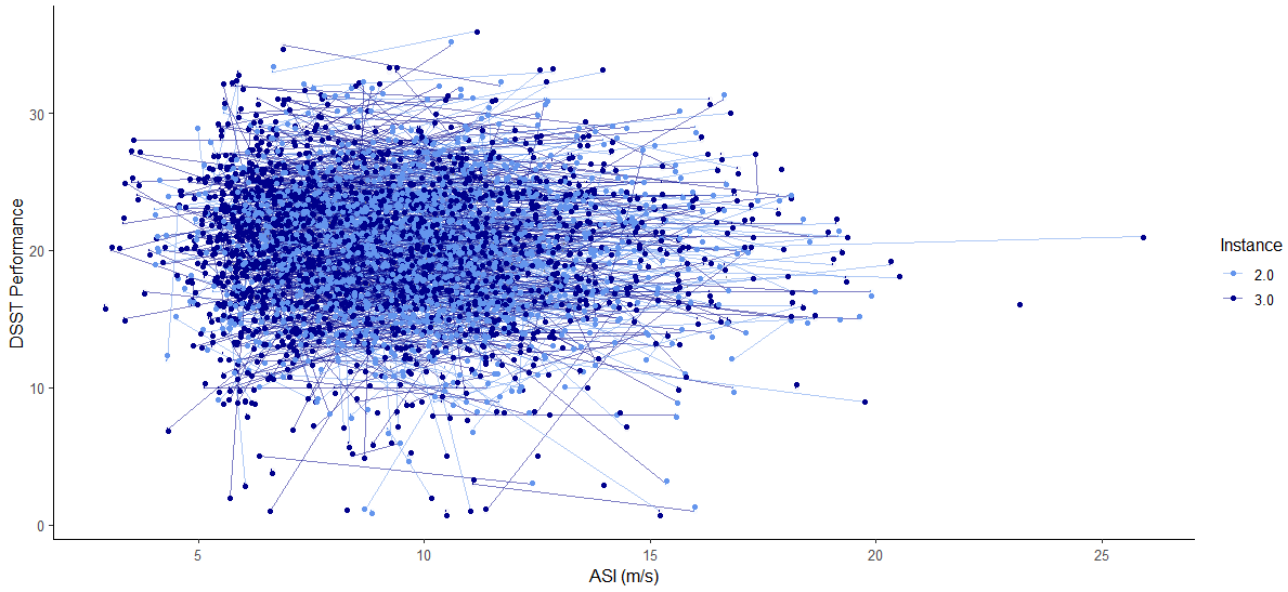

Figure 17. Association of changes in ASI (m/s) and changes in Digit Symbol Substitution Test performance over 2.5 ± 1 years (range 1.1-6.9 years). Each individual line indicates a single participant's trajectory over the two instances (instance 2.0 and 3.0) (N = 1834).

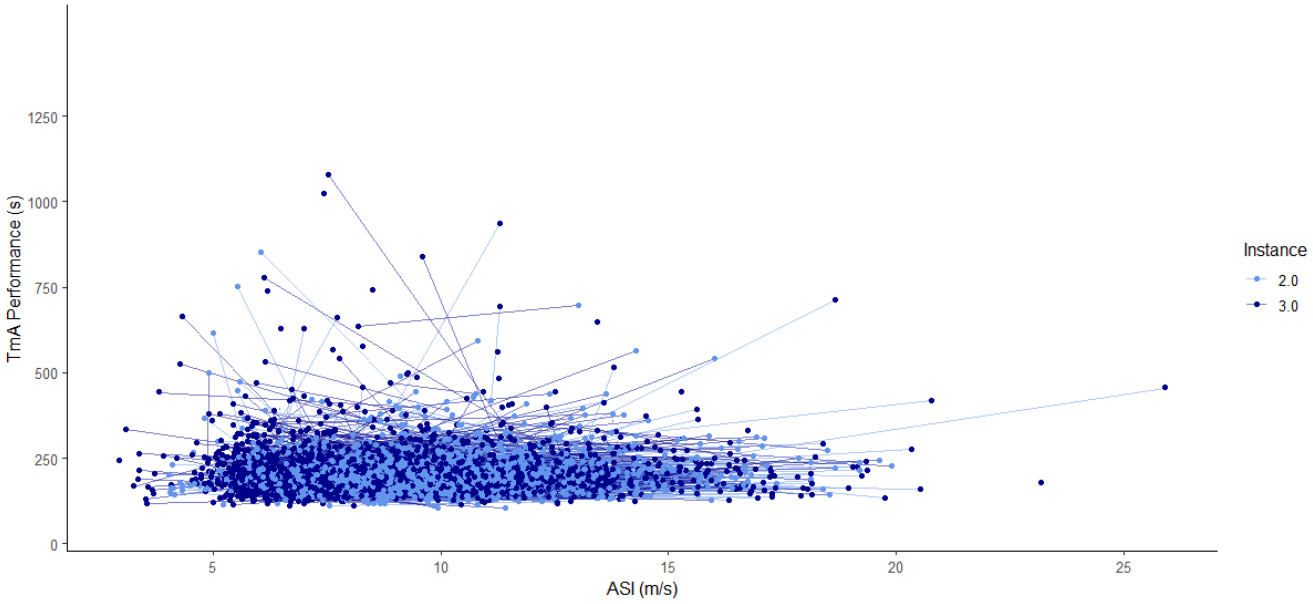

Figure 18. Association of changes in ASI (m/s) and changes in Trail Making Test part A performance over 2.5 ± 1 years (range 1.1-6.9 years). Each individual line indicates a single participant's trajectory over the two instances (instance 2.0 and 3.0) (N = 1845).

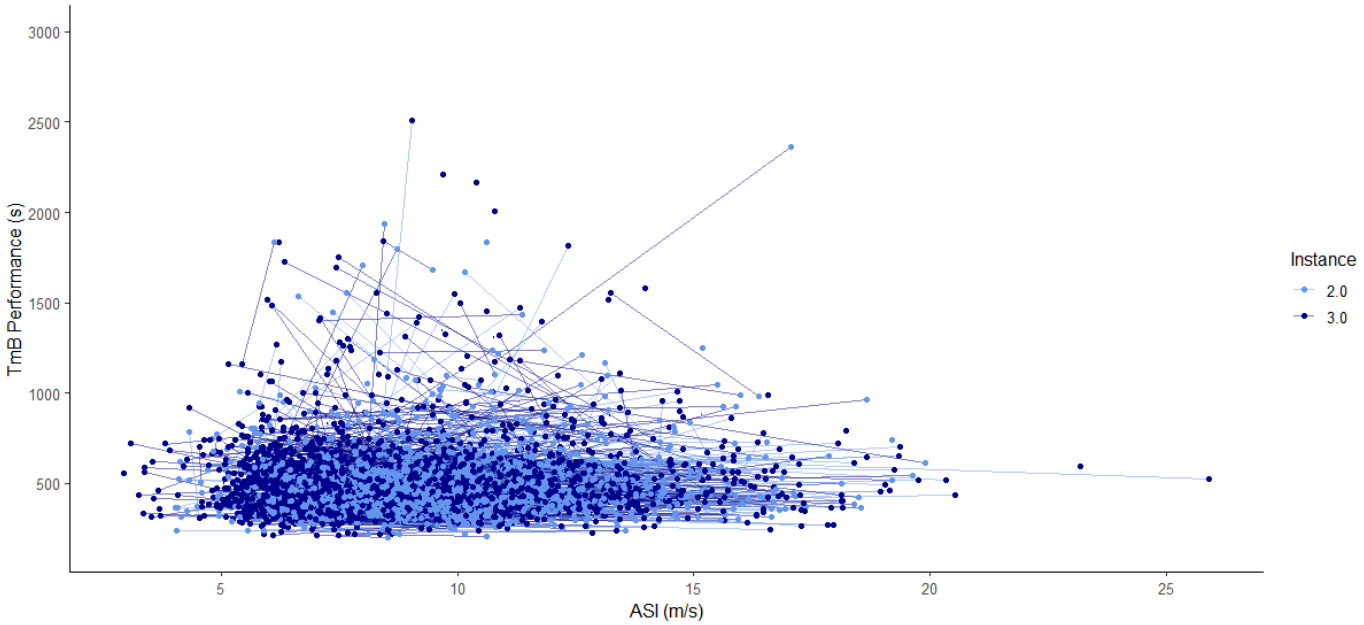

Figure 19. Association of changes in ASI (m/s) and changes in Trail Making Test Part B performance over 2.5 ± 1 years (range 1.1-6.9 years). Each individual line indicates a single participant's trajectory over the two instances (instance 2.0 and 3.0) (N = 1845).

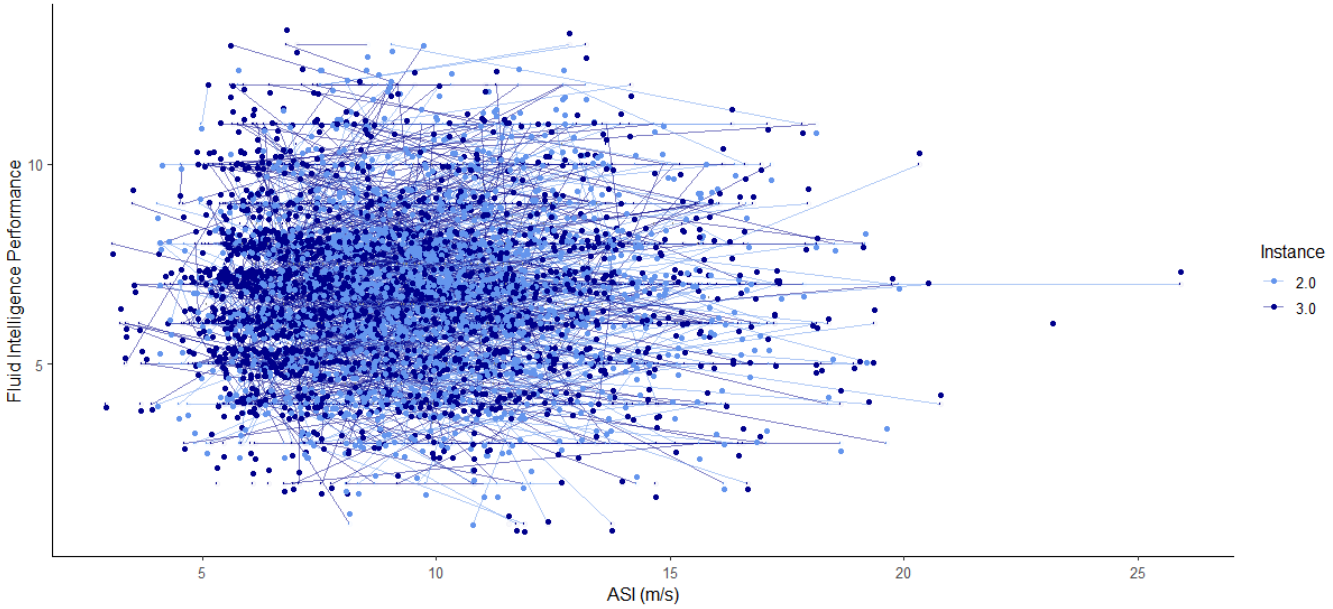

Figure 20. Association of changes in ASI (m/s) and changes in Fluid Intelligence Test performance over 2.5 ± 1 years (range 1.1-6.9 years). Each individual line indicates a single participant's trajectory over the two instances (instance 2.0 and 3.0) (N = 1835).

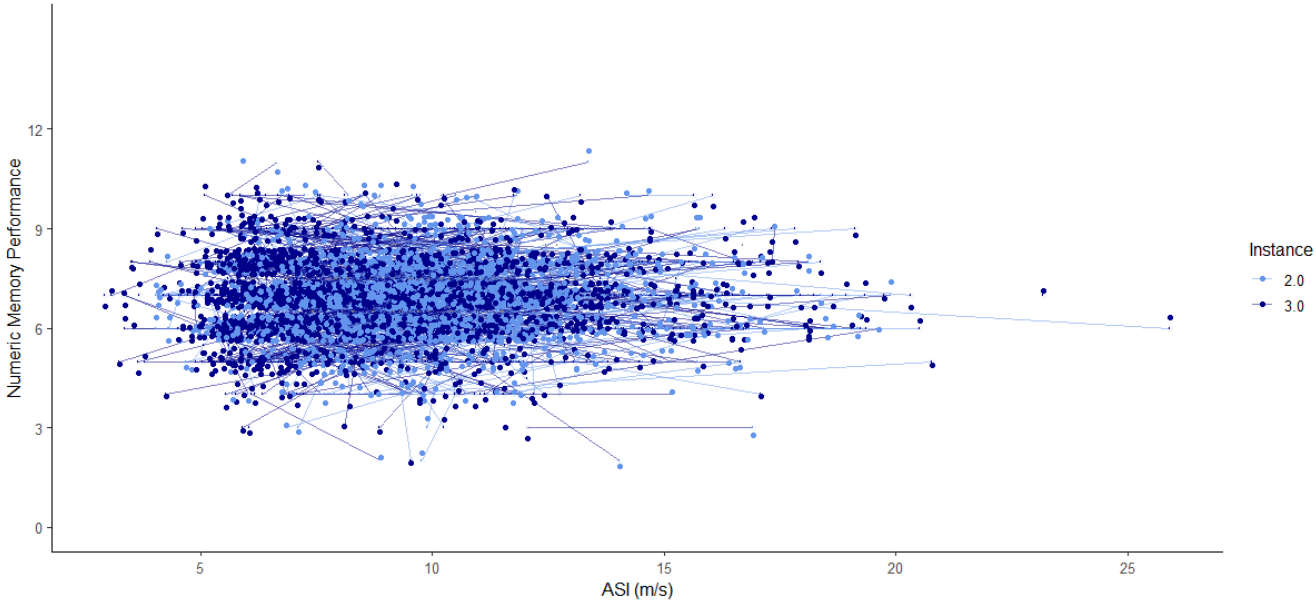

Figure 21. Association of changes in ASI (m/s) and changes Numeric Memory Test performance over 2.5 ± 1 years (range 1.1-6.9 years). Each individual line indicates a single participant's trajectory over the two instances (instance 2.0 and 3.0) (N = 1845).

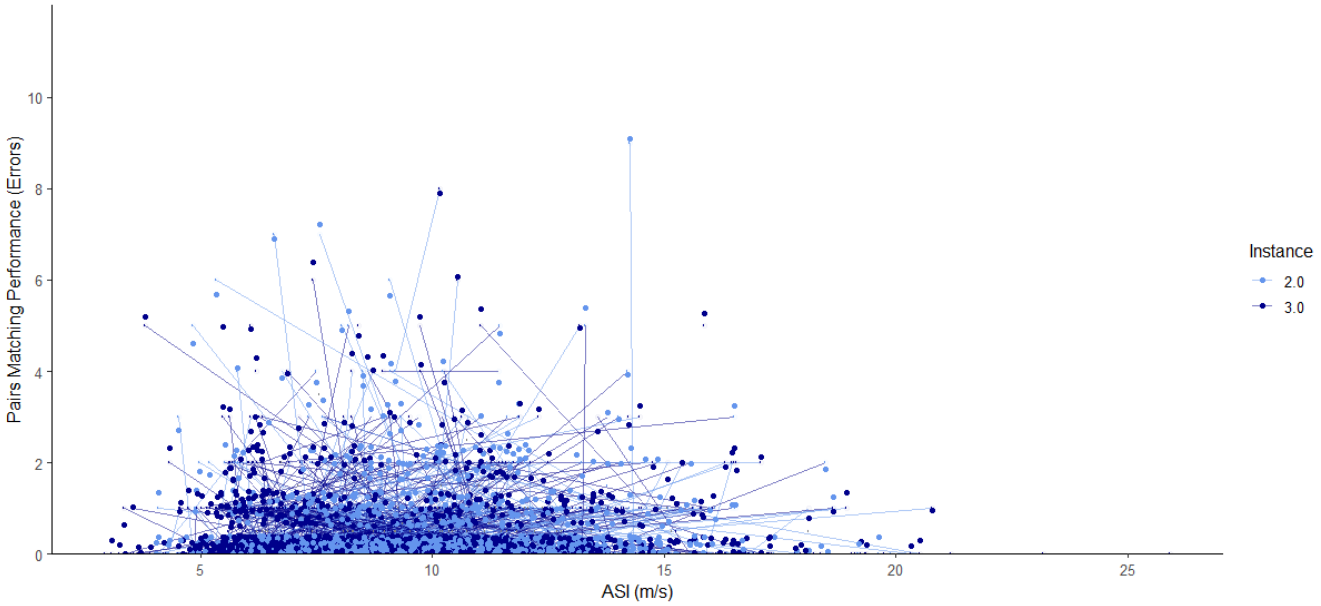

Figure 22. Association of changes in ASI (m/s) and changes in Pairs Matching Test performance over 2.5 ± 1 years (range 1.1-6.9 years). Each individual line indicates a single participant's trajectory over the two instances (instance 2.0 and 3.0) (N = 1845).

Objective 2 – Linear Regression Results

Regional grey matter (GM) cortical thickness

Following our linear regression analysis (N = 630) using baseline ASI as our independent variable and adjusting for age, our models determined that there was a significant association of baseline ASI on regional cortical thickness at the first imaging visit (8.5 ± 1.02 years post baseline) in four of 26 cortical regions prior to post-hoc correction for multiple comparisons. The regions in which there was a significant association between baseline ASI and cortical thickness at the first imaging visit included: left and right inferior parietal cortices (***p* = 0.034 and 0.049**, respectively), the right hemisphere inferior temporal cortex (***p* = 0.018**), and the left hemisphere middle temporal lobe (***p* = 0.014**). Following post-hoc correction for multiple comparisons using the Holm-Bonferroni method, there was no significant effect of baseline ASI on regional cortical thickness at the first imaging visit (8.5 ± 1.05 years follow-up from baseline). Similarly, prior to post-hoc correction there was a significant association between ASI at baseline and cortical thickness at the second imaging visit for four of 26 cortical regions including: the left hemisphere caudal middle frontal gyri (***p* = 0.023**), left and right hemisphere inferior parietal cortices (***p* = 0.028** for both regions), and the right hemisphere inferior temporal lobe (***p* = 0.012**). Following post-hoc correction for multiple comparisons using the Holm-Bonferroni method, the association between baseline ASI and cortical thickness at the second imaging visit (11± 1.02 years follow-up from baseline) remained significant in only the right hemisphere inferior temporal lobe (**adjusted *p* = 0.048**). There was a significant association between age and regional cortical thicknesses at the first imaging visit in all but four of 26 regions prior to correction (right hemisphere caudal middle frontal gyri, right hemisphere rostral anterior cingulate, bilateral hippocampus), and at the second imaging visit in all but one of 26 regions (right hemisphere rostral anterior cingulate). The

association between age and cortical thickness remained significant following post-hoc correction for multiple comparisons in all but one region for the first imaging visit (left hemisphere inferior temporal cortex) and all but four regions for the second imaging visit (right hemisphere caudal middle frontal gyri, left and right hemisphere parahippocampus, right hemisphere posterior cingulate). The raw and adjusted p values for each cortical region can be found in *Table 5.* The raw linear regression model outputs for all cortical regions can be found in *Appendix B (B1-B26)*.

Whole brain grey matter volume (GMV) and white matter hyperintensities (WMH) volume

Following linear regression analysis using baseline ASI as our independent variable and adjusting for age, it was determined that there was a significant effect of baseline ASI on whole brain GMV at both the first imaging visit (***p* = 0.015**) and the second imaging visit (***p* = 0.030**). There was a significant association between age and whole brain GMV for both imaging visits (***p* < 0.001**). In contrast, there was no effect of baseline ASI on WMH volume at either the first ($p = 0.45$) or the second ($p = 0.08$) imaging visits, however there was a significant association of age at both imaging visits (***p* < 0.001**). Raw p values for the relationship between baseline ASI and GMV and WMH at each imaging visit can be found in *Table 5*. Raw linear regression model outputs for outcomes of GMV and WMH volume can be found in *Appendix B27* and *B28,* respectively.

Cognitive performance

Following our linear regression analyses investigating the association between baseline ASI adjusted for age and cognitive outcomes, our models determined that prior to post-hoc correction, baseline ASI was only associated with Pairs Matching Test performance at the first imaging visit (***p* = 0.034)** and was not associated with performance of any cognitive tests at the second imaging

visit. Following post-hoc correction, there was no association between baseline ASI and cognitive performance for any of the tests included in analysis. There was a significant association of age on four of six cognitive tests at the first imaging visit (DSST, TmA, TmB, Pairs Matching), and on four of six cognitive tests at the second imaging visit (DSST, TmA, TmB, Numeric Memory) prior to correction. Following post-hoc correction the association between age and cognitive performance at each imaging visit remained significant in all regions except for the Numeric Memory Test performance at the second imaging visit. Raw and adjusted p values for the relationship between baseline ASI and cognitive performance at each imaging visit can be found in *Table 5*. Raw linear model outputs for each cognitive test analyzed can be found in *Appendix B (B29-B34)*.

Discussion

This is the first study to date to investigate the longitudinal role of arterial stiffness on changes in regional GM cortical thickness and builds on other work done as part of the SMART-MR study (N = 526, age 59 ± 10 years) and the Whitehall II study (N = 542 age 63.9 ± 5.2 years) who investigated the longitudinal influence of arterial stiffness on brain volumes (GMV, WMH volume)(Jochemsen et al., 2015; Suri et al., 2020) and cognitive function (Suri et al., 2020). To our knowledge, our study used the largest cohort to date (N = 1858) for investigating the longitudinal relationship between indices of arterial stiffness and both structural and functional brain outcomes. Brain structure was assessed via outcome measures of regional GM cortical thicknesses across 26 brain regions (13 per hemisphere), whole brain GMV, and WMH volume, and brain function was assessed via cognitive performance in six tests which included the Digit Symbol Substitution Test, Trail Making Test Parts A And B, Fluid Intelligence Test, Numeric

Memory Test, and Pairs Matching Test. We investigated the longitudinal influence of arterial stiffness (measured by ASI) on structural and functional brain outcomes as part of two objectives. The first objective was to determine whether changes in ASI over 2.5 ± 1 years were associated with changes in structural and functional brain outcomes. For Objective 1 we used robust linear mixed effects models to consider variability at the individual level, allowing each individual subject to be significantly different at baseline (random intercepts), as well as a different trajectory of changes in brain structure and function. The use of robust linear mixed effects models allowed us to identify and consider outliers without necessitating their exclusion by reweighing of residuals according to their distance from the model fit. Visualization of all robust linear mixed effects model fits can be found in *Appendix A*. The random effects term of individual subject added significant value to our analysis models, explaining up to 84% of the variance for changes in brain structure models including all regional GM cortical thickness models, whole brain GMV, and WMH models and as much as 60% of the variance for our brain function models which included cognitive performance for all six tests of interest. The variance explained by random effects is calculated as the difference between marginal vs conditional R^2. Full model outputs for each outcome can be found in *Appendix A and* marginal and conditional R^2 can be found at the bottom of each output table in *Appendix A*. The second objective aimed to examine whether ASI was significantly associated with brain structure and function when preceding imaging visits 1 and 2 by 8.5 ± 1.05 and 11 ± 1.02 years, respectively. For Objective 2, we used a smaller subsample of our full sample (N = 630 subjects with baseline ASI data and brain structure and function data at each imaging visit) and conducted linear regression analysis with baseline ASI as our independent variable (adjusted for age) and brain structure and function at imaging visit 1 and imaging visit 2

as our dependent variables. All linear regression model outputs for each outcome at both the first and second imaging visits can be found in *Appendix B*.

Objective 1. Longitudinal influence of ASI has a non-significant contribution to reductions in GM cortical thickness, but no effect on whole brain GMV, WMH volume or cognitive performance

In the context of GM cortical thickness, there was no statistically significant effect of ASI over the 2.5 ± 1 years between imaging visits on any of the 26 cortical regions analyzed when interpreting our findings based on adjusted p-values. However, estimates for each of our statistical models did suggest that changes in ASI was associated with non-significant reductions in cortical thickness in all regions analyzed ranging from 0.001-0.006mm change in cortical thickness per m/s increase of ASI over the 2.5 ± 1 years between imaging visits. Literature suggests that reductions in cortical thickness of approximately 0.002-0.006mm per year is a part of the normal aging process, and any reductions in cortical thickness beyond 0.006mm per year (reported as 0.06mm reduction per decade) may potentially be considered pathological (Thambisetty et al., 2010). While the influence of ASI alone was not statistically significant, taken alongside the effect of age, which was statistically significant in 25 of our 26 brain regions (range of estimates: 0.001-0.008mm reduction in cortical thickness per year), the effect of changes in ASI on cortical thickness (0.0004-0.0024mm reduction in cortical thickness per year) within the time between imaging visits may have an additive effect to drive individuals outside of the range of normal aging and potentially into a pathological range of reductions in cortical thickness. Our analyses determined the regions that were most affected by changes in ASI over 2.5 ± 1 years included the caudal anterior and caudal middle frontal gyri, the superior temporal cortex, both superior and inferior parietal

cortices, and the middle temporal lobe. This is in line with much of the literature of the effect of aging on regional cortical thickness, as the most robust changes in brain structure occur in the frontal, temporal, and parietal regions independent of pathology (Fjell et al., 2009, 2014; Ramanoël et al., 2018; Storsve et al., 2014; Thambisetty et al., 2010). Our findings of the effect of ASI on brain regions agree with the literature that points to a greater vulnerability in anterior regions within the context of changes in brain structure (Lemaitre et al., 2012). While this anterior-posterior gradient has typically been associated with age, our findings suggest this relationship may also be present related to arterial stiffness. Greater vulnerability of anterior brain regions has been suggested to be connected to the "last in-first out" theory of brain aging, suggesting that later maturing brain regions responsible for higher order cognitive tasks are the most vulnerable (Fjell et al., 2014). We observed significant sex differences in the rate of cortical thinning in 10 cortical regions, including frontal, parietal, parahippocampal, temporal regions, and occipital regions. These regions demonstrating sex differences in the rate of cortical thinning are consistent with the findings from Thambisetty *et al.,* (N = 66), as well as Driscoll *et al*., (N = 138) who similarly found pronounced sex differences in the rate of cortical thinning in the frontal, parietal, postcentral, parahippocampal, and temporal regions (Driscoll et al., 2009; Thambisetty et al., 2010). In both studies, they observed that in all regions in which sex differences were detected, all regions indicated that males had greater rates of cortical atrophy compared to females. Where our findings deviate from the findings from the two studies mentioned above is that we observed a greater rate of cortical thinning in frontal, temporal, and occipital regions in males compared to females, while females demonstrated a greater rate of cortical thinning in parietal and hippocampal regions. It is important to note that any sex-based differences observed in the current study should be interpreted

with caution, as we did not specifically design our analyses to detect sex differences by using sex-stratified analyses, and rather included sex as a covariate in our models.

We also found a significant effect of waist to hip ratio in four right hemisphere cortical regions including the caudal anterior cingulate, caudal middle frontal gyri, rostral middle frontal gyri, and lateral occipital lobe. While there was only a significant effect of waist to hip ratio in four cortical regions, our findings partially support the findings from Kim et al., (N = 1777) who observed an inverted U-shaped association between waist to hip ratio and cortical thickness, particularly in the frontal cortical regions (Kim et al., 2015). Seemingly, the inverted U-shaped relationship between waist to hip ratio also exists in other metrics of abdominal obesity, as found in work by Cho and colleagues, who observed a similar relationship when examining the relationship between visceral fat and cortical thickness (Cho et al., 2021).

For whole brain grey matter volume, there was no observed effect of changes in ASI over the 2.5 ± 1 years between imaging visits. The relationship between arterial stiffness and lower brain volumes has been frequently observed cross-sectionally, however the longitudinal relationship between the two remains controversial. Both the SMART-MR and Whitehall II study each had both longitudinal and cross-sectional components. Our findings support the longitudinal findings from SMART-MR, in which there was no significant relationship between arterial stiffness and the progression of whole brain grey matter atrophy over a duration of 4 years (Jochemsen et al., 2015). Our findings are also in line with the longitudinal findings from the Whitehall II imaging study, in which there was no longitudinal association between arterial stiffening and total GM

density (Suri et al., 2020). In contrast, cross-sectional literature suggests that there is indeed an association between indices of vascular stiffness and whole brain volume. Tsao and colleagues observed a significant association between PWV and total brain volume that was equivalent to 1.2 years of aging (Tsao et al., 2013). Mitchell and colleagues observed a similar relationship between indices of arterial stiffness and whole brain GMV, in which elevations in pulsatility index were associated with significantly reduced GMV (Mitchell et al., 2011). One possible reason for the discrepancy in the literature is that the present study and both the SMART-MR and Whitehall II studies were, at least partially, longitudinal in nature (follow up over 2.5 ± 1 year, 4.1 ± 0.55 years, and 4 years respectively), while the other studies referenced were cross-sectional associations (Jochemsen et al., 2015; Suri et al., 2020; Tsao et al., 2013; Mitchell et al., 2011). The cross-sectional component of the SMART-MR study also observed a significant association between arterial stiffness and total GMV. While in the present study there was no significant effect of ASI on whole brain GMV over the time interval between imaging visits, there was a significant effect of age independently (***p* < 0.001**). Our model estimates suggested that per year increase in age there was an associated 3.599mL reduction in whole brain GMV. These estimates are comparable to findings from Lemaitre *et al.,* in which there was an observed 3.68mL reduction in whole brain GMV per year in otherwise healthy older adults, and when expressed as a percent reduction in whole brain GMV (~0.45%), fall into the normal range of relative reductions in whole brain GMV believed to be within the range of 0.2-0.7% per year (Lemaitre et al., 2012; Enzinger et al., 2005; Scahill et al., 2003; Sluimer et al., 2008). Our findings also suggested that men had a significantly steeper decline in GMV over time when compared to women, which is in agreement with much of the literature (Armstrong et al., 2019; Driscoll et al., 2009; Pacheco et al., 2015). Our findings of a significant association between waist to hip ratio and whole brain GMV are also in line with

what is typically observed in the literature, which suggests that elevations in abdominal obesity across metrics of BMI, waist to hip ratio or body fat percentage are associated with lower whole brain GMV (Debette et al., 2014; Hamer & Batty, 2019).

There was no significant effect of changes in ASI on WMH volume over the 2.5 ± 1 years between imaging visits, and similar to the findings for GMV, this contributes to the inconsistent findings across the literature. Cross-sectionally, Mitchell *et al.,* and Tsao and *et al.,* both found a significant association between cfPWV and elevations in WMH volume, with their statistical models estimating a 0.1mL and a 0.05mL increase in WMH volume per SD increase in cfPWV, respectively (Mitchell et al., 2011; Tsao et al., 2013). Our findings resemble the longitudinal findings from the SMART-MR and Whitehall II studies in which there was no association between arterial stiffness and increased WMH volume over the 4-year duration of both studies (Jochemsen et al., 2015; Suri et al., 2020). We did however observe a significant effect of age on WMH volume, in which our model estimates a 0.167mL increase in WMH volume per year increase in age. This model estimate falls within the consensus range across the literature of ~0-0.4mL increase in WMH per year associated with normal aging (Ramirez et al., 2016; Garde et al., 2005; Kramer et al., 2007; Raz et al., 2012; Silbert et al., 2008; Wolfson et al., 2013). Our models did not identify any effect of sex on explaining the variance in the WMH volumes for this cohort of individuals. This finding is inconsistent with much of the literature pointing to a trend that otherwise healthy elderly women typically demonstrate a greater progression of WMH volume compared to men (Fatemi et al., 2018; van den Heuvel et al., 2004; van Dijk et al., 2008). Our models did identify a significant effect of waist to hip ratio on WMH progression (***p* < 0.001**), which confirms and extends the literature that points to obesity and visceral adiposity as an independent predictor of

WMH progression (Kim et al., 2017; Lampe et al., 2019; Yamashiro et al., 2014). Following the additional analysis of the subset with WMH volume <15mL, we observed no change in the relationship between changes in ASI and WMH volume (p = 0.83). Visualization of the relationship between changes in ASI and WMH volume in both the full cohort model and the model with WMH volume <15mL can be seen in *Figure 15* and *Figure 16*, respectively.

The relationship between arterial stiffness and cognitive function has been reported previously (Alvarez-Bueno et al., 2020). In the present study, we did not identify any relationship between changes in ASI and cognitive performance across the six tests included in analysis over the time interval between imaging visits. The absence of an observed relationship between the rate of arterial stiffening and cognitive function in our study is in line with recent work conducted as part of the Whitehall II imaging study, in which changes in aortic stiffness were not related to cognitive function (Suri et al., 2020). The domain in which changes in ASI over 2.5 ± 1 years had the largest effect was the domain of fluid intelligence, which does not corroborate much of the literature that suggests executive function is the domain that is most vulnerable to elevations in arterial stiffness and vascular aging cross-sectionally, a domain in which we observed no effect of changes in ASI over the time interval between imaging visits (Mitchell et al., 2011; Nilsson et al., 2014). Other studies (Rotterdam study and the Sydney Memory and Ageing Study) investigating the longitudinal influence of arterial stiffness on cognitive function agree with our findings, in which no relationship between changes in arterial stiffness and cognitive function across several domains including attention, memory, and executive function were identified (Poels et al., 2007; Singer et al., 2013), whereas work as part of the Framingham cohort study did identify an association between aortic stiffness and cognitive performance in the domains of processing speed and

executive function (Pase et al., 2016). While there was no significant effect of the change in ASI on cognitive performance for any of our six tests included in analysis, as expected, and frequently reported in the literature, following post-hoc correction there was a significant effect of age for five of six tests analyzed over the duration of 2.5 ± 1 years between imaging visits (Cornelis et al., 2019; Harada et al., 2013). Our robust linear mixed models did identify a significant impact of sex on 4 of 6 tests analyzed including the TmA, Fluid Intelligence Test, Numeric Memory Test, And Pairs Matching Test. Evidence from the literature suggests that females maintain superior cognitive performance in the domains of reasoning, memory, verbal recognition, perceptuomotor speed and integration, and semantic fluency with advancing age compared to males, whereas males typically have greater performance in executive function and visuospatial tasks with advancing age (De Frias et al., 2006; McCarrey et al., 2016; Nichols et al., 2020). Our findings point to males exhibiting a steeper decline in cognitive functions in the domains of executive function, visuospatial ability, and processing speed (TmA), as well as episodic memory (Pairs Matching). In contrast, females showed a steeper decline in cognitive function in the domains of fluid intelligence, verbal logic, and reasoning (Fluid Intelligence Test) and short-term memory (Numeric Memory Test). These findings of the effect of sex as it pertains to cognitive function are largely in conflict with much of the literature directly investigating sex-based differences in cognitive function (Lee et al., 2022). The interpretability of our sex-difference observations is somewhat limited as sex was only included as a covariate, and no specific analyses to uncover sex differences were conducted. We also found a significant effect of waist to hip ratio in four of six cognitive tests analyzed (DSST, Fluid Intelligence Test, Numeric Memory Test, Pairs Matching Test). The association between indices of abdominal obesity and cognitive function has been

reported frequently in the literature, and our findings corroborate the existence of this association (Liu et al., 2019; Zhang et al., 2018).

Objective 2. Baseline ASI is associated with lower whole brain GMV, but not regional GM cortical thickness, WMH volume, or cognitive performance over a follow-up of 8-11 years.

We observed a significant association between baseline ASI and grey matter cortical thickness in four regions at the first imaging visit (8.5 ± 1.05 years post baseline) and four regions at the second imaging visit (11 ± 1.02 years post baseline) prior to post-hoc correction for multiple comparisons. Following post-hoc correction none of those associations remained significant except for the right hemisphere inferior temporal lobe at the second imaging visit. The regions in which there was an association detected included primarily frontal, temporal, and parietal cortical regions. Much of the literature suggests that these regions are also the most vulnerable to age-related atrophy (Fjell et al., 2009, 2014; Ramanoël et al., 2018; Storsve et al., 2014; Thambisetty et al., 2010). According to model estimates, each m/s increase in baseline ASI independently contributed to a non-significant reduction in cortical thickness ranging from 0.001-0.005mm 8-11 years later. We also detected a significant effect of baseline ASI after adjusting for age on whole brain GMV at both the first (***p* = 0.015**) and second (***p* = 0.03**) imaging visits. For the first and second imaging visits, our model estimates suggests that each m/s increase in baseline ASI contributed to a 1.330 and a 1.153mL reduction in whole brain GMV, respectively. We did not observe any significant association between baseline ASI on WMH volume at either imaging visit. These findings agree with the finding from the Whitehall II study in which no significant association between arterial stiffness and brain structure when PWV preceded brain measurements by 5.9 ± 1.4 years (Suri et al., 2020). Taken together, our findings do not suggest that there is a temporal lag between the

expression of arterial stiffness and future changes in GM cortical thickness or WMH volume, and this relationship is still likely primarily mediated by natural age-related changes in brain structure. While there was no statistical association between baseline ASI and GM cortical thickness or WMH volume approximately a decade later, there was a significant effect of baseline ASI on whole brain GMV. The effect of baseline ASI on future whole brain GMV may be of interest, as grey matter atrophy beyond what would be expected in normal aging by even marginal amounts, may lead to neurological complications such as impaired cognitive function (Arvanitakis et al., 2016; Pasha et al., 2015; Soriano-Raya et al., 2012).

Much like most of the structural outcomes analyzed, there was no significant association of baseline ASI and cognitive performance 8-11 years later in the current study. Our observations of no association between baseline ASI and cognitive performance are in contrast with the findings from the Whitehall II study, which observed a significant association of baseline PWV and cognitive performance 5.9 ± 1.4 years post baseline assessment (Suri et al., 2020). The Whitehall II study found that baseline PWV was related to impaired cognitive performance, largely driven by semantic fluency and verbal learning (Suri et al., 2020). The Whitehall II study similarly saw no longitudinal association of the rate of arterial stiffening and changes in cognitive function (Objective 1), but instead a relationship between arterial stiffening and cognitive performance when the stiffness measure preceded the cognitive assessments (Objective 2). Our findings suggest that when correcting for age, there was no effect of baseline ASI on cognitive performance. Taken together, our findings as well as the findings from the Whitehall II study supports the growing understanding that long-term chronic exposure to vascular aging or pathology in the years

preceding older adulthood, rather than late-life vascular aging, may be more representative of stiffness related cognitive decline (Livingston et al., 2020; Suri et al., 2020).

Strengths and Limitations

Strengths

There are several strengths to the current study. This is the first study to investigate the longitudinal relationship between arterial stiffness on regional GM cortical thicknesses and builds on previous work looking at arterial stiffness on whole brain GMV, WMH and cognitive performance. Furthermore, this is the first study to assess longitudinal changes of arterial stiffness on structural (regional GM cortical thickness, GMV, WMH volumes) and functional (cognitive performance) in a single cohort of individuals. Via the UK Biobank, we were able to test the relationship between changes in ASI and brain structure and function in a large sample of 1858 healthy subjects (age 61 ± 7 years). Beyond the large sample size, the longitudinal nature of the UK Biobank dataset allowed us to track changes in outcomes within subjects over 2.5 ± 1 years for our linear mixed effects models (Objective 1) and for up to 11 ± 1.02 years in our linear models (Objective 2). The UK Biobank is a multicenter study, and thereby strengthens the work in the current study as it includes subjects from across the UK, as opposed to a community dwelling cohort which may limit generalizability. Another strength of the present study is the use of *a priori* simulation-based power calculations by creating a mock dataset with expected differences in outcome values extracted from literature. We based our power calculations around conservative changes in effects of interest that reflected the changes expected to be a product of the normal aging process. Despite using conservative changes in outcomes over time for the mock dataset, we were still sufficiently powered at N = 1858 to detect true effects where they might exist for all outcomes of interest. In

addition, using robust linear mixed effects models we were able to fit each individual subject as random effects, allowing us to consider the variability at the individual subject level and significantly improved the amount of variance explained by our statistical models. The use of robust models as opposed to a standard linear mixed effects model meant we were also able to handle and consider outliers without their removal from the sample. This was done by reweighing different outliers based on their deviance from the model fits for each outcome (*Appendix A*). The inclusion of covariates of age, sex, waist to hip ratio, years between visits, and physical activity allowed us to explain more variance in our statistical models and assess the independent effect of changes in ASI over time more accurately.

Limitations

There were several limitations to the current study. Despite the utility in using mock data for estimating sample size, all the effect sizes used to create the mock dataset were unidirectional, (i.e., trended in the direction that is representative of the overall relationship for each variable). For example, GMV decreased on average ~3mL per timepoint for each individual subject in the mock dataset. While relevant for the detection of our conservative effects of interest (reductions in cortical thickness), this approach does not accurately model the variability of individual subjects across all variables. Future work should attempt to create more random variation in mock data, where values can increase, decrease, or stay the same to more accurately represent longitudinal changes that would be observed in a real large-scale cohort study such as the UK Biobank. However, regardless of the unidirectionality of the effect sizes used in the mock data, we still included a much higher sample size than what was required for all variables as illustrated by our sample size calculations.

Other limitations include the use of ASI over PWV as a measure of arterial stiffness. While ASI is a more feasible approach for a large-scale cohort like the UK Biobank study due to its quick and uncomplicated administration requiring little to no training, we nonetheless interpret our results with caution as our independent variable was not measured using the gold standard approach of PWV. Another potential limitation in the generalizability of the current study is the use of WMH volume as a primary outcome measure. Some evidence suggests that WMH can be ill-defined and imaging abnormalities have potential to be misclassified as lesions therefore confounding results and reducing the validity of the WMH volume measures. Furthermore, some findings suggest that WMH can get smaller or disappear over time, once again pointing to reduced validity of WMH volume as a measure of permanent and clinically meaningful cerebral white matter damage (Wardlaw et al., 2015).

Another limitation is the use of only two time points for all imaging and cognitive data. While we were able to track subjects over time, additional data would improve interpretability of findings related to the association between arterial stiffness and brain health. While sex was considered by its inclusion as a covariate for the linear mixed effects model analyses, the effect of sex is limited in its interpretability in the present work as we did not run a sex-specific analysis (i.e., stratify by sex). The inclusion of physical activity as a covariate, while justified, may be somewhat limited in its ability to truly explain the relationship between physical activity and the progression of changes in brain structure and function. The physical activity variable used in the present study was a self-report measure and only represented the frequency (days per week) of moderate physical activity

of 10+ minutes per day. A more empirical and physiologically relevant measure such as metabolic equivalent (MET) or volume of oxygen consumption (VO_2) may be more accurate assessment of the role physical activity plays on the progression of brain aging.

We also did not consider ethnicity, education, or socioeconomic status, which all may have been useful inclusions as covariates in our statistical models. There is precedence for differences in arterial stiffness across ethnicities, and inclusion of ethnicity in statistical models may aid in discerning potential ethnic differences in the relationship between arterial stiffness and brain health (Snijder et al., 2015). The same can be said for education and socioeconomic status, as both have been well established as predictors of all-cause cardiovascular risk (Stringhini et al., 2017; Dégano et al., 2017). Our selection of cortical regions included in analyses, while justified based on cognitive domains of interest, may have also overlooked the potential relationship between arterial stiffness and grey matter atrophy in regions not included in the present study.

Future Work

The UK Biobank and other longitudinal cohort studies of the same nature are constantly growing and expanding on the scope of the studies. Future work should aim to investigate additional timepoints to deepen the current understanding of how normal age-related arterial stiffening affects brain structure and function over a longer range of years. The UK Biobank continues to add data to the database and the addition of follow up imaging data will only bolster the current understanding of the longitudinal relationships between vascular and brain health. Additional UK Biobank imaging data that is released can add valuable insight into the trajectory of changes in

brain structure, as a third imaging visit would be ~8 years after the first imaging visit and ~16 years post baseline. Longitudinal data spanning nearly two decades provides a unique opportunity to track the same individuals and significantly expand on our current understanding of the links between vascular function and the trajectory of brain aging.

Future work should also aim to consider different levels of WMH even within a healthy subset. Despite filtering and only including healthy subjects, there was a wide range of observed WMH volumes in the current cohort. Greater consideration into what a healthy aging brain may look like in the context of WMH volume may provide a more nuanced look at the role of vascular health in otherwise healthy subjects. Additionally, using a measure of susceptibility weighted images (SWI) over WMH volume could provide critical information on the state of brain structure, microbleeds and white matter integrity in future studies. Available as part of the UK Biobank database, SWI is an MRI sequence that has garnered significant clinical support for lesion visualization (Tate et al., 2017). SWI is suggested to be a more precise approach for the detection of small microbleeds, and can be up to six times more sensitive in the detection of subtle lesions, microbleeds, or axonal injury when compared to other sequencing approaches (Tate et al., 2017; Tong et al., 2003).

Future longitudinal studies should also aim to use a more validated measurement approach than ASI. Using a gold-standard approach for the measurement of arterial stiffness such as tonometry or MRI derived PWV can increase validity and provide a stronger measure of arterial stiffness, potentially yielding additional insight into the relationship between vascular aging and brain structure and function. Additionally, focusing on and directly investigating sex differences that

may exist within the relationship of vascular health and brain aging both pre- and post-menopause is an important area that should be studied further, as evidence suggests arterial stiffness is drastically increased in women-post menopause (Zaydun et al., 2006). Finally, future studies should aim to include a more diverse sample, including different ethnic and socioeconomic backgrounds, as well as those who are living with diseases that have been identified as risk factors for vascular or neurological pathology to deepen the understanding of the relationship between vascular and brain health in unique populations.

Key Findings

Overall, our findings suggest that there is a non-significant effect of arterial stiffness on brain aging both structurally (through regional GM cortical thicknesses, whole brain GMV and WMH) and functionally (through six cognitive tests). Our findings of an anterior region vulnerability bias as well as our individual model estimates for the role of arterial stiffness on structural changes in the brain suggest that arterial stiffness may contribute to accelerate brain aging compared to the normal aging process. Elevations in ASI contributed to cortical thinning equivalent to up to ~30% of the annual rate of cortical thinning associated with age observed in our model estimates (ASI contributed to 0.0004-0.0024mm reduction in GM cortical thickness per year; age contributed to 0.001-0.008mm reduction in GM cortical thickness per year). As such, late-life arterial stiffening taken alongside the effect of age may have an additive effect and drive individuals beyond the normal age-related rate into pathological ranges of cortical thinning. Atrophy of grey matter beyond the rate associated with normal aging may put individuals at a greater risk for the development of cognitive impairment or the progression of neurodegenerative disease including vascular dementia, Parkinson's disease, and Alzheimer's disease. We found no association

between either the progression of arterial stiffness (Objective 1) or arterial stiffness at baseline (Objective 2) and WMH volume in the present study. After adjusting for age, our models determined that most changes in WMH volume were driven by age in both our longitudinal and cross-sectional analyses. Similarly, we found that there was no association between changes in and cognitive performance across six tests longitudinally, and no association of baseline ASI on cognitive assessment after 8-11 years post-baseline after adjusting for effects of age. Taken together, we propose that arterial stiffness may have an additive effect when taken together with age-related declines in cortical thickness to drive individuals outside of the range of grey matter atrophy that is part of the normal aging process, while changes in WMH volume and declines in cognitive performance seem to be driven primarily by age. Finally, while changes in ASI were not associated with reductions in GMV longitudinally, there was a significant association between baseline ASI and GMV 8-11 years later, even after adjusting for effects of age, suggesting that the relationship between arterial stiffness and whole brain grey matter atrophy may potentially be more time dependent, requiring long-term chronic exposure to elevations in arterial stiffness.

Conclusion

To our knowledge, we have provided the first evidence of the independent role of arterial stiffening on longitudinal changes in regional GM cortical thickness. We also provide additional insight into the independent effect of arterial stiffening on brain structure and function in healthy middle- and older aged adults, extending previous work. The findings from the present study suggest that in otherwise healthy middle- to older-aged adults from the UK Biobank cohort, there is a minimal effect of arterial stiffness on brain structure and function both longitudinally over 2.5 ± 1 years and when measures of arterial stiffness preceded brain measures by 8-11 years. We also find that

in otherwise-healthy subjects, changes in brain structure and function are primarily a product of aging, not indices of arterial stiffness. The association of arterial stiffness and total grey matter volume nearly a decade later may suggest that changes in global brain structure are the product of prolonged, chronic exposure to vascular pathology rather than acute changes. The delayed relationship between arterial stiffness and whole brain grey matter volume may be indicative of the subclinical nature of arterial stiffness measures and could point to a potential treatment window for the onset of arterial stiffness and subsequent expression of structural changes within the brain.

REFERENCES

Alfaro-Almagro, F., Jenkinson, M., Bangerter, N. K., Andersson, J. L. R., Griffanti, L., Douaud, G., Sotiropoulos, S. N., Jbabdi, S., Hernandez-Fernandez, M., Vallee, E., Vidaurre, D., Webster, M., McCarthy, P., Rorden, C., Daducci, A., Alexander, D. C., Zhang, H., Dragonu, I., Matthews, P. M., … Smith, S. M. (2018). Image processing and Quality Control for the first 10,000 brain imaging datasets from UK Biobank. *NeuroImage*, *166*, 400–424. https://doi.org/10.1016/j.neuroimage.2017.10.034

AlGhatrif, M., Strait, J. B., Morrell, C. H., Canepa, M., Wright, J., Elango, P., Scuteri, A., Najjar, S. S., Ferrucci, L., & Lakatta, E. G. (2013). Longitudinal trajectories of arterial stiffness and the role of blood pressure: The Baltimore Longitudinal Study of Aging. *Hypertension (Dallas, Tex. : 1979)*, *62*(5), 934–941. PubMed. https://doi.org/10.1161/HYPERTENSIONAHA.113.01445

Alosco, M. L., Gunstad, J., Xu, X., Clark, U. S., Labbe, D. R., Riskin-Jones, H. H., Terrero, G., Schwarz, N. F., Walsh, E. G., Poppas, A., Cohen, R. A., & Sweet, L. H. (2014). The Impact of Hypertension on Cerebral Perfusion and Cortical Thickness in Older Adults. *Journal of the American Society of Hypertension : JASH*, *8*(8), 561–570. https://doi.org/10.1016/j.jash.2014.04.002

Armstrong, N. M., An, Y., Beason-Held, L., Doshi, J., Erus, G., Ferrucci, L., Davatzikos, C., & Resnick, S. M. (2019). Sex differences in brain aging and predictors of neurodegeneration in cognitively healthy older adults. *Neurobiology of Aging*, *81*, 146–156. https://doi.org/10.1016/j.neurobiolaging.2019.05.020

Arsalidou, M., Pawliw-Levac, M., Sadeghi, M., & Pascual-Leone, J. (2018). Brain areas associated with numbers and calculations in children: Meta-analyses of fMRI studies.

Developmental Cognitive Neuroscience, *30*, 239–250. https://doi.org/10.1016/j.dcn.2017.08.002

Arvanitakis, Z., Fleischman, D. A., Arfanakis, K., Leurgans, S. E., Barnes, L. L., & Bennett, D. A. (2016). Association of white matter hyperintensities and gray matter volume with cognition in older individuals without cognitive impairment. *Brain Structure and Function*, *221*(4), 2135–2146. https://doi.org/10.1007/s00429-015-1034-7

Baddeley Alan. (1992). Working Memory. *Science*, *255*(5044), 556–559. https://doi.org/10.1126/science.1736359

Badji, A., Sabra, D., Bherer, L., Cohen-Adad, J., Girouard, H., & Gauthier, C. J. (2019). Arterial stiffness and brain integrity: A review of MRI findings. *Ageing Research Reviews*, *53*, 100907. https://doi.org/10.1016/j.arr.2019.05.001

Bates, D., Mächler, M., Bolker, B., & Walker, S. (2015). Fitting Linear Mixed-Effects Models Using lme4. *Journal of Statistical Software*, *67*(1), 1–48. https://doi.org/10.18637/jss.v067.i01

Belz, G. G. (1995). Elastic properties and Windkessel function of the human aorta. *Cardiovascular Drugs and Therapy*, *9*(1), 73–83. https://doi.org/10.1007/BF00877747

Beres, C. A., & Baron, A. (1981). Improved Digit Symbol Substitution by Older Women as a Result of Extended Practice1. *Journal of Gerontology*, *36*(5), 591–597. https://doi.org/10.1093/geronj/36.5.591

Bowie, C. R., & Harvey, P. D. (2006). Administration and interpretation of the Trail Making Test. *Nature Protocols*, *1*(5), 2277–2281. https://doi.org/10.1038/nprot.2006.390

Buck, S., Bastos, F., Baldeweg, T., & Vargha-Khadem, F. (2021). The Pair Test: A computerised measure of learning and memory. *Behavior Research Methods*, *53*(2), 928–942. https://doi.org/10.3758/s13428-020-01470-9

Calabia, J., Torguet, P., Garcia, M., Garcia, I., Martin, N., Guasch, B., Faur, D., & Vallés, M. (2011). Doppler ultrasound in the measurement of pulse wave velocity: Agreement with the Complior method. *Cardiovascular Ultrasound*, *9*, 13–13. PubMed. https://doi.org/10.1186/1476-7120-9-13

Castaneda, D., Esparza, A., Ghamari, M., Soltanpur, C., & Nazeran, H. (2018). A review on wearable photoplethysmography sensors and their potential future applications in health care. *International Journal of Biosensors & Bioelectronics*, *4*(4), 195–202. PubMed. https://doi.org/10.15406/ijbsbe.2018.04.00125

Cecelja, M., & Chowienczyk, P. (2009). Dissociation of Aortic Pulse Wave Velocity With Risk Factors for Cardiovascular Disease Other Than Hypertension. *Hypertension*, *54*(6), 1328–1336. https://doi.org/10.1161/HYPERTENSIONAHA.109.137653

Chae, C. U., Pfeffer, M. A., Glynn, R. J., Mitchell, G. F., Taylor, J. O., & Hennekens, C. H. (1999). Increased pulse pressure and risk of heart failure in the elderly. *JAMA*, *281*(7), 634–639. https://doi.org/10.1001/jama.281.7.634

Chen, P.-Y., Chen, C.-L., Hsu, Y.-C., & Tseng, W.-Y. I. (2020). Fluid intelligence is associated with cortical volume and white matter tract integrity within multiple-demand system across adult lifespan. *NeuroImage*, *212*, 116576. https://doi.org/10.1016/j.neuroimage.2020.116576

Cho, J., Seo, S., Kim, W.-R., Kim, C., & Noh, Y. (2021). Association Between Visceral Fat and Brain Cortical Thickness in the Elderly: A Neuroimaging Study. *Frontiers in Aging Neuroscience*, *13*. https://doi.org/10.3389/fnagi.2021.694629

Chutinet, A., & Rost, N. S. (2014). White matter disease as a biomarker for long-term cerebrovascular disease and dementia. *Current Treatment Options in Cardiovascular Medicine*, *16*(3), 292–292. PubMed. https://doi.org/10.1007/s11936-013-0292-z

Cochrane, A., Simmering, V., & Green, C. S. (2019). Fluid intelligence is related to capacity in memory as well as attention: Evidence from middle childhood and adulthood. *PloS One*, *14*(8), e0221353–e0221353. PubMed. https://doi.org/10.1371/journal.pone.0221353

Cornelis, M. C., Wang, Y., Holland, T., Agarwal, P., Weintraub, S., & Morris, M. C. (2019). Age and cognitive decline in the UK Biobank. *PloS One*, *14*(3), e0213948–e0213948. PubMed. https://doi.org/10.1371/journal.pone.0213948

Dale, A. M., Fischl, B., & Sereno, M. I. (1999). Cortical Surface-Based Analysis: I. Segmentation and Surface Reconstruction. *NeuroImage*, *9*(2), 179–194. https://doi.org/10.1006/nimg.1998.0395

Darwich, M. A., Langevin, F., & Darwich, K. (2015). Local Pulse Wave Velocity Estimation in the Carotids Using Dynamic MR Sequences. In *Journal of Biomedical Science and Engineering: Vol. Vol.08No.04* (p. 10).

De Frias, C. M., Nilsson, L.-G., & Herlitz, A. (2006). Sex differences in cognition are stable over a 10-year period in adulthood and old age. *Aging, Neuropsychology, and Cognition*, *13*(3–4), 574–587.

Debette, S., & Markus, H. S. (2010). The clinical importance of white matter hyperintensities on brain magnetic resonance imaging: Systematic review and meta-analysis. *BMJ (Clinical Research Ed.)*, *341*, c3666–c3666. PubMed. https://doi.org/10.1136/bmj.c3666

Debette, S., Wolf, C., Lambert, J.-C., Crivello, F., Soumaré, A., Zhu, Y.-C., Schilling, S., Dufouil, C., Mazoyer, B., Amouyel, P., Tzourio, C., & Elbaz, A. (2014). Abdominal obesity and lower gray matter volume: A Mendelian randomization study. *Neurobiology of Aging*, *35*(2), 378–386. https://doi.org/10.1016/j.neurobiolaging.2013.07.022

Dégano, I. R., Marrugat, J., Grau, M., Salvador-González, B., Ramos, R., Zamora, A., Martí, R., & Elosua, R. (2017). The association between education and cardiovascular disease incidence is mediated by hypertension, diabetes, and body mass index. *Scientific Reports*, *7*(1), 12370–12370. PubMed. https://doi.org/10.1038/s41598-017-10775-3

Desikan, R. S., Ségonne, F., Fischl, B., Quinn, B. T., Dickerson, B. C., Blacker, D., Buckner, R. L., Dale, A. M., Maguire, R. P., Hyman, B. T., Albert, M. S., & Killiany, R. J. (2006). An automated labeling system for subdividing the human cerebral cortex on MRI scans into gyral based regions of interest. *NeuroImage*, *31*(3), 968–980. https://doi.org/10.1016/j.neuroimage.2006.01.021

Dickstein, D. L., Walsh, J., Brautigam, H., Stockton, S. D., Gandy, S., & Hof, P. R. (2010). Role of Vascular Risk Factors and Vascular Dysfunction in Alzheimer's Disease. *Mount Sinai Journal of Medicine: A Journal of Translational and Personalized Medicine*, *77*(1), 82–102. https://doi.org/10.1002/msj.20155

Driscoll, I., Davatzikos, C., An, Y., Wu, X., Shen, D., Kraut, M., & Resnick, S. M. (2009). Longitudinal pattern of regional brain volume change differentiates normal aging from MCI. *Neurology*, *72*(22), 1906. https://doi.org/10.1212/WNL.0b013e3181a82634

Enzinger, C., Fazekas, F., Matthews, P. M., Ropele, S., Schmidt, H., Smith, S., & Schmidt, R. (2005). Risk factors for progression of brain atrophy in aging. *Neurology*, *64*(10), 1704. https://doi.org/10.1212/01.WNL.0000161871.83614.BB

Fatemi, F., Kantarci, K., Graff-Radford, J., Preboske, G. M., Weigand, S. D., Przybelski, S. A., Knopman, D. S., Machulda, M. M., Roberts, R. O., Mielke, M. M., Petersen, R. C., Jack, C. R., Jr, & Vemuri, P. (2018). Sex differences in cerebrovascular pathologies on FLAIR in cognitively unimpaired elderly. *Neurology*, *90*(6), e466–e473. PubMed. https://doi.org/10.1212/WNL.0000000000004913

Feng, L., Bi, X., & Zhang, H. (2021). Brain Regions Identified as Being Associated With Verbal Reasoning Through the Use of Imaging Regression via Internal Variation. *Journal of the American Statistical Association*, *116*(533), 144–158. https://doi.org/10.1080/01621459.2020.1766468

Fernandes, V. R. S., Polak, J. F., Cheng, S., Rosen, B. D., Carvalho, B., Nasir, K., McClelland, R., Hundley, G., Pearson, G., O'Leary, D. H., Bluemke, D. A., & Lima, J. A. C. (2008). Arterial Stiffness Is Associated With Regional Ventricular Systolic and Diastolic Dysfunction. *Arteriosclerosis, Thrombosis, and Vascular Biology*, *28*(1), 194–201. https://doi.org/10.1161/ATVBAHA.107.156950

Fischl, B., & Dale, A. (2000). Fischl B, Dale AM. Measuring the thickness of the human cerebral cortex from magnetic resonance images. Proc Natl Acad Sci USA 97: 11050-11055. *Proceedings of the National Academy of Sciences of the United States of America*, *97*, 11050–11055. https://doi.org/10.1073/pnas.200033797

Fischl, B., Salat, D. H., Busa, E., Albert, M., Dieterich, M., Haselgrove, C., van der Kouwe, A., Killiany, R., Kennedy, D., Klaveness, S., Montillo, A., Makris, N., Rosen, B., & Dale, A.

M. (2002). Whole Brain Segmentation: Automated Labeling of Neuroanatomical Structures in the Human Brain. *Neuron*, *33*(3), 341–355. https://doi.org/10.1016/S0896-6273(02)00569-X

Fjell, A. M., McEvoy, L., Holland, D., Dale, A. M., Walhovd, K. B., & Alzheimer's Disease Neuroimaging Initiative. (2014). What is normal in normal aging? Effects of aging, amyloid and Alzheimer's disease on the cerebral cortex and the hippocampus. *Progress in Neurobiology*, *117*, 20–40. PubMed. https://doi.org/10.1016/j.pneurobio.2014.02.004

Franklin, S. S., Gustin, W., Wong, N. D., Larson, M. G., Weber, M. A., Kannel, W. B., & Levy, D. (1997). Hemodynamic patterns of age-related changes in blood pressure. The Framingham Heart Study. *Circulation*, *96*(1), 308–315. https://doi.org/10.1161/01.cir.96.1.308

Fung, K., Ramírez, J., Warren, H. R., Aung, N., Lee, A. M., Tzanis, E., Petersen, S. E., & Munroe, P. B. (2019). Genome-wide association study identifies loci for arterial stiffness index in 127,121 UK Biobank participants. *Scientific Reports*, *9*(1), 9143. https://doi.org/10.1038/s41598-019-45703-0

Garde, E., Lykke Mortensen, E., Rostrup, E., & Paulson, O. B. (2005). Decline in intelligence is associated with progression in white matter hyperintensity volume. *Journal of Neurology, Neurosurgery, and Psychiatry*, *76*(9), 1289–1291. PubMed. https://doi.org/10.1136/jnnp.2004.055905

Godia, E. C., Madhok, R., Pittman, J., Trocio, S., Ramas, R., Cabral, D., Sacco, R. L., & Rundek, T. (2007). Carotid Artery Distensibility. *Journal of Ultrasound in Medicine : Official Journal of the American Institute of Ultrasound in Medicine*, *26*(9), 1157–1165.

Gottfredson, L. S. (1997). Why g matters: The complexity of everyday life. *Intelligence*, *24*(1), 79–132.

Green, P., & MacLeod, C. J. (2016). SIMR: an R package for power analysis of generalized linear mixed models by simulation. *Methods in Ecology and Evolution*, *7*(4), 493–498. https://doi.org/10.1111/2041-210X.12504

Griffanti, L., Zamboni, G., Khan, A., Li, L., Bonifacio, G., Sundaresan, V., Schulz, U. G., Kuker, W., Battaglini, M., Rothwell, P. M., & Jenkinson, M. (2016). BIANCA (Brain Intensity AbNormality Classification Algorithm): A new tool for automated segmentation of white matter hyperintensities. *NeuroImage*, *141*, 191–205. PubMed. https://doi.org/10.1016/j.neuroimage.2016.07.018

Gupta, A., Nair, S., Schweitzer, A. D., Kishore, S., Johnson, C. E., Comunale, J. P., Tsiouris, A. J., & Sanelli, P. C. (2012). Neuroimaging of cerebrovascular disease in the aging brain. *Aging and Disease*, *3*(5), 414–425. PubMed.

Hajjar, I., Goldstein, F. C., Martin, G. S., & Quyyumi, A. A. (2016). Roles of Arterial Stiffness and Blood Pressure in Hypertension-Associated Cognitive Decline in Healthy Adults. *Hypertension*, *67*(1), 171–175. https://doi.org/10.1161/HYPERTENSIONAHA.115.06277

Hamer, M., & Batty, G. D. (2019). Association of body mass index and waist-to-hip ratio with brain structure. *Neurology*, *92*(6), e594. https://doi.org/10.1212/WNL.0000000000006879

Harada, C. N., Natelson Love, M. C., & Triebel, K. L. (2013). Normal cognitive aging. *Clinics in Geriatric Medicine*, *29*(4), 737–752. PubMed. https://doi.org/10.1016/j.cger.2013.07.002

Hoiland, R. L., Bain, A. R., Rieger, M. G., Bailey, D. M., & Ainslie, P. N. (2016). Hypoxemia, oxygen content, and the regulation of cerebral blood flow. *American Journal of Physiology-Regulatory, Integrative and Comparative Physiology*, *310*(5), R398–R413. https://doi.org/10.1152/ajpregu.00270.2015

Holwerda, S. W., Luehrs, R. E., DuBose, L., Collins, M. T., Wooldridge, N. A., Stroud, A. K., Fadel, P. J., Abboud, F. M., & Pierce, G. L. (2019). Elevated Muscle Sympathetic Nerve Activity Contributes to Central Artery Stiffness in Young and Middle-Age/Older Adults. *Hypertension*, *73*(5), 1025–1035. https://doi.org/10.1161/HYPERTENSIONAHA.118.12462

Holwerda, S. W., Luehrs, R. E., DuBose, L. E., Majee, R., & Pierce, G. L. (2019). Sex and age differences in the association between sympathetic outflow and central elastic artery wall thickness in humans. *American Journal of Physiology-Heart and Circulatory Physiology*, *317*(3), H552–H560. https://doi.org/10.1152/ajpheart.00275.2019

Humphrey, J. D., & Tellides, G. (2019). Central artery stiffness and thoracic aortopathy. *American Journal of Physiology-Heart and Circulatory Physiology*, *316*(1), H169–H182. https://doi.org/10.1152/ajpheart.00205.2018

Hunter, J. E. (1986). Cognitive ability, cognitive aptitudes, job knowledge, and job performance. *Journal of Vocational Behavior*, *29*(3), 340–362.

Hussain, R., Zubair, H., Pursell, S., & Shahab, M. (2018). Neurodegenerative Diseases: Regenerative Mechanisms and Novel Therapeutic Approaches. *Brain Sciences*, *8*(9), 177. https://doi.org/10.3390/brainsci8090177

Hutton, C., Draganski, B., Ashburner, J., & Weiskopf, N. (2009). A comparison between voxel-based cortical thickness and voxel-based morphometry in normal aging. *NeuroImage*, *48*(2), 371–380. https://doi.org/10.1016/j.neuroimage.2009.06.043

Iadecola, C., Yaffe, K., Biller, J., Bratzke, L. C., Faraci, F. M., Gorelick, P. B., Gulati, M., Kamel, H., Knopman, D. S., Launer, L. J., Saczynski, J. S., Seshadri, S., & Zeki Al Hazzouri, A. (2016). Impact of Hypertension on Cognitive Function: A Scientific Statement From the American Heart Association. *Hypertension*, *68*(6), e67–e94. https://doi.org/10.1161/HYP.0000000000000053

Jaeger, J. (2018). Digit Symbol Substitution Test: The Case for Sensitivity Over Specificity in Neuropsychological Testing. *Journal of Clinical Psychopharmacology*, *38*(5), 513–519. PubMed. https://doi.org/10.1097/JCP.0000000000000941

Jagust, W., Harvey, D., Mungas, D., & Haan, M. (2005). Central Obesity and the Aging Brain. *Archives of Neurology*, *62*(10), 1545–1548. https://doi.org/10.1001/archneur.62.10.1545

Jochemsen, H. M., Muller, M., Bots, M. L., Scheltens, P., Vincken, K. L., Mali, W. P. T. M., van der Graaf, Y., Geerlings, M. I., & SMART Study Group. (2015). Arterial stiffness and progression of structural brain changes: The SMART-MR study. *Neurology*, *84*(5), 448–455. https://doi.org/10.1212/WNL.0000000000001201

Kaufman, A. S., & Horn, J. L. (1996). Age changes on tests of fluid and crystallized ability for women and men on the Kaufman Adolescent and Adult Intelligence Test (KAIT) at ages 17–94 years. *Archives of Clinical Neuropsychology*, *11*(2), 97–121.

Kim, H. J., Kim, C., Jeon, S., Kang, M., Kim, Y. J., Lee, J.-M., Shin, H.-Y., Cho, H., Ye, B. S., Kim, J.-H., Jang, E. Y., Cho, J., Na, D. L., Rexrode, K. M., & Seo, S. W. (2015). Association of Body Fat Percentage and Waist-hip Ratio With Brain Cortical Thickness:

A Study Among 1777 Cognitively Normal Subjects. *Alzheimer Disease & Associated Disorders*, *29*(4). https://journals.lww.com/alzheimerjournal/Fulltext/2015/10000/Association_of_Body_Fat_Percentage_and_Waist_hip.2.aspx

Kim, K., Seo, H., Kwak, M., & Kim, D. (2017). Visceral obesity is associated with white matter hyperintensity and lacunar infarct. *International Journal of Obesity*, *41*(5), 683–688.

Klapwijk, E. T., van de Kamp, F., van der Meulen, M., Peters, S., & Wierenga, L. M. (2019). Qoala-T: A supervised-learning tool for quality control of FreeSurfer segmented MRI data. *NeuroImage*, *189*, 116–129. https://doi.org/10.1016/j.neuroimage.2019.01.014

Kohn, J. C., Lampi, M. C., & Reinhart-King, C. A. (2015). Age-related vascular stiffening: Causes and consequences. *Frontiers in Genetics*, *6*, 112–112. PubMed. https://doi.org/10.3389/fgene.2015.00112

Koller, M. (2016). robustlmm: An R Package for Robust Estimation of Linear Mixed-Effects Models. *Journal of Statistical Software*, *75*(6), 1–24. https://doi.org/10.18637/jss.v075.i06

Kramer, J. H., Mungas, D., Reed, B. R., Wetzel, M. E., Burnett, M. M., Miller, B. L., Weiner, M. W., & Chui, H. C. (2007). Longitudinal MRI and cognitive change in healthy elderly. *Neuropsychology*, *21*(4), 412–418. PubMed. https://doi.org/10.1037/0894-4105.21.4.412

Lacolley, P., Regnault, V., & Laurent, S. (2020). Mechanisms of Arterial Stiffening. *Arteriosclerosis, Thrombosis, and Vascular Biology*, *40*(5), 1055–1062. https://doi.org/10.1161/ATVBAHA.119.313129

Lamar, M., H. Rubin, L., Ajilore, O., Charlton, R., Zhang, A., Yang, S., Cohen, J., & Kumar, A. (2015). What Metabolic Syndrome Contributes to Brain Outcomes in African American & Caucasian Cohorts. *Current Alzheimer Research*, *12*(7), 640–647.

Lampe, L., Zhang, R., Beyer, F., Huhn, S., Kharabian Masouleh, S., Preusser, S., Bazin, P.-L., Schroeter, M. L., Villringer, A., & Witte, A. V. (2019). Visceral obesity relates to deep white matter hyperintensities via inflammation. *Annals of Neurology*, *85*(2), 194–203. PubMed. https://doi.org/10.1002/ana.25396

Laurent, S., Cockcroft, J., Van Bortel, L., Boutouyrie, P., Giannattasio, C., Hayoz, D., Pannier, B., Vlachopoulos, C., Wilkinson, I., Struijker-Boudier, H., & on behalf of the European Network for Non-invasive Investigation of Large Arteries. (2006). Expert consensus document on arterial stiffness: Methodological issues and clinical applications. *European Heart Journal*, *27*(21), 2588–2605. https://doi.org/10.1093/eurheartj/ehl254

Lee, B. H., Richard, J. E., de Leon, R. G., Yagi, S., & Galea, L. A. M. (n.d.). *Sex Differences in Cognition Across Aging* (pp. 1–50). Springer Berlin Heidelberg. https://doi.org/10.1007/7854_2022_309

Lemaitre, H., Goldman, A., Sambataro, F., Verchinski, B., Meyer-Lindenberg, A., Weinberger, D., & Mattay, V. (2012). Normal age-related brain morphometric changes: Nonuniformity across cortical thickness, surface area and grey matter volume? *Neurobiology of Aging*, *33*(3), 617.e1-617.e9. https://doi.org/10.1016/j.neurobiolaging.2010.07.013

Liu, Z., Yang, H., Chen, S., Cai, J., & Huang, Z. (2019). The association between body mass index, waist circumference, waist–hip ratio and cognitive disorder in older adults. *Journal of Public Health*, *41*(2), 305–312. https://doi.org/10.1093/pubmed/fdy121

Llewellyn, D. J., Lang, I. A., Xie, J., Huppert, F. A., Melzer, D., & Langa, K. M. (2008). Framingham Stroke Risk Profile and poor cognitive function: A population-based study. *BMC Neurology*, *8*(1), 12. https://doi.org/10.1186/1471-2377-8-12

Lohse, K. R., Shen, J., & Kozlowski, A. J. (2020). Modeling Longitudinal Outcomes: A Contrast of Two Methods. *Journal of Motor Learning and Development*, *8*(1), 145–165. https://doi.org/10.1123/jmld.2019-0007

Magezi, D. A. (2015). Linear mixed-effects models for within-participant psychology experiments: An introductory tutorial and free, graphical user interface (LMMgui). *Frontiers in Psychology*, *6*, 2. https://doi.org/10.3389/fpsyg.2015.00002

Makedonov, I., Black, S. E., & MacIntosh, B. J. (2013). Cerebral small vessel disease in aging and Alzheimer's disease: A comparative study using MRI and SPECT. *European Journal of Neurology*, *20*(2), 243–250. https://doi.org/10.1111/j.1468-1331.2012.03785.x

McCarrey, A. C., An, Y., Kitner-Triolo, M. H., Ferrucci, L., & Resnick, S. M. (2016). Sex differences in cognitive trajectories in clinically normal older adults. *Psychology and Aging*, *31*(2), 166.

McNeish, D., & Matta, T. (2018). Differentiating between mixed-effects and latent-curve approaches to growth modeling. *Behavior Research Methods*, *50*(4), 1398–1414. https://doi.org/10.3758/s13428-017-0976-5

Messerli, F., Frohlich, E., & Ventura, H. (1985). Arterial compliance in essential hypertension. *J Cardiovasc Pharmacol*, *7 Suppl 2*, S33-5. PubMed. https://doi.org/10.1097/00005344-198507002-00007

Millar, P. J., Notarius, C. F., Haruki, N., & Floras, J. S. (2019). Heart Failure–Specific Relationship Between Muscle Sympathetic Nerve Activity and Aortic Wave Reflection.

Journal of Cardiac Failure, *25*(5), 404–408. https://doi.org/10.1016/j.cardfail.2019.03.005

MILLASSEAU, S. C., KELLY, R. P., RITTER, J. M., & CHOWIENCZYK, P. J. (2002). Determination of age-related increases in large artery stiffness by digital pulse contour analysis. *Clinical Science*, *103*(4), 371–377. https://doi.org/10.1042/cs1030371

Millasseau, S. C., Stewart, A. D., Patel, S. J., Redwood, S. R., & Chowienczyk, P. J. (2005). Evaluation of Carotid-Femoral Pulse Wave Velocity. *Hypertension*, *45*(2), 222–226. https://doi.org/10.1161/01.HYP.0000154229.97341.d2

Mitchell, G. F. (2008). Effects of central arterial aging on the structure and function of the peripheral vasculature: Implications for end-organ damage. *Journal of Applied Physiology (Bethesda, Md.: 1985)*, *105*(5), 1652–1660. https://doi.org/10.1152/japplphysiol.90549.2008

Mitchell, G. F. (2014). Arterial Stiffness and Hypertension: Chicken or Egg? *Hypertension*, *64*(2), 210–214. https://doi.org/10.1161/HYPERTENSIONAHA.114.03449

Mitchell, G. F., van Buchem, M. A., Sigurdsson, S., Gotal, J. D., Jonsdottir, M. K., Kjartansson, Ó., Garcia, M., Aspelund, T., Harris, T. B., Gudnason, V., & Launer, L. J. (2011). Arterial stiffness, pressure and flow pulsatility and brain structure and function: The Age, Gene/Environment Susceptibility—Reykjavik study. *Brain : A Journal of Neurology*, *134*(Pt 11), 3398–3407. PubMed. https://doi.org/10.1093/brain/awr253

Mitchell, G. F., Vasan, R. S., Keyes, M. J., Parise, H., Wang, T. J., Larson, M. G., D'Agostino, R. B., Kannel, W. B., Levy, D., & Benjamin, E. J. (2007). Pulse pressure and risk of new-onset atrial fibrillation. *JAMA*, *297*(7), 709–715. https://doi.org/10.1001/jama.297.7.709

Molarius, A., Seidell, J., Sans, S., Tuomilehto, J., & Kuulasmaa, K. (1999). Waist and hip circumferences, and waist-hip ratio in 19 populations of the WHO MONICA Project. *International Journal of Obesity*, *23*(2), 116–125. https://doi.org/10.1038/sj.ijo.0800772

Nardone, M., Floras, J. S., & Millar, P. J. (2020). Sympathetic neural modulation of arterial stiffness in humans. *American Journal of Physiology-Heart and Circulatory Physiology*, *319*(6), H1338–H1346. https://doi.org/10.1152/ajpheart.00734.2020

Neisser, U., Boodoo, G., Bouchard Jr, T. J., Boykin, A. W., Brody, N., Ceci, S. J., Halpern, D. F., Loehlin, J. C., Perloff, R., & Sternberg, R. J. (1996). Intelligence: Knowns and unknowns. *American Psychologist*, *51*(2), 77.

Nichols, E. S., Wild, C. J., Owen, A. M., & Soddu, A. (2020). Cognition across the lifespan: Age, gender, and sociodemographic influences. *BioRxiv*, 804765. https://doi.org/10.1101/804765

Oberg, A. L., & Mahoney, D. W. (2007). Linear Mixed Effects Models. In W. T. Ambrosius (Ed.), *Topics in Biostatistics* (pp. 213–234). Humana Press. https://doi.org/10.1007/978-1-59745-530-5_11

Pacheco, J., Goh, J. O., Kraut, M. A., Ferrucci, L., & Resnick, S. M. (2015). Greater cortical thinning in normal older adults predicts later cognitive impairment. *Neurobiology of Aging*, *36*(2), 903–908. https://doi.org/10.1016/j.neurobiolaging.2014.08.031

Panizzon, M. S., Fennema-Notestine, C., Eyler, L. T., Jernigan, T. L., Prom-Wormley, E., Neale, M., Jacobson, K., Lyons, M. J., Grant, M. D., Franz, C. E., Xian, H., Tsuang, M., Fischl, B., Seidman, L., Dale, A., & Kremen, W. S. (2009). Distinct genetic influences on cortical surface area and cortical thickness. *Cerebral Cortex (New York, N.Y. : 1991)*, *19*(11), 2728–2735. PubMed. https://doi.org/10.1093/cercor/bhp026

Pasha, E. P., Kaur, S. S., Gonzales, M. M., Machin, D. R., Kasischke, K., Tanaka, H., & Haley, A. P. (2015). Vascular function, cerebral cortical thickness, and cognitive performance in middle-aged Hispanic and non-Hispanic Caucasian adults. *Journal of Clinical Hypertension (Greenwich, Conn.)*, *17*(4), 306–312. https://doi.org/10.1111/jch.12512

Patenaude, B., Smith, S. M., Kennedy, D. N., & Jenkinson, M. (2011). A Bayesian model of shape and appearance for subcortical brain segmentation. *NeuroImage*, *56*(3), 907–922. https://doi.org/10.1016/j.neuroimage.2011.02.046

Pereira, T., Correia, C., & Cardoso, J. (2015). Novel Methods for Pulse Wave Velocity Measurement. *Journal of Medical and Biological Engineering*, *35*(5), 555–565. PubMed. https://doi.org/10.1007/s40846-015-0086-8

Raichle Marcus E. & Gusnard Debra A. (2002). Appraising the brain's energy budget. *Proceedings of the National Academy of Sciences*, *99*(16), 10237–10239. https://doi.org/10.1073/pnas.172399499

Rajzer, M. W., Wojciechowska, W., Klocek, M., Palka, I., Brzozowska-Kiszka, M., & Kawecka-Jaszcz, K. (2008). Comparison of aortic pulse wave velocity measured by three techniques: Complior, SphygmoCor and Arteriograph. *Journal of Hypertension*, *26*(10). https://journals.lww.com/jhypertension/Fulltext/2008/10000/Comparison_of_aortic_pulse_wave_velocity_measured.14.aspx

Ramanoël, S., Hoyau, E., Kauffmann, L., Renard, F., Pichat, C., Boudiaf, N., Krainik, A., Jaillard, A., & Baciu, M. (2018). Gray Matter Volume and Cognitive Performance During Normal Aging. A Voxel-Based Morphometry Study. *Frontiers in Aging Neuroscience*, *10*. https://www.frontiersin.org/article/10.3389/fnagi.2018.00235

Ramirez, J., McNeely, A. A., Berezuk, C., Gao, F., & Black, S. E. (2016). Dynamic Progression of White Matter Hyperintensities in Alzheimer's Disease and Normal Aging: Results from the Sunnybrook Dementia Study. *Frontiers in Aging Neuroscience*, *8*, 62. https://doi.org/10.3389/fnagi.2016.00062

Raz, N., Yang, Y., Dahle, C. L., & Land, S. (2012). Volume of white matter hyperintensities in healthy adults: Contribution of age, vascular risk factors, and inflammation-related genetic variants. *Imaging Brain Aging and Neurodegenerative Disease*, *1822*(3), 361–369. https://doi.org/10.1016/j.bbadis.2011.08.007

Reitan, R. M., & Wolfson, D. (2004). The Trail Making Test as an initial screening procedure for neuropsychological impairment in older children. *Archives of Clinical Neuropsychology*, *19*(2), 281–288.

Resnick, S. M., Pham, D. L., Kraut, M. A., Zonderman, A. B., & Davatzikos, C. (2003). Longitudinal magnetic resonance imaging studies of older adults: A shrinking brain. *The Journal of Neuroscience : The Official Journal of the Society for Neuroscience*, *23*(8), 3295–3301. PubMed. https://doi.org/10.1523/JNEUROSCI.23-08-03295.2003

S. R. Alty, N. Angarita-Jaimes, S. C. Millasseau, & P. J. Chowienczyk. (2007). Predicting Arterial Stiffness From the Digital Volume Pulse Waveform. *IEEE Transactions on Biomedical Engineering*, *54*(12), 2268–2275. https://doi.org/10.1109/TBME.2007.897805

Said, M. A., Eppinga, R. N., Lipsic, E., Verweij, N., & van der Harst, P. (2018). Relationship of arterial stiffness index and pulse pressure with cardiovascular disease and mortality. *Journal of the American Heart Association*, *7*(2), e007621.

Salvi, P., Lio, G., Labat, C., Ricci, E., Pannier, B., & Benetos, A. (2004). Validation of a new non-invasive portable tonometer for determining arterial pressure wave and pulse wave velocity: The PulsePen device. *Journal of Hypertension*, *22*(12). https://journals.lww.com/jhypertension/Fulltext/2004/12000/Validation_of_a_new_non_invasive_portable.10.aspx

Scahill, R. I., Frost, C., Jenkins, R., Whitwell, J. L., Rossor, M. N., & Fox, N. C. (2003). A Longitudinal Study of Brain Volume Changes in Normal Aging Using Serial Registered Magnetic Resonance Imaging. *Archives of Neurology*, *60*(7), 989–994. https://doi.org/10.1001/archneur.60.7.989

Schmidt, R., Ropele, S., Enzinger, C., Petrovic, K., Smith, S., Schmidt, H., Matthews, P. M., & Fazekas, F. (2005). White matter lesion progression, brain atrophy, and cognitive decline: The Austrian stroke prevention study. *Annals of Neurology*, *58*(4), 610–616. https://doi.org/10.1002/ana.20630

Scuteri, A., Nilsson, P. M., Tzourio, C., Redon, J., & Laurent, S. (2011). Microvascular brain damage with aging and hypertension: Pathophysiological consideration and clinical implications. *Journal of Hypertension*, *29*(8). https://journals.lww.com/jhypertension/Fulltext/2011/08000/Microvascular_brain_damage_with_aging_and.1.aspx

Silbert, L. C., Howieson, D. B., Dodge, H., & Kaye, J. A. (2009). Cognitive impairment risk. *Neurology*, *73*(2), 120. https://doi.org/10.1212/WNL.0b013e3181ad53fd

Silbert, L. C., Nelson, C., Howieson, D. B., Moore, M. M., & Kaye, J. A. (2008). Impact of white matter hyperintensity volume progression on rate of cognitive and motor decline. *Neurology*, *71*(2), 108. https://doi.org/10.1212/01.wnl.0000316799.86917.37

Singh, V., Chertkow, H., Lerch, J. P., Evans, A. C., Dorr, A. E., & Kabani, N. J. (2006). Spatial patterns of cortical thinning in mild cognitive impairment and Alzheimer's disease. *Brain*, *129*(11), 2885–2893. https://doi.org/10.1093/brain/awl256

Sluimer, J. D., van der Flier, W. M., Karas, G. B., Fox, N. C., Scheltens, P., Barkhof, F., & Vrenken, H. (2008). Whole-Brain Atrophy Rate and Cognitive Decline: Longitudinal MR Study of Memory Clinic Patients. *Radiology*, *248*(2), 590–598. https://doi.org/10.1148/radiol.2482070938

Snijder, M. B., Stronks, K., Agyemang, C., Busschers, W. B., Peters, R. J., & van den Born, B.-J. H. (2015). Ethnic differences in arterial stiffness the Helius study. *International Journal of Cardiology*, *191*, 28–33. https://doi.org/10.1016/j.ijcard.2015.04.234

Sørensen, L., Pai, A., Anker, C., Balas, I., Lillholm, M., Igel, C., & Nielsen, M. (n.d.). *Dementia Diagnosis using MRI Cortical Thickness, Shape, Texture, and Volumetry*.

Soriano-Raya, J. J., Miralbell, J., López-Cancio, E., Bargalló, N., Arenillas, J. F., Barrios, M., Cáceres, C., Toran, P., Alzamora, M., Dávalos, A., & Mataró, M. (2012). Deep versus Periventricular White Matter Lesions and Cognitive Function in a Community Sample of Middle-Aged Participants. *Journal of the International Neuropsychological Society*, *18*(5), 874–885. https://doi.org/10.1017/S1355617712000677

Stakos, D. A., Tziakas, D. N., Chalikias, G. K., Mitrousi, K., Tsigalou, C., & Boudoulas, H. (2010). Associations Between Collagen Synthesis and Degradation and Aortic Function in Arterial Hypertension. *American Journal of Hypertension*, *23*(5), 488–494. https://doi.org/10.1038/ajh.2010.2

Steinberg, B. A., Bieliauskas, L. A., Smith, G. E., & Ivnik, R. J. (2005). Mayo's Older Americans Normative Studies: Age- and IQ-Adjusted Norms for the Trail-Making Test,

the Stroop Test, and MAE Controlled Oral Word Association Test. *The Clinical Neuropsychologist*, *19*(3–4), 329–377. https://doi.org/10.1080/13854040590945210

Stringhini, S., Carmeli, C., Jokela, M., Avendaño, M., Muennig, P., Guida, F., Ricceri, F., d'Errico, A., Barros, H., Bochud, M., Chadeau-Hyam, M., Clavel-Chapelon, F., Costa, G., Delpierre, C., Fraga, S., Goldberg, M., Giles, G. G., Krogh, V., Kelly-Irving, M., … Zins, M. (2017). Socioeconomic status and the 25 × 25 risk factors as determinants of premature mortality: A multicohort study and meta-analysis of 1·7 million men and women. *The Lancet*, *389*(10075), 1229–1237. https://doi.org/10.1016/S0140-6736(16)32380-7

Sudlow, C., Gallacher, J., Allen, N., Beral, V., Burton, P., Danesh, J., Downey, P., Elliott, P., Green, J., Landray, M., Liu, B., Matthews, P., Ong, G., Pell, J., Silman, A., Young, A., Sprosen, T., Peakman, T., & Collins, R. (2015). UK Biobank: An Open Access Resource for Identifying the Causes of a Wide Range of Complex Diseases of Middle and Old Age. *PLOS Medicine*, *12*(3), e1001779. https://doi.org/10.1371/journal.pmed.1001779

Suri, S., Chiesa, S. T., Zsoldos, E., Mackay, C. E., Filippini, N., Griffanti, L., Mahmood, A., Singh-Manoux, A., Shipley, M. J., Brunner, E. J., Kivimäki, M., Deanfield, J. E., & Ebmeier, K. P. (2020). *Accelerated aortic stiffness is associated with brain structure, perfusion and cognition in the Whitehall II Imaging Sub-study* [Preprint]. Cardiovascular Medicine. https://doi.org/10.1101/2020.07.01.20142612

Sutton-Tyrrell, K., Najjar, S. S., Boudreau, R. M., Venkitachalam, L., Kupelian, V., Simonsick, E. M., Havlik, R., Lakatta, E. G., Spurgeon, H., Kritchevsky, S., Pahor, M., Bauer, D., Newman, A., & Health ABC Study. (2005). Elevated aortic pulse wave velocity, a marker of arterial stiffness, predicts cardiovascular events in well-functioning older

adults. *Circulation*, *111*(25), 3384–3390. https://doi.org/10.1161/CIRCULATIONAHA.104.483628

Swierblewska, E., Hering, D., Kara, T., Kunicka, K., Kruszewski, P., Bieniaszewski, L., Boutouyrie, P., Somers, V. K., & Narkiewicz, K. (2010). An independent relationship between muscle sympathetic nerve activity and pulse wave velocity in normal humans. *Journal of Hypertension*, *28*(5). https://journals.lww.com/jhypertension/Fulltext/2010/05000/An_independent_relationship_between_muscle.16.aspx

Tanaka, H., Dinenno, F. A., & Seals, D. R. (2017). Reductions in central arterial compliance with age are related to sympathetic vasoconstrictor nerve activity in healthy men. *Hypertension Research*, *40*(5), 493–495. https://doi.org/10.1038/hr.2016.182

Tarumi, T., Khan, M. A., Liu, J., Tseng, B. M., Parker, R., Riley, J., Tinajero, C., & Zhang, R. (2014). Cerebral Hemodynamics in Normal Aging: Central Artery Stiffness, Wave Reflection, and Pressure Pulsatility. *Journal of Cerebral Blood Flow & Metabolism*, *34*(6), 971–978. https://doi.org/10.1038/jcbfm.2014.44

Tate, D. F., Gusman, M., Kini, J., Reid, M., Velez, C. S., Drennon, A. M., Cooper, D. B., Kennedy, J. E., Bowles, A. O., Bigler, E. D., Lewis, J. D., Ritter, J., & York, G. E. (2017). Susceptibility Weighted Imaging and White Matter Abnormality Findings in Service Members With Persistent Cognitive Symptoms Following Mild Traumatic Brain Injury. *Military Medicine*, *182*(3–4), e1651–e1658. https://doi.org/10.7205/MILMED-D-16-00132

Thambisetty, M., Wan, J., Carass, A., An, Y., Prince, J. L., & Resnick, S. M. (2010). Longitudinal changes in cortical thickness associated with normal aging. *NeuroImage*, *52*(4), 1215–1223. https://doi.org/10.1016/j.neuroimage.2010.04.258

The Reference Values for Arterial Stiffness' Collaboration. (2010). Determinants of pulse wave velocity in healthy people and in the presence of cardiovascular risk factors: 'Establishing normal and reference values.' *European Heart Journal*, *31*(19), 2338–2350. https://doi.org/10.1093/eurheartj/ehq165

Tong, K. A., Ashwal, S., Holshouser, B. A., Shutter, L. A., Herigault, G., Haacke, E. M., & Kido, D. K. (2003). Hemorrhagic Shearing Lesions in Children and Adolescents with Posttraumatic Diffuse Axonal Injury: Improved Detection and Initial Results. *Radiology*, *227*(2), 332–339. https://doi.org/10.1148/radiol.2272020176

Tsao, C. W., Seshadri, S., Beiser, A. S., Westwood, A. J., Decarli, C., Au, R., Himali, J. J., Hamburg, N. M., Vita, J. A., Levy, D., Larson, M. G., Benjamin, E. J., Wolf, P. A., Vasan, R. S., & Mitchell, G. F. (2013). Relations of arterial stiffness and endothelial function to brain aging in the community. *Neurology*, *81*(11), 984–991. PubMed. https://doi.org/10.1212/WNL.0b013e3182a43e1c

van den Heuvel, D. M. J., Admiraal-Behloul, F., ten Dam, V. H., Olofsen, H., Bollen, E. L. E. M., Murray, H. M., Blauw, G. J., Westendorp, R. G. J., de Craen, A. J. M., & van Buchem, M. A. (2004). Different progression rates for deep white matter hyperintensities in elderly men and women. *Neurology*, *63*(9), 1699. https://doi.org/10.1212/01.WNL.0000143058.40388.44

van Dijk, E. J., Prins, N. D., Vrooman, H. A., Hofman, A., Koudstaal, P. J., & Breteler, M. M. B. (2008). Progression of Cerebral Small Vessel Disease in Relation to Risk Factors and

Cognitive Consequences. *Stroke*, *39*(10), 2712–2719. https://doi.org/10.1161/STROKEAHA.107.513176

van Sloten, T. T., Protogerou, A. D., Henry, R. M. A., Schram, M. T., Launer, L. J., & Stehouwer, C. D. A. (2015). Association between arterial stiffness, cerebral small vessel disease and cognitive impairment: A systematic review and meta-analysis. *Neuroscience and Biobehavioral Reviews*, *53*, 121–130. PubMed. https://doi.org/10.1016/j.neubiorev.2015.03.011

Vlachopoulos Charalambos, Aznaouridis Konstantinos, & Stefanadis Christodoulos. (2010). Prediction of Cardiovascular Events and All-Cause Mortality With Arterial Stiffness. *Journal of the American College of Cardiology*, *55*(13), 1318–1327. https://doi.org/10.1016/j.jacc.2009.10.061

Wagenseil, J. E., & Mecham, R. P. (2012). Elastin in large artery stiffness and hypertension. *Journal of Cardiovascular Translational Research*, *5*(3), 264–273. PubMed. https://doi.org/10.1007/s12265-012-9349-8

Waldmann, B. W., Dickson, A. L., Monahan, M. C., & Kazelskis, R. (1992). The relationship between intellectual ability and adult performance on the trail making test and the symbol digit modalities test. *Journal of Clinical Psychology*, *48*(3), 360–363. https://doi.org/10.1002/1097-4679(199205)48:3<360::AID-JCLP2270480314>3.0.CO;2-P

Walsh, K. W. (1978). *Neuropsychology: A clinical approach.* (p. 371). Churchill Livingstone.

Wardlaw, J. M., Valdés Hernández, M. C., & Muñoz-Maniega, S. (n.d.). What are White Matter Hyperintensities Made of? *Journal of the American Heart Association*, *4*(6), e001140. https://doi.org/10.1161/JAHA.114.001140

Wen, W., Zhu, W., He, Y., Kochan, N. A., Reppermund, S., Slavin, M. J., Brodaty, H., Crawford, J., Xia, A., & Sachdev, P. (2011). Discrete Neuroanatomical Networks Are Associated with Specific Cognitive Abilities in Old Age. *The Journal of Neuroscience*, *31*(4), 1204. https://doi.org/10.1523/JNEUROSCI.4085-10.2011

Wiesmann, M., Kiliaan, A. J., & Claassen, J. A. (2013). Vascular Aspects of Cognitive Impairment and Dementia. *Journal of Cerebral Blood Flow & Metabolism*, *33*(11), 1696–1706. https://doi.org/10.1038/jcbfm.2013.159

Winkler, A. M., Kochunov, P., Blangero, J., Almasy, L., Zilles, K., Fox, P. T., Duggirala, R., & Glahn, D. C. (2010). Cortical Thickness or Grey Matter Volume? The Importance of Selecting the Phenotype for Imaging Genetics Studies. *NeuroImage*, *53*(3), 1135–1146. https://doi.org/10.1016/j.neuroimage.2009.12.028

Wolfson, L., Wakefield, D. B., Moscufo, N., Kaplan, R. F., Hall, C. B., Schmidt, J. A., Guttmann, C. R. G., & White, W. B. (2013). Rapid Buildup of Brain White Matter Hyperintensities Over 4 Years Linked to Ambulatory Blood Pressure, Mobility, Cognition, and Depression in Old Persons. *The Journals of Gerontology: Series A*, *68*(11), 1387–1394. https://doi.org/10.1093/gerona/glt072

Woodman, R. J., Kingwell, B. A., Beilin, L. J., Hamilton, S. E., Dart, A. M., & Watts, G. F. (2005). Assessment of central and peripheral arterial stiffness*: Studies indicating the need to use a combination of techniques. *American Journal of Hypertension*, *18*(2), 249–260. https://doi.org/10.1016/j.amjhyper.2004.08.038

Xu, C., Zarins, C. K., Pannaraj, P. S., Bassiouny, H. S., & Glagov, S. (2000). Hypercholesterolemia Superimposed by Experimental Hypertension Induces Differential

Distribution of Collagen and Elastin. *Arteriosclerosis, Thrombosis, and Vascular Biology*, *20*(12), 2566–2572. https://doi.org/10.1161/01.ATV.20.12.2566

Y. Zhang, M. Brady, & S. Smith. (2001). Segmentation of brain MR images through a hidden Markov random field model and the expectation-maximization algorithm. *IEEE Transactions on Medical Imaging*, *20*(1), 45–57. https://doi.org/10.1109/42.906424

Yamashiro, K., Tanaka, R., Tanaka, Y., Miyamoto, N., Shimada, Y., Ueno, Y., Urabe, T., & Hattori, N. (2014). Visceral fat accumulation is associated with cerebral small vessel disease. *European Journal of Neurology*, *21*(4), 667–673.

Zaydun, G., Tomiyama, H., Hashimoto, H., Arai, T., Koji, Y., Yambe, M., Motobe, K., Hori, S., & Yamashina, A. (2006). Menopause is an independent factor augmenting the age-related increase in arterial stiffness in the early postmenopausal phase. *Atherosclerosis*, *184*(1), 137–142. https://doi.org/10.1016/j.atherosclerosis.2005.03.043

Zhang, T., Yan, R., Chen, Q., Ying, X., Zhai, Y., Li, F., Wang, X., He, F., Ye, C., & Lin, J. (2018). Body mass index, waist-to-hip ratio and cognitive function among Chinese elderly: A cross-sectional study. *BMJ Open*, *8*(10), e022055–e022055. PubMed. https://doi.org/10.1136/bmjopen-2018-022055

Zieman, S. J., Melenovsky, V., & Kass, D. A. (2005). Mechanisms, Pathophysiology, and Therapy of Arterial Stiffness. *Arteriosclerosis, Thrombosis, and Vascular Biology*, *25*(5), 932–943. https://doi.org/10.1161/01.ATV.0000160548.78317.29

Appendices

Appendix A. Linear Mixed Effects Model Outputs and Model Fits

Appendix A1a). Left Hemisphere Caudal Anterior Cingulate Cortical Thickness Linear Mixed Effects Model Output

	LH Caudal Anterior Cingulate (mm)		
Predictors	*Estimates*	*CI*	*p*
(Intercept)	3.073	2.927 – 3.219	**<0.001**
ASI	0.003	-0.001 – 0.007	0.125
Instance [3 0]	0.100	0.044 – 0.157	**0.001**
Years between visits	-0.021	-0.031 – -0.010	**<0.001**
Waist to hip ratio	-0.155	-0.294 – -0.016	**0.029**
Age	-0.003	-0.005 – -0.002	**<0.001**
Sex	-0.006	-0.034 – 0.021	0.649
Physical Activity	0.001	-0.002 – 0.005	0.479
ASI * Instance [3 0]	-0.006	-0.011 – -0.002	**0.010**
Random Effects			
σ^2	0.03		
$\tau_{00\ eid}$	0.04		
ICC	0.58		
$N_{\ eid}$	1855		
Observations	3620		
Marginal R^2 / Conditional R^2	0.019 / 0.586		

Appendix A1b). Left Hemisphere Caudal Anterior Cingulate Cortical Thickness Linear Mixed Effects Model Fit

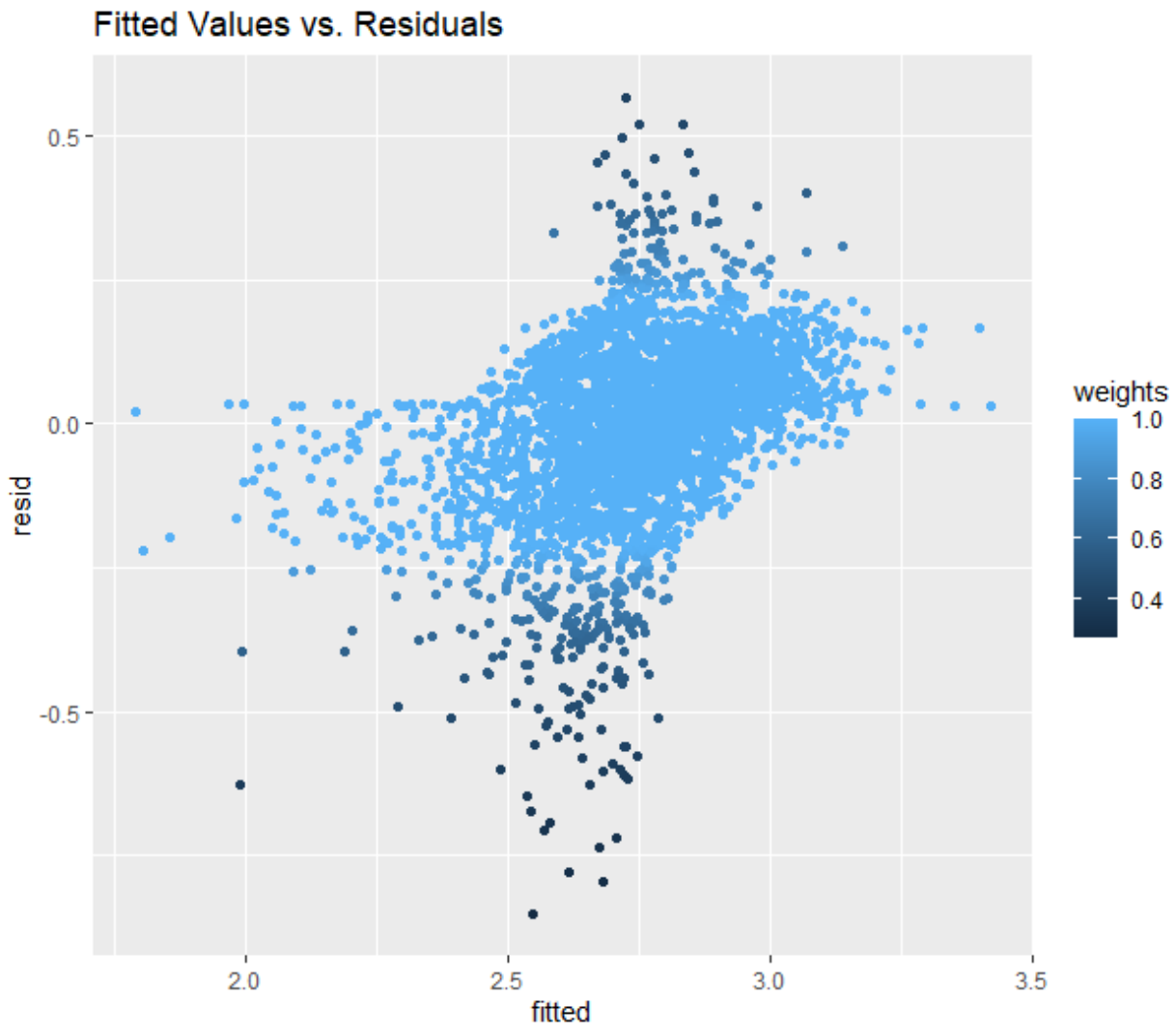

A2a). Right Hemisphere Caudal Anterior Cingulate Cortical Thickness Linear Mixed Effects Model Output

	RH Caudal Anterior Cingulate (mm)		
Predictors	*Estimates*	*CI*	*p*
(Intercept)	3.144	3.075 – 3.214	**<0.001**
ASI	0.001	-0.001 – 0.002	0.413
Instance [3 0]	-0.001	-0.023 – 0.021	0.930
Years between visits	0.007	0.003 – 0.011	**0.002**
Waist to hip ratio	0.079	0.019 – 0.139	**0.010**
Age	-0.006	-0.007 – -0.005	**<0.001**
Sex	-0.014	-0.027 – 0.000	0.054
Physical Activity	-0.001	-0.002 – 0.001	0.428
ASI * Instance [3 0]	-0.002	-0.003 – 0.000	0.091
Random Effects			
σ^2	0.00		
$\tau_{00\ eid}$	0.01		
ICC	0.79		
$N_{\ eid}$	1855		
Observations	3620		
Marginal R^2 / Conditional R^2	0.103 / 0.810		

Appendix A2b). Right Hemisphere Caudal Anterior Cingulate Cortical Thickness Linear Mixed Effects Model Fit

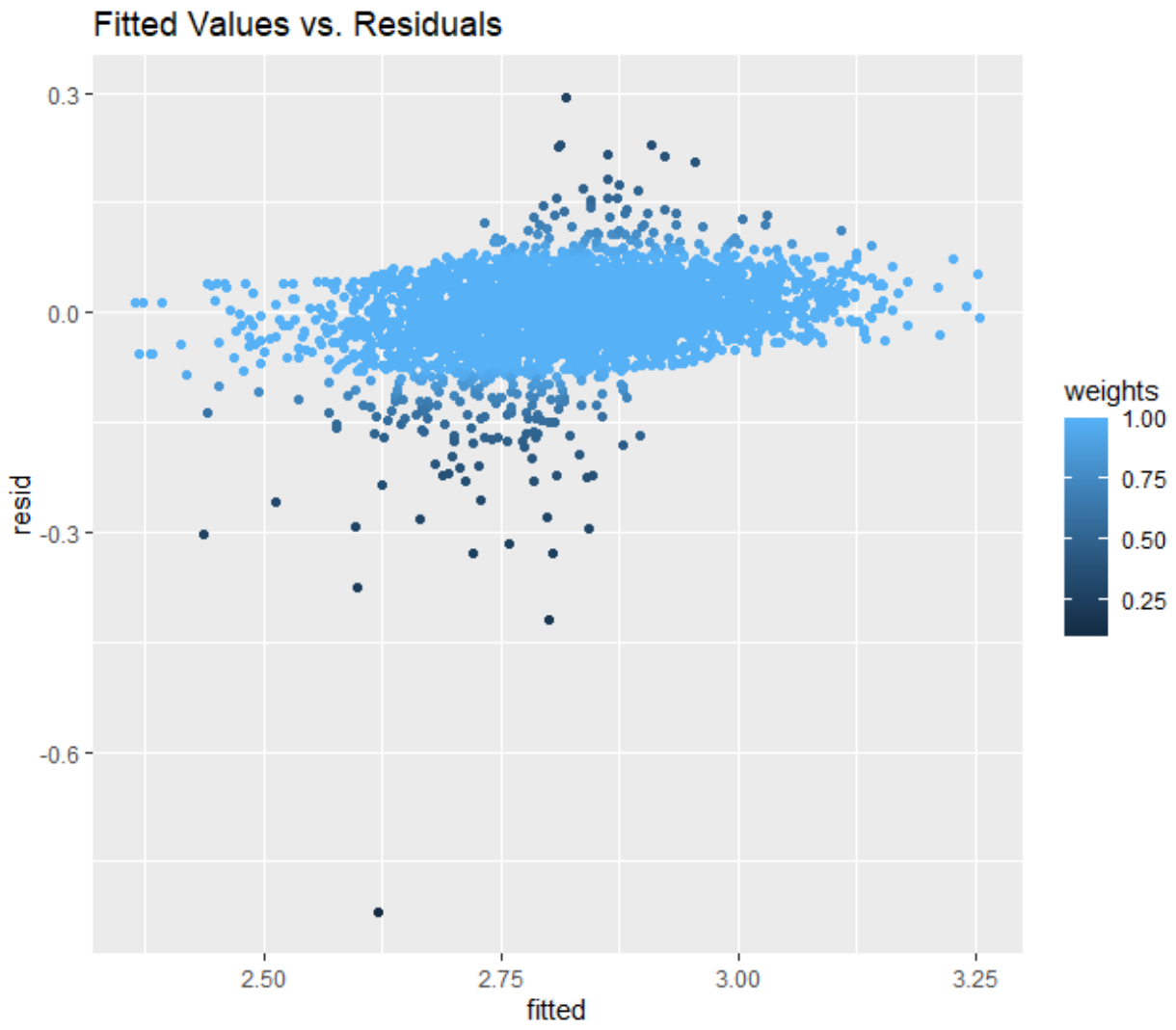

Appendix A3a). Left Hemisphere Caudal Middle Frontal Gyri Cortical Thickness Linear Mixed Effects Model Output

	LH Caudal Middle Frontal gyri(mm)		
Predictors	*Estimates*	*CI*	*p*
(Intercept)	3.242	3.171 – 3.313	**<0.001**
ASI	0.001	-0.000 – 0.003	0.052
Instance [3 0]	0.009	-0.012 – 0.031	0.393
Years between visits	0.006	0.002 – 0.010	**0.006**
Waist to hip ratio	-0.019	-0.079 – 0.041	0.531
Age	-0.006	-0.007 – -0.005	**<0.001**
Sex	-0.006	-0.020 – 0.008	0.421
Physical Activity	-0.001	-0.003 – 0.000	0.125
ASI * Instance [3 0]	-0.002	-0.004 – -0.000	**0.034**
Random Effects			
σ^2	0.00		
$\tau_{00\ eid}$	0.02		
ICC	0.81		
$N_{\ eid}$	1855		
Observations	3620		
Marginal R^2 / Conditional R^2	0.090 / 0.828		

Appendix A3b). Left Hemisphere Caudal Middle Frontal Gyri Cortical Thickness Linear Mixed Effects Model Fit

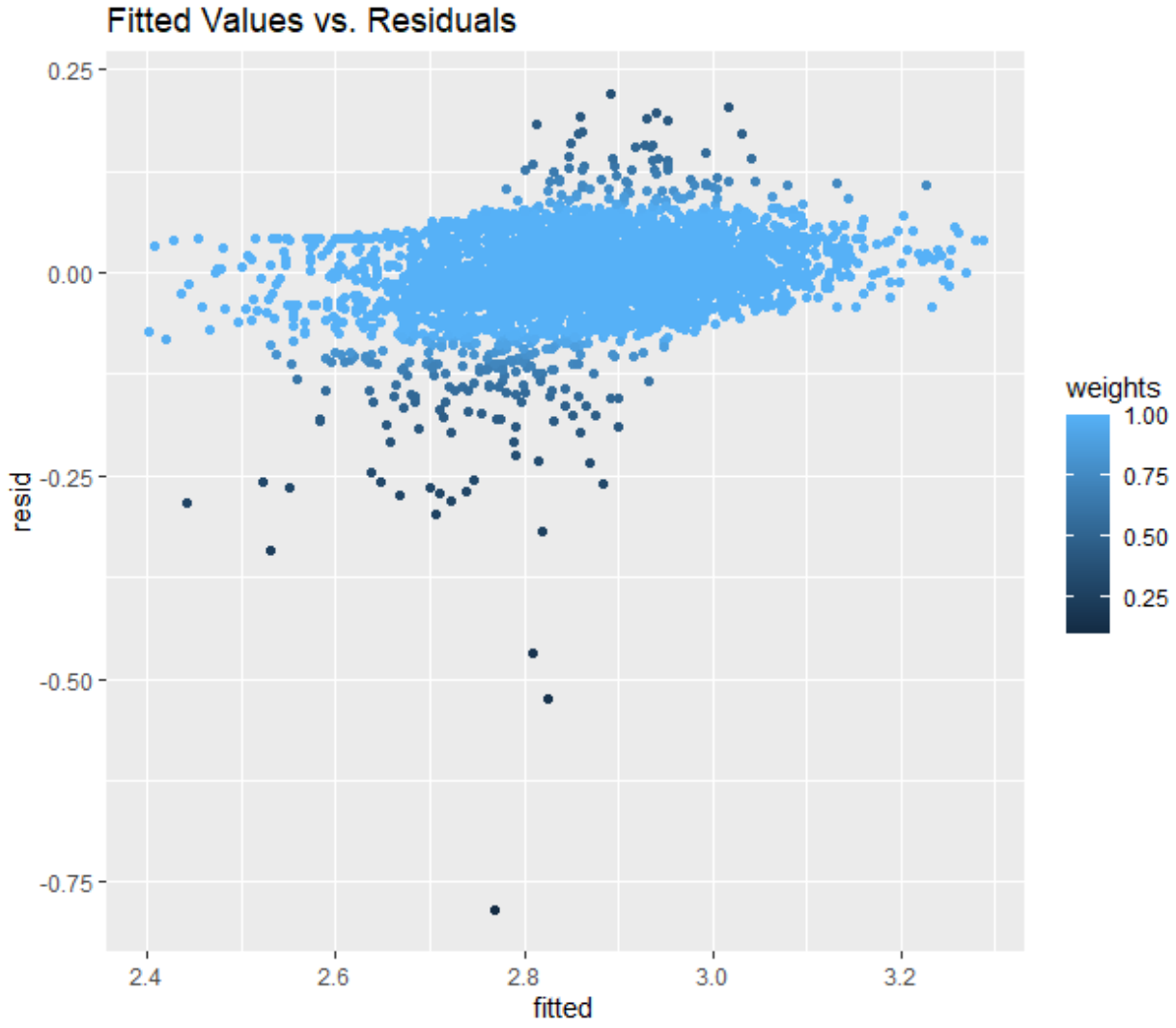

Appendix A4a). Right Hemisphere Caudal Middle Frontal Gyri Cortical Thickness Linear Mixed Effects Model Output

	RH Caudal Middle Frontal gyri (mm)		
Predictors	*Estimates*	*CI*	*p*
(Intercept)	1.929	1.860 – 1.997	**<0.001**
ASI	0.001	-0.000 – 0.003	0.064
Instance [3 0]	0.016	-0.006 – 0.037	0.150
Years between visits	-0.000	-0.004 – 0.004	0.903
Waist to hip ratio	0.102	0.043 – 0.161	**0.001**
Age	-0.001	-0.002 – -0.001	**0.001**
Sex	0.019	0.006 – 0.033	**0.005**
Physical Activity	-0.001	-0.002 – 0.001	0.436
ASI * Instance [3 0]	-0.002	-0.004 – -0.000	**0.036**
Random Effects			
σ^2	0.00		
$\tau_{00\ eid}$	0.01		
ICC	0.78		
$N_{\ eid}$	1855		
Observations	3620		
Marginal R^2 / Conditional R^2	0.021 / 0.789		

Appendix A4b). Right Hemisphere Caudal Middle Frontal Gyri Cortical Thickness Linear Mixed Effects Model Fit

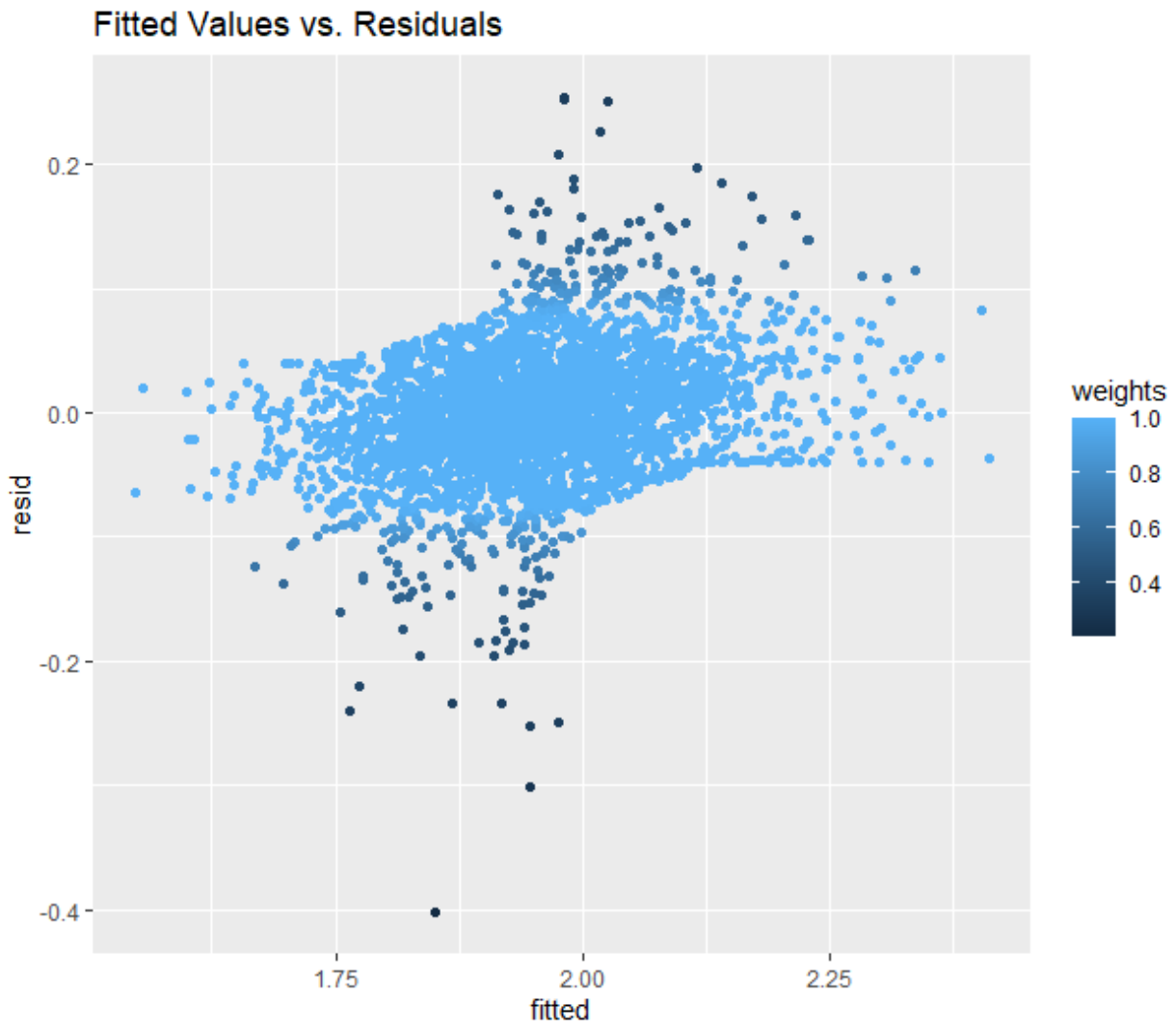

Appendix A5a). Left Hemisphere Rostral Anterior Cingulate Cortical Thickness Linear Mixed Effects Model Output

	LH Rostral Anterior Cingulate (mm)		
Predictors	*Estimates*	*CI*	*p*
(Intercept)	3.164	3.068 – 3.260	**<0.001**
ASI	-0.000	-0.002 – 0.002	0.953
Instance [3 0]	0.022	-0.011 – 0.054	0.194
Years between visits	-0.008	-0.015 – -0.002	**0.007**
Waist to hip ratio	-0.062	-0.148 – 0.025	0.162
Age	-0.003	-0.004 – -0.002	**<0.001**
Sex	-0.000	-0.019 – 0.018	0.961
Physical Activity	-0.001	-0.003 – 0.002	0.550
ASI * Instance [3 0]	-0.001	-0.004 – 0.001	0.356
Random Effects			
σ^2	0.01		
$\tau_{00\ eid}$	0.02		
ICC	0.73		
$N_{\ eid}$	1855		
Observations	3620		
Marginal R^2 / Conditional R^2	0.023 / 0.732		

Appendix A5b). Left Hemisphere Rostral Anterior Cingulate Cortical Thickness Linear Mixed Effects Model Fit

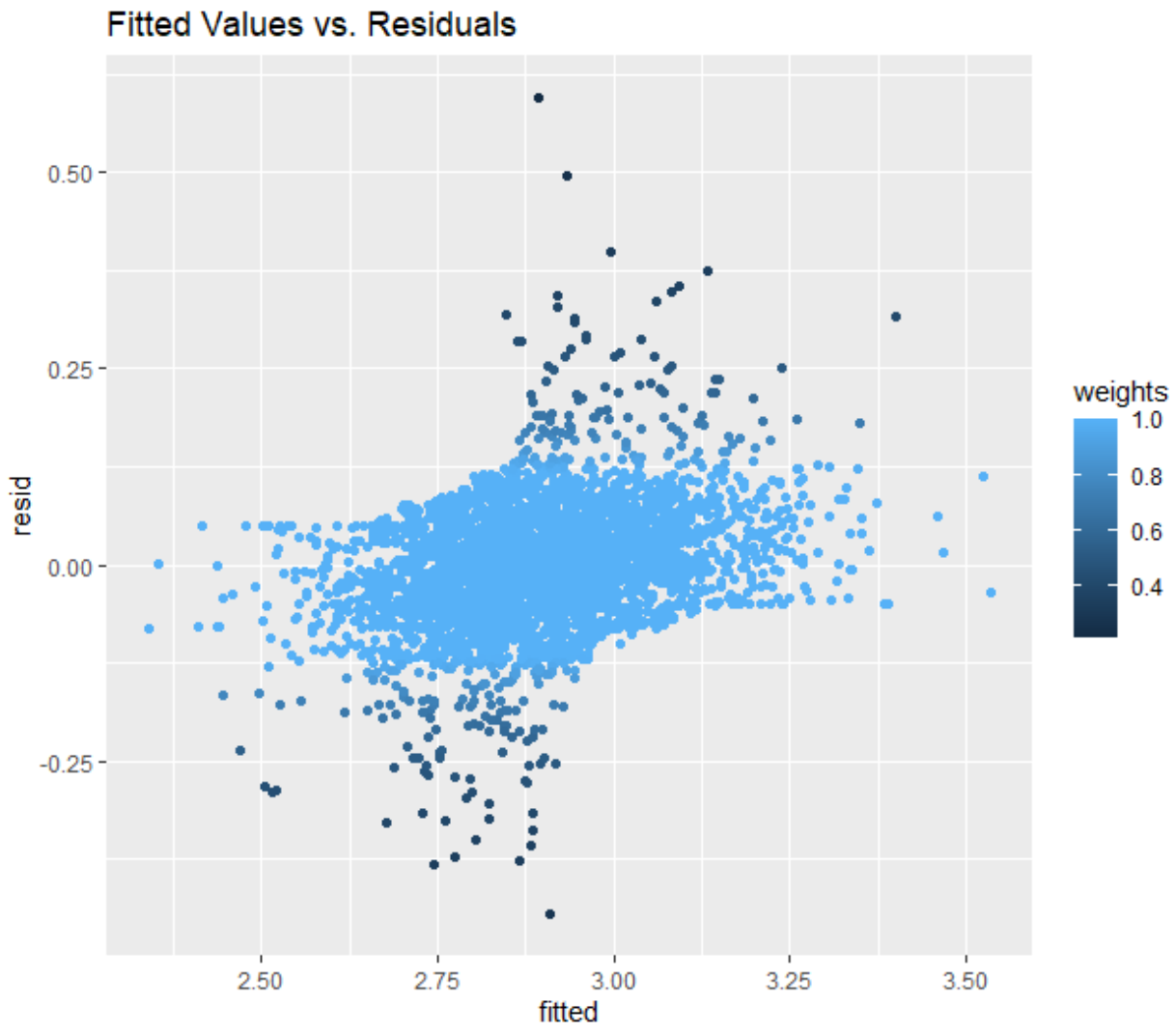

Appendix A6a). Right Hemisphere Rostral Anterior Cingulate Cortical Thickness Linear Mixed Effects Model Output

	RH Rostral Anterior Cingulate (mm)		
Predictors	*Estimates*	*CI*	*p*
(Intercept)	3.076	2.977 – 3.176	**<0.001**
ASI	-0.002	-0.004 – 0.001	0.122
Instance [3 0]	0.016	-0.019 – 0.051	0.361
Years between visits	-0.009	-0.016 – -0.003	**0.005**
Waist to hip ratio	-0.077	-0.169 – 0.014	0.097
Age	-0.001	-0.002 – 0.000	0.065
Sex	0.024	0.005 – 0.043	**0.013**
Physical Activity	0.002	-0.001 – 0.004	0.142
ASI * Instance [3 0]	-0.001	-0.004 – 0.002	0.632
Random Effects			
σ^2	0.01		
$\tau_{00\ eid}$	0.02		
ICC	0.69		
$N_{\ eid}$	1855		
Observations	3620		
Marginal R^2 / Conditional R^2	0.009 / 0.695		

Appendix A6b). Right Hemisphere Rostral Anterior Cingulate Cortical Thickness Linear Mixed Effects Model Fit

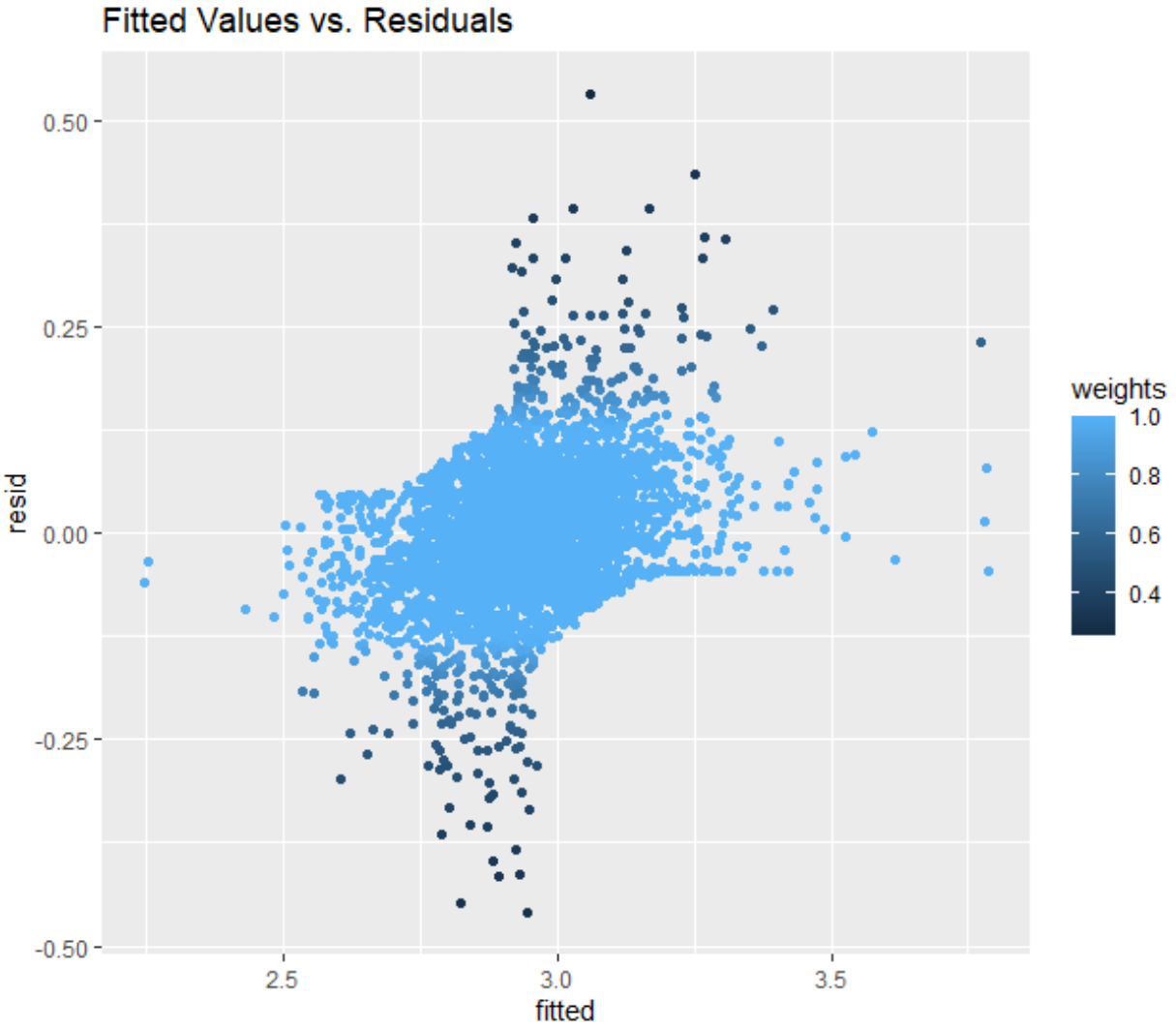

Appendix A7a). Left Hemisphere Rostral Middle Frontal Gyri Cortical Thickness Linear Mixed Effects Model Output

	LH Rostral Middle Frontal gyri (mm)		
Predictors	*Estimates*	*CI*	*p*
(Intercept)	3.043	2.981 – 3.106	**<0.001**
ASI	0.001	-0.000 – 0.003	0.060
Instance [3 0]	0.007	-0.012 – 0.026	0.465
Years between visits	0.001	-0.002 – 0.005	0.508
Waist to hip ratio	-0.010	-0.064 – 0.043	0.712
Age	-0.006	-0.007 – -0.005	**<0.001**
Sex	0.013	0.001 – 0.026	**0.039**
Physical Activity	-0.001	-0.002 – 0.001	0.456
ASI * Instance [3 0]	-0.001	-0.003 – 0.001	0.217
Random Effects			
σ^2	0.00		
$\tau_{00\ eid}$	0.01		
ICC	0.79		
$N_{\ eid}$	1855		
Observations	3620		
Marginal R^2 / Conditional R^2	0.114 / 0.818		

Appendix A7b). Left Hemisphere Rostral Middle Frontal Gyri Cortical Thickness Linear Mixed Effects Model Fit

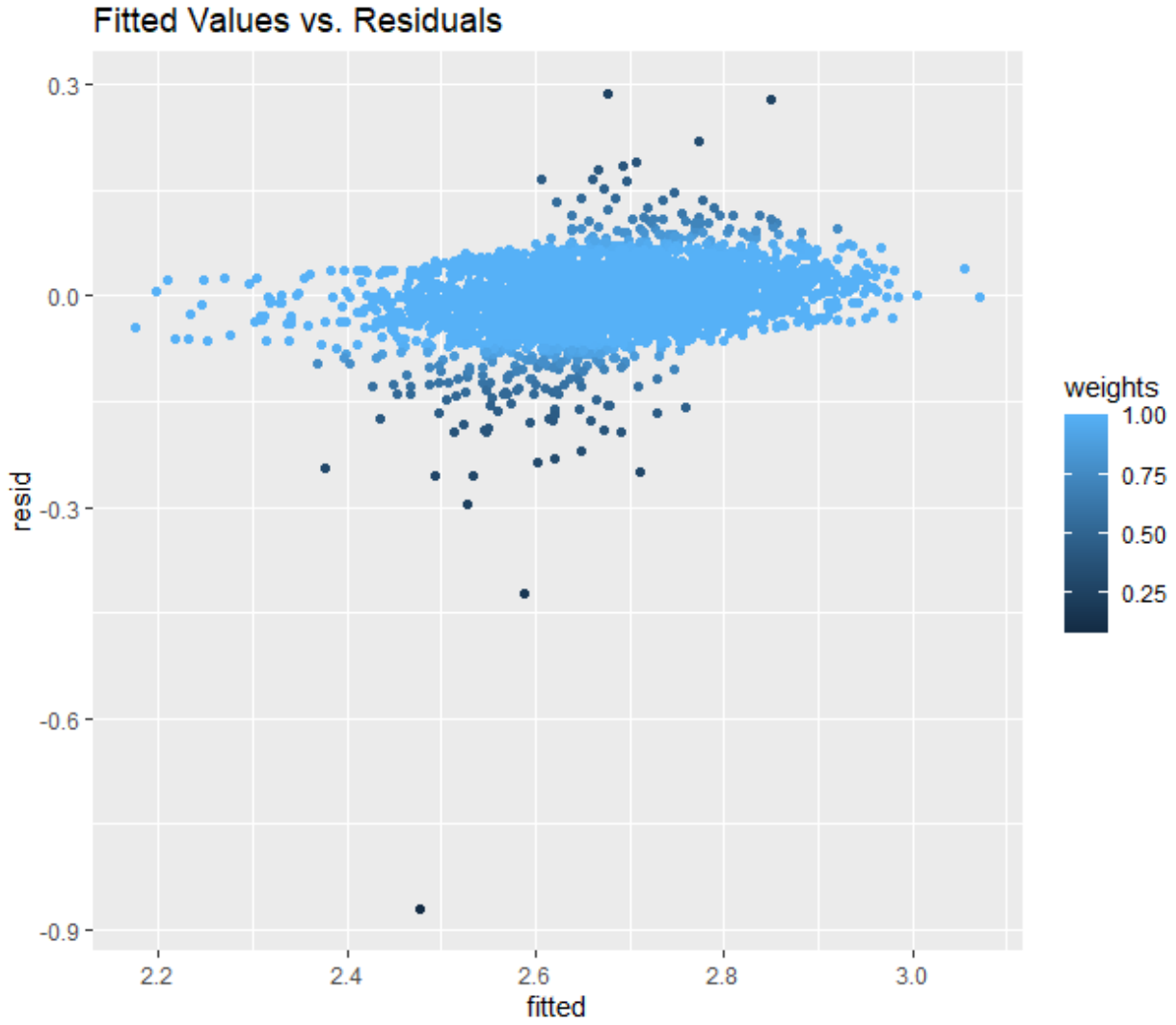

Appendix A8a). Right Hemisphere Rostral Middle Frontal Gyri Cortical Thickness Linear Mixed Effects Model Output

	RH Rostral Middle Frontal gyri (mm)		
Predictors	*Estimates*	*CI*	*p*
(Intercept)	2.895	2.838 – 2.951	**<0.001**
ASI	0.000	-0.001 – 0.002	0.502
Instance [3 0]	0.002	-0.016 – 0.019	0.853
Years between visits	0.001	-0.002 – 0.004	0.530
Waist to hip ratio	0.096	0.047 – 0.145	**<0.001**
Age	-0.006	-0.006 – -0.005	**<0.001**
Sex	0.002	-0.009 – 0.014	0.686
Physical Activity	-0.000	-0.001 – 0.001	0.749
ASI * Instance [3 0]	-0.001	-0.002 – 0.001	0.297
Random Effects			
σ^2	0.00		
$\tau_{00\ eid}$	0.01		
ICC	0.79		
$N_{\ eid}$	1855		
Observations	3620		
Marginal R^2 / Conditional R^2	0.127 / 0.812		

Appendix A8b). Right Hemisphere Rostral Middle Frontal Gyri Cortical Thickness Linear Mixed Effects Model Fit

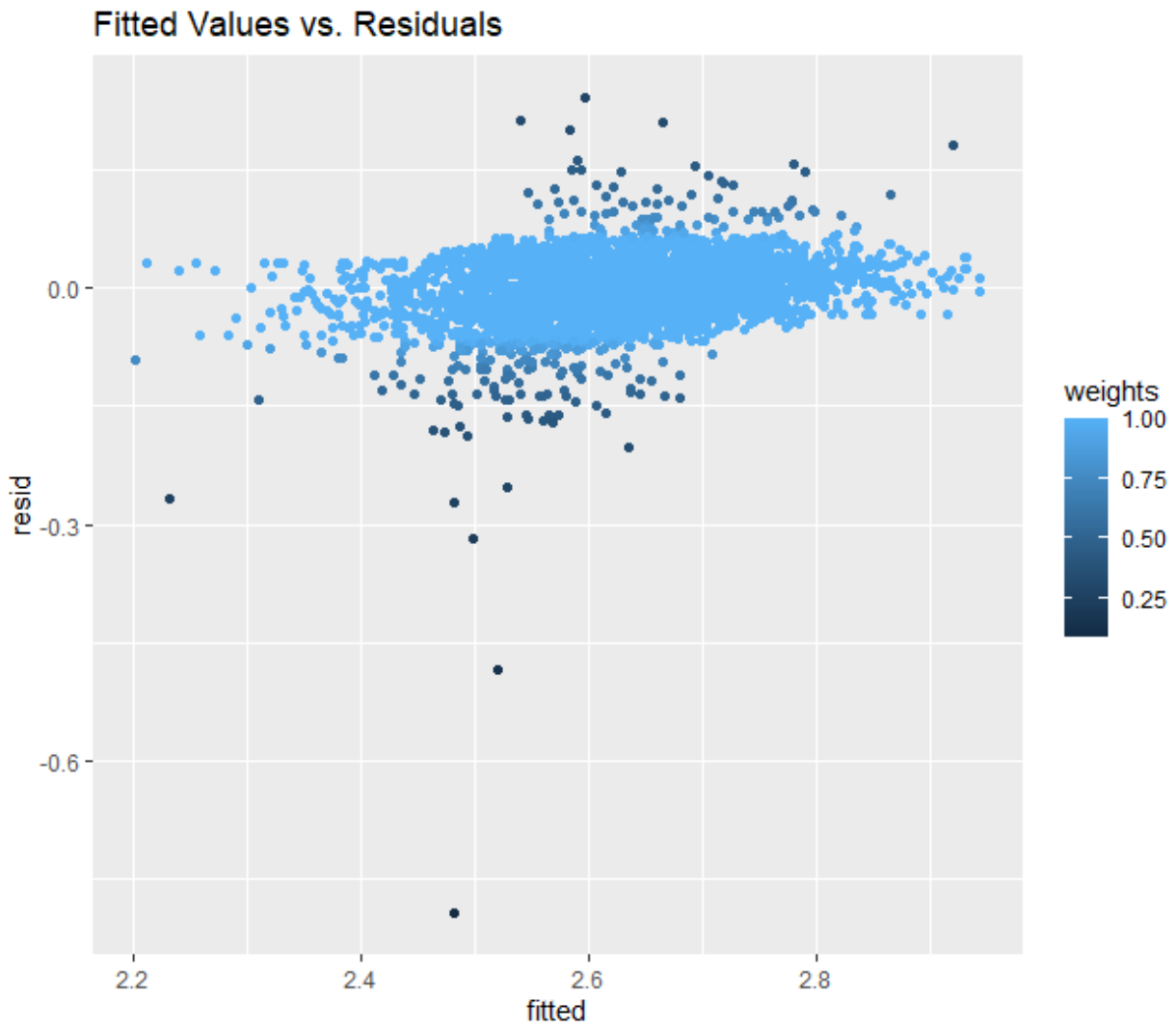

Appendix A9a). Left Hemisphere Superior Frontal Gyri Cortical Thickness Linear Mixed Effects Model Output

	LH Superior Frontal Gyri (mm)		
Predictors	*Estimates*	*CI*	*p*
(Intercept)	3.429	3.362 – 3.497	**<0.001**
ASI	0.002	0.000 – 0.003	**0.026**
Instance [3 0]	-0.003	-0.024 – 0.019	0.807
Years between visits	0.008	0.004 – 0.012	**<0.001**
Waist to hip ratio	-0.008	-0.066 – 0.051	0.791
Age	-0.008	-0.008 – -0.007	**<0.001**
Sex	-0.006	-0.020 – 0.007	0.366
Physical Activity	-0.001	-0.003 – 0.000	0.142
ASI * Instance [3 0]	-0.002	-0.004 – 0.000	0.053
Random Effects			
σ^2	0.00		
$\tau_{00\ eid}$	0.01		
ICC	0.79		
$N_{\ eid}$	1855		
Observations	3620		
Marginal R^2 / Conditional R^2	0.160 / 0.820		

Appendix A9b). Left Hemisphere Superior Frontal Gyri Cortical Thickness Linear Mixed Effects Model Fit

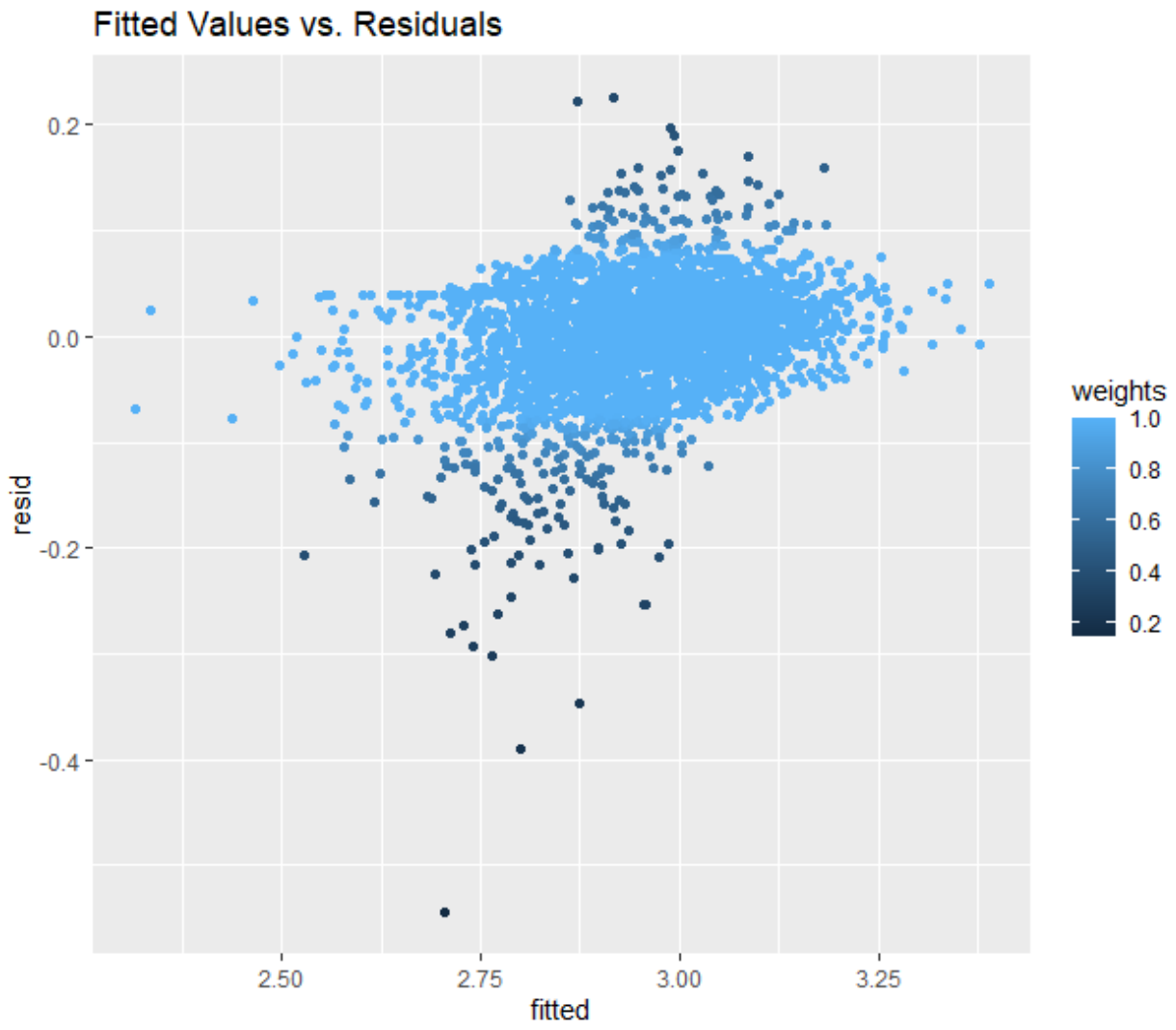

Appendix A10a). Right Hemisphere Superior Frontal Gyri Cortical Thickness Linear Mixed Effects Model Output

	RH Superior Frontal Gyri (mm)		
Predictors	*Estimates*	*CI*	*p*
(Intercept)	3.290	3.227 – 3.353	**<0.001**
ASI	0.001	-0.000 – 0.002	0.187
Instance [3 0]	-0.001	-0.021 – 0.020	0.931
Years between visits	0.006	0.002 – 0.010	**0.002**
Waist to hip ratio	0.054	-0.001 – 0.110	0.056
Age	-0.007	-0.008 – -0.006	**<0.001**
Sex	-0.014	-0.027 – -0.002	**0.024**
Physical Activity	-0.000	-0.002 – 0.001	0.661
ASI * Instance [3 0]	-0.002	-0.003 – 0.000	0.058
Random Effects			
σ^2	0.00		
$\tau_{00\ eid}$	0.01		
ICC	0.76		
$N_{\ eid}$	1855		
Observations	3620		
Marginal R^2 / Conditional R^2	0.151 / 0.797		

Appendix A10b). Right Hemisphere Superior Frontal Gyri Cortical Thickness Linear Mixed Effects Model Fit

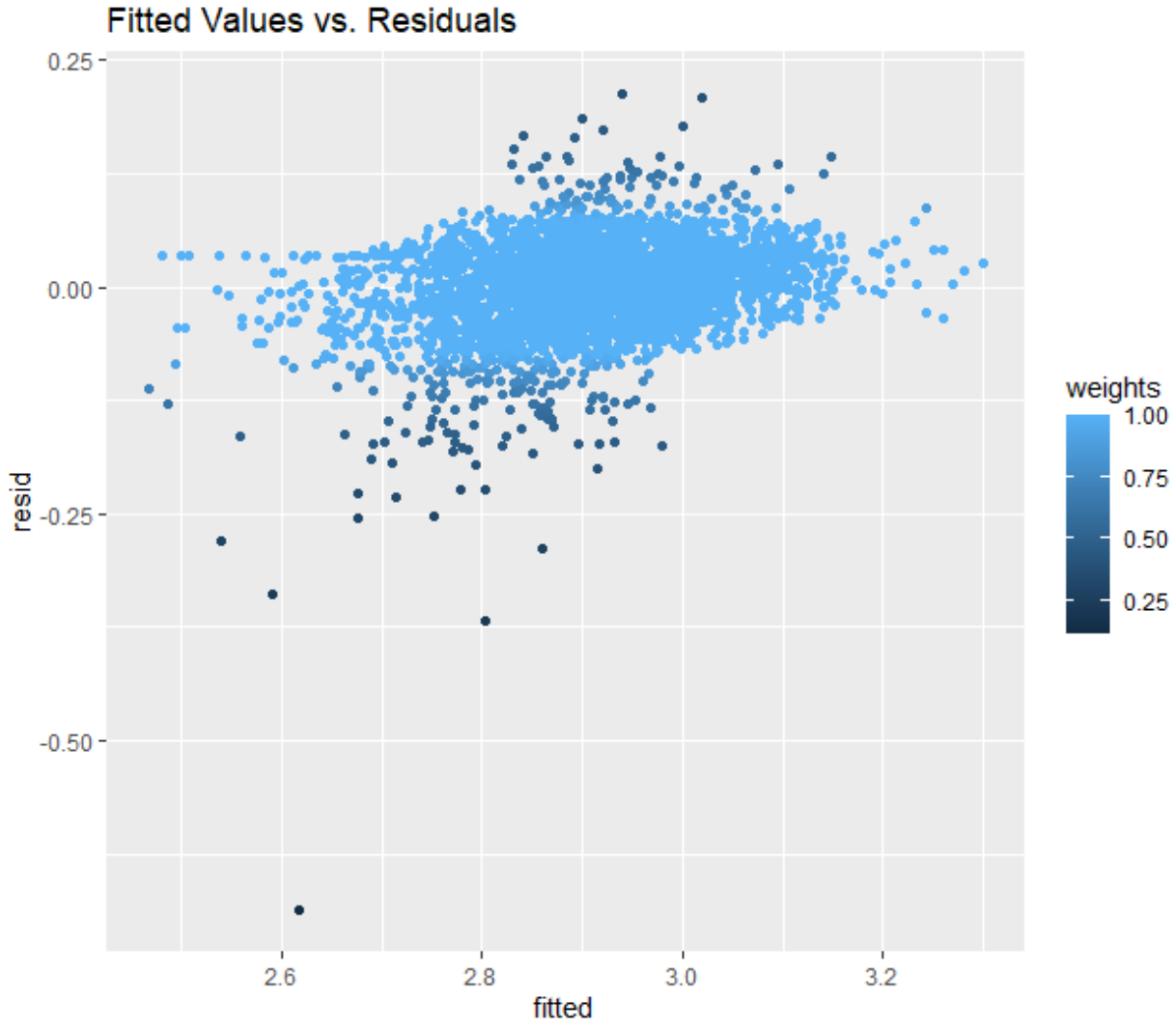

Appendix A11a). Left Hemisphere Superior Parietal Cortex Cortical Thickness Linear Mixed Effects Model Output

	LH Superior Parietal Cortex (mm)		
Predictors	*Estimates*	*CI*	*p*
(Intercept)	2.753	2.689 – 2.817	**<0.001**
ASI	0.002	0.001 – 0.003	**0.005**
Instance [3 0]	-0.010	-0.031 – 0.010	0.320
Years between visits	0.010	0.006 – 0.014	**<0.001**
Waist to hip ratio	0.018	-0.037 – 0.074	0.517
Age	-0.005	-0.006 – -0.004	**<0.001**
Sex	-0.006	-0.018 – 0.007	0.391
Physical Activity	-0.002	-0.003 – -0.000	**0.038**
ASI * Instance [3 0]	-0.001	-0.003 – 0.000	0.158
Random Effects			
σ^2	0.00		
$\tau_{00\ eid}$	0.01		
ICC	0.78		
$N_{\ eid}$	1855		
Observations	3620		
Marginal R^2 / Conditional R^2	0.084 / 0.794		

Appendix A11b). Left Hemisphere Superior Parietal Cortex Cortical Thickness Linear Mixed Effects Model Fit

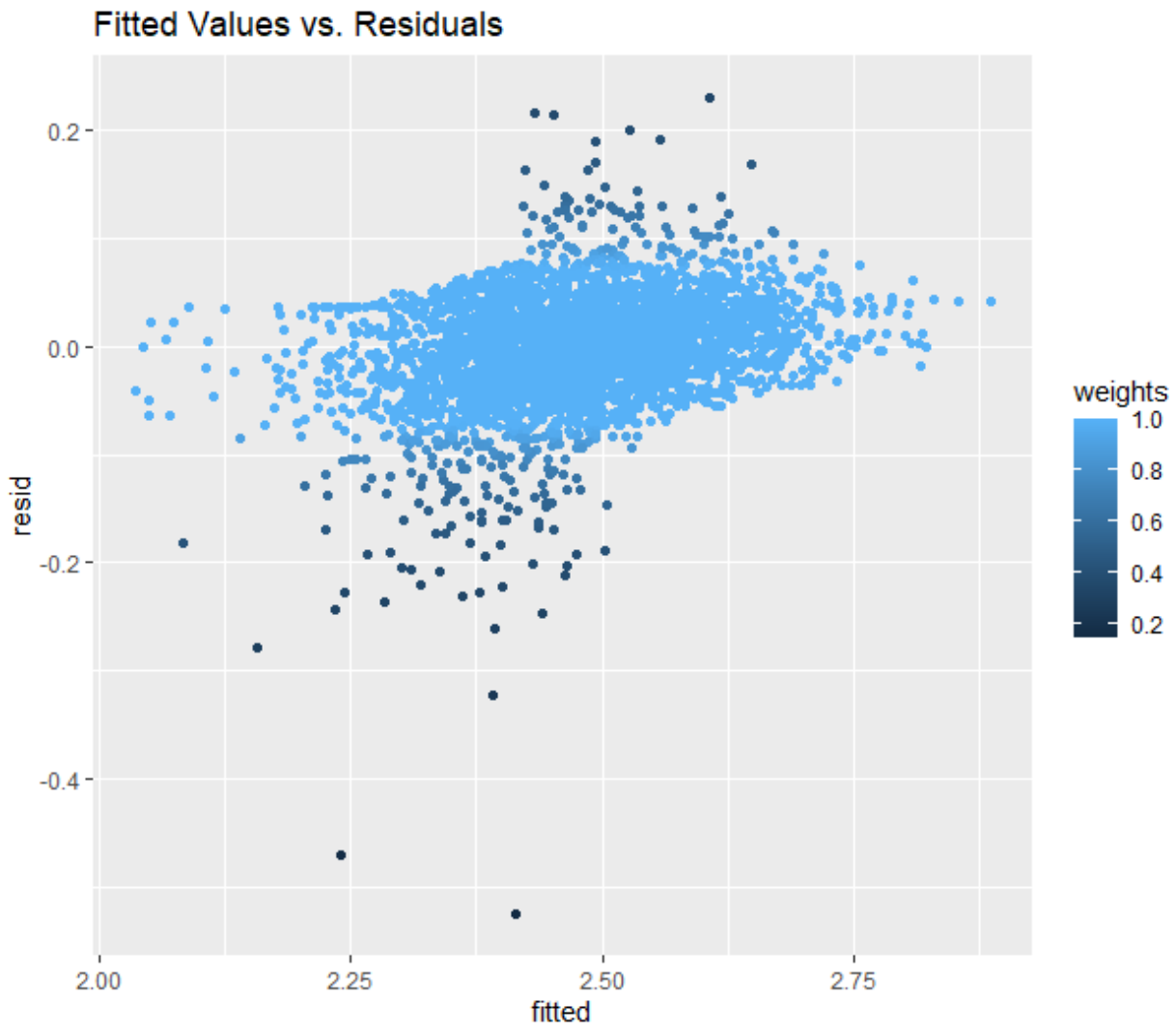

Appendix A12a). Right Hemisphere Superior Parietal Cortex Cortical Thickness Linear Mixed Effects Model Output

	RH Superior Parietal Cortex (mm)		
Predictors	*Estimates*	*CI*	*p*
(Intercept)	2.722	2.657 – 2.786	**<0.001**
ASI	0.001	0.000 – 0.003	**0.042**
Instance [3 0]	0.006	-0.015 – 0.026	0.588
Years between visits	0.005	0.002 – 0.009	**0.006**
Waist to hip ratio	0.068	0.011 – 0.124	**0.019**
Age	-0.005	-0.006 – -0.005	**<0.001**
Sex	-0.024	-0.037 – -0.011	**<0.001**
Physical Activity	-0.000	-0.002 – 0.001	0.631
ASI * Instance [3 0]	-0.002	-0.004 – -0.000	**0.025**
Random Effects			
σ^2	0.00		
$\tau_{00\ eid}$	0.01		
ICC	0.78		
$N_{\ eid}$	1855		
Observations	3620		
Marginal R^2 / Conditional R^2	0.099 / 0.801		

Appendix A12b). Right Hemisphere Superior Parietal Cortex Cortical Thickness Linear Mixed Effects Model Fit

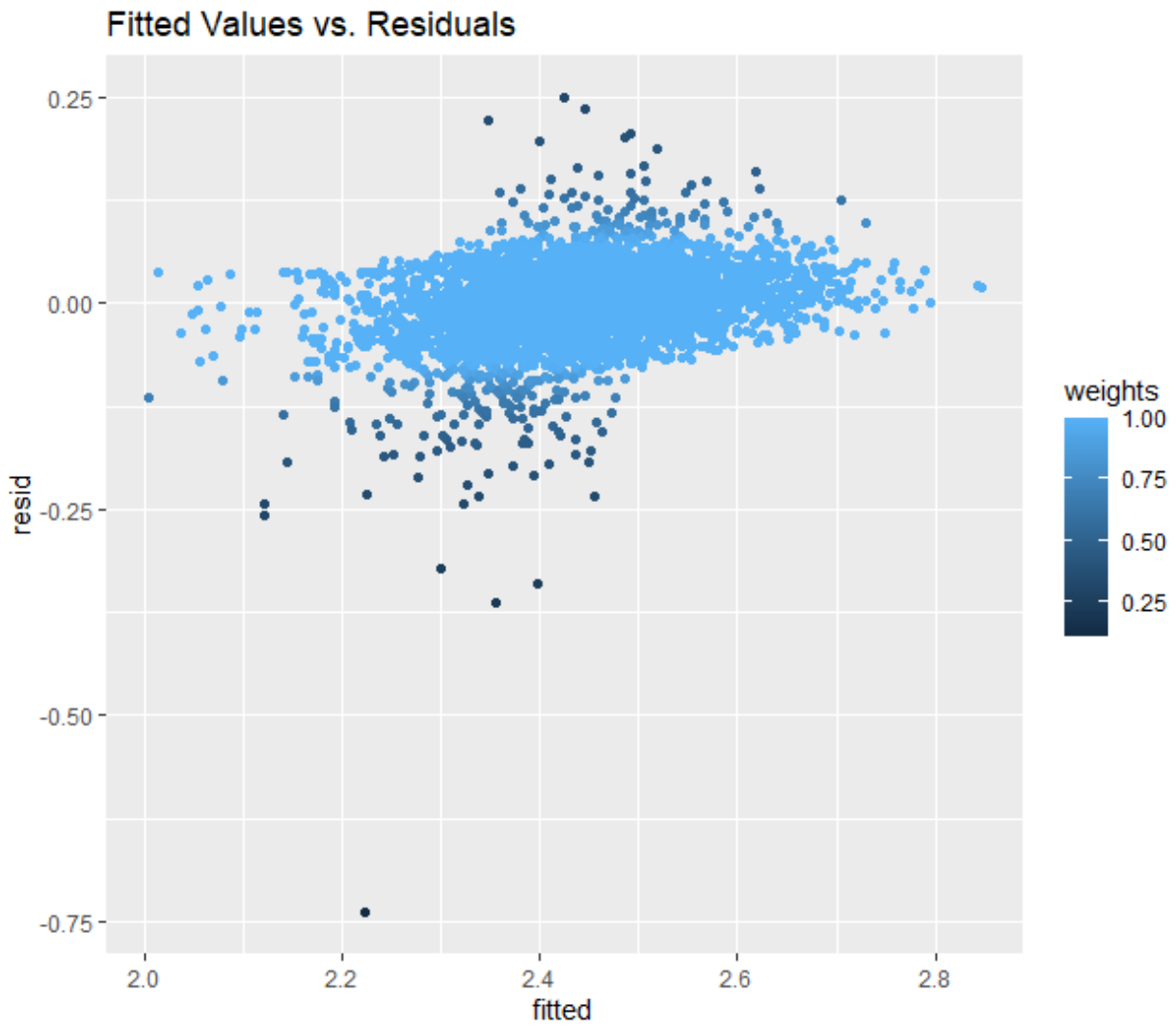

Appendix A13a). Left Hemisphere Inferior Parietal Cortex Cortical Thickness Linear Mixed Effects Model Output

	LH Inferior Parietal Cortex (mm)		
Predictors	*Estimates*	*CI*	*p*
(Intercept)	3.004	2.946 – 3.062	**<0.001**
ASI	0.002	0.001 – 0.003	**0.003**
Instance [3 0]	0.004	-0.013 – 0.022	0.630
Years between visits	0.005	0.002 – 0.008	**0.004**
Waist to hip ratio	0.003	-0.046 – 0.052	0.910
Age	-0.005	-0.006 – -0.004	**<0.001**
Sex	-0.013	-0.025 – -0.002	**0.026**
Physical Activity	-0.001	-0.002 – 0.000	0.061
ASI * Instance [3 0]	-0.002	-0.003 – -0.000	**0.023**
Random Effects			
σ^2	0.00		
$\tau_{00\ eid}$	0.01		
ICC	0.81		
$N_{\ eid}$	1855		
Observations	3620		
Marginal R^2 / Conditional R^2	0.106 / 0.828		

Appendix A13b). Left Hemisphere Inferior Parietal Cortex Cortical Thickness Linear Mixed Effects Model Fit

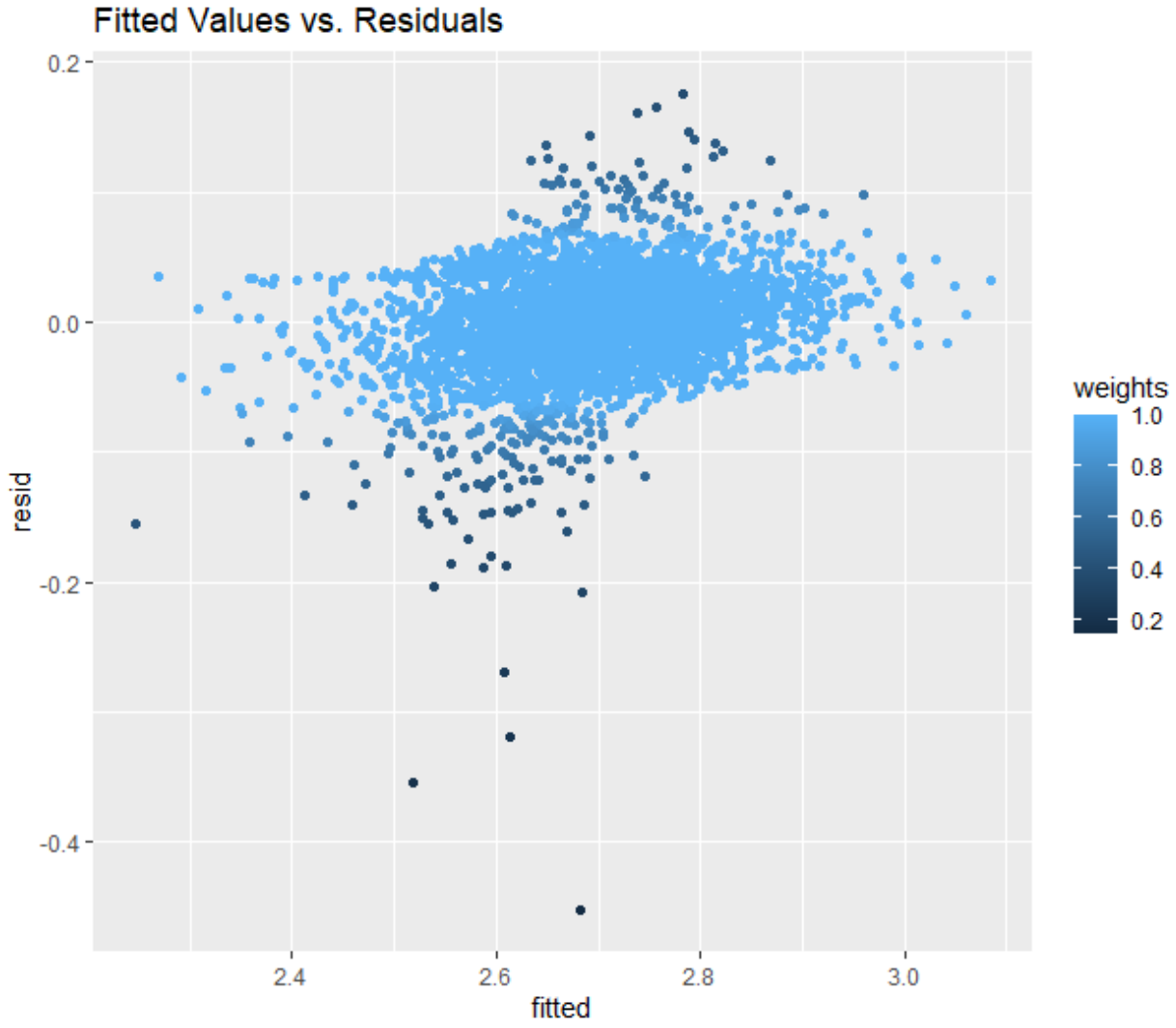

Appendix A14a). Right Hemisphere Inferior Parietal Cortex Cortical Thickness Linear Mixed Effects Model Output

	RH Inferior Parietal Cortex (mm)		
Predictors	*Estimates*	*CI*	*p*
(Intercept)	3.045	2.985 – 3.106	**<0.001**
ASI	0.001	0.000 – 0.002	**0.045**
Instance [3 0]	0.004	-0.014 – 0.022	0.648
Years between visits	0.003	-0.000 – 0.006	0.083
Waist to hip ratio	0.059	0.009 – 0.109	**0.021**
Age	-0.006	-0.007 – -0.005	**<0.001**
Sex	-0.011	-0.023 – 0.001	0.074
Physical Activity	-0.001	-0.002 – 0.001	0.408
ASI * Instance [3 0]	-0.001	-0.003 – 0.000	0.090
Random Effects			
σ^2	0.00		
$\tau_{00\ eid}$	0.01		
ICC	0.82		
$N_{\ eid}$	1855		
Observations	3620		
Marginal R^2 / Conditional R^2	0.125 / 0.845		

Appendix A14b). Right Hemisphere Inferior Parietal Cortex Cortical Thickness Linear Mixed Effects Model Fit

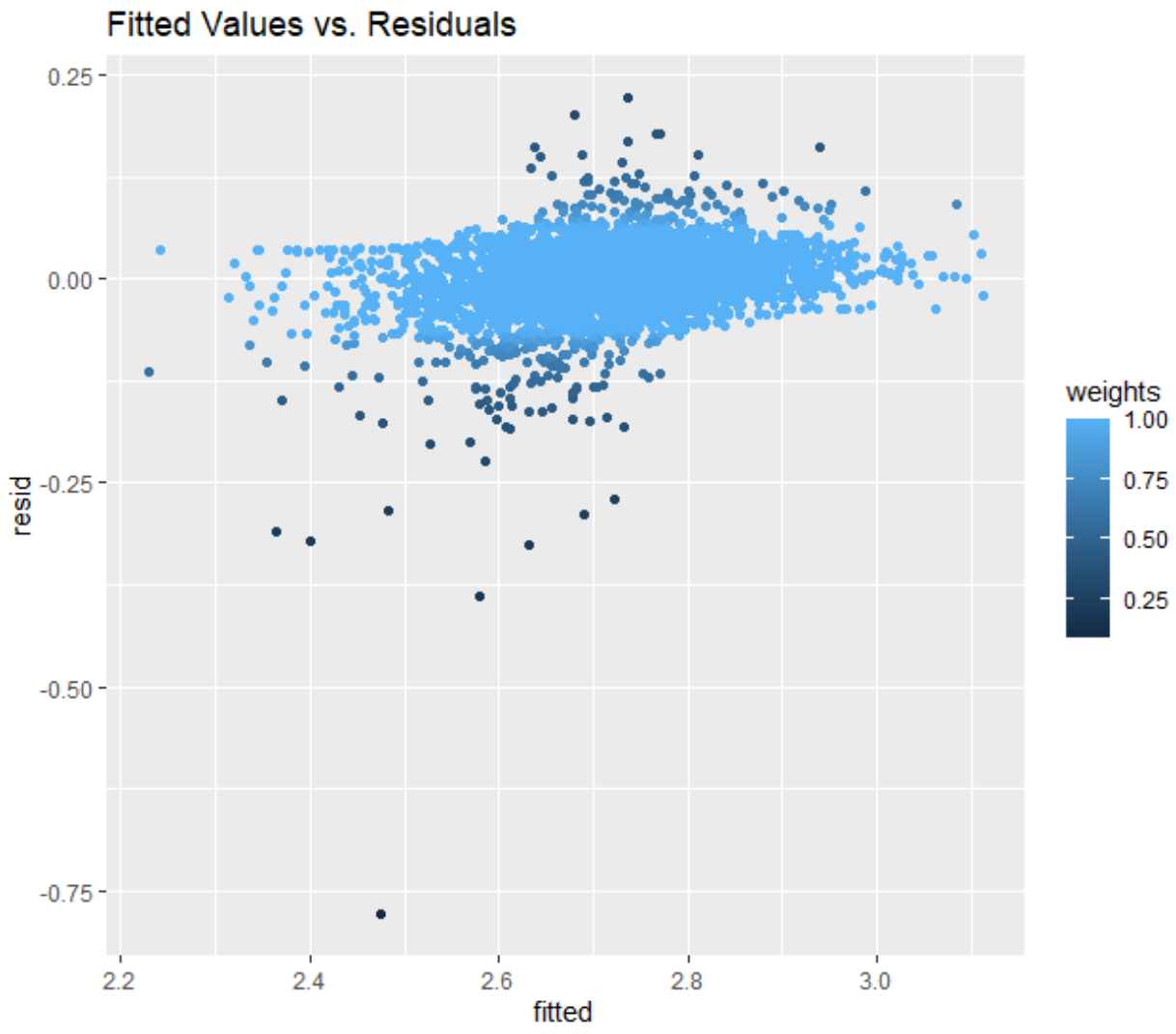

Appendix A15a). Left Hemisphere Superior Temporal Cortex Cortical Thickness Linear Mixed Effects Model Output

	LH Superior Temporal Cortex (mm)		
Predictors	*Estimates*	*CI*	*p*
(Intercept)	3.433	3.352 – 3.515	**<0.001**
ASI	0.002	0.000 – 0.004	**0.035**
Instance [3 0]	0.016	-0.011 – 0.044	0.239
Years between visits	-0.001	-0.006 – 0.004	0.757
Waist to hip ratio	-0.075	-0.148 – -0.002	**0.044**
Age	-0.007	-0.008 – -0.006	**<0.001**
Sex	0.027	0.011 – 0.043	**0.001**
Physical Activity	-0.001	-0.003 – 0.001	0.345
ASI * Instance [3 0]	-0.002	-0.004 – 0.000	0.104
Random Effects			
σ^2	0.01		
$\tau_{00\ eid}$	0.02		
ICC	0.74		
$N_{\ eid}$	1855		
Observations	3620		
Marginal R^2 / Conditional R^2	0.096 / 0.764		

Appendix A15b). Left Hemisphere Superior Temporal Cortex Cortical Thickness Linear Mixed Effects Model Fit

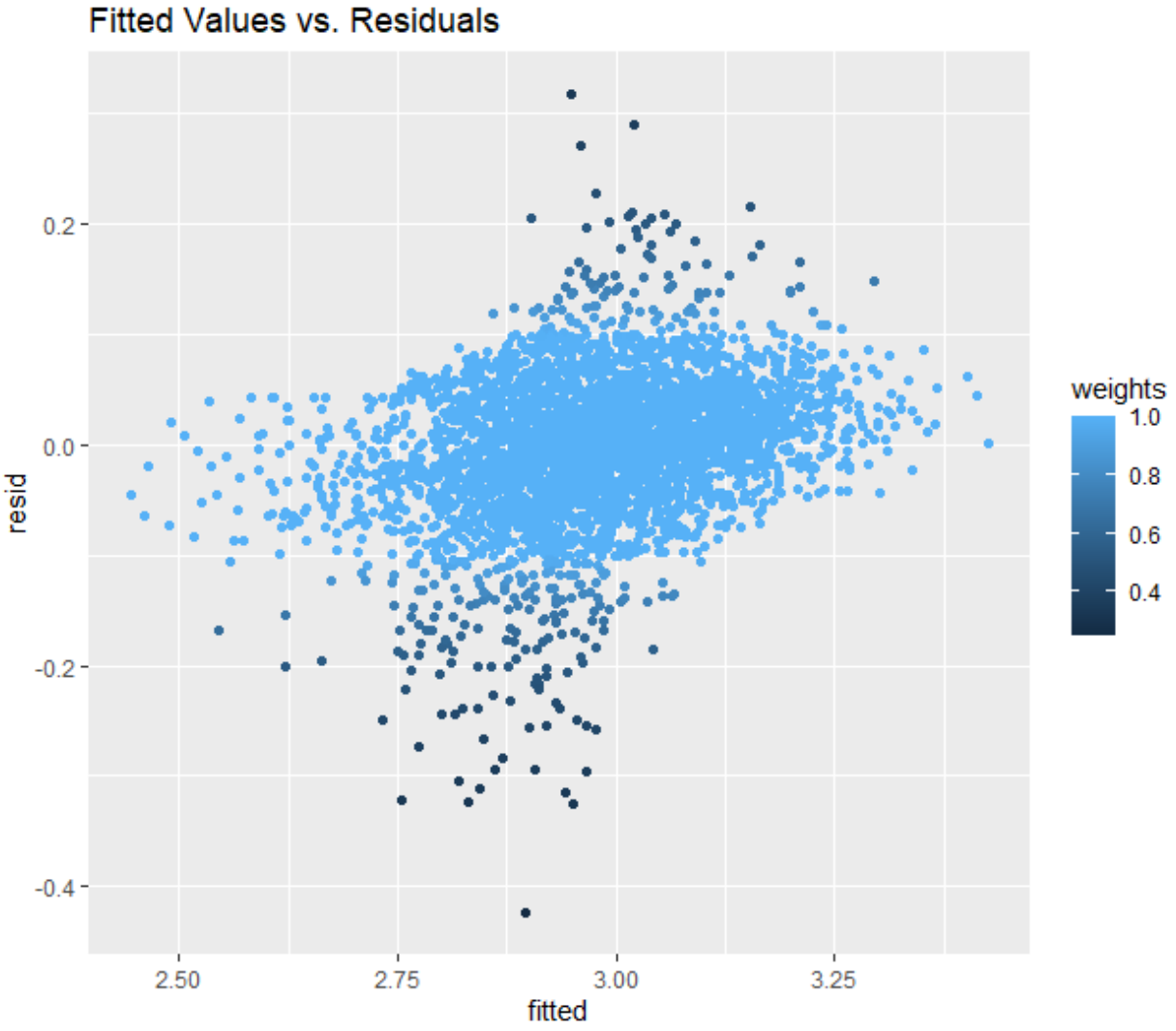

Appendix A16a). Right Hemisphere Superior Temporal Cortex Cortical Thickness Linear Mixed Effects Model Output

	RH Superior Temporal Cortex (mm)		
Predictors	*Estimates*	*CI*	*p*
(Intercept)	3.501	3.422 – 3.579	**<0.001**
ASI	0.001	-0.001 – 0.003	0.197
Instance [3 0]	0.016	-0.011 – 0.043	0.240
Years between visits	0.001	-0.004 – 0.006	0.666
Waist to hip ratio	0.041	-0.030 – 0.112	0.260
Age	-0.008	-0.009 – -0.007	**<0.001**
Sex	0.008	-0.007 – 0.023	0.293
Physical Activity	0.000	-0.001 – 0.002	0.673
ASI * Instance [3 0]	-0.003	-0.005 – -0.000	**0.019**
Random Effects			
σ^2	0.01		
$\tau_{00\ eid}$	0.02		
ICC	0.72		
$N_{\ eid}$	1855		
Observations	3620		
Marginal R^2 / Conditional R^2	0.138 / 0.758		

Appendix A16b). Right Hemisphere Superior Temporal Cortex Cortical Thickness Linear Mixed Effects Model Fit

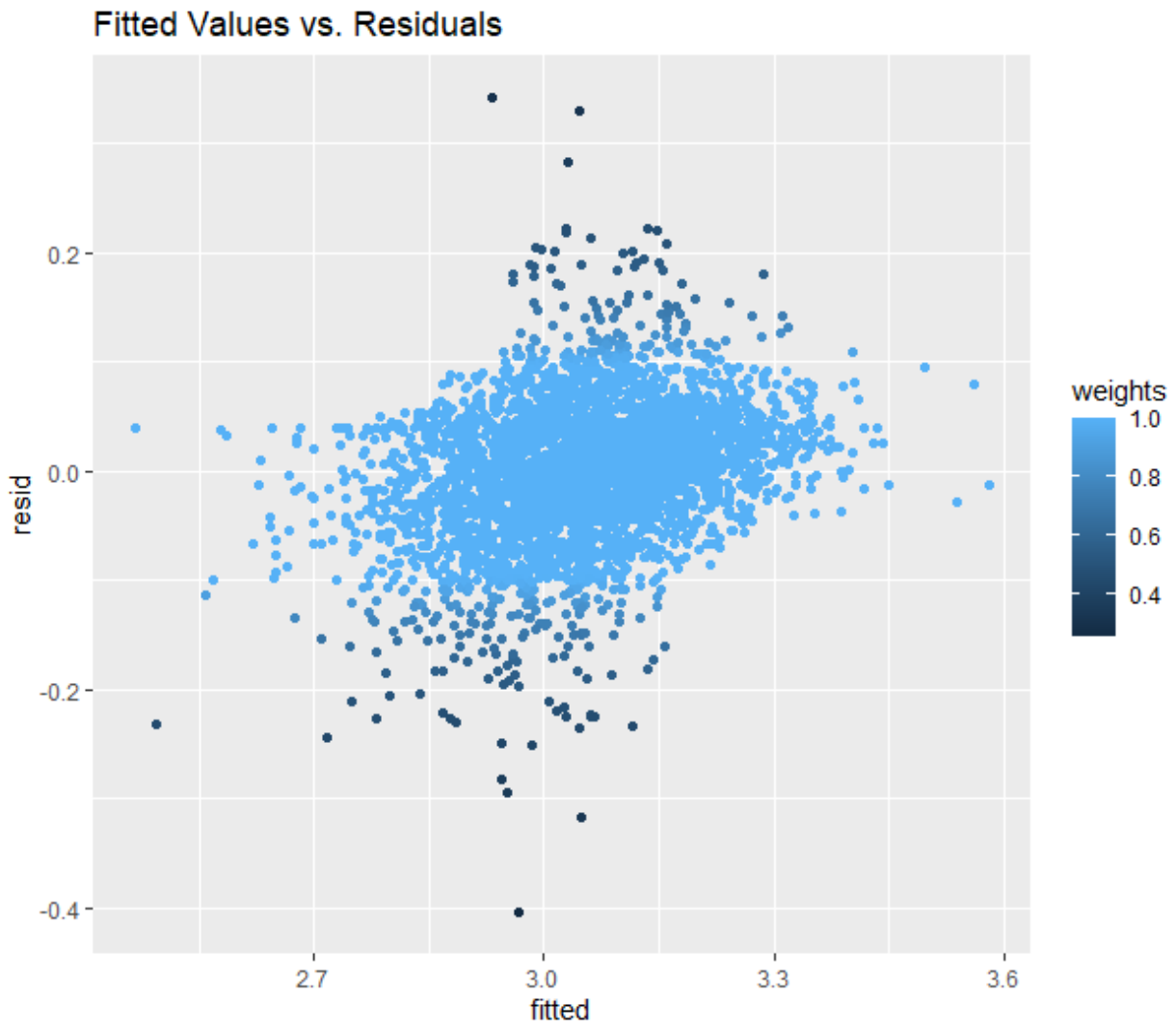

Appendix A17a). Left Hemisphere Middle Temporal Lobe Cortical Thickness Linear Mixed Effects Model Output

	LH Middle Temporal Lobe (mm)		
Predictors	*Estimates*	*CI*	*p*
(Intercept)	3.208	3.133 – 3.284	**<0.001**
ASI	0.002	-0.000 – 0.003	0.054
Instance [3 0]	0.020	-0.005 – 0.044	0.123
Years between visits	-0.003	-0.007 – 0.002	0.284
Waist to hip ratio	-0.090	-0.157 – -0.023	**0.008**
Age	-0.004	-0.005 – -0.003	**<0.001**
Sex	0.039	0.024 – 0.054	**<0.001**
Physical Activity	-0.000	-0.002 – 0.001	0.634
ASI * Instance [3 0]	-0.002	-0.004 – -0.000	**0.031**
Random Effects			
σ^2	0.01		
$\tau_{00\ eid}$	0.02		
ICC	0.74		
$N_{\ eid}$	1855		
Observations	3620		
Marginal R^2 / Conditional R^2	0.055 / 0.759		

Appendix A17b). Left Hemisphere Middle Temporal Lobe Cortical Thickness Linear Mixed Effects Model Fit

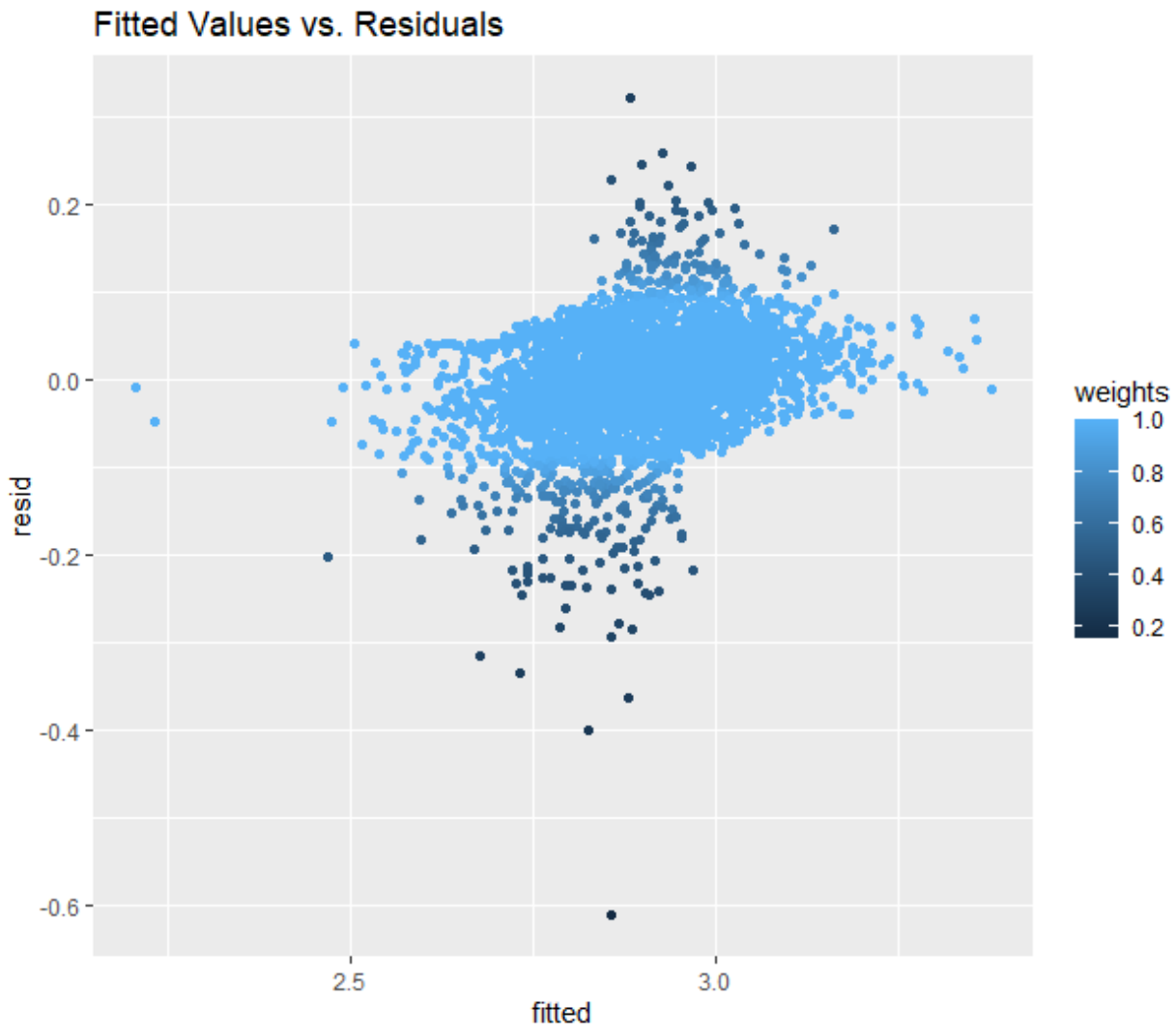

Appendix A18a). Right Hemisphere Middle Temporal Lobe Cortical Thickness Linear Mixed Effects Model Output

	RH Middle Temporal Lobe (mm)		
Predictors	*Estimates*	*CI*	*p*
(Intercept)	3.234	3.161 – 3.306	**<0.001**
ASI	0.001	-0.000 – 0.003	0.103
Instance [3 0]	0.018	-0.006 – 0.042	0.151
Years between visits	-0.000	-0.005 – 0.004	0.877
Waist to hip ratio	0.052	-0.013 – 0.117	0.117
Age	-0.005	-0.006 – -0.004	**<0.001**
Sex	0.019	0.005 – 0.033	**0.010**
Physical Activity	-0.000	-0.002 – 0.002	0.901
ASI * Instance [3 0]	-0.002	-0.004 – -0.000	**0.035**
Random Effects			
σ^2	0.00		
$\tau_{00\ eid}$	0.01		
ICC	0.74		
$N_{\ eid}$	1855		
Observations	3620		
Marginal R^2 / Conditional R^2	0.070 / 0.759		

Appendix A18b). Right Hemisphere Middle Temporal Lobe Cortical Thickness Linear Mixed Effects Model Fit

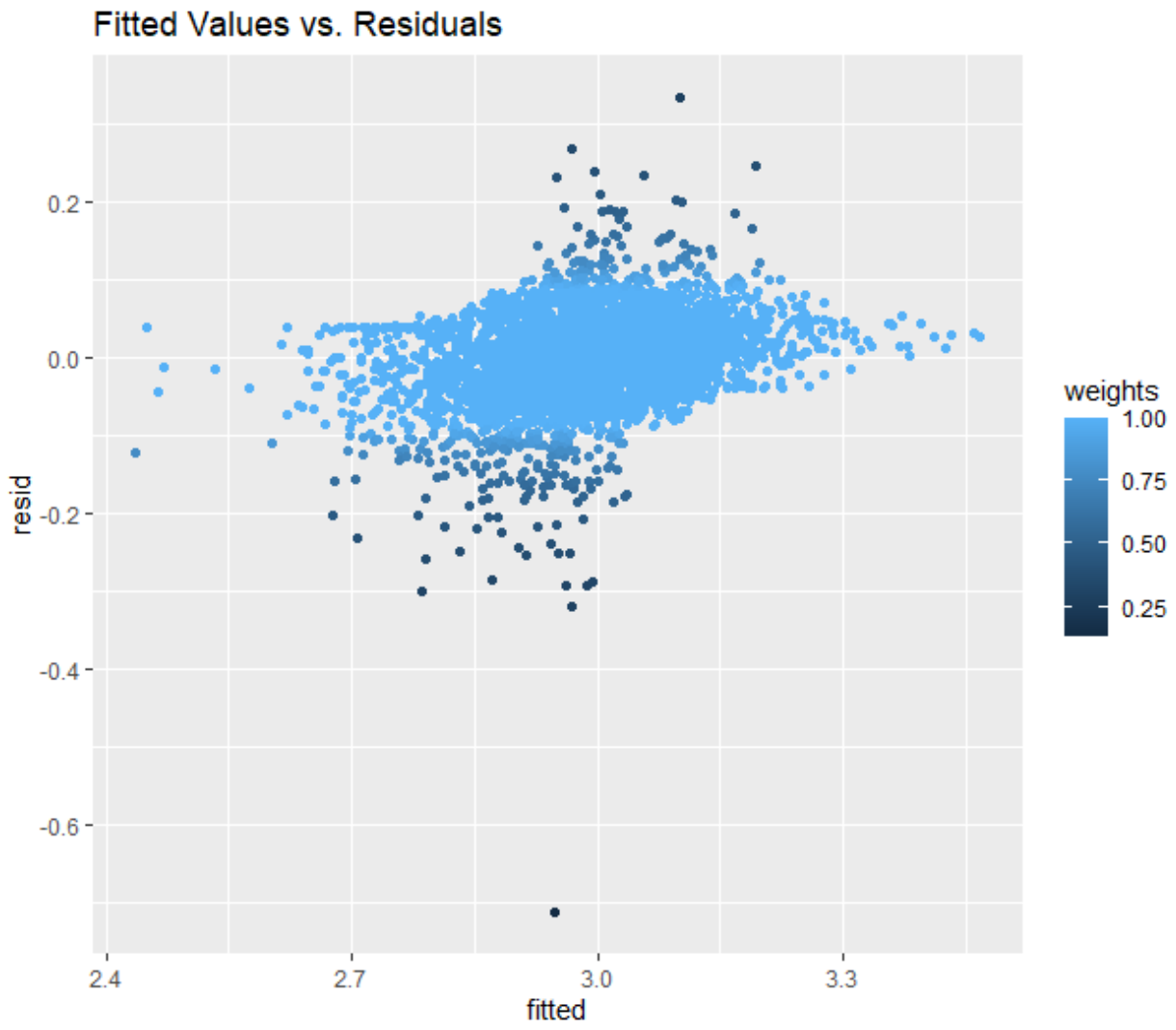

Appendix A19a). Left Hemisphere Inferior Temporal Lobe Cortical Thickness Linear Mixed Effects Model Output

	LH Inferior Temporal Cortex (mm)		
Predictors	*Estimates*	*CI*	*p*
(Intercept)	3.233	3.164 – 3.301	**<0.001**
ASI	0.001	-0.000 – 0.003	0.114
Instance [3 0]	0.017	-0.005 – 0.039	0.133
Years between visits	-0.003	-0.007 – 0.001	0.190
Waist to hip ratio	-0.019	-0.080 – 0.041	0.528
Age	-0.003	-0.004 – -0.002	**<0.001**
Sex	0.030	0.016 – 0.043	**<0.001**
Physical Activity	-0.000	-0.002 – 0.001	0.829
ASI * Instance [3 0]	-0.002	-0.004 – -0.000	**0.041**
Random Effects			
σ^2	0.00		
$\tau_{00\ eid}$	0.01		
ICC	0.76		
$N_{\ eid}$	1855		
Observations	3620		
Marginal R^2 / Conditional R^2	0.039 / 0.772		

Appendix A19b). Left Hemisphere Inferior Temporal Lobe Cortical Thickness Linear Mixed Effects Model Fit

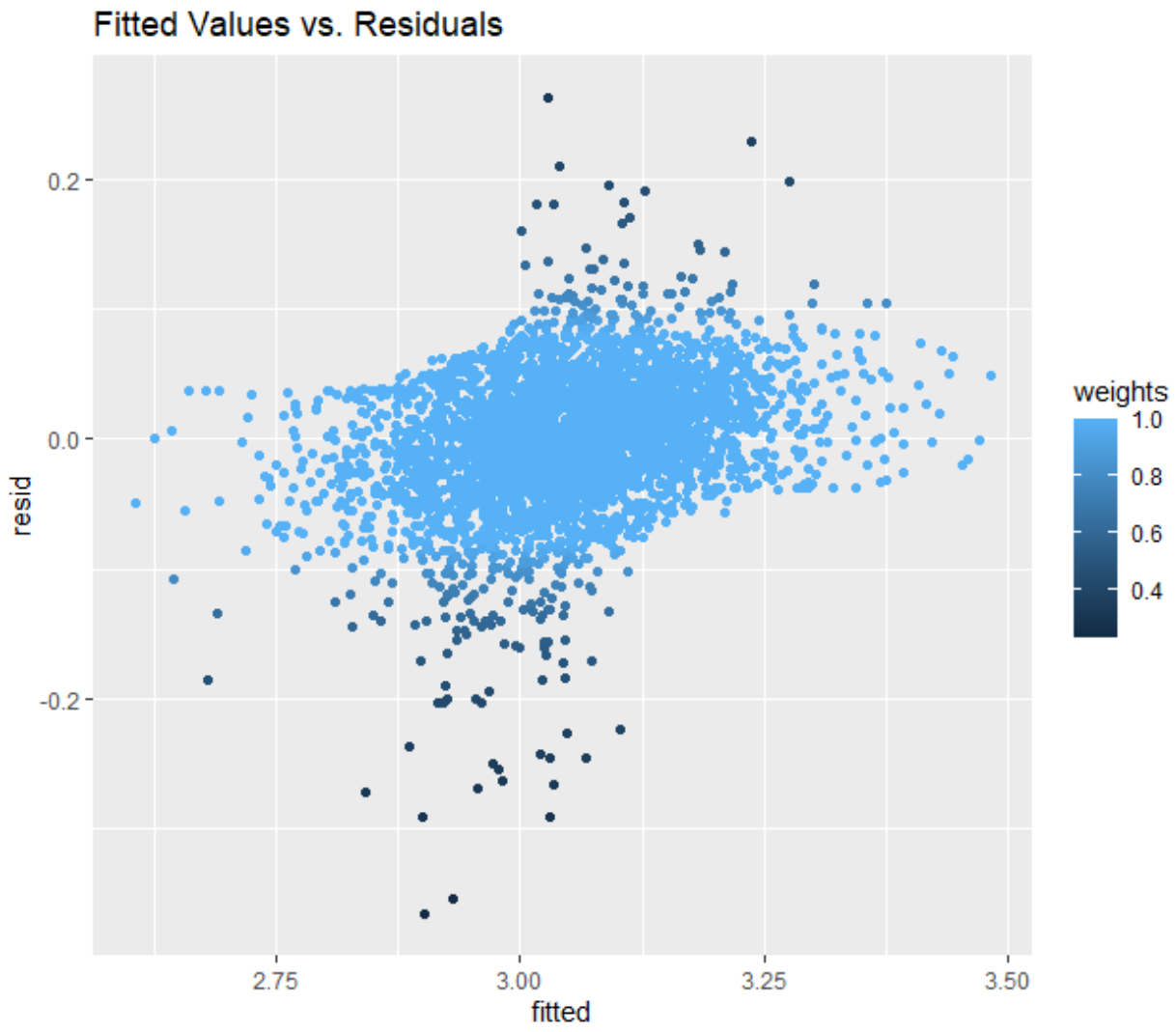

Appendix A20a). Right Hemisphere Inferior Temporal Lobe Cortical Thickness Linear Mixed Effects Model Output

	RH Inferior Temporal Cortex (mm)		
Predictors	*Estimates*	*CI*	*p*
(Intercept)	3.178	3.111 – 3.245	**<0.001**
ASI	0.001	-0.001 – 0.002	0.402
Instance [3 0]	0.007	-0.014 – 0.027	0.528
Years between visits	0.002	-0.002 – 0.005	0.442
Waist to hip ratio	0.024	-0.032 – 0.081	0.402
Age	-0.003	-0.004 – -0.002	**<0.001**
Sex	0.005	-0.008 – 0.018	0.467
Physical Activity	-0.000	-0.002 – 0.001	0.764
ASI * Instance [3 0]	-0.002	-0.003 – 0.000	0.057
Random Effects			
σ^2	0.00		
$\tau_{00\ eid}$	0.01		
ICC	0.80		
$N_{\ eid}$	1855		
Observations	3620		
Marginal R^2 / Conditional R^2	0.027 / 0.807		

Appendix A20b). Right Hemisphere Inferior Temporal Lobe Cortical Thickness Linear Mixed Effects Model Fit

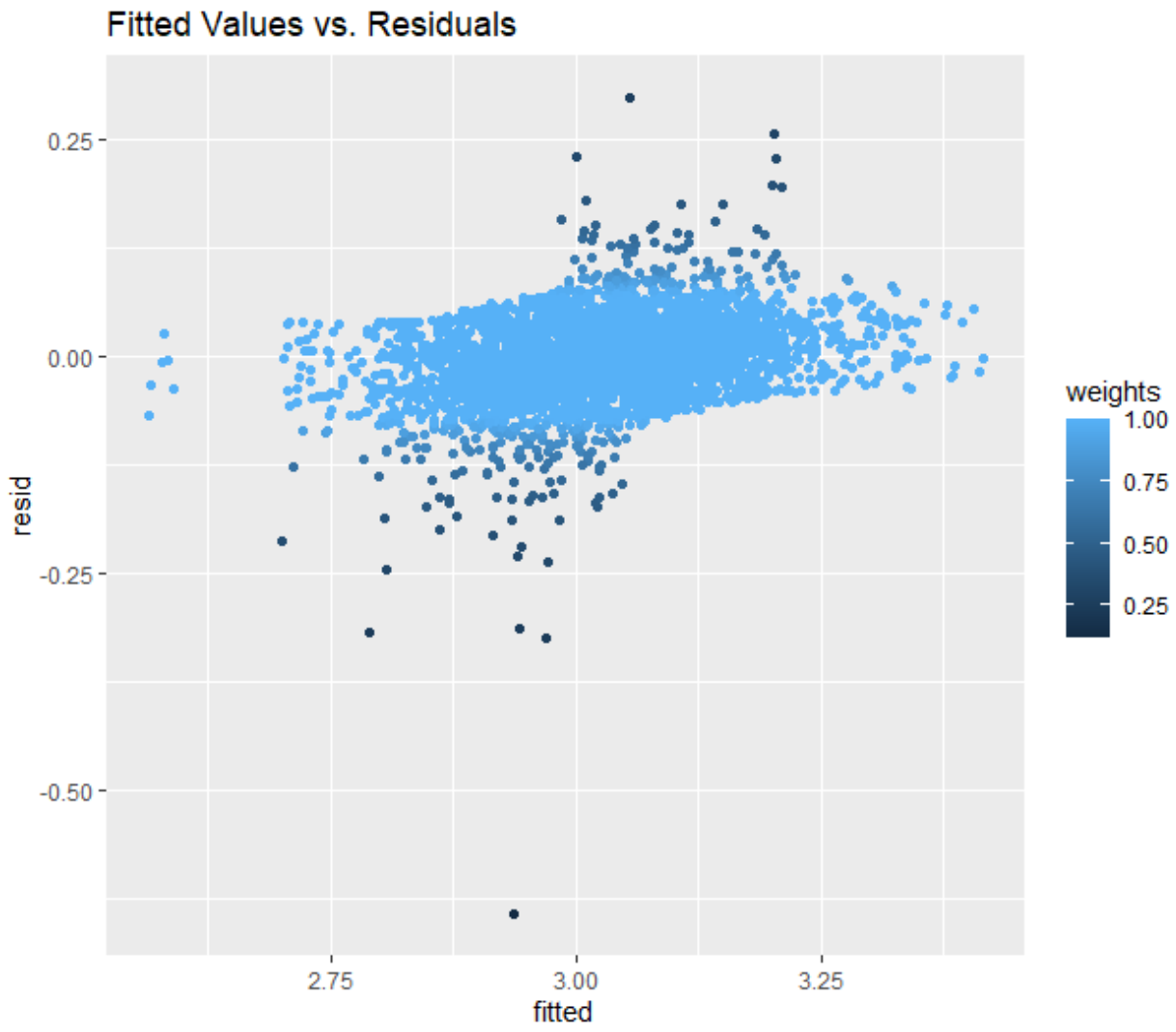

Appendix A21a). Left Hemisphere Parahippocampus Cortical Thickness Linear Mixed Effects Model Output

	LH Parahippocampus (mm)		
Predictors	*Estimates*	*CI*	*p*
(Intercept)	3.046	2.905 – 3.187	**<0.001**
ASI	0.001	-0.001 – 0.004	0.383
Instance [3 0]	0.037	-0.001 – 0.075	0.058
Years between visits	-0.004	-0.011 – 0.003	0.282
Waist to hip ratio	-0.039	-0.150 – 0.072	0.490
Age	-0.003	-0.005 – -0.002	**<0.001**
Sex	-0.065	-0.094 – -0.035	**<0.001**
Physical Activity	-0.000	-0.003 – 0.003	0.839
ASI * Instance [3 0]	-0.004	-0.007 – -0.000	**0.030**
Random Effects			
σ^2	0.01		
$\tau_{00\ eid}$	0.07		
ICC	0.86		
N_{eid}	1855		
Observations	3620		
Marginal R^2 / Conditional R^2	0.023 / 0.866		

Appendix A21b). Left Hemisphere Parahippocampus Cortical Thickness Linear Mixed Effects Model Fit

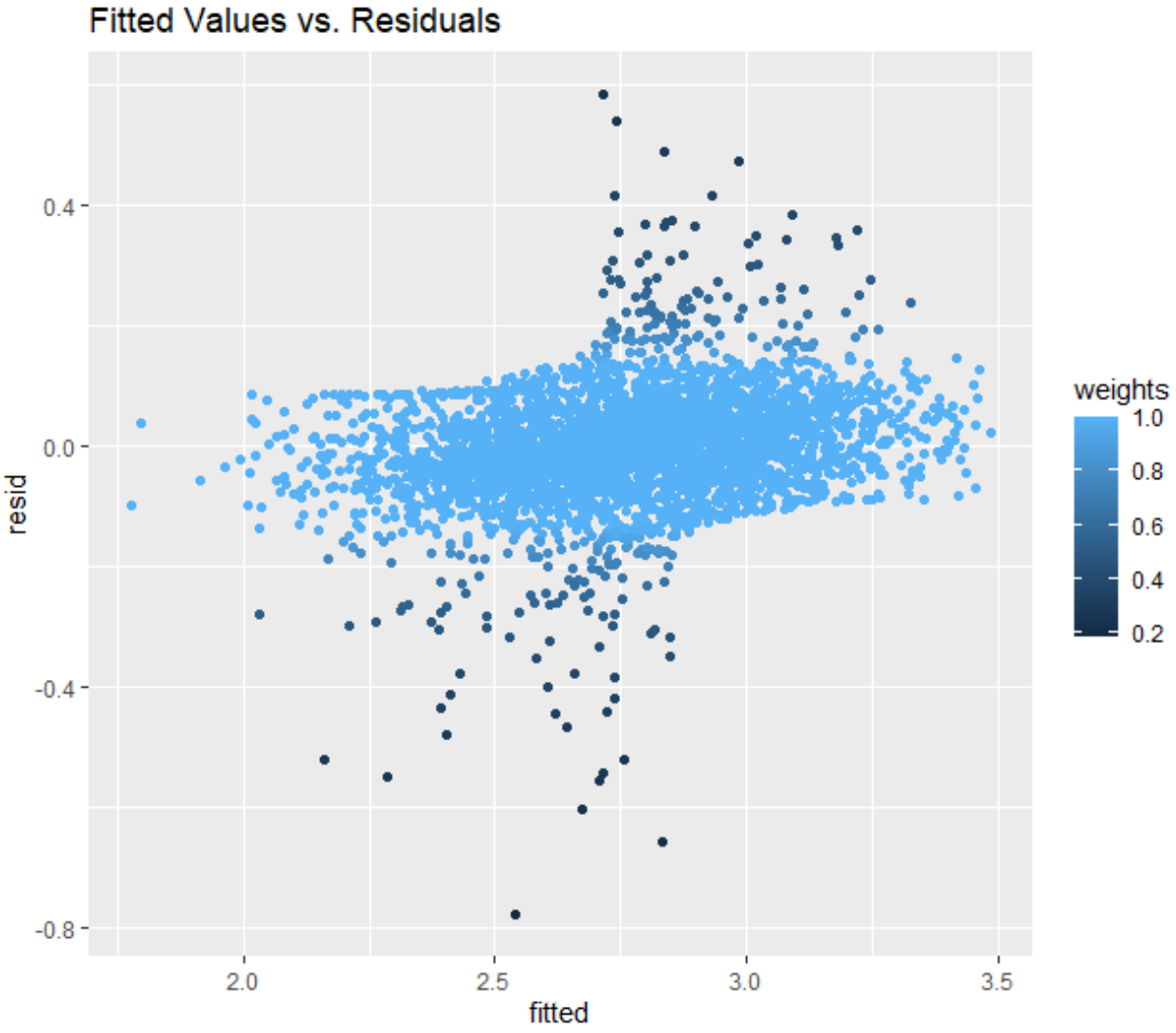

Appendix A22a). Right Hemisphere Parahippocampus Cortical Thickness Linear Mixed Effects Model Output

	RH Parahippocampus (mm)		
Predictors	*Estimates*	*CI*	*p*
(Intercept)	2.875	2.752 – 2.997	**<0.001**
ASI	-0.001	-0.003 – 0.002	0.606
Instance [3 0]	0.013	-0.024 – 0.050	0.492
Years between visits	-0.002	-0.009 – 0.005	0.582
Waist to hip ratio	0.048	-0.055 – 0.151	0.364
Age	-0.003	-0.004 – -0.001	**0.001**
Sex	-0.095	-0.120 – -0.071	**<0.001**
Physical Activity	0.003	-0.000 – 0.005	0.054
ASI * Instance [3 0]	-0.001	-0.005 – 0.002	0.358
Random Effects			
σ^2	0.01		
$\tau_{00\ eid}$	0.05		
ICC	0.81		
$N_{\ eid}$	1855		
Observations	3620		
Marginal R^2 / Conditional R^2	0.043 / 0.818		

Appendix A22b). Right Hemisphere Parahippocampus Cortical Thickness Linear Mixed Effects Model Fit

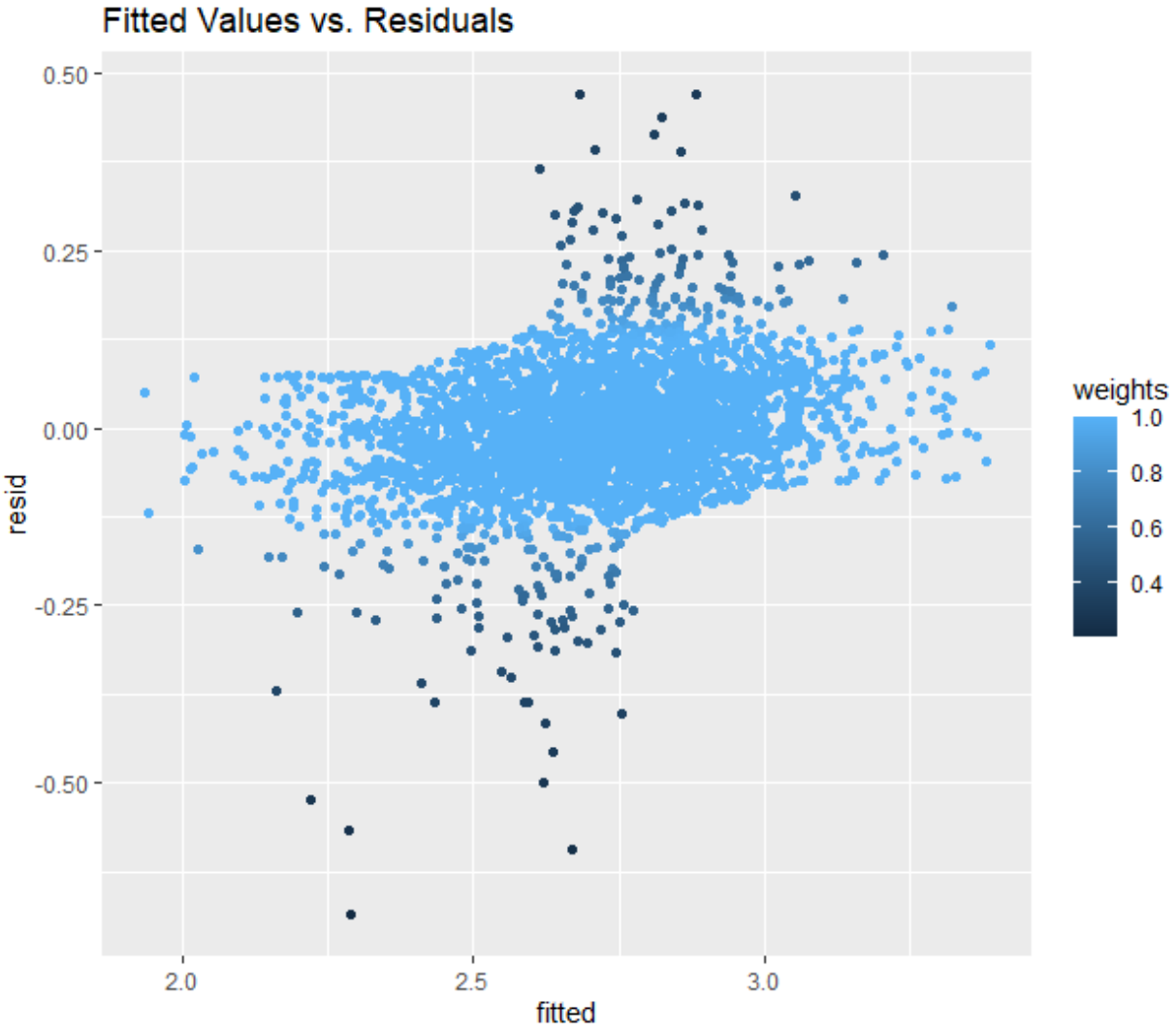

Appendix A23a). Left Hemisphere Lateral Occipital Lobe Cortical Thickness Linear Mixed Effects Model Output

	LH Lateral Occipital Lobe (mm)		
Predictors	*Estimates*	*CI*	*p*
(Intercept)	2.420	2.355 – 2.485	**<0.001**
ASI	0.002	0.001 – 0.004	**0.005**
Instance [3 0]	-0.001	-0.022 – 0.020	0.939
Years between visits	0.003	-0.001 – 0.007	0.102
Waist to hip ratio	0.067	0.009 – 0.124	**0.022**
Age	-0.003	-0.004 – -0.002	**<0.001**
Sex	0.020	0.008 – 0.033	**0.002**
Physical Activity	-0.002	-0.004 – -0.001	**0.007**
ASI * Instance [3 0]	-0.002	-0.003 – 0.000	0.076
Random Effects			
σ^2	0.00		
$\tau_{00\ eid}$	0.01		
ICC	0.76		
$N_{\ eid}$	1855		
Observations	3620		
Marginal R^2 / Conditional R^2	0.045 / 0.769		

Appendix A23b). Left Hemisphere Lateral Occipital Lobe Cortical Thickness Linear Mixed Effects Model Fit

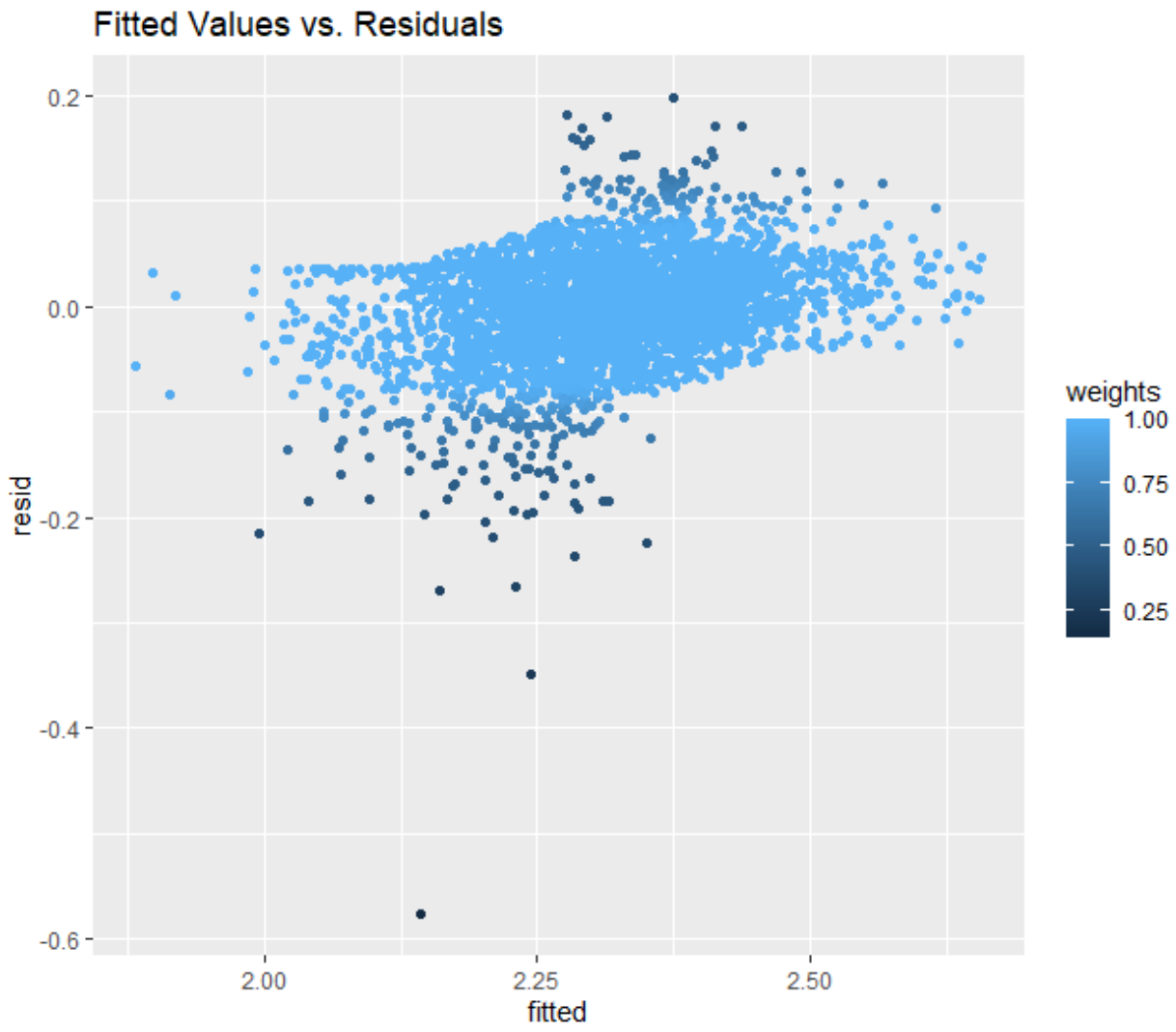

Appendix A24a). Right Hemisphere Lateral Occipital Lobe Cortical Thickness Linear Mixed Effects Model Output

	RH Lateral Occipital Lobe (mm)		
Predictors	*Estimates*	*CI*	*p*
(Intercept)	2.461	2.395 – 2.528	**<0.001**
ASI	0.001	-0.000 – 0.002	0.167
Instance [3 0]	0.013	-0.007 – 0.033	0.194
Years between visits	0.000	-0.004 – 0.004	0.921
Waist to hip ratio	0.090	0.034 – 0.147	**0.002**
Age	-0.003	-0.004 – -0.003	**<0.001**
Sex	0.019	0.006 – 0.033	**0.004**
Physical Activity	-0.001	-0.002 – 0.001	0.363
ASI * Instance [3 0]	-0.002	-0.004 – -0.000	**0.037**
Random Effects			
σ^2	0.00		
$\tau_{00\ eid}$	0.01		
ICC	0.80		
$N_{\ eid}$	1855		
Observations	3620		
Marginal R^2 / Conditional R^2	0.045 / 0.812		

Appendix A24b). Right Hemisphere Lateral Occipital Lobe Cortical Thickness Linear Mixed Effects Model Fit

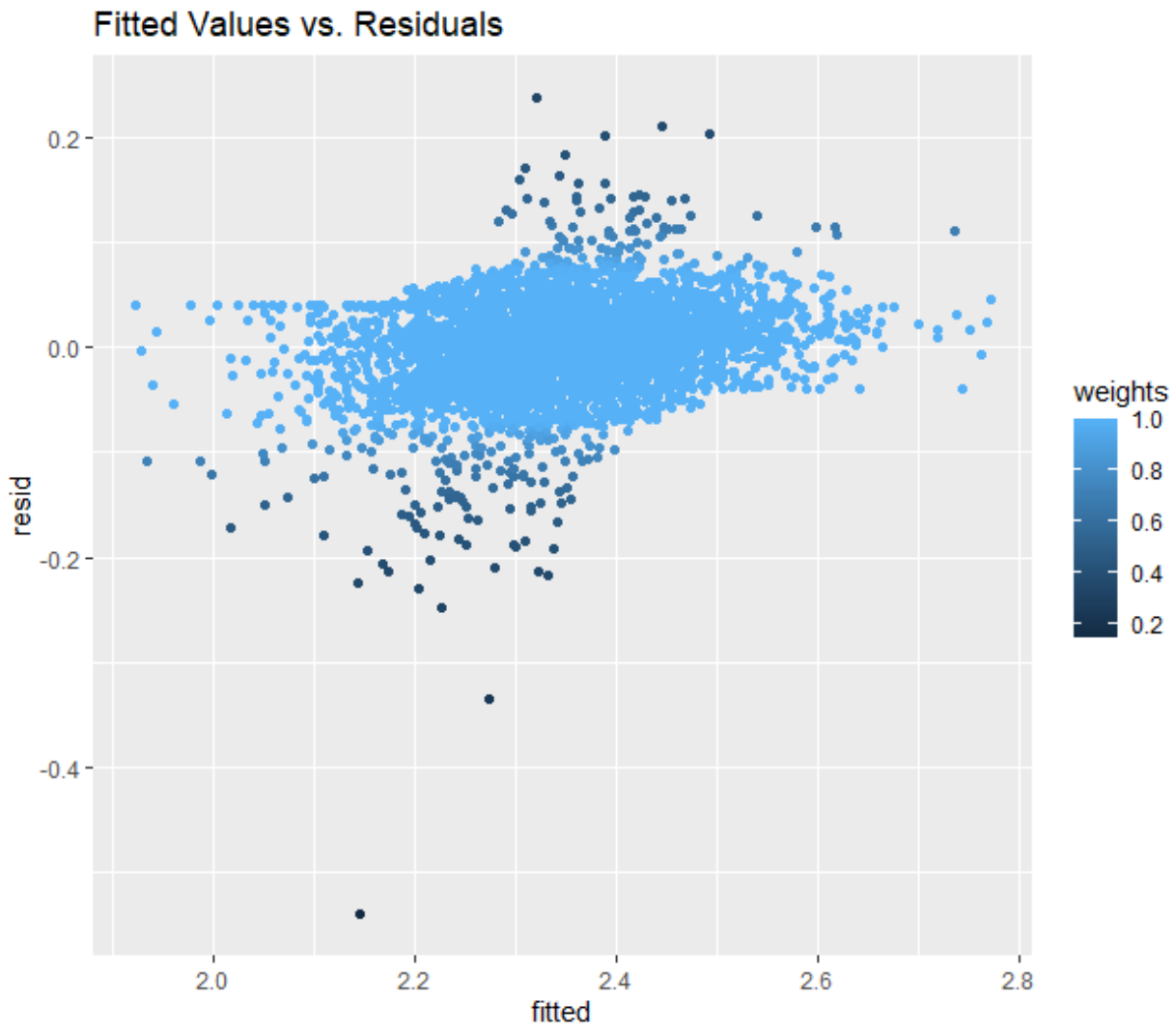

Appendix A25a). Left Hemisphere Posterior Cingulate Cortical Thickness Linear Mixed Effects Model Output

	LH Posterior Cingulate (mm)		
Predictors	*Estimates*	*CI*	*p*
(Intercept)	2.907	2.819 – 2.995	**<0.001**
ASI	0.001	-0.001 – 0.003	0.146
Instance [3 0]	0.028	0.000 – 0.057	**0.049**
Years between visits	-0.007	-0.013 – -0.002	**0.007**
Waist to hip ratio	-0.015	-0.092 – 0.062	0.700
Age	-0.003	-0.004 – -0.002	**<0.001**
Sex	-0.012	-0.030 – 0.005	0.165
Physical Activity	0.000	-0.002 – 0.002	0.830
ASI * Instance [3 0]	-0.002	-0.005 – 0.000	0.072
Random Effects			
σ^2	0.01		
$\tau_{00\ eid}$	0.02		
ICC	0.77		
$N_{\ eid}$	1855		
Observations	3620		
Marginal R^2 / Conditional R^2	0.026 / 0.772		

Appendix A25b). Left Hemisphere Posterior Cingulate Cortical Thickness Linear Mixed Effects Model Fit

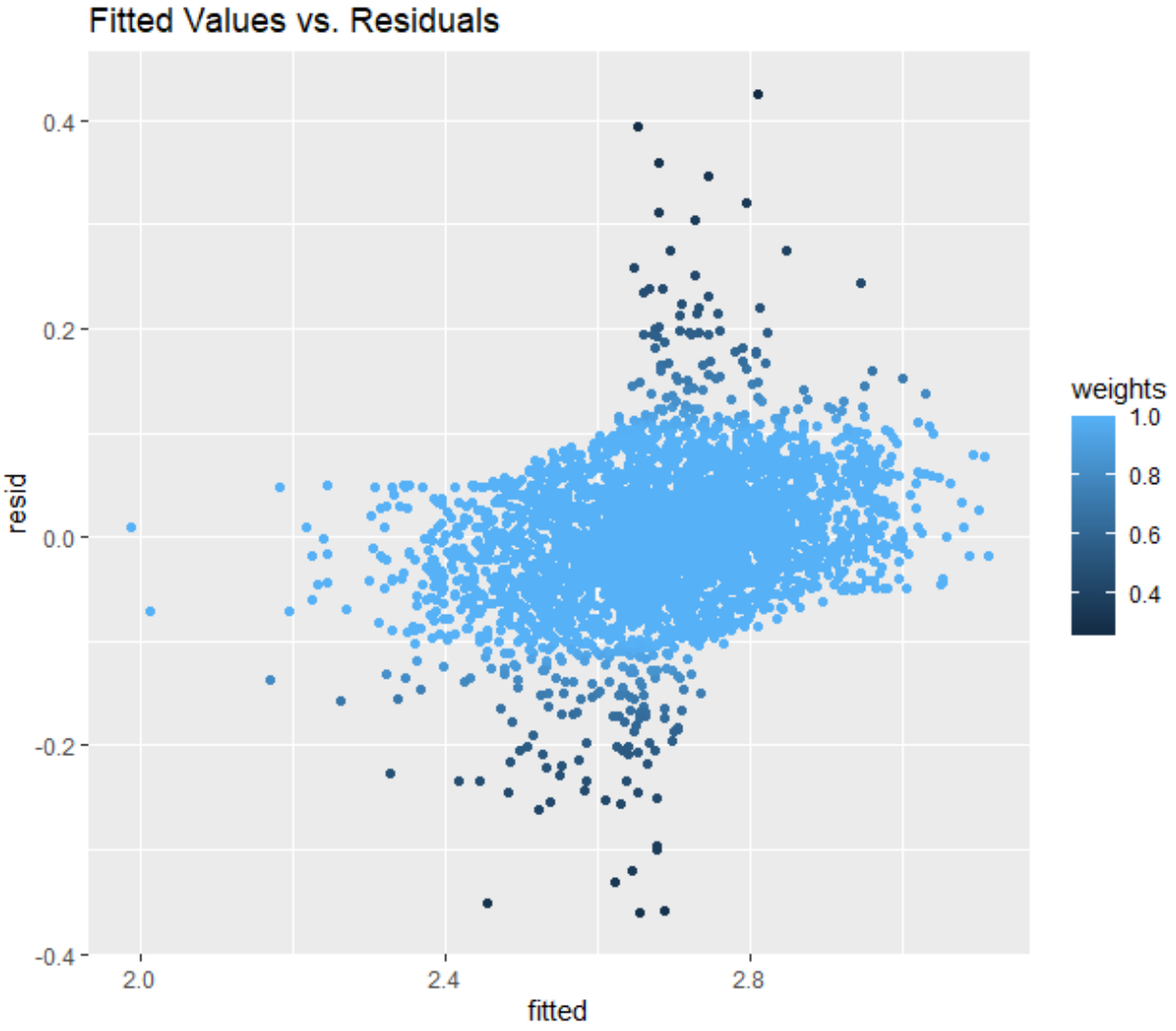

Appendix A26a). Right Hemisphere Posterior Cingulate Cortical Thickness Linear Mixed Effects Model Output

	RH Posterior Cingulate (mm)		
Predictors	*Estimates*	*CI*	*p*
(Intercept)	2.912	2.821 – 3.004	**<0.001**
ASI	0.001	-0.001 – 0.003	0.331
Instance [3 0]	0.023	-0.008 – 0.053	0.149
Years between visits	-0.009	-0.015 – -0.003	**0.002**
Waist to hip ratio	-0.025	-0.107 – 0.057	0.548
Age	-0.003	-0.004 – -0.002	**<0.001**
Sex	-0.026	-0.044 – -0.008	**0.004**
Physical Activity	0.000	-0.002 – 0.002	0.832
ASI * Instance [3 0]	-0.001	-0.004 – 0.001	0.296
Random Effects			
σ^2	0.01		
$\tau_{00\ eid}$	0.02		
ICC	0.73		
$N_{\ eid}$	1855		
Observations	3620		
Marginal R^2 / Conditional R^2	0.028 / 0.735		

Appendix A26b). Right Hemisphere Posterior Cingulate Cortical Thickness Linear Mixed Effects Model Fit

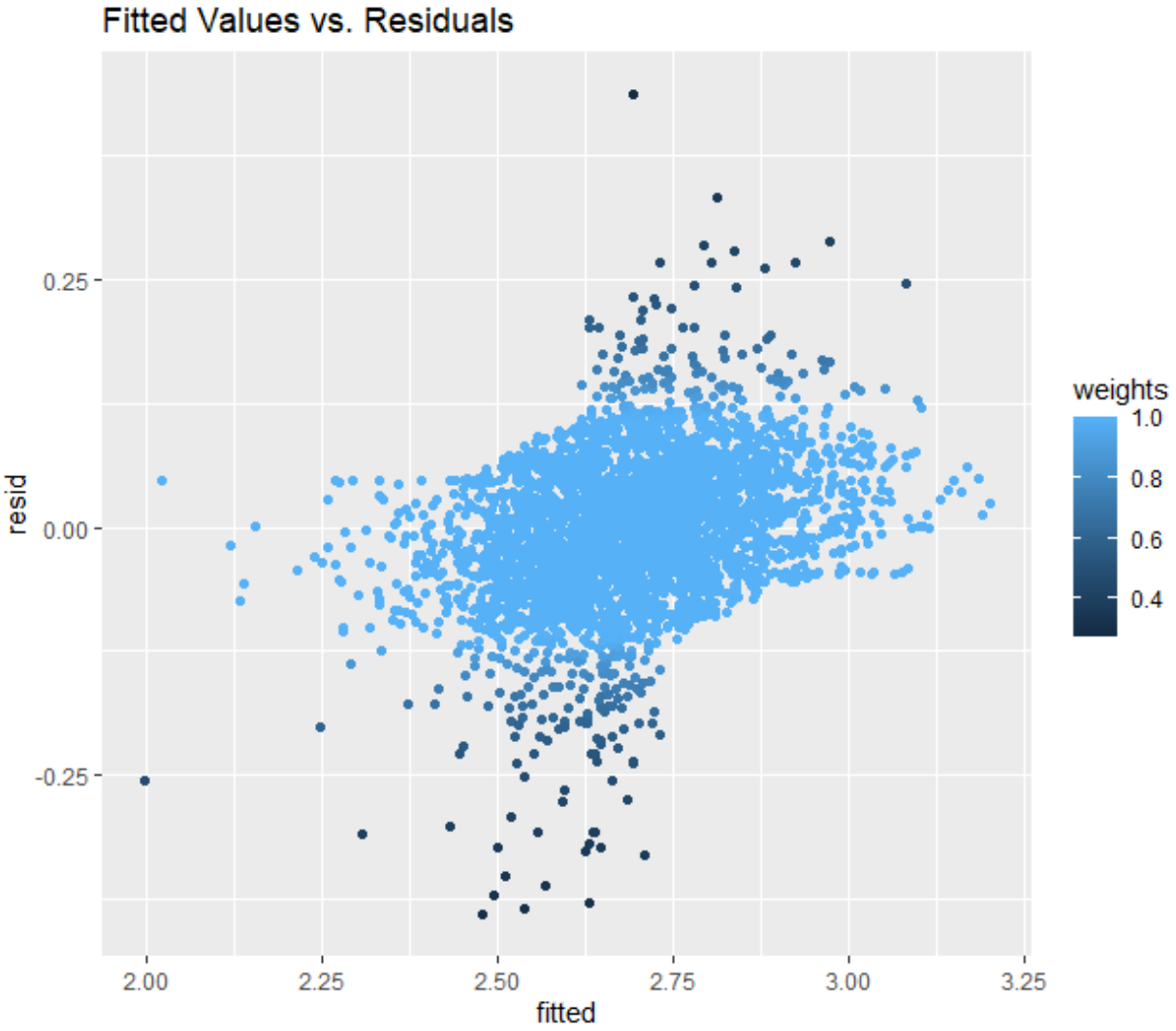

Appendix A27a). Whole Brain Grey Matter Volume Linear Mixed Effects Model Output

	GMV (mL)		
Predictors	*Estimates*	*CI*	*p*
(Intercept)	1046.836	1031.393 – 1062.279	**<0.001**
ASI	0.002	-0.225 – 0.229	0.988
Instance [3 0]	-4.214	-7.455 – -0.973	**0.011**
Years between visits	1.262	0.615 – 1.910	**<0.001**
Waist to hip ratio	-12.652	-22.478 – -2.825	**0.012**
Age	-3.599	-3.816 – -3.383	**<0.001**
Sex	-20.484	-23.892 – -17.076	**<0.001**
Physical Activity	-0.012	-0.260 – 0.235	0.922
ASI * Instance [3 0]	0.042	-0.231 – 0.316	0.761
Random Effects			
σ^2	83.97		
$\tau_{00\ eid}$	1135.46		
ICC	0.93		
$N_{\ eid}$	1858		
Observations	3709		
Marginal R^2 / Conditional R^2	0.417 / 0.960		

Appendix A27b). Whole Brain Grey Matter Volume Linear Mixed Effects Model Fit

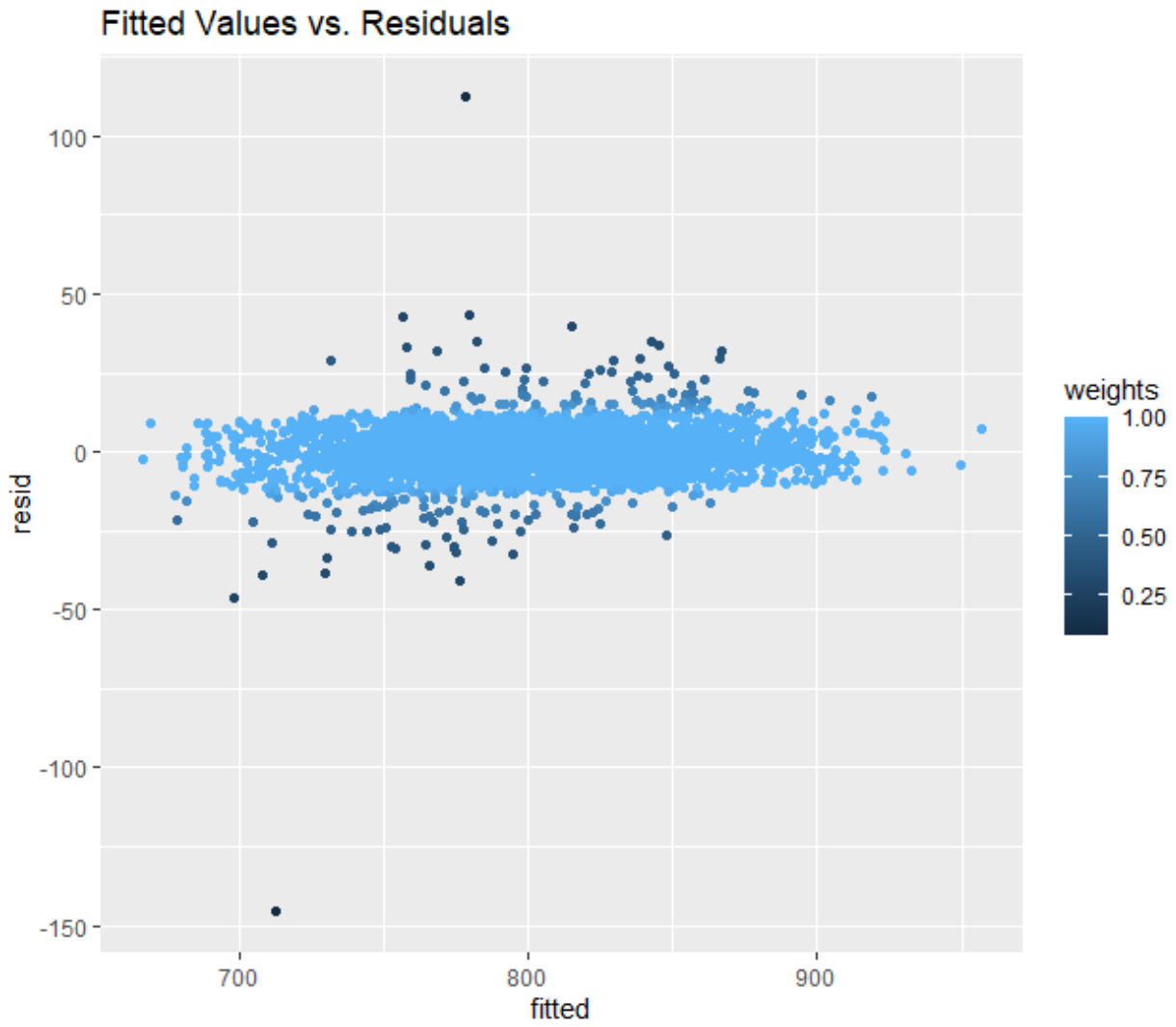

Appendix A28a). White Matter Hyperintensities Volume Linear Mixed Effects Model Output

	WMH (mL)		
Predictors	*Estimates*	*CI*	*p*
(Intercept)	-8.934	-10.041 – -7.827	**<0.001**
ASI	-0.013	-0.036 – 0.011	0.281
Instance [3 0]	-0.302	-0.640 – 0.035	0.079
Years between visits	0.092	0.028 – 0.157	**0.005**
Waist to hip ratio	2.053	1.116 – 2.989	**<0.001**
Age	0.167	0.154 – 0.180	**<0.001**
Sex	0.137	-0.086 – 0.359	0.228
Physical Activity	0.011	-0.013 – 0.036	0.361
ASI * Instance [3 0]	0.003	-0.026 – 0.031	0.842
Random Effects			
σ^2	0.97		
$\tau_{00\ eid}$	3.85		
ICC	0.80		
$N_{\ eid}$	1858		
Observations	3709		
Marginal R^2 / Conditional R^2	0.251 / 0.849		

Appendix A28b). White Matter Hyperintensities Volume Linear Mixed Effects Model Fit

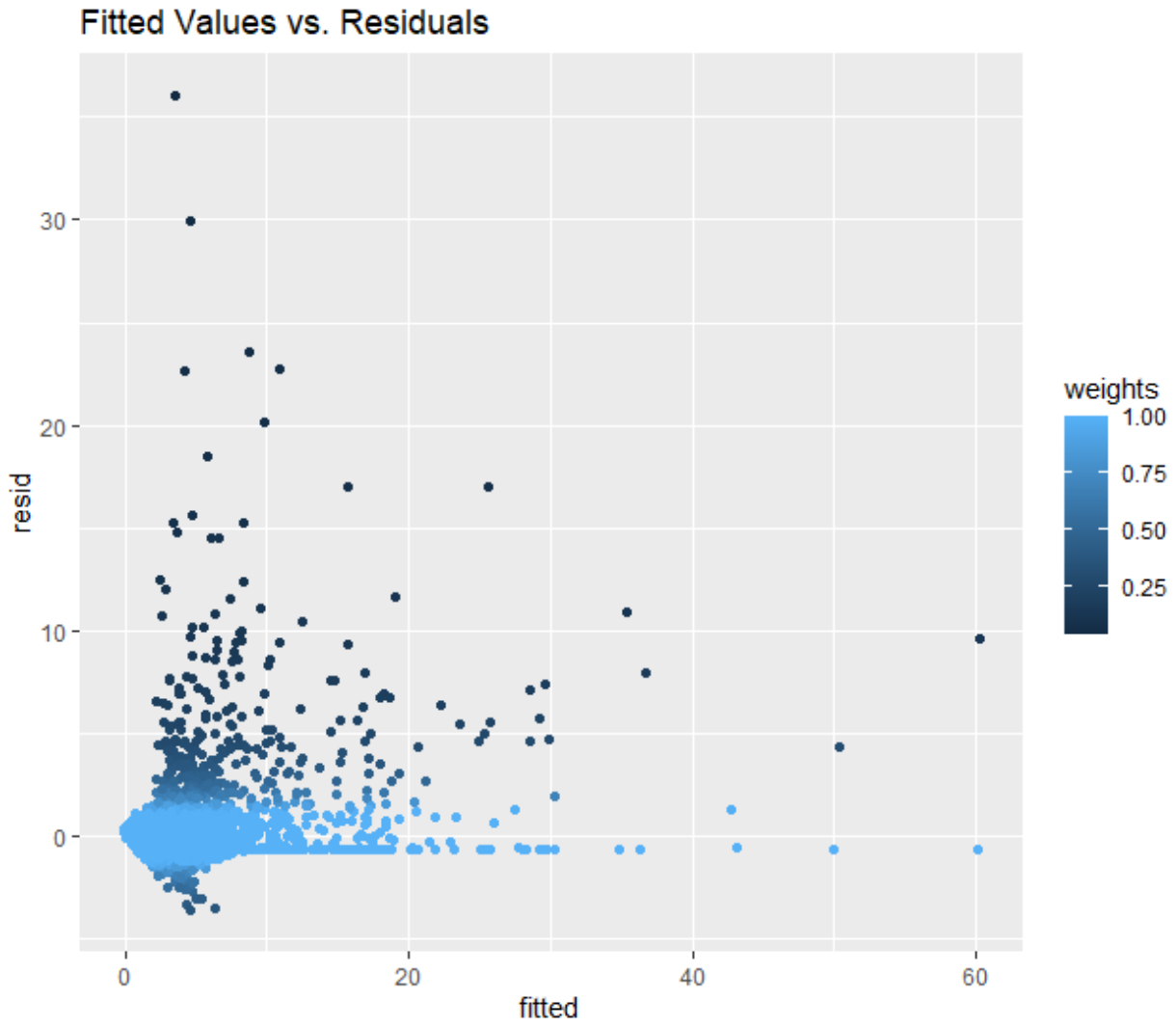

Appendix A29a). Digit Symbol Substitution Test Performance Linear Mixed Effects Model Output

	DSST Performance		
Predictors	*Estimates*	*CI*	*p*
(Intercept)	39.31	36.79 – 41.84	**<0.001**
ASI	-0.01	-0.08 – 0.06	0.860
Instance [3 0]	0.72	-0.25 – 1.68	0.144
Years between visits	-0.00	-0.19 – 0.18	0.993
Waist to hip ratio	-2.87	-5.24 – -0.51	**0.017**
Age	-0.27	-0.30 – -0.24	**<0.001**
Sex	0.14	-0.32 – 0.60	0.558
Physical Activity	-0.01	-0.08 – 0.05	0.721
ASI * Instance [3 0]	-0.01	-0.09 – 0.07	0.809
Random Effects			
σ^2	7.60		
$\tau_{00\ eid}$	10.94		
ICC	0.59		
$N_{\ eid}$	1834		
Observations	3241		
Marginal R^2 / Conditional R^2	0.172 / 0.661		

Appendix A29b). Digit Symbol Substitution Test Performance Linear Mixed Effects Model Fit

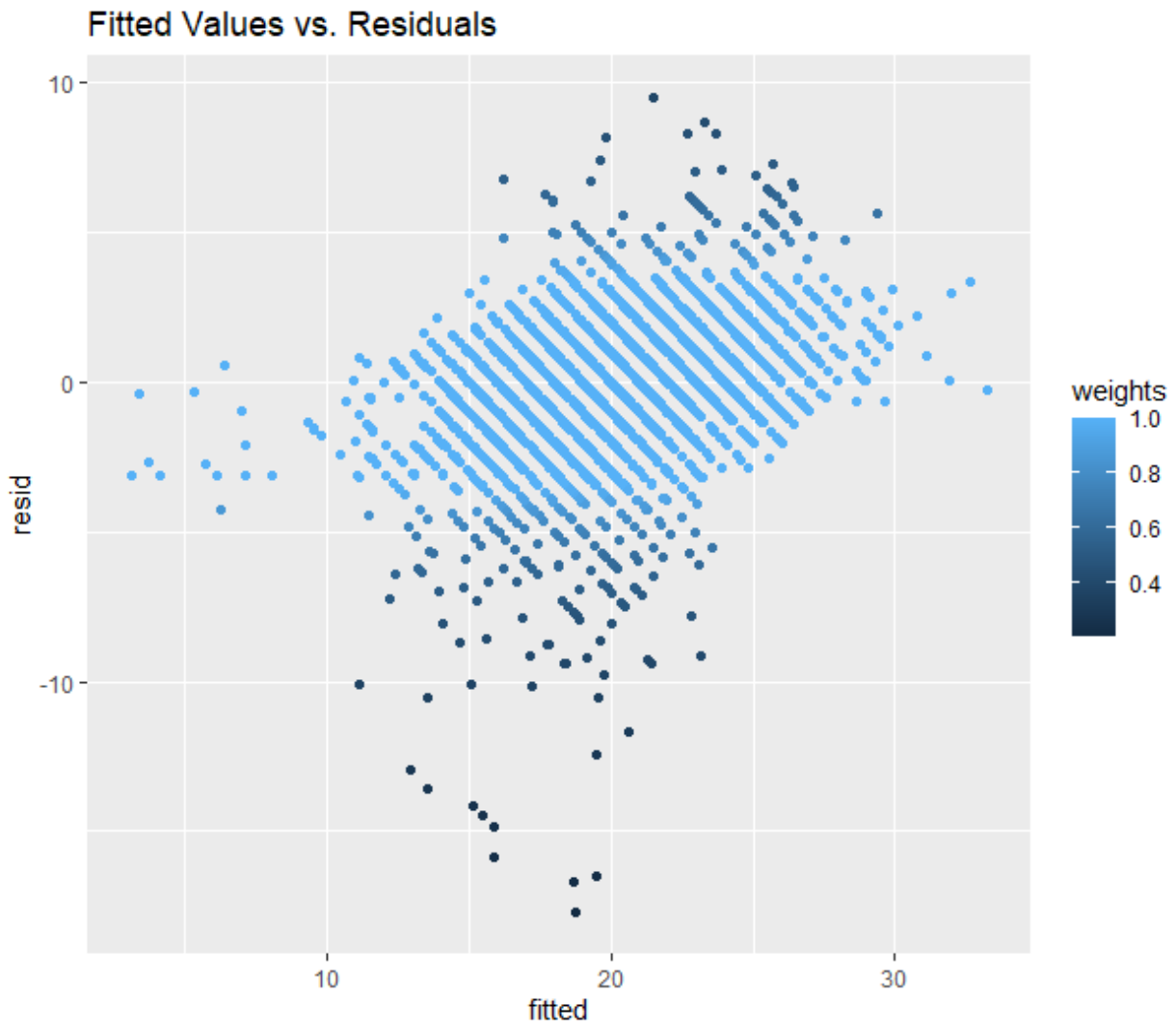

Appendix A30a). Trail Making Test Part A Performance Linear Mixed Effects Model Output

	TmA Performance		
Predictors	*Estimates*	*CI*	*p*
(Intercept)	66.06	39.36 – 92.76	**<0.001**
ASI	0.42	-0.53 – 1.37	0.381
Instance [3 0]	8.38	-5.06 – 21.82	0.222
Years between visits	-1.34	-3.51 – 0.83	0.226
Waist to hip ratio	-2.82	-29.22 – 23.57	0.834
Age	2.11	1.86 – 2.35	**<0.001**
Sex	6.58	2.04 – 11.12	**0.005**
Physical Activity	0.19	-0.58 – 0.95	0.627
ASI * Instance [3 0]	-0.71	-1.90 – 0.49	0.247
Random Effects			
σ^2	2351.24		
$\tau_{00\ eid}$	0.00		
ICC	0.00		
$N_{\ eid}$	1845		
Observations	3293		
Marginal R^2 / Conditional R^2	0.097 / 0.097		

Appendix A30b). Trail Making Test Part A Performance Linear Mixed Effects Model Fit

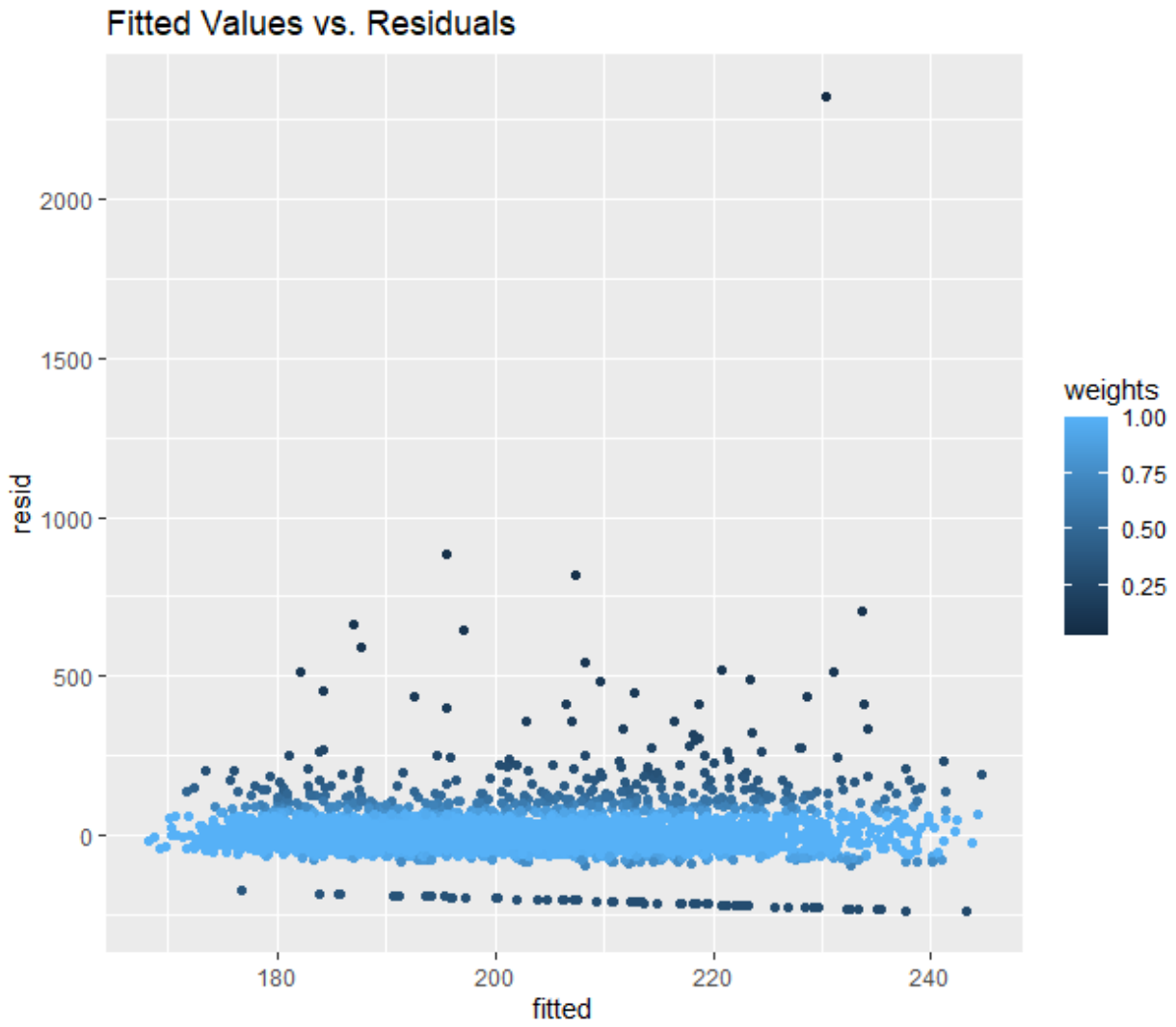

Appendix A31a). Trail Making Test Part B Performance Linear Mixed Effects Model Output

	TmB Performance		
Predictors	*Estimates*	*CI*	*p*
(Intercept)	25.44	-56.51 – 107.38	0.543
ASI	-1.26	-3.42 – 0.89	0.249
Instance [3 0]	-21.81	-51.88 – 8.26	0.155
Years between visits	-1.75	-7.70 – 4.21	0.565
Waist to hip ratio	28.34	-47.30 – 103.98	0.463
Age	7.26	6.39 – 8.12	**<0.001**
Sex	7.17	-7.87 – 22.21	0.350
Physical Activity	0.82	-1.26 – 2.89	0.441
ASI * Instance [3 0]	1.62	-1.00 – 4.24	0.225
Random Effects			
σ^2	7249.35		
$\tau_{00\ eid}$	12885.09		
ICC	0.64		
N_{eid}	1845		
Observations	3293		
Marginal R^2 / Conditional R^2	0.123 / 0.684		

Appendix A31b). Trail Making Test Part B Performance Linear Mixed Effects Model Fit

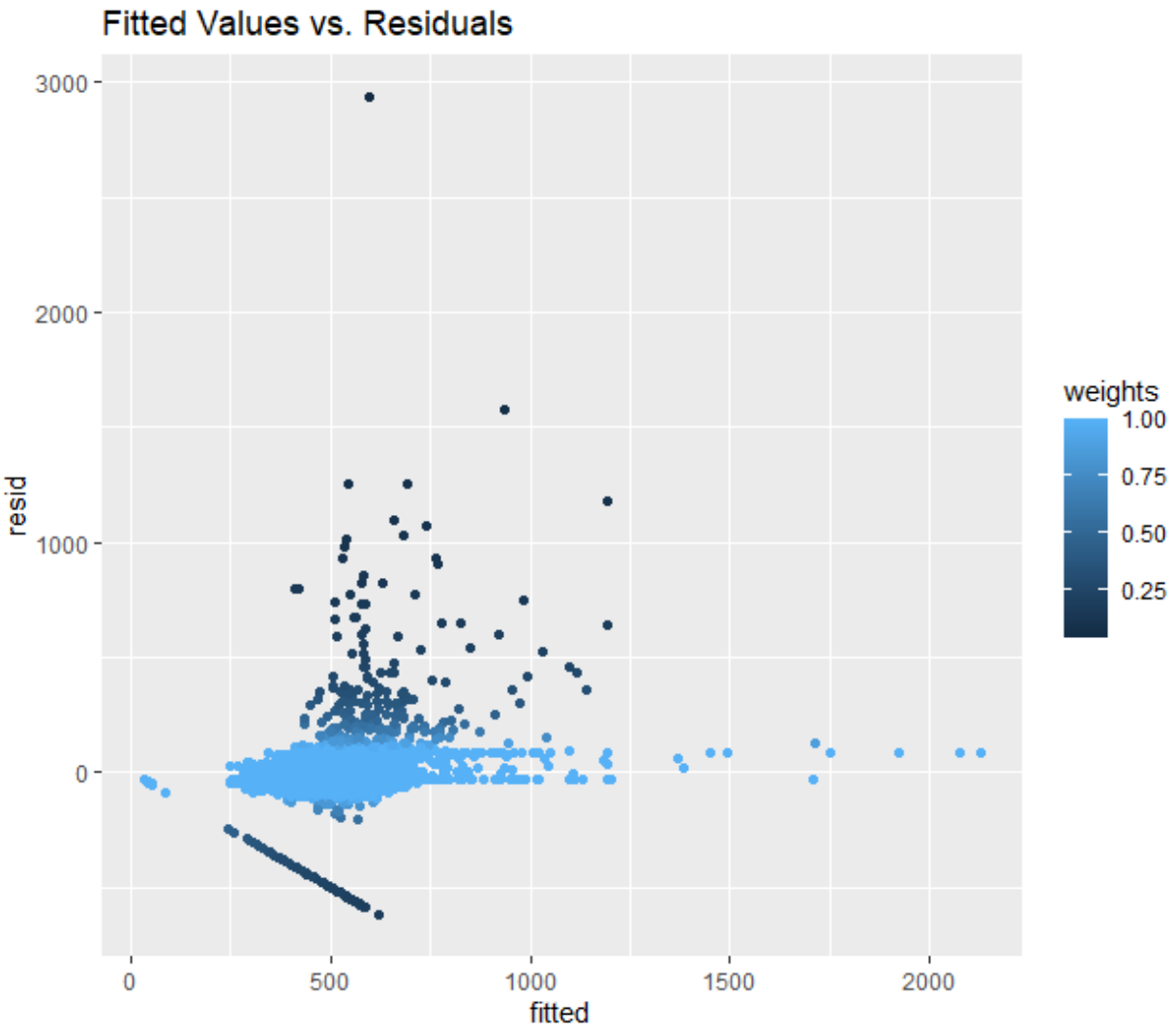

Appendix A32a). Fluid Intelligence Test Performance Linear Mixed Effects Model Output

	Fluid Intelligence Performance		
Predictors	*Estimates*	*CI*	*p*
(Intercept)	8.32	7.23 – 9.41	**<0.001**
ASI	0.02	-0.00 – 0.05	0.083
Instance [3 0]	0.52	0.13 – 0.91	**0.009**
Years between visits	-0.04	-0.11 – 0.03	0.226
Waist to hip ratio	-1.19	-2.21 – -0.18	**0.021**
Age	-0.01	-0.03 – -0.00	**0.019**
Sex	0.28	0.07 – 0.48	**0.009**
Physical Activity	-0.03	-0.05 – 0.00	0.068
ASI * Instance [3 0]	-0.04	-0.07 – -0.00	**0.029**
Random Effects			
σ^2	1.29		
$\tau_{00\ eid}$	2.55		
ICC	0.66		
$N_{\ eid}$	1835		
Observations	3380		
Marginal R^2 / Conditional R^2	0.007 / 0.666		

Appendix A32b). Fluid Intelligence Test Performance Linear Mixed Effects Model Fit

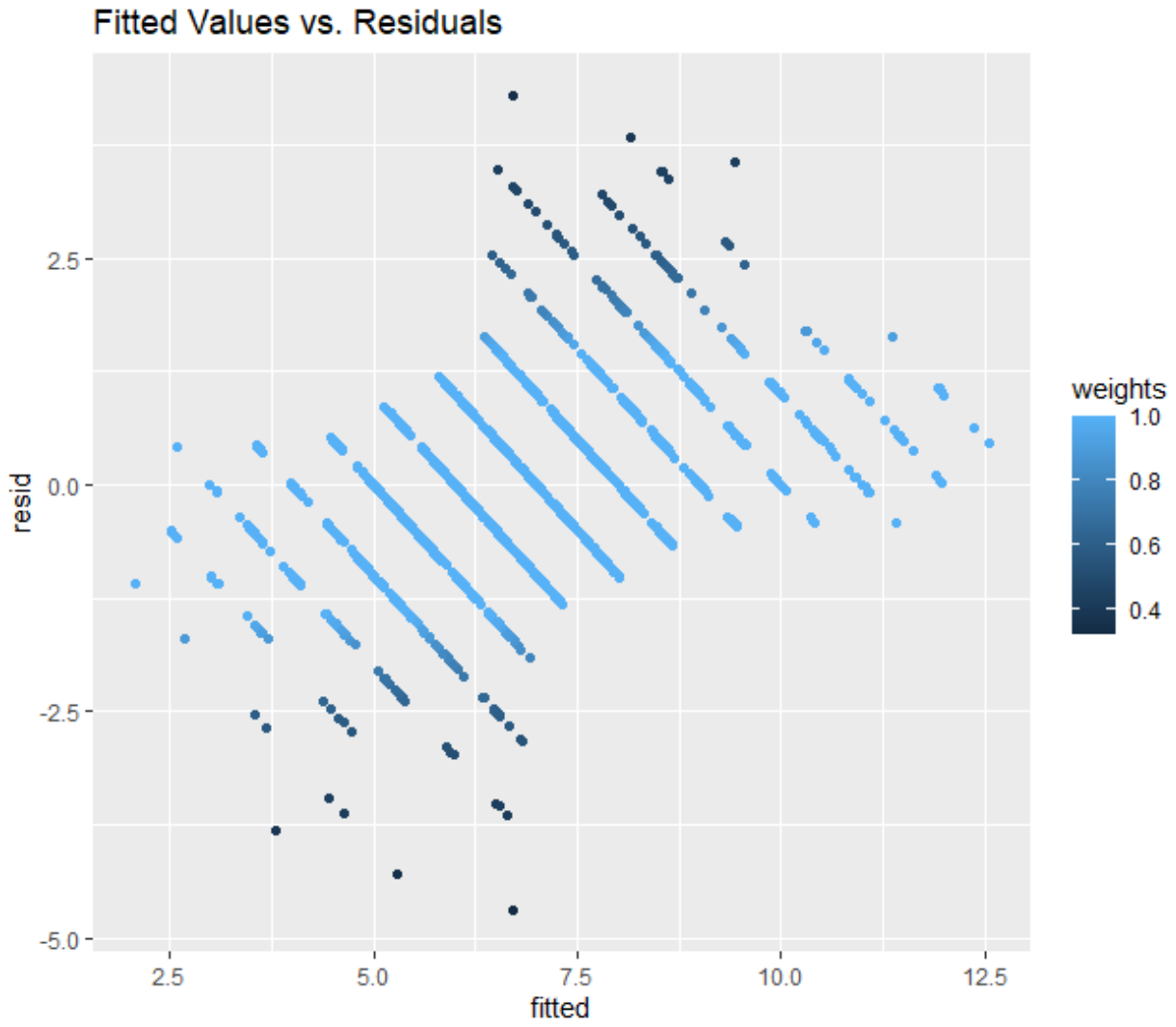

Appendix A33a). Numeric Memory Test Performance Linear Mixed Effects Model Output

	Numeric Memory Performance		
Predictors	*Estimates*	*CI*	*p*
(Intercept)	8.71	8.04 – 9.39	**<0.001**
ASI	0.02	-0.00 – 0.04	0.053
Instance [3 0]	-0.04	-0.31 – 0.23	0.775
Years between visits	0.06	0.01 – 0.11	**0.019**
Waist to hip ratio	-1.21	-1.86 – -0.57	**<0.001**
Age	-0.02	-0.03 – -0.01	**<0.001**
Sex	0.31	0.19 – 0.44	**<0.001**
Physical Activity	-0.01	-0.03 – 0.01	0.415
ASI * Instance [3 0]	-0.01	-0.03 – 0.02	0.646
Random Effects			
σ^2	0.66		
$\tau_{00\ eid}$	0.67		
ICC	0.50		
$N_{\ eid}$	1845		
Observations	3300		
Marginal R^2 / Conditional R^2	0.027 / 0.517		

Appendix A33b). Numeric Memory Test Performance Linear Mixed Effects Model Fit

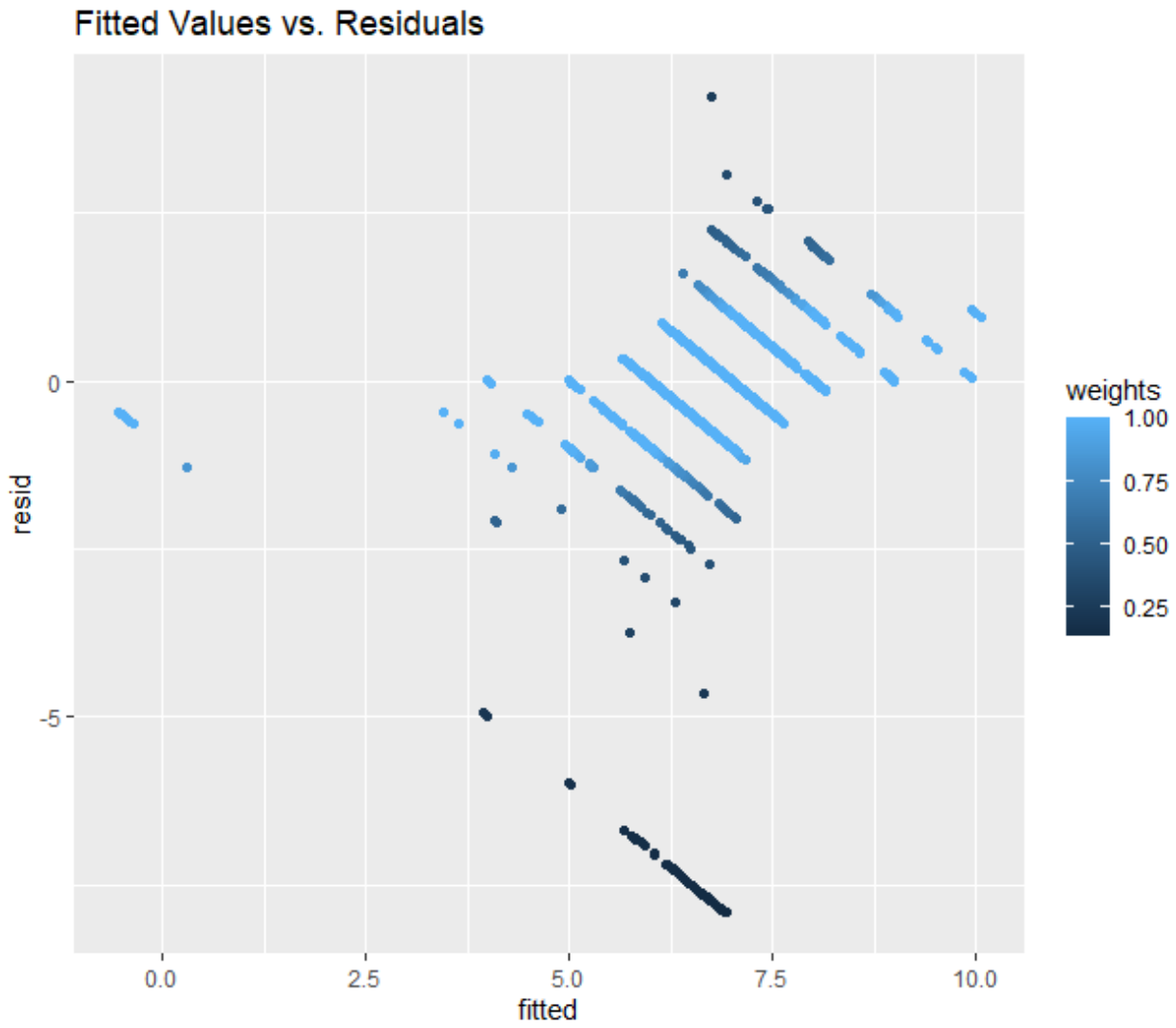

Appendix A34a). Pairs Matching Test Performance Linear Mixed Effects Model Output

	Pairs Matching Performance		
Predictors	*Estimates*	*CI*	*p*
(Intercept)	-0.00	-0.00 – -0.00	**<0.001**
ASI	0.00	-0.00 – 0.00	0.693
Instance [3 0]	-0.00	-0.00 – 0.00	0.402
Years between visits	0.00	-0.00 – 0.00	0.518
Waist to hip ratio	0.00	0.00 – 0.00	**0.014**
Age	0.00	0.00 – 0.00	**<0.001**
Sex	-0.00	-0.00 – -0.00	**0.001**
Physical Activity	0.00	-0.00 – 0.00	0.302
ASI * Instance [3 0]	0.00	-0.00 – 0.00	0.742
Random Effects			
σ^2	0.00		
$\tau_{00\ eid}$	0.00		
ICC	0.00		
$N_{\ eid}$	1845		
Observations	3440		
Marginal R^2 / Conditional R^2	0.014 / 0.014		

Appendix A34b). Pairs Matching Test Performance Linear Mixed Effects Model Fit

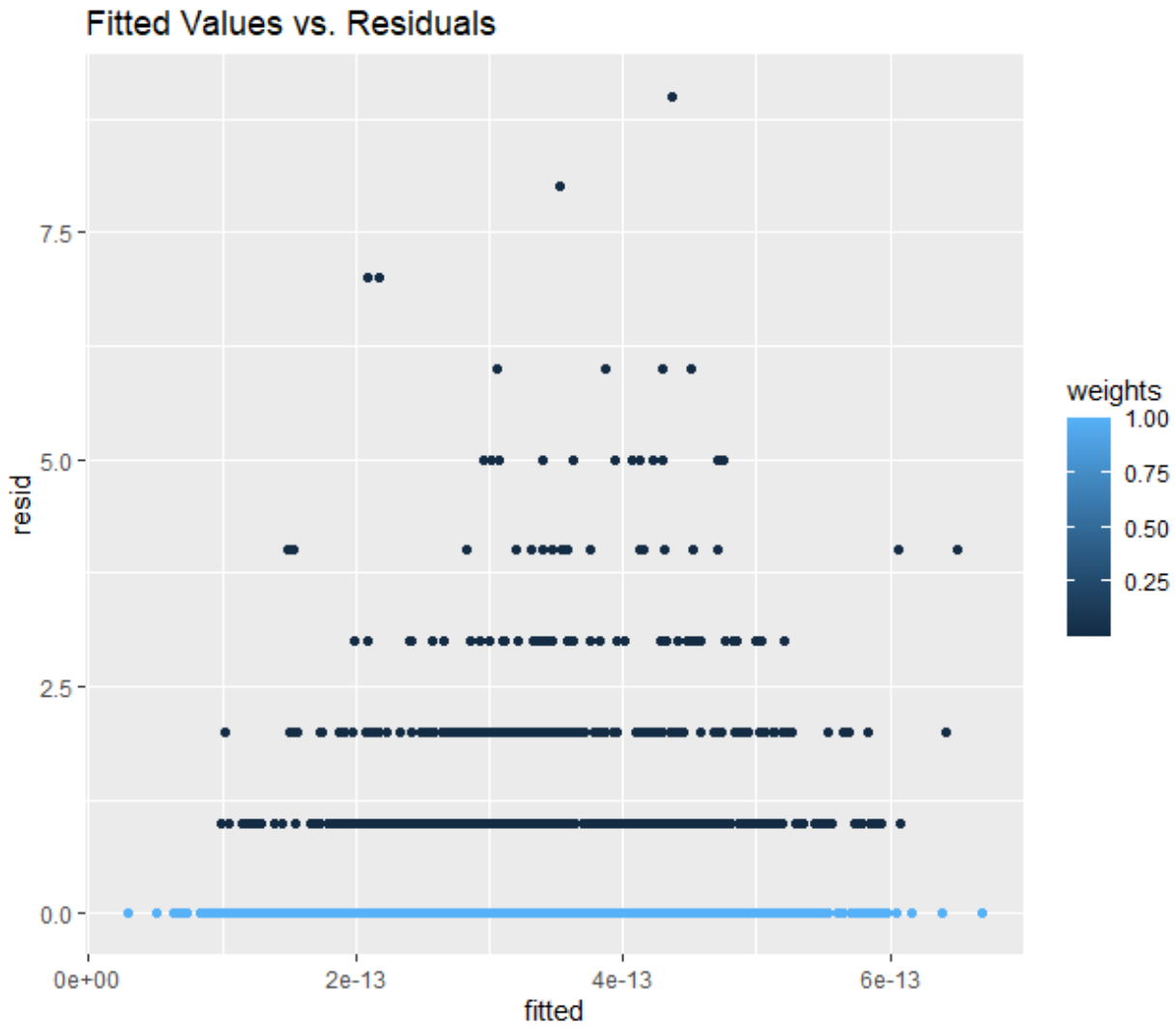

Appendix B. Linear Regression Model Outputs for Imaging Visits 1 and 2

B1. Left Hemisphere Caudal Anterior Cingulate Cortical Thickness

B1a). Linear Regression Model Output Imaging Visit 1

	LH Caudal Anterior Cingulate at First Imaging Visit		
Predictors	*Estimates*	*CI*	*p*
(Intercept)	3.031	2.875 – 3.186	**<0.001**
ASI at baseline	-0.003	-0.011 – 0.004	0.394
Age	-0.005	-0.008 – -0.002	**0.001**
Observations	639		
R^2 / R^2 adjusted	0.021 / 0.018		

B1b). Linear Regression Model Output Imaging Visit 2

	LH Caudal Anterior Cingulate at First Imaging Visit		
Predictors	*Estimates*	*CI*	*p*
(Intercept)	2.986	2.822 – 3.150	**<0.001**
ASI at baseline	0.005	-0.004 – 0.013	0.268
Age	-0.006	-0.009 – -0.003	**0.001**
Observations	630		
R^2 / R^2 adjusted	0.022 / 0.019		

B2. Right Hemisphere Caudal Anterior Cingulate Cortical Thickness

B2a). Linear Regression Model Output Imaging Visit 1

	RH Caudal Anterior Cingulate at First Imaging Visit		
Predictors	*Estimates*	*CI*	*p*
(Intercept)	3.220	3.141 – 3.298	**<0.001**
ASI at baseline	-0.001	-0.005 – 0.003	0.487
Age	-0.007	-0.008 – -0.006	**<0.001**
Observations	639		
R^2 / R^2 adjusted	0.131 / 0.129		

B2b). Linear Regression Model Output Imaging Visit 2

	RH Caudal Anterior Cingulate at Second Imaging Visit		
Predictors	*Estimates*	*CI*	*p*
(Intercept)	2.986	2.822 – 3.150	**<0.001**
ASI at baseline	0.005	-0.004 – 0.013	0.268
Age	-0.006	-0.009 – -0.003	**<0.001**
Observations	630		
R^2 / R^2 adjusted	0.022 / 0.019		

B3. Left Hemisphere Caudal Middle Frontal Gyri Cortical Thickness

B3a). Linear Regression Model Output Imaging Visit 1

	LH Caudal Middle Frontal Gyri at First Imaging Visit		
Predictors	*Estimates*	*CI*	*p*
(Intercept)	3.287	3.204 – 3.370	**<0.001**
ASI at baseline	-0.004	-0.008 – 0.000	0.053
Age	-0.007	-0.009 – -0.006	**<0.001**
Observations	639		
R^2 / R^2 adjusted	0.133 / 0.131		

B3b). Linear Regression Model Output Imaging Visit 2

	LH Caudal Middle Frontal Gyri at Second Imaging Visit		
Predictors	*Estimates*	*CI*	*p*
(Intercept)	3.333	3.246 – 3.420	**<0.001**
ASI at baseline	-0.005	-0.010 – -0.001	**0.023**
Age	-0.008	-0.010 – -0.006	**<0.001**
Observations	630		
R^2 / R^2 adjusted	0.158 / 0.156		

B4. Right Hemisphere Caudal Middle Frontal Gyri Cortical Thickness

B4a). Linear Regression Model Output Imaging Visit 1

	RH Caudal Middle Frontal Gyri at First Imaging Visit		
Predictors	*Estimates*	*CI*	*p*
(Intercept)	2.010	1.926 – 2.094	**<0.001**
ASI at baseline	0.003	-0.001 – 0.007	0.161
Age	-0.002	-0.003 – 0.000	0.059
Observations	639		
R^2 / R^2 adjusted	0.007 / 0.004		

B4b). Linear Regression Model Output Imaging Visit 2

	RH Caudal Middle Frontal Gyri at Second Imaging Visit		
Predictors	*Estimates*	*CI*	*p*
(Intercept)	2.064	1.983 – 2.146	**<0.001**
ASI at baseline	0.001	-0.003 – 0.005	0.528
Age	-0.002	-0.004 – -0.001	**0.002**
Observations	630		
R^2 / R^2 adjusted	0.015 / 0.012		

B5. Left Hemisphere Rostral Anterior Cingulate Cortical Thickness

B5a). Linear Regression Model Output Imaging Visit 1

	LH Rostral Anterior Cingulate at First Imaging Visit		
Predictors	*Estimates*	*CI*	*p*
(Intercept)	3.102	2.992 – 3.212	**<0.001**
ASI at baseline	-0.001	-0.007 – 0.004	0.615
Age	-0.003	-0.006 – -0.001	**0.001**
Observations	639		
R^2 / R^2 adjusted	0.020 / 0.016		

B5b). Linear Regression Model Output Imaging Visit 2

	LH Rostral Anterior Cingulate at Second Imaging Visit		
Predictors	*Estimates*	*CI*	*p*
(Intercept)	3.108	2.995 – 3.221	**<0.001**
ASI at baseline	-0.001	-0.006 – 0.005	0.845
Age	-0.004	-0.006 – -0.002	**<0.001**
Observations	630		
R^2 / R^2 adjusted	0.025 / 0.022		

B6. Right Hemisphere Rostral Anterior Cingulate Cortical Thickness

B6a). Linear Regression Model Output Imaging Visit 1

	RH Rostral Anterior Cingulate at First Imaging Visit		
Predictors	*Estimates*	*CI*	*p*
(Intercept)	2.973	2.862 – 3.084	**<0.001**
ASI at baseline	0.003	-0.002 – 0.009	0.258
Age	-0.001	-0.003 – 0.001	0.302
Observations	639		
R^2 / R^2 adjusted	0.003 / -0.000		

B6b). Linear Regression Model Output Imaging Visit 2

	RH Rostral Anterior Cingulate at Second Imaging Visit		
Predictors	*Estimates*	*CI*	*p*
(Intercept)	2.948	2.837 – 3.059	**<0.001**
ASI at baseline	-0.001	-0.006 – 0.005	0.848
Age	-0.000	-0.002 – 0.002	0.779
Observations	630		
R^2 / R^2 adjusted	0.000 / -0.003		

B7. Left Hemisphere Rostral Middle Frontal Gyri Cortical Thickness

B7a). Linear Regression Model Output Imaging Visit 1

	LH Rostral Middle Frontal Gyri at First Imaging Visit		
Predictors	*Estimates*	*CI*	*p*
(Intercept)	3.076	3.005 – 3.147	**<0.001**
ASI at baseline	-0.001	-0.005 – 0.002	0.515
Age	-0.007	-0.008 – -0.006	**<0.001**
Observations	639		
R^2 / R^2 adjusted	0.159 / 0.156		

B7b). Linear Regression Model Output Imaging Visit 2

	LH Rostral Middle Frontal Gyri at Second Imaging Visit		
Predictors	*Estimates*	*CI*	*p*
(Intercept)	3.097	3.020 – 3.174	**<0.001**
ASI at baseline	-0.002	-0.006 – 0.002	0.343
Age	-0.008	-0.009 – -0.006	**<0.001**
Observations	630		
R^2 / R^2 adjusted	0.164 / 0.162		

B8. Right Hemisphere Rostral Middle Frontal Gyri Cortical Thickness

B8a). Linear Regression Model Output Imaging Visit 1

	RH Rostral Middle Frontal Gyri at First Imaging Visit		
Predictors	*Estimates*	*CI*	*p*
(Intercept)	2.976	2.912 – 3.040	**<0.001**
ASI at baseline	-0.000	-0.004 – 0.003	0.844
Age	-0.006	-0.008 – -0.005	**<0.001**
Observations	639		
R^2 / R^2 adjusted	0.151 / 0.148		

B8b). Linear Regression Model Output Imaging Visit 2

	RH Rostral Middle Frontal Gyri at Second Imaging Visit		
Predictors	*Estimates*	*CI*	*p*
(Intercept)	3.031	2.962 – 3.101	**<0.001**
ASI at baseline	-0.001	-0.005 – 0.002	0.457
Age	-0.008	-0.009 – -0.006	**<0.001**
Observations	630		
R^2 / R^2 adjusted	0.183 / 0.180		

B9. Left Hemisphere Superior Frontal Gyri Cortical Thickness

B9a). Linear Regression Model Output Imaging Visit 1

	LH Superior Frontal Gyri at First Imaging Visit		
Predictors	*Estimates*	*CI*	*p*
(Intercept)	3.451	3.376 – 3.526	**<0.001**
ASI at baseline	-0.004	-0.007 – 0.000	0.058
Age	-0.009	-0.010 – -0.007	**<0.001**
Observations	639		
R^2 / R^2 adjusted	0.208 / 0.205		

B9b). Linear Regression Model Output Imaging Visit 2

	LH Superior Frontal Gyri at Second Imaging Visit		
Predictors	*Estimates*	*CI*	*p*
(Intercept)	3.492	3.411 – 3.573	**<0.001**
ASI at baseline	-0.003	-0.007 – 0.001	0.151
Age	-0.010	-0.011 – -0.008	**<0.001**
Observations	630		
R^2 / R^2 adjusted	0.229 / 0.227		

B10. Right Hemisphere Superior Frontal Gyri Cortical Thickness

B10a). Linear Regression Model Output Imaging Visit 1

	RH Superior Frontal Gyri at First Imaging Visit		
Predictors	*Estimates*	*CI*	*p*
(Intercept)	3.324	3.255 – 3.394	**<0.001**
ASI at baseline	-0.001	-0.005 – 0.002	0.452
Age	-0.007	-0.009 – -0.006	**<0.001**
Observations	639		
R^2 / R^2 adjusted	0.172 / 0.169		

B10b). Linear Regression Model Output Imaging Visit 2

	RH Superior Frontal Gyri at Second Imaging Visit		
Predictors	*Estimates*	*CI*	*p*
(Intercept)	3.397	3.322 – 3.472	**<0.001**
ASI at baseline	-0.003	-0.007 – 0.000	0.088
Age	-0.009	-0.010 – -0.007	**<0.001**
Observations	630		
R^2 / R^2 adjusted	0.217 / 0.214		

B11. Left Hemisphere Superior Parietal Cortex Cortical Thickness

B11a). Linear Regression Model Output Imaging Visit 1

	LH Superior Parietal Cortex at First Imaging Visit		
Predictors	*Estimates*	*CI*	*p*
(Intercept)	2.792	2.722 – 2.863	**<0.001**
ASI at baseline	-0.002	-0.005 – 0.002	0.331
Age	-0.006	-0.007 – -0.004	**<0.001**
Observations	639		
R^2 / R^2 adjusted	0.110 / 0.107		

B11b). Linear Regression Model Output Imaging Visit 2

	LH Superior Parietal Cortex at Second Imaging Visit		
Predictors	*Estimates*	*CI*	*p*
(Intercept)	2.875	2.797 – 2.952	**<0.001**
ASI at baseline	-0.002	-0.006 – 0.002	0.244
Age	-0.007	-0.009 – -0.006	**<0.001**
Observations	630		
R^2 / R^2 adjusted	0.153 / 0.150		

B12. Right Hemisphere Superior Parietal Cortex Cortical Thickness

B12a). Linear Regression Model Output Imaging Visit 1

	RH Superior Parietal Cortex at First Imaging Visit		
Predictors	*Estimates*	*CI*	*p*
(Intercept)	2.789	2.716 – 2.861	**<0.001**
ASI at baseline	-0.002	-0.006 – 0.001	0.210
Age	-0.006	-0.007 – -0.005	**<0.001**
Observations	639		
R^2 / R^2 adjusted	0.119 / 0.116		

B12b). Linear Regression Model Output Imaging Visit 2

	RH Superior Parietal Cortex at Second Imaging Visit		
Predictors	*Estimates*	*CI*	*p*
(Intercept)	2.874	2.797 – 2.952	**<0.001**
ASI at baseline	-0.003	-0.007 – 0.001	0.098
Age	-0.008	-0.009 – -0.006	**<0.001**
Observations	630		
R^2 / R^2 adjusted	0.168 / 0.165		

B13. Left Hemisphere Inferior Parietal Cortex Cortical Thickness

B13a). Linear Regression Model Output Imaging Visit 1

	LH Inferior Parietal Cortex at First Imaging Visit		
Predictors	*Estimates*	*CI*	*p*
(Intercept)	3.000	2.933 – 3.068	**<0.001**
ASI at baseline	-0.004	-0.007 – -0.000	**0.034**
Age	-0.005	-0.006 – -0.004	**<0.001**
Observations	639		
R^2 / R^2 adjusted	0.113 / 0.110		

B13b). Linear Regression Model Output Imaging Visit 2

	LH Inferior Parietal Cortex at Second Imaging Visit		
Predictors	*Estimates*	*CI*	*p*
(Intercept)	3.075	3.003 – 3.146	**<0.001**
ASI at baseline	-0.004	-0.008 – -0.000	**0.028**
Age	-0.007	-0.008 – -0.005	**<0.001**
Observations	630		
R^2 / R^2 adjusted	0.162 / 0.159		

B14. Right Hemisphere Inferior Parietal Cortex Cortical Thickness

B14a). Linear Regression Model Output Imaging Visit 1

	RH Inferior Parietal Cortex at First Imaging Visit		
Predictors	*Estimates*	*CI*	*p*
(Intercept)	3.098	3.026 – 3.170	**<0.001**
ASI at baseline	-0.004	-0.007 – -0.000	**0.049**
Age	-0.006	-0.008 – -0.005	**<0.001**
Observations	639		
R^2 / R^2 adjusted	0.143 / 0.140		

B14b). Linear Regression Model Output Imaging Visit 2

	RH Inferior Parietal Cortex at Second Imaging Visit		
Predictors	*Estimates*	*CI*	*p*
(Intercept)	3.161	3.085 – 3.237	**<0.001**
ASI at baseline	-0.004	-0.008 – -0.000	**0.028**
Age	-0.008	-0.009 – -0.006	**<0.001**
Observations	630		
R^2 / R^2 adjusted	0.183 / 0.181		

B15. Left Hemisphere Superior Temporal Cortex Cortical Thickness

B15a). Linear Regression Model Output Imaging Visit 1

	LH Superior Temporal Cortex at First Imaging Visit		
Predictors	*Estimates*	*CI*	*p*
(Intercept)	2.792	2.722 – 2.863	**<0.001**
ASI at baseline	-0.002	-0.005 – 0.002	0.331
Age	-0.006	-0.007 – -0.004	**<0.001**
Observations	639		
R^2 / R^2 adjusted	0.110 / 0.107		

B15b). Linear Regression Model Output Imaging Visit 2

	LH Superior Temporal Cortex at Second Imaging Visit		
Predictors	*Estimates*	*CI*	*p*
(Intercept)	2.875	2.797 – 2.952	**<0.001**
ASI at baseline	-0.002	-0.006 – 0.002	0.244
Age	-0.007	-0.009 – -0.006	**<0.001**
Observations	630		
R^2 / R^2 adjusted	0.153 / 0.150		

B16. Right Hemisphere Superior Temporal Cortex Cortical Thickness

B16a). Linear Regression Model Output Imaging Visit 1

	RH Superior Temporal Cortex at First Imaging Visit		
Predictors	*Estimates*	*CI*	*p*
(Intercept)	2.789	2.716 – 2.861	**<0.001**
ASI at baseline	-0.002	-0.006 – 0.001	0.210
Age	-0.006	-0.007 – -0.005	**<0.001**
Observations	639		
R^2 / R^2 adjusted	0.119 / 0.116		

B16b). Linear Regression Model Output Imaging Visit 2

	RH Superior Temporal Cortex at First Imaging Visit		
Predictors	*Estimates*	*CI*	*p*
(Intercept)	2.874	2.797 – 2.952	**<0.001**
ASI at baseline	-0.003	-0.007 – 0.001	0.098
Age	-0.008	-0.009 – -0.006	**<0.001**
Observations	630		
R^2 / R^2 adjusted	0.168 / 0.165		

B17. Left Hemisphere Middle Temporal Lobe Cortical Thickness

B17a). Linear Regression Model Output Imaging Visit 1

	LH Middle Temporal Lobe at First Imaging Visit		
Predictors	*Estimates*	*CI*	*p*
(Intercept)	3.146	3.065 – 3.226	**<0.001**
ASI at baseline	-0.005	-0.009 – -0.001	**0.014**
Age	-0.004	-0.005 – -0.002	**<0.001**
Observations	639		
R^2 / R^2 adjusted	0.054 / 0.051		

B17b). Linear Regression Model Output Imaging Visit 2

	LH Middle Temporal Lobe at Second Imaging Visit		
Predictors	*Estimates*	*CI*	*p*
(Intercept)	3.179	3.094 – 3.264	**<0.001**
ASI at baseline	-0.004	-0.009 – 0.000	0.058
Age	-0.005	-0.007 – -0.003	**<0.001**
Observations	630		
R^2 / R^2 adjusted	0.072 / 0.069		

B18. Right Hemisphere Middle Temporal Lobe Cortical Thickness

B18a). Linear Regression Model Output Imaging Visit 1

	RH Middle Temporal Lobe at First Imaging Visit		
Predictors	*Estimates*	*CI*	*p*
(Intercept)	3.315	3.232 – 3.397	**<0.001**
ASI at baseline	-0.000	-0.005 – 0.004	0.869
Age	-0.006	-0.007 – -0.004	**<0.001**
Observations	639		
R^2 / R^2 adjusted	0.086 / 0.083		

B18b). Linear Regression Model Output Imaging Visit 2

	RH Middle Temporal Lobe at Second Imaging Visit		
Predictors	*Estimates*	*CI*	*p*
(Intercept)	3.338	3.254 – 3.421	**<0.001**
ASI at baseline	-0.002	-0.006 – 0.002	0.331
Age	-0.006	-0.008 – -0.005	**<0.001**
Observations	630		
R^2 / R^2 adjusted	0.103 / 0.101		

B19. Left Hemisphere Inferior Temporal Cortex Cortical Thickness

B19a). Linear Regression Model Output Imaging Visit 1

	LH Inferior Temporal Cortex at First Imaging Visit		
Predictors	*Estimates*	*CI*	*p*
(Intercept)	3.186	3.109 – 3.264	**<0.001**
ASI at baseline	-0.001	-0.005 – 0.003	0.539
Age	-0.002	-0.004 – -0.001	**0.003**
Observations	639		
R^2 / R^2 adjusted	0.017 / 0.014		

B19b). Linear Regression Model Output Imaging Visit 2

	LH Inferior Temporal Cortex at Second Imaging Visit		
Predictors	*Estimates*	*CI*	*p*
(Intercept)	3.236	3.157 – 3.315	**<0.001**
ASI at baseline	-0.002	-0.006 – 0.002	0.401
Age	-0.003	-0.005 – -0.002	**<0.001**
Observations	630		
R^2 / R^2 adjusted	0.039 / 0.036		

B20. Right Hemisphere Inferior Temporal Cortex Cortical Thickness

B20a). Linear Regression Model Output Imaging Visit 1

	RH Inferior Temporal Cortex at First Imaging Visit		
Predictors	*Estimates*	*CI*	*p*
(Intercept)	3.238	3.163 – 3.312	**<0.001**
ASI at baseline	-0.005	-0.008 – -0.001	**0.018**
Age	-0.003	-0.004 – -0.002	**<0.001**
Observations	639		
R^2 / R^2 adjusted	0.047 / 0.044		

B20b). Linear Regression Model Output Imaging Visit 2

	RH Inferior Temporal Cortex at Second Imaging Visit		
Predictors	*Estimates*	*CI*	*p*
(Intercept)	3.263	3.183 – 3.342	**<0.001**
ASI at baseline	-0.005	-0.009 – -0.001	**0.012**
Age	-0.004	-0.005 – -0.002	**<0.001**
Observations	630		
R^2 / R^2 adjusted	0.059 / 0.056		

B21. Left Hemisphere Parahippocampus Cortical Thickness

B21a). Linear Regression Model Output Imaging Visit 1

	LH Parahippocampus at First Imaging Visit		
Predictors	*Estimates*	*CI*	*p*
(Intercept)	2.890	2.724 – 3.056	**<0.001**
ASI at baseline	-0.008	-0.016 – 0.000	0.061
Age	-0.001	-0.004 – 0.003	0.722
Observations	639		
R^2 / R^2 adjusted	0.007 / 0.004		

B21b). Linear Regression Model Output Imaging Visit 2

	LH Parahippocampus at Second Imaging Visit		
Predictors	*Estimates*	*CI*	*p*
(Intercept)	2.995	2.826 – 3.165	**<0.001**
ASI at baseline	-0.004	-0.012 – 0.005	0.398
Age	-0.004	-0.007 – -0.000	**0.024**
Observations	630		
R^2 / R^2 adjusted	0.012 / 0.009		

B22. Right Hemisphere Parahippocampus Cortical Thickness

B22a). Linear Regression Model Output Imaging Visit 1

	RH Parahippocampus at First Imaging Visit		
Predictors	*Estimates*	*CI*	*p*
(Intercept)	2.866	2.725 – 3.006	**<0.001**
ASI at baseline	-0.002	-0.009 – 0.005	0.655
Age	-0.003	-0.005 – 0.000	0.055
Observations	639		
R^2 / R^2 adjusted	0.007 / 0.004		

B22b). Linear Regression Model Output Imaging Visit 2

	RH Parahippocampus at Second Imaging Visit		
Predictors	*Estimates*	*CI*	*p*
(Intercept)	2.971	2.832 – 3.111	**<0.001**
ASI at baseline	-0.007	-0.014 – 0.000	0.063
Age	-0.004	-0.007 – -0.001	**0.004**
Observations	630		
R^2 / R^2 adjusted	0.025 / 0.022		

B23. Left Hemisphere Lateral Occipital Lobe Cortical Thickness

B23a). Linear Regression Model Output Imaging Visit 1

	LH Lateral Occipital Cortex at First Imaging Visit		
Predictors	*Estimates*	*CI*	*p*
(Intercept)	2.496	2.424 – 2.569	**<0.001**
ASI at baseline	-0.002	-0.006 – 0.002	0.265
Age	-0.003	-0.004 – -0.002	**<0.001**
Observations	639		
R^2 / R^2 adjusted	0.035 / 0.032		

B23b). Linear Regression Model Output Imaging Visit 2

	LH Lateral Occipital Cortex at Second Imaging Visit		
Predictors	*Estimates*	*CI*	*p*
(Intercept)	2.555	2.479 – 2.630	**<0.001**
ASI at baseline	-0.001	-0.005 – 0.002	0.461
Age	-0.005	-0.006 – -0.003	**<0.001**
Observations	630		
R^2 / R^2 adjusted	0.067 / 0.064		

B24. Right Hemisphere Lateral Occipital Lobe Cortical Thickness

B24a). Linear Regression Model Output Imaging Visit 1

	RH Lateral Occipital Cortex at First Imaging Visit		
Predictors	*Estimates*	*CI*	*p*
(Intercept)	2.530	2.449 – 2.610	**<0.001**
ASI at baseline	0.000	-0.004 – 0.004	0.913
Age	-0.003	-0.005 – -0.002	**<0.001**
Observations	639		
R^2 / R^2 adjusted	0.031 / 0.028		

B24b). Linear Regression Model Output Imaging Visit 2

	RH Lateral Occipital Cortex at Second Imaging Visit		
Predictors	*Estimates*	*CI*	*p*
(Intercept)	2.561	2.481 – 2.641	**<0.001**
ASI at baseline	-0.001	-0.005 – 0.004	0.788
Age	-0.004	-0.006 – -0.003	**<0.001**
Observations	630		
R^2 / R^2 adjusted	0.046 / 0.043		

B25. Left Hemisphere Posterior Cingulate Cortical Thickness

B25a). Linear Regression Model Output Imaging Visit 1

	LH Posterior Cingulate at First Imaging Visit		
Predictors	*Estimates*	*CI*	*p*
(Intercept)	2.915	2.819 – 3.011	**<0.001**
ASI at baseline	0.001	-0.004 – 0.006	0.764
Age	-0.004	-0.006 – -0.003	**<0.001**
Observations	639		
R^2 / R^2 adjusted	0.035 / 0.032		

B25b). Linear Regression Model Output Imaging Visit 2

	LH Posterior Cingulate at Second Imaging Visit		
Predictors	*Estimates*	*CI*	*p*
(Intercept)	2.907	2.807 – 3.006	**<0.001**
ASI at baseline	0.003	-0.002 – 0.008	0.261
Age	-0.005	-0.007 – -0.003	**<0.001**
Observations	630		
R^2 / R^2 adjusted	0.041 / 0.038		

B26. Right Hemisphere Posterior Cingulate Cortical Thickness

B26a). Linear Regression Model Output Imaging Visit 1

	RH Posterior Cingulate at First Imaging Visit		
Predictors	*Estimates*	*CI*	*p*
(Intercept)	2.902	2.797 – 3.006	**<0.001**
ASI at baseline	0.000	-0.005 – 0.005	0.955
Age	-0.004	-0.006 – -0.002	**<0.001**
Observations	639		
R^2 / R^2 adjusted	0.023 / 0.020		

B26b). Linear Regression Model Output Imaging Visit 2

	RH Posterior Cingulate at Second Imaging Visit		
Predictors	*Estimates*	*CI*	*p*
(Intercept)	2.862	2.757 – 2.967	**<0.001**
ASI at baseline	-0.003	-0.009 – 0.002	0.237
Age	-0.003	-0.005 – -0.001	**0.004**
Observations	630		
R^2 / R^2 adjusted	0.020 / 0.017		

B27. Whole Brain Grey Matter Volume

B27a). Linear Regression Model Output Imaging Visit 1

	GMV at first imaging visit		
Predictors	*Estimates*	*CI*	*p*
(Intercept)	1013.081	991.947 – 1034.215	**<0.001**
ASI at baseline	-1.330	-2.401 – -0.259	**0.015**
Age	-3.687	-4.087 – -3.287	**<0.001**
Observations	650		
R^2 / R^2 adjusted	0.373 / 0.371		

B27b). Linear Regression Model Output Imaging Visit 2

	GMV at second imaging visit		
Predictors	*Estimates*	*CI*	*p*
(Intercept)	1006.801	986.206 – 1027.397	**<0.001**
ASI at baseline	-1.153	-2.197 – -0.109	**0.030**
Age	-3.791	-4.181 – -3.401	**<0.001**
Observations	650		
R^2 / R^2 adjusted	0.394 / 0.393		

B28. White Matter Hyperintensity Volume

B28a). Linear Regression Model Output Imaging Visit 1

	WMH at first imaging visit		
Predictors	*Estimates*	*CI*	*p*
(Intercept)	-8.015	-10.213 – -5.817	**<0.001**
ASI at baseline	0.043	-0.068 – 0.155	0.446
Age	0.214	0.173 – 0.256	**<0.001**
Observations	650		
R^2 / R^2 adjusted	0.151 / 0.149		

B28b). Linear Regression Model Output Imaging Visit 2

	WMH at second imaging visit		
Predictors	*Estimates*	*CI*	*p*
(Intercept)	-10.109	-12.885 – -7.332	**<0.001**
ASI at baseline	0.124	-0.016 – 0.265	0.083
Age	0.253	0.201 – 0.306	**<0.001**
Observations	650		
R^2 / R^2 adjusted	0.144 / 0.142		

B29. Digit Symbol Substitution Test Performance

B29a). Linear Regression Model Output Imaging Visit 1

	DSST at first imaging visit		
Predictors	*Estimates*	*CI*	*p*
(Intercept)	31.528	28.582 – 34.473	**<0.001**
ASI at baseline	0.021	-0.130 – 0.173	0.782
Age	-0.219	-0.275 – -0.163	**<0.001**
Observations	511		
R^2 / R^2 adjusted	0.109 / 0.106		

B29b). Linear Regression Model Output Imaging Visit 2

	DSST at second imaging visit		
Predictors	*Estimates*	*CI*	*p*
(Intercept)	34.765	31.851 – 37.680	**<0.001**
ASI at baseline	0.029	-0.120 – 0.177	0.706
Age	-0.284	-0.339 – -0.229	**<0.001**
Observations	619		
R^2 / R^2 adjusted	0.149 / 0.146		

B30. Trail Making Test Part A Performance

B30a). Linear Regression Model Output Imaging Visit 1

	TmA at first imaging visit		
Predictors	*Estimates*	*CI*	*p*
(Intercept)	121.688	78.471 – 164.904	**<0.001**
ASI at baseline	-0.419	-2.626 – 1.788	0.709
Age	1.705	0.883 – 2.527	**<0.001**
Observations	515		
R^2 / R^2 adjusted	0.032 / 0.029		

B30b). Linear Regression Model Output Imaging Visit 2

	TmA at second imaging visit		
Predictors	*Estimates*	*CI*	*p*
(Intercept)	36.148	-15.888 – 88.185	0.173
ASI at baseline	-1.411	-4.070 – 1.248	0.298
Age	3.596	2.611 – 4.581	**<0.001**
Observations	634		
R^2 / R^2 adjusted	0.076 / 0.073		

B31. Trail Making Test Part B Performance

B31a). Linear Regression Model Output Imaging Visit 1

	TmB at first imaging visit		
Predictors	*Estimates*	*CI*	*p*
(Intercept)	194.465	60.150 – 328.779	**0.005**
ASI at baseline	-4.062	-10.922 – 2.798	0.245
Age	6.627	4.072 – 9.182	**<0.001**
Observations	515		
R^2 / R^2 adjusted	0.048 / 0.045		

B31b). Linear Regression Model Output Imaging Visit 2

	TmB at second imaging visit		
Predictors	*Estimates*	*CI*	*p*
(Intercept)	64.800	-81.880 – 211.480	0.386
ASI at baseline	1.799	-5.696 – 9.294	0.638
Age	8.209	5.431 – 10.987	**<0.001**
Observations	634		
R^2 / R^2 adjusted	0.057 / 0.054		

B32. Fluid Intelligence Test Performance

B32a). Linear Regression Model Output Imaging Visit 1

	Fluid Intelligence at first imaging visit		
Predictors	*Estimates*	*CI*	*p*
(Intercept)	6.355	5.116 – 7.593	**<0.001**
ASI at baseline	-0.029	-0.093 – 0.034	0.368
Age	0.013	-0.011 – 0.036	0.296
Observations	559		
R^2 / R^2 adjusted	0.003 / -0.001		

B32b). Linear Regression Model Output Imaging Visit 2

	Fluid Intelligence at second imaging visit		
Predictors	*Estimates*	*CI*	*p*
(Intercept)	7.536	6.372 – 8.700	**<0.001**
ASI at baseline	-0.011	-0.071 – 0.048	0.709
Age	-0.013	-0.035 – 0.009	0.250
Observations	621		
R^2 / R^2 adjusted	0.003 / -0.000		

B33. Numeric Memory Test Performance

B33a). Linear Regression Model Output Imaging Visit 1

	Numeric Memory at first imaging visit		
Predictors	*Estimates*	*CI*	*p*
(Intercept)	7.722	6.782 – 8.662	**<0.001**
ASI at baseline	-0.022	-0.070 – 0.026	0.364
Age	-0.014	-0.032 – 0.004	0.120
Observations	518		
R^2 / R^2 adjusted	0.008 / 0.004		

B33b). Linear Regression Model Output Imaging Visit 2

	Numeric Memory at second imaging visit		
Predictors	*Estimates*	*CI*	*p*
(Intercept)	8.098	7.147 – 9.049	**<0.001**
ASI at baseline	-0.025	-0.074 – 0.023	0.307
Age	-0.023	-0.041 – -0.005	**0.013**
Observations	634		
R^2 / R^2 adjusted	0.015 / 0.011		

B34. Pairs Matching Test Performance

B34a). Linear Regression Model Output Imaging Visit 1

	Pairs Matching at first imaging visit		
Predictors	*Estimates*	*CI*	*p*
(Intercept)	0.657	-1.017 – 2.331	0.441
ASI at baseline	-0.093	-0.178 – -0.007	**0.034**
Age	0.069	0.037 – 0.101	**<0.001**
Observations	564		
R^2 / R^2 adjusted	0.033 / 0.029		

B34b). Linear Regression Model Output Imaging Visit 2

	Pairs Matching at second imaging visit		
Predictors	*Estimates*	*CI*	*p*
(Intercept)	1.609	0.049 – 3.170	**0.043**
ASI at baseline	0.031	-0.048 – 0.111	0.438
Age	0.026	-0.004 – 0.055	0.087
Observations	634		
R^2 / R^2 adjusted	0.007 / 0.004		